ҚАЗАҚСТАН РЕСПУБЛИКАСЫ
ҒЫЛЫМ ЖӘНЕ ЖОҒАРЫ БІЛІМ МИНИСТРЛІГІ

SATBAYEV UNIVERSITY
МЕТАЛЛУРГИЯ ЖӘНЕ КЕН БАЙЫТУ ИНСТИТУТЫ

ISSN 2616-6445 (Online)
ISSN 2224-5243 (Print)
DOI 10.31643/2018/166445

Минералдық шикізаттарды кешенді пайдалану

1(344)

Комплексное Использование Минерального Сырья

Complex Use of Mineral Resources

ҚАҢТАР-НАУРЫЗ 2028
JANUARY-MARCH 2028
ЯНВАРЬ-МАРТ 2028

ЖЫЛЫНА 4 РЕТ ШЫҒАДЫ
QUARTERLY JOURNAL
ВЫХОДИТ 4 РАЗА В ГОД

ЖУРНАЛ 1978 ЖЫЛДАН БАСТАП ШЫҒАДЫ
JOURNAL HAS BEEN PUBLISHING SINCE 1978
ЖУРНАЛ ИЗДАЕТСЯ С 1978 ГОДА

АЛМАТЫ - 2028

Редакция мекен жайы:
«Металлургия және кен байыту институты» АҚ
050010, Қазақстан Республикасы, Алматы қ., Шевченко к-сі, Уәлиханов к-нің қиылысы, 29/133,
Fax. +7 (727) 298-45-03, Tel. +7-(727) 298-45-02, +7 (727) 298-45-19
E mail: journal@kims-imio.kz, product-service@kims-imio.kz
http://kims-imio.com/index.php/main

«Минералдық шикізаттарды кешенді пайдалану» журналы ғылыми жұмыстардың негізгі нәтижелерін жариялау үшін Қазақстан Республикасы Білім және ғылым министірлігінің Білім және ғылым сапасын қамтамасыз ету комитеті ұсынған ғылыми басылымдар тізіміне енгізілген.
Меншік иесі: «Металлургия және кен байыту институты» АҚ

Журнал Қазақстан Республикасының Ақпарат және коммуникация министрлігінің Байланыс, ақпараттандыру және бұқаралық ақпарат құралдары саласындағы мемлекеттік бақылау комитетінде қайта тіркелген

2016 ж. 18 қазандағы № 16180-Ж Куәлігі

Address:
"Institute of Metallurgy and Ore Beneficiation" JSC
29/133 Shevchenko Street, corner of Ch. Valikhanov Street, Almaty, 050010, Kazakhstan
Fax. +7 (727) 298-45-03, Tel. +7-(727) 298-45-02, +7 (727) 298-45-19
E mail: journal@kims-imio.kz, product-service@kims-imio.kz
http://kims-imio.com/index.php/main

The Journal "Complex Use of Mineral Resources" is included in the List of publications recommended by the Committee for Control in the Sphere of Education and Science of the Ministry of Education and Science of the Republic of Kazakhstan for the publication of the main results of scientific activities.
Owner: "Institute of Metallurgy and Ore Beneficiation" JSC

The Journal was re-registered by the Committee for State Control in the Sphere of Communication, Information and Mass Media of the Ministry of Information and Communication of the Republic of Kazakhstan.

Certificate № 16180-Ж since October 18, 2016

Адрес редакции:
АО «Институт металлургии и обогащения»
050010, Республика Казахстан, г. Алматы, ул. Шевченко, уг. ул. Валиханова, 29/133,
Fax. +7 (727) 298-45-03, Tel. +7 (727) 298-45-02, +7 (727) 298-45-19
E mail: journal@kims-imio.kz, product-service@kims-imio.kz
http://kims-imio.com/index.php/main

Журнал «Комплексное использование минерального сырья» включен в Перечень изданий, рекомендуемых Комитетом по контролю в сфере образования и науки Министерства образования и науки Республики Казахстан для публикации основных результатов научной деятельности.
Собственник: АО «Институт металлургии и обогащения»

Журнал перерегистрирован в Комитете государственного контроля в области связи, информатизации и средств массовой информации
Министерства информации и коммуникации Республики Казахстан
Свидетельство № 16180-Ж от 18 октября 2016 г.

Crossref
DOI: 10.31643/2028/6445.01
Mining & Mineral Processing

Acid and Thermal Activation of Clay Separated from Kaoline for Uranium Purification

[1]Maldybayev G., [2]Gerassyova N., [1*]Sharipov R., [1]Zhangabayeva A., [1]El-Sayed Negim, [1]Khambarqyzy A., [1] Kylyshkanov M., [3] Bekbayeva L., [1] Balgimbayeva U., [4]Moshera Samy

[1]Kazakh British Technical University, Almaty, Kazakhstan
[2]LLC Deep Core Analytics, Almaty, Kazakhstan
[3]Al-Farabi Kazakh National University, Almaty, Kazakhstan
[4] National Research Centre, Dokki, Giza, Egypt

** Corresponding author email: r.sharipov@kbtu.kz*

Received: *February 28, 2026*
Peer-reviewed: *March 18, 2026*
Accepted: *April 2, 2026*

ABSTRACT
Clay minerals are commonly used as adsorbents due to their wide availability, large specific surface area, and cation exchange capabilities, making them suitable for removing heavy metal ions from wastewater. This study investigated the activation of clay by acid and thermal treatment to obtain an adsorbent for the purification of uranium from impurities such as iron and magnesium. Acid modification of clay samples was carried out with sulfuric acid (15%) at a temperature of 80–90 °C for 3 hours. While the activation of the clay using the thermal process was performed at 600–650 °C for 12–24 hours. X-Ray Diffraction, Electron Paramagnetic Resonance (EPR), and Fourier Transform Infrared Spectroscopy (FTIR) were used to analyse the clay's chemical composition and structural changes before and after activation. FTIR identified free OH groups and hydrated SiO2. EPR showed a high level of paramagnetic centers linked to structural defects and oxygen vacancies, which contribute to the material's strong adsorption and catalytic activity. After acid treatment, the clay particles exhibited a notable rise in specific surface area, expanding from 35.2 m^2/g to 342.5 m^2/g. Additionally, the specific pore volume grew substantially, increasing from 0.024 cm^3/g to 0.30 cm^3/g.

Keywords: clay, acid activation, thermal activation, uranium.

Information about authors:

Galymzhan Maldybayev — *PhD, Associate Professor, Laboratory of Advanced Materials and Technologies, Kazakh British Technical University, 050000, St. Tole bi, 59, Almaty, Kazakhstan. Email: g.maldybaev@kbtu.kz*

Gerassyova Natalya — *Doctoral student, LLC Deep Core Analytics, al-Farabi av., 17/1 b5B, 050059, Almaty, Kazakhstan. Email: tatoline2001@gmail.com*

Rustam Sharipov — *PhD, Assistant Professor, Laboratory of Advanced Materials and Technologies, Kazakh British Technical University, 050000, St. Tole bi, 59, Almaty, Kazakhstan. Email: r.sharipov@kbtu.kz*

Assem Zhangabayeva — *Researcher, Laboratory of Advanced Materials and Technologies, Kazakh British Technical University, 050000, St. Tole bi, 59, Almaty, Kazakhstan. Email: a.zhangabayeva@kbtu.kz*

El-Sayed Negim — *PhD, Professor, School of Materials Science and Green Technologies, Kazakh British Technical University, 050000, St. Tole bi, 59, Almaty, Kazakhstan. Email: elashmawi5@yahoo.com*

Aigerim Khambarqyzy — *Researcher, Laboratory of Advanced Materials and Technologies, Kazakh British Technical University, 050000, St. Tole bi, 59, Almaty, Kazakhstan. Email: a.khambarkyzy@kbtu.kz*

Manarbek Kylyshkanov — *Doctor of Physico-Mathematical Sciences, Laboratory of Advanced Materials and Technologies, Kazakh British Technical University, 050000, St. Tole bi, 59, Almaty, Kazakhstan. Email: kylyshkanov@mail.ru*

Lyazzat Bekbayeva — *PhD, Associate Professor, National Nanotechnology Open Laboratory, Al-Farabi Kazakh National University, 050040, Al-Farabi av., Almaty, Kazakhstan. Email: lyazzat_bk2019@mail.ru*

Ulpan Balgimbayeva — *PhD, Laboratory of Advanced Materials and Technologies, Kazakh British Technical University, 050000, St. Tole bi, 59, Almaty, Kazakhstan. Email: u.balgimbaeva@kbtu.kz*

Moshera Samy — *PhD, Polymers and Pigments Department, National Research Centre, 33 El Buhouth St., Dokki, Giza 12622, Egypt. Email: moshera_samy1984@yahoo.com; ORCID ID: https://orcid.org/0000-0002-7272-4134*

Introduction

In industrial water systems, silicon is present in multiple physicochemical forms based on different factors, including its solubility and degree of aggregation: as monomeric soluble silicon dioxide (SiO_2), as colloidal aggregates ($SiO_2 \cdot nH_2O$), and in the solid phase as sand, silt, or silicate minerals [[1], [2], [3]]. In uranium hydrometallurgy, the ionic and colloidal forms are dominant, significantly affecting the efficiency of technological processes, including sorption, equipment corrosion, and scale formation [4]. There are

different types of silicon depends on factors such as pH, temperature, ionic strength, and what's in the solution. When uranium ores undergo in-situ leaching with sulfuric acid, silicon primarily dissolves as an impurity that reduces the efficiency of uranium extraction [4]. Sulfuric acid ion exchange process for uranium ores reacts with aluminosilicate minerals such as kaolinite, chlorite, hydromica, and coffinite, producing silicic acid that can polymerize into high-molecular-weight compounds [6]. These compounds accumulate and infiltrate in anion exchange resins, causing significant improvement in silicification, reducing uranium capacity, increasing hydraulic resistance, impeding desorption and denitration, and degrading mechanical properties. Silicon content in waste resins may reach 12–15 wt.%, so removal is necessary either before sorption or from saturated resins [[7], [8]]. Several methods are available for removing silicon from industrial solutions, including adsorption, ion exchange, reverse osmosis, electrodialysis, chemical precipitation, and extraction [[3], [4],[4]]. In uranium environments, adsorption is preferred due to its selectivity and cost-effectiveness. It offers low energy use, adsorbent regeneration, environmental safety, and process flexibility. Adsorption may occur through physical forces (van der Waals) or chemisorption, which forms stronger chemical bonds between the adsorbate and adsorbent [[2], [9], [10]]. Physical adsorption occurs due to weak intermolecular forces and the condensation of molecules within the pores of a solid, whereas chemical adsorption (chemisorption) involves the formation of chemical bonds between the sorbate molecule and the active sites on the adsorbent surface on the adsorbent surface [[2],[11]]. Chemisorption results in the formation of an adsorbate monolayer and is often irreversible, making it particularly effective for the deep extraction of target components. A thorough understanding of adsorption mechanisms is necessary for both the design and optimization of industrial processes, as well as for the accurate characterization of the porous structure of materials [12]. Ion exchange is used to purify, separate, and recover ion-containing solutions using solid materials such as resins, membranes, and minerals. However, this method requires significant capital and operating costs, especially when resin regeneration and waste disposal are required [[13], [14], [15], [16]]. Chemical precipitation is used to convert dissolved substances into a solid phase, but is ineffective for removing trace contaminants and produces large amounts of sludge requiring further processing [[14], [15]]. Reverse osmosis is a membrane process that uses pressure to selectively remove ions and molecules through a semipermeable membrane. Electrodialysis allows for the selective extraction of ions using an electric field, but also produces concentrated waste streams [[15], [16], [17], [18]. It is effective for desalination but is limited in application due to the high cost of the membranes and sensitivity to fouling [[19], [20], [21]]. Electrolysis is used to extract elements from solutions but has limited application in the context of silicon removal [22], [23], [24], [25]]. Sulfuric acid in-situ leaching of uranium ores results in the transfer of uranium and several other elements from the ore-bearing rocks into the productive solution, leading to contamination of the productive solutions with ballast impurities. During the sorption extraction of uranium, these impurities behave differently and can be classified according to their behavior as inert, depressant, or toxic. In sulfuric acid environments, silicic acid is the most significant toxic impurity. The transfer of silicon into productive solutions is caused by reactions between sulfuric acid and aluminosilicates, chlorites, hydromicas, and the uranium-bearing mineral coffinite.

The goal of this study is to develop process modes and parameters for producing effective chemical adsorbents based on an aluminosilicate carrier, as well as to study the distribution and behavior of silicon in uranium sorption processing cycles.

Experimental part

Materials

Samples of kaolin ore from the Kostanay region were preliminarily crushed using a jaw crusher, Allis Mineral Systems (model N184T17FB12C), until a particle size was achieved at which all the material passed through a sieve with an aperture of 0.074 mm. The resulting crushed material was then processed in a Denver flotation cell equipped with a two-blade impeller. During processing, water was added to obtain a dense, homogeneous pulp; the solids content was not quantitatively controlled. At the final stage, the pulp was subjected to sieve analysis using Tyler sieves with additional dilution by water.

Method for separating clay and sand fractions from kaolin ore

The reactivity and practical of minerals are largely determined by the degree of structural order within their crystal lattices. The diversity of layered silicates stems from the presence of not only silicon–oxygen tetrahedra but also aluminum - and iron – oxygen tetrahedra. When tetravalent silicon (Si^{4+}) is substituted by trivalent aluminum (Al^{3+}), charge neutrality must be preserved through the

incorporation of compensating cations such as K^+, Na^+, or Ca^{2+}. The formation of active centers requires the gradual disruption of polyaluminosilicate frameworks. As a result, the process flow has been improved by introducing a preliminary separation of the ore into clay and sand fractions using a hydrocyclone system [[26], [27], [28], [29], [30]]. The results of test trials on clay–sand separation are presented in Table 1.

Table 1 shows that ore separation concentrates about 30% Al_2O_3 and 50% SiO_2 of the feedstock mass in the clay fraction. The conversion of Al_2O_3 into the clay fraction reaches 60–80%. As a result, adding the siphon separation step to ore preparation significantly impacts the process on a large scale; it mechanically activates the material, essentially "shaking" the aluminosilicate structures. Acid activation of the original clay mass.

Acid activation removes Fe and Mg impurities, breaks down inert minerals, and increases the surface area and porosity of clay, enhancing its adsorption and catalytic properties.

When treated with sulfuric acid (H_2SO_4), oxides and hydroxides of transition and alkaline earth metals are converted into soluble sulfate forms:

$$Fe_2O_3 + 3\ H_2SO_4 \rightarrow Fe_2(SO_4)_3 + 3\ H_2O$$
$$MgO + H_2SO_4 \rightarrow MgSO_4 + H_2O$$

Furthermore, controlled acid treatment facilitates the partial removal of adsorbed impurities and improves access to the material's pore system. However, excessively intense treatment can leach out structural aluminum and destroy the underlying aluminosilicate lattice, resulting in reduced product quality. Therefore, it is necessary to carefully control the acid concentration, process temperature, treatment duration, and solid-to-liquid ratio.

Preliminary modification of the structure and properties of mineral raw materials under the influence of chemical and physical factors creates optimal conditions for subsequent leaching and the formation of a developed porous structure.

To perform the acid treatment, 100 g of calcined and crushed clay material was loaded into the reactor, then 1 liter of a 15% H_2SO_4 solution was added at room temperature, and the system was heated to 80-90 °C. The process was carried out with vigorous stirring (~300 rpm) for 3 hours, with periodic sampling of the solid and liquid phases at 30, 60, 120, and 180 minutes to assess the reaction kinetics. Upon completion of the treatment, the mixture was cooled to ~40 °C and filtered, separating the liquid and solid phases.

The precipitate was washed with several portions of water until the filtrate pH reached approximately 6.5–7.0 and the conductivity was close to the initial value, monitoring the parameters with a pH meter. The purified solid residue was dried at 105 °C to constant weight.

Table 1 – Technological parameters of siphon-based ore separation: sieve analysis of the feed ore, detailing the mass fractions of aluminum and silicon within the size classes of both the hydrocyclone overflow and underflow (sand) streams.

No.	Separation product	Tormentation		Al_2O_3		Distribution Al_2O_3	SiO_2		Distribution SiO_2
		G	%	%	G	%	%	G	%
1	Raw ore	1866	100	20.97	391.3		60.75	1133	
	Clay	1323	71	23.95	316.8	81	56.78	751	66.3
	Sands	543	29	13.72	74.5	19	70.35	382	33.7
2	Raw ore	1855	100	22.24	412.5		61.4	1138	
	Clay	1292	69.6	25.91	334.75	81.1	56.72	732	64.3
	Sands	563	30.4	13.81	77.75	18.9	72.11	406	35.7
3	Source ore	3256	100	20.72	674.6		60.38	1965	
	Clay	1463	45	30.32	443.5	65.8	46.42	679	34.55
	Sands	1793	55	12.88	231.1	34.2	71.7	1286	65.44
4s	Raw ore	1960	100	22.88	448.4		56.12	1099	
	Clay	848.8	43.3	30.1	255.5	57	47.52	403	36.7
	Sands	1111.2	56.7	17.35	192.9	43	62.63	696	63.3

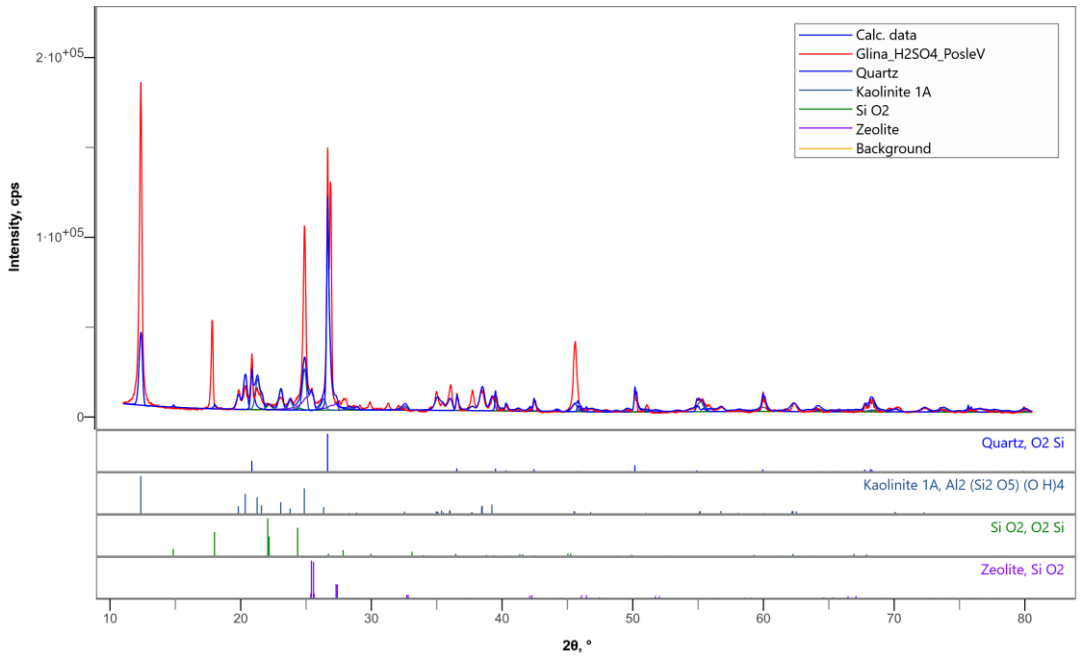

Figure 1 – X-ray diffraction pattern of kaolin clay after leaching

Table 2 – Phase composition of the sample determined by XRD

Component		Formula	Mass fraction, %
A	Quartz	SiO_2	33.7
B	Kaolinite 1A	$Al_2(Si_2O_5)(OH)_4$	50.7
C	Silicon dioxide	SiO_2	2.4
D	Zeolite	SiO_2	13.2

Figure 1 and Table 2 X-ray diffraction (XRD) analysis results show that the resulting material does not meet the expected characteristics required to form an active component based on the metakaolin mineral. This result indicates incomplete transformation of the original kaolinite into metakaolin, which may be due to insufficient dehydroxylation. Furthermore, the potential for the formation of secondary silicate compounds leads to a decrease in the proportion of free aluminum oxide in the composition. These deviations limit the potential for further use of the material as a chemical adsorbent.

Thermal activation of kaolin clay

Thermal activation of clay minerals involves treating natural clay at elevated temperatures, which causes the removal of adsorbed gases and water molecules and leads to the formation of a free surface. However, upon reaching certain temperatures characteristic of each specific mineral, the crystal lattice can partially disintegrate or completely collapse, which reduces the surface activity of the material. Based on the results of differential thermal analysis and thermogravimetry, it was established that the sample contains: quartz - less than 40%, kaolinite - about 50%, hydromica - 4.4%, chlorite - less than 1%, goethite - 1.6%, as well as thermally inert components - less than 5%. When heated, the characteristic features of the thermal behavior of these minerals did not show noticeable differences from the behavior of the components of the original ore.

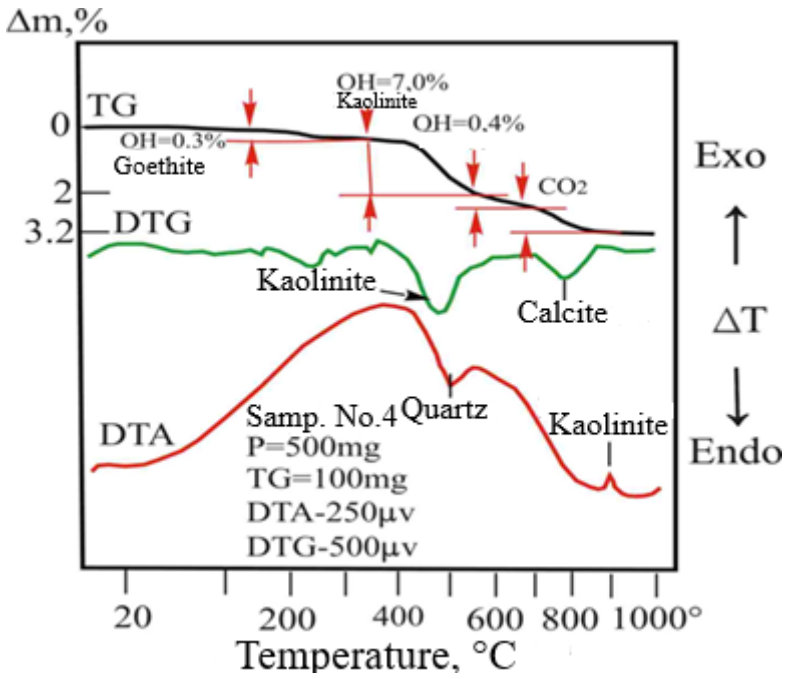

Mineral composition: quartz <80%, kaolinite – 12.1%, mica – 2.5%, goethite – 1.6%, calcite – 1.8%, TIM ~5%

Figure 2 - Derivative diagram of the clay fraction

Table 3 - Mineral and material composition of kaolin ore based on the results of thermal analysis

Sample name	Mineral and material composition of rocks, %													PP, 1000º C, %
	Quartz	Kaolinite	Hydromica	Mica	Chlorite	Calcite	Goethite	Hematite	TIM	Other minerals	H_2O	HE	CO_2	
Aluminosilicate carrier	<40	50.0	4.4	0.3	<1	-	1.6	-	5.0	-	0.4	7.8	-	8.2
Note: TIM – thermally inert minerals PS, diopside, etc. PPP –loss on ignition														

Figure 2 and Table 3 illustrate the results of DTA-TG-DTG analysis, which confirm the presence of hydroxyl and carbonate compounds in the sample and also allow us to determine the optimal range of thermal activation temperatures – from 600 to 700 °C, at which the dehydroxylation of kaolinite is completed and reactive metakaolin is formed without significant loss of structure and with the preservation of active adsorption centers. Up to 200 °C, a slight decrease in mass is observed, associated with the removal of physically adsorbed moisture and dehydration of the mineral surface. Around 250 °C - a small change in mass due to the removal of hydroxyl groups from goethite (OH ≈ 0.3%). In the range of 400–550 °C, there is an intense endothermic decrease in mass associated with the dehydroxylation of kaolinite (OH ≈ 7%), which leads to the formation of metakaolin. Around 600 °C, there is a weak peak of mica dehydroxylation (OH ≈ 0.4%). In the range of 700–850 °C, CO_2 is released,

corresponding to the decomposition of calcite ($CaCO_3 \rightarrow CaO + CO_2$). Above 900 °C, recrystallization of kaolinite begins with the formation of high-temperature phases (mullite, quartz) [[31], [32]].

Thus, thermal activation of clay minerals is possible at temperatures above 500°C. Puncture losses contribute to the formation of voids and new active centers, the structural elements of which in zeolites are SiO_4 and AlO_4 tetrahedra, connected at their corners to form cavities and channels through which hydrated cations, water, and other molecules can diffuse [33].

Based on the above, the solid product after leaching was subjected to additional thermal activation at 600–650 °C for 12–24 hours to stabilize the structure and increase the specific surface area. The resulting activated material was analyzed using X-ray diffraction (XRD), as shown in Figure 3 and Table 4.

X-ray diffraction analysis revealed that after heat treatment, partial amorphization of the aluminosilicate component was observed in the sample, accompanied by the disappearance of characteristic kaolinite reflections. This confirms the formation of metakaolin—an amorphous, reactive phase formed through dehydroxylation and the breakdown of the mineral's layered structure. The diffraction pattern reveals an increase in the amorphous background in the 15–35° 2θ range, reflecting an increase in the number of defective structural regions acting as active adsorption sites. The remaining quartz reflections and minor iron silicate peaks correspond to thermally stable impurities that do not participate in the formation of the active component. Thus, the resulting metakaolin possesses a developed defective surface capable of effectively binding silicon in solutions and providing increased sorption activity.

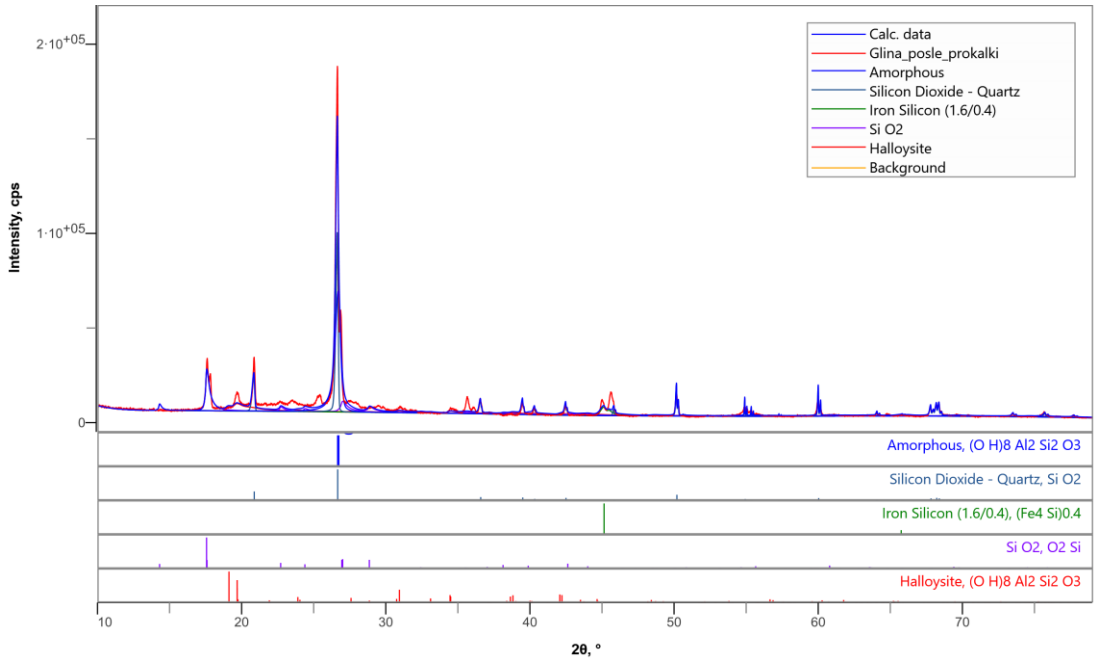

Figure 3 – X-ray diffraction pattern of kaolin clay after heat treatment

Table 4 – Phase composition of the sample determined by XRD

Component		Formula	Mass fraction, %
A	Silicon dioxide - Quartz	SiO_2	34.96
B	Iron silicide (1.6/0.4)	$(Fe_4Si)_{0.4}$	2.74
C	Silicon dioxide	SiO_2	26.2
D	Metakaolin	$Al_2Si_2O_3(OH)_8$	36.1

Results and Discussion

FT-IR analysis of the obtained chemical adsorbent

The predominance of hydrated silica indicates a highly amorphous matrix with inclusions of crystalline Al and Fe phases (metakaolin). This combination of phases explains the observed combination of broad background bands and several sharp peaks in XRD/IR: amorphous SiO_2 provides the background "flat" component, while the crystalline phases are responsible for the narrow peaks and characteristic OH/Si–O peaks. For technological applications, this implies high reactivity and absorption capacity (due to hydrated SiO_2), as well as the presence of stable mineral phases that influence thermal stability and behavior during heat treatment/chemical extraction.

The absorption spectrum in Figure 4 exhibits various vibrations above 3000 cm^{-1}. Absorption at 3400 cm^{-1} is attributed to absorbed water in the bulk phase (film water and water in inclusions), while the region around 3304 cm^{-1} is associated with the absorption of water molecules disturbed by the crystal's surface field. Under the influence of this field, the distances between the charges of water's molecular dipoles are slightly increased compared to the average distance in the bulk phase. This reduces bond rigidity and the vibration frequency.

Absorption at 3478 cm^{-1} in kaolin clay is characteristic of molecular water. Deformation vibrations of H_2O in mineral crystals are observed at higher frequencies (1620 cm^{-1}). This is attributed to the fact that water molecules in the crystal are bound by stronger hydrogen bonds.

The absorption band for the practically free OH group in kaolinite is around ~3600 cm^{-1}, the absorption band of water is around ~3450 cm^{-1}, and the absorption band for short hydrogen bonds O-H...O is around ~3300 cm^{-1}. The spectrum band of 1620 cm^{-1} is related to the deformation vibrations of the OH bond. Thus, the crystalline form of the original product is transformed predominantly into an ionic state, which determines the physicochemical properties of the leaching residue.

Study of the specific surface area and porosity of the chemical adsorbent

The specific surface area and pore structure parameters of the original kaolin clays and the resulting chemical adsorbent were studied using low-temperature nitrogen adsorption using the BET method. The results show a significant change in textural characteristics after activation treatment (Table 5). The measurements were performed using a SORBTOMETR-M instrument.

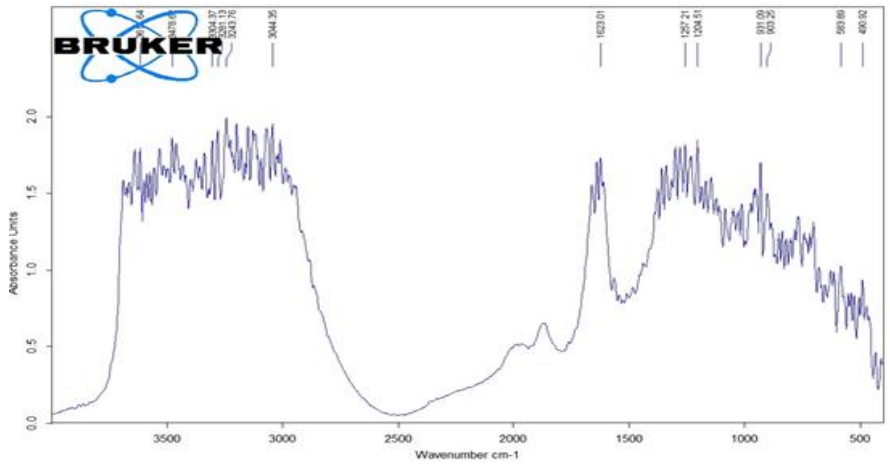

Figure 4 – FTIR spectra of chemical adsorbent

Table 5 – Specific surface area, specific volume and average pore size of the active component

Sample	Specific surface area, m^2/g	Specific pore volume, cm^3	Average pore size, angstroms
Original kaolin	35.2	0.024	1.52
Chemical adsorbent	342.5	0.30	1.95

The starting material has a relatively low specific surface area of 35.2 m²/g, a small specific pore volume (0.024 cm³/g), and an average pore size of about 1.52 Å, which corresponds to the dense, poorly developed porous structure of the natural mineral.

After activation, a sharp increase in the specific surface area to 342.5 m²/g is observed, exceeding the initial value by more than an order of magnitude. The specific pore volume increases to 0.30 cm³/g, indicating significant development of the microporous and mesoporous structure. The average pore size remains virtually unchanged (1.95 Å), indicating that the treatment primarily increases the number of active pores rather than changes their size.

Thus, the activation treatment ensures the formation of a highly developed porous structure, significantly increasing the specific surface area of the material. This directly enhances the effectiveness of the active component as a sorbent, improving the accessibility of active sites and the adsorption capacity of the material.

Study of the patterns of occurrence, content, and form of silicon compounds at different stages of processing uranium-containing solutions

To study methods for neutralizing silicon poisoning of the resin, the behavior of silicon in a uranium-containing solution was first studied. Silicon dioxide, SiO_2, is the anhydride of a series of silicic acids, whose composition can be expressed by the general formula $xSiO_2 \times yH_2O$, where x and y are integers.

x = 1, y = 1:$SiO_2 \times H_2O$, i.e. H_2SiO_3 – metasilicic acid;

x = 1, y = 2:$SiO_2 \times 2H_2O$, i.e. H_4SiO_4 – orthosilicic acid;

x = 2, y = 1:$2SiO_2 \times H_2O$, i.e. $H_2Si_2O_5$ – dimethylsilicic acid.

According to many researchers, the solubility of silicic acid at room temperature is 0.01–0.017% (calculated as SiO_2). As the temperature increases, its solubility increases, reaching 0.04% at 94 °C. Silicic acid is a very weak electrolyte. Its dissociation constant is 2×10-10. The pH of an aqueous silicic acid solution is approximately 4.0–4.5. Data on the solubility of amorphous silicon dioxide are presented in Table 6.

In natural waters, silicon compounds are found in dissolved, suspended, and colloidal states, the quantitative relationships between which are determined by the chemical composition of the water, temperature, pH, and other factors.

The dissolved forms are mainly represented by molecular orthosilicic acid $H_4SiO_4(SiO_2 \cdot 2H_2O)$, metasilicic $H_2SiO_3(SiO_2 \cdot H_2O)$, disilicic $H_2Si_2O_5$ $(2SiO_2 \cdot H_2O)$, and other acids with different numbers of SiO_2 and H_2O, products of their dissociation and association, as well as silicon-organic compounds. Polymeric and colloidal forms of silicic acid have a variable composition of the type $mSiO_2\ nH_2O$ (m and n are integers).

In aqueous solutions, the monomer silicic acid can be found primarily in five forms: H_4SiO_4, H_3SiO^{4-}, $H_2SiO_4^{2-}$, $HSiO_4^{3-}$, and SiO_4^{4-}. The ratio of silicic acid forms in water is determined by the dissociation constants of each of the stages. Figure 5 shows the dependence of the distribution of forms of dissolved silicon on the pH of the environment, from which it follows that in natural waters, the main part of silicic acid is in a molecularly dissolved form.

Therefore, during ion exchange, silicon begins to be absorbed as the medium transitions to an alkaline region, where it exists in an ionic form. This is achieved in practice by a highly basic anion exchange resin in the absence of strong acid anions. Thus, silicon in a process uranium-containing solution in the pH range up to 8.0 is monosilicic acid, which undergoes a polycondensation reaction as shown in Figure 5. In the pH range of 2.0 to 3.0, the polycondensation rate is minimal. Silicic acid cannot react chemically with other elements up to a pH of 8.0.

Table 6 – Dependence of the solubility of amorphous silicon dioxide on the pH of the solution at 25 °C

pH	1.0	2.0	3.0	4.2	5.7	7.7	10.26	10.6
Solubility, %	0.014	0.015	0.015	0.013	0.011	0.010	0.019	0.112

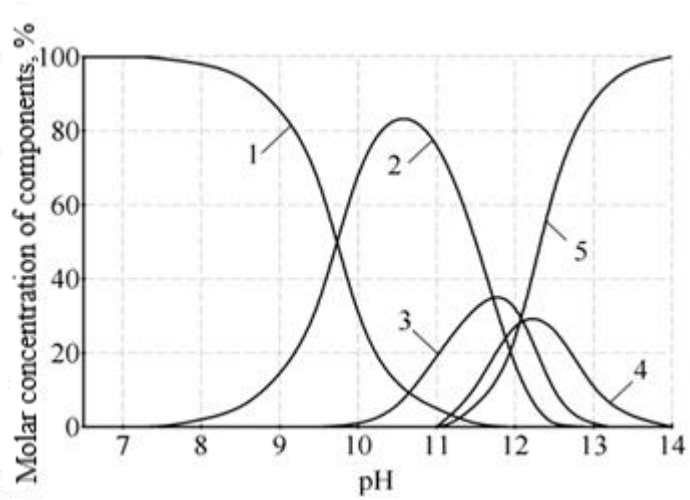

1 – H_4SiO_4; 2 – $H_3SiO_4^-$; 3 – $H_2SiO_4^{2-}$; 4 – $HSiO_4^{3-}$; 5 – SiO_4^{4-}

Figure 5 – Dependence of the ratio of silicic acid forms on the pH of the medium

Conclusions

The process modes for producing the active component for synthesizing chemical adsorbents based on kaolin or were developed. Hydrocyclone separation of kaolin ore enabled enrichment of the clay fraction in Al_2O_3 to 60–80% of the total content in the feedstock, ensuring high reactivity of subsequent products. Acid activation of the resulting clay mass with sulfuric acid (15%, 80–90 °C, 3 h) allowed for the partial removal of iron and magnesium impurities, increasing the availability of the aluminosilicate structure for further modification. To form the active phase, metakaolin-heat treatment was performed at 600–650 °C for 12–24 hours. The results of differential thermal analysis (DTA-TG-DTG) and X-ray diffraction (XRD) confirmed the completion of kaolinite dehydroxylation and the formation of an amorphous, reactive phase with a defective structure capable of effectively interacting with silicon compounds. The phase composition of the final product includes quartz (34.96%), metakaolin (36.1%), and amorphous silicon dioxide (26.2%), which meets the requirements for materials used as sorbents. The physicochemical characteristics of the obtained chemical adsorbent showed a significant improvement in textural properties compared to the original kaolin: the specific surface area increased from 35.2 m^2/g to 342.5 m^2/g, and the specific pore volume increased from 0.024 cm^3/g to 0.30 cm3/g. This indicates the formation of a developed microporous structure, ensuring high accessibility of active centers for sorption. IR spectroscopy confirmed the presence of free OH groups and hydrated forms of SiO_2.

Conflicts of interest. Authors declare no conflict of interest.

CRediT author statement: G. Maldybayev, N. Gerassyova: Conceptualization, Methodology, Software. R. Sharipov: Data curation, Writing draft preparation.: Visualization, Investigation. A. Zhangabayeva: Supervision. E. Negim: Software, Validation. A. Khambarqyzy, M. Kylyshkanov, L. Bekbayeva, U. Balgimbayeva U, M. Samy: Reviewing and Editing.

Acknowledgements. This research was funded by the Committee of Science of the Ministry of Science and Higher Education of the Republic of Kazakhstan (Grant No. BR28713471 Development of methods for increasing the extraction of uranium from uranium-containing solutions by effectively reducing the content of silicon compounds).

Cite this article as: Maldybayev G, Gerassyova N, Sharipov R, Zhangabayeva A, El-Sayed Negim, Khambarqyzy A, M. Kylyshkanov, Bekbayeva L, Balgimbayeva U, Moshera Samy. Acid and Thermal Activation of Clay Separated from Kaoline for Uranium Purification. Kompleksnoe Ispolzovanie Mineralnogo Syra = Complex Use of Mineral Resources. 2028; 344(1):5-17. https://doi.org/10.31643/2028/6445.01

Уранды тазарту үшін каолиннен бөлінген саздың қышқылды және термиялық активтенуі

[1] Малдыбаев Ғ., [2]Герасёва Н., [1] Шарипов Р., [1] Жаңабаева Ә., [1]El-Sayed Negim, [1]Хамбарқызы Ә., [1] Қылышқанов М., [3] Бекбаева Л., [1] Балгимбаева У., [4]Moshera Samy

[1] Қазақстан- Британ Техникалық Университеті Алматы, Қазақстан
[2]ЖШС Deep Core Analytics, Алматы, Қазақстан
[3] Әл-Фараби атындағы Қазақ Ұлттық Университеті, Алматы, Қазақстан
[4] Ұлттық зерттеу орталығы, Докки, Гиза, Египет

Мақала келді: *28 ақпан 2026*
Сараптамадан өтті: *18 наурыз 2026*
Қабылданды: 2 *сәуір 2026*

Саз минералдарын әдетте адсорбенттер ретінде пайдаланылады, себебі олар қолжетімді және аумақты меншікті бет ауданында катион алмасу қабілетіне байланысты адсорбент ретінде кеңінен қолданылады, бұл оларды ағынды сулардан ауыр металл иондарын кетіруге жарамды етеді. Бұл зерттеу темір мен магний сияқты қоспалардан уранды тазартуға арналған қоспа алу үшін саздың қышқыл мен және термиялық өңдеу арқылы активтенуін зерттеді. Саз үлгілерінің қышқылдық модификациясы күкірт қышқылымен (15%) 80-90 °C температурада 3 сағат бойы жүргізілді. Сазды термиялық процестің көмегімен активтендіру 600-650 °c температурада 12-24 сағат ішінде жүргізілді. Саздың химиялық құрамын және активацияға дейін және одан кейінгі құрылымдық өзгерістерді талдау үшін рентгендік дифракция, электронды парамагниттік резонанс (ЭПР) және Фурье түрлендіруінің инфрақызыл спектроскопиясы (FTIR) қолданылды.Бос ОН топтары және гидратталған SiO_2 FTIR көмегімен анықталды. ЭПР құрылымдық ақауларымен және оттегінің жетіспеушілігімен байланысты парамагниттік орталықтардың жоғары деңгейін көрсетті, бұл материалдың күшті адсорбциясы мен каталитикалық белсенділігіне ықпал етеді. Қышқылмен өңдеуден кейін саз бөлшектерінің меншікті беткі ауданы 35,2 $м^2$/г-нан 342,5 $м^2$/г-ға дейін кеңейіп айтарлықтай өсуін көрсетті. Сонымен қатар, кеуектердің меншікті көлемі айтарлықтай өсіп, 0,024 $см^3$/г-нан 0,30 $см^3$/г-ға дейін өсті.

Түйінді сөздер: саз, қышқылды активтендіру, термиялық активтендіру, уран.

Авторлар туралы ақпарат:

Ғалымжан Малдыбаев *PhD, қауымдастырылған-профессор, Перспективті Материалдар мен Технологиялар зертханасы, Қазақстан-Британ Техникалық Университеті, 050000, Төле би көшесі, 59, Алматы, Қазақстан. Email: g.maldybaev@kbtu.kz*

Наталья Герасёва *Докторант, ЖШС Deep Core Analytics, 050059, Аль-Фараби даңғылы, 17/1 к5Б, Алматы, Қазақстан. Email: tatoline2001@gmail.com*

Рустам Шарипов *PhD, ассистент-профессор, Перспективті Материалдар мен Технологиялар зертханасы, Қазақстан-Британ Техникалық Университеті, 050000,Төле би көшесі, 59, Алматы, Қазақстан. Email: r.sharipov@kbtu.kz*

Әсем Жаңабаева *Ғылыми қызметкер, Перспективті Материалдар мен Технологиялар зертханасы, Қазақстан-Британ Техникалық Университеті, 050000,Төле би көшесі, 59, Алматы, Қазақстан. Email: a.zhangabayeva@kbtu.kz*

El-Sayed Negim *PhD, Материалтану және жасыл технологиялар мектебінің профессоры, Қазақстан-Британ Техникалық Университеті, 050000, Төле би көшесі, 59, Алматы, Қазақстан. Email: elashmawi5@yahoo.com*

Әйгерім Хамбарқызы *Ғылыми қызметкер, Перспективті Материалдар мен Технологиялар зертханасы, Қазақстан-Британ Техникалық Университеті, 050000,Төле би көшесі, 59, Алматы, Қазақстан. Email: a.khambarkyzy@kbtu.kz*

Манарбек Кылышканов *Физ.-мат. ғ. докторы, Перспективті Материалдар мен Технологиялар зертханасы, Қазақстан-Британ Техникалық Университеті, 050000, Төле би көшесі, 59, Алматы, Қазақстан. Email: kylyshkanov@mail.ru*

Ләззат Бекбаева *PhD, қауымдастырылған-профессор, Ашық Түрдегі Нанотехнологиялық Зертхана, Әл-Фараби атындағы Қаз¥У, 050040, әл-Фараби даңғылы, 71, Алматы, Қазақстан. Email: lyazzat_bk2019@mail.ru*

Улпан Балгимбаева *PhD, Ғылым және инновациялар департаменті, Коммерцияландыру секторы, Қазақстан-Британ Техникалық Университеті, 050000, Төле би көшесі, 59, Алматы, Қазақстан. Email: u.balgimbaeva@kbtu.kz*

Moshera Samy *PhD, Полимерлер мен пигменттер кафедрасы, Ұлттық зерттеу орталығы, Әл-Бухут көшесі, 33, Докки, Гиза, 12622, Египет. Email: moshera_samy1984@yahoo.com; ORCID ID: https://orcid.org/0000-0002-7272-4134*

Кислотная и термическая активация глины, выделенной из каолина, для очистки урана

[1] Малдыбаев Г., [2]Герасёва Н., [1] Шарипов Р., [1] Жанабаева А., [1]El-Sayed Negim, [1]Хамбаркызы А., [1] Кылышканов М., [3] Бекбаева Л., [1] Балгимбаева У., [4]Moshera Samy

[1] Казахстанско-Британский технический университет, Алматы, Казахстан
[2]ТОО Deep Core Analytics, Алматы, Казахстан
[3]Казахский национальный университет им. Аль-Фараби, Алматы, Казахстан
[4]Национальный исследовательский центр, Докки, Гиза, 12622, Египет

Поступила: *28 февраля 2026*
Рецензирование: *18 марта 2026*
Принята в печать: *2 апреля 2026*

АННОТАЦИЯ

Глинистые минералы широко используются в качестве адсорбентов из-за их широкой доступности, большой удельной поверхности и способности к катионообмену, что делает их пригодными для удаления ионов тяжелых металлов из сточных вод. В этом исследовании изучалась активация глины кислотой и термической обработкой с получением добавки для очистки урана от примесей, таких как железо и магний. Кислотную модификацию образцов глины проводили серной кислотой (15%) при температуре 80-90°C в течение 3 часов. В то время как активацию глины термическим способом проводили при температуре 600-650°C в течение 12-24 часов. Для анализа химического состава глины и структурных изменений до и после активации были использованы методы рентгеновской дифракции, электронного парамагнитного резонанса (ЭПР), инфракрасной спектроскопии с преобразованием Фурье (ИК-ФУРЬЕ). С помощью ИК-ФУРЬЕ были определены свободные ОН-группы и гидратированный SiO_2. ЭПР показал высокий уровень парамагнитных центров, связанных со структурными дефектами и кислородными вакансиями, которые способствуют сильной адсорбционной и каталитической активности материала. После кислотной обработки удельная поверхность глинистых частиц заметно увеличилась с 35,2 $м^2$/г до 342,5 $м^2$/г. Кроме того, существенно увеличился удельный объем пор, увеличившись с 0,024 $см^3$/г до 0,30 $см^3$/г.

Ключевые слова: глина, кислотная активация, термическая активация, уран.

Информация об авторах:

Галымжан Малдыбаев — *PhD, Ассоциированный-профессор, Лаборатория перспективных материалов и технологий, Казахстанско-Британский технический университет, 050000, ул. Толе би, 59, Алматы, Казахстан. Email: g.maldybaev@kbtu.kz*

Наталья Герасёва — *Докторант, ТОО Deep Core Analytics, проспект Аль-Фараби, 17/1 к5Б, 050059, Алматы, Казахстан. Email: tatoline2001@gmail.com*

Рустам Шарипов — *PhD, Ассистент-профессор, Лаборатория перспективных материалов и технологий, Казахстанско-Британский технический университет, 050000, ул. Толе би, 59, Алматы, Казахстан. Email: r.sharipov@kbtu.kz*

Асем Жанабаева — *Научный сотрудник, Лаборатория перспективных материалов и технологий, Казахстанско-Британский технический университет, 050000, ул. Толе би, 59, Алматы, Казахстан. Email: a.zhangabayeva@kbtu.kz*

El-Sayed Negim — *PhD, Профессор Школы материаловедения и зеленых технологий, Казахстанско-Британский технический университет, 050000, ул. Толе би, 59, Алматы, Казахстан. Email: elashmawi5@yahoo.com*

Айгерим Хамбаркызы — *Научный сотрудник, Лаборатория перспективных материалов и технологий, Казахстанско-Британский технический университет, 050000, ул. Толе би, 59, Алматы, Казахстан. Email: a.khambarkyzy@kbtu.kz*

Манарбек Кылышканов — *Д.физ.-мат.наук, Лаборатория перспективных материалов и технологий, Казахстанско-Британский технический университет, 050000, ул. Толе би, 59, Алматы, Казахстан. Email: kylyshkanov@mail.ru*

Ляззат Бекбаева — *PhD, Ассоциированный-профессор, Лаборатория нанотехнологии открытого типа, КазНУ им. Аль-Фараби, 050040, проспект Аль-Фараби, 71, Алматы, Казахстан. Email: lyazzat_bk2019@mail.ru*

Улпан Балгимбаева — *PhD, Департамент науки и инноваций, Сектор коммерциализации, Казахстанско-Британский технический университет, 050000, ул. Толе би, 59, Алматы, Казахстан. Email: u.balgimbaeva@kbtu.kz*

Moshera Samy — *PhD, Кафедра полимеров и пигментов, Национальный исследовательский центр, ул. Эль-Бохут, 33, Докки, Гиза, 12622, Египет. Email: moshera_samy1984@yahoo.com; ORCID ID: https://orcid.org/0000-0002-7272-4134*

References

[1] Teng W, Liu S, Zhang X, Zhang F, Yang X, Xu M, Hou J. Reliability Treatment of Silicon in Oilfield Wastewater by Electrocoagulation. Water. 2023; 15:206. https://doi.org/10.3390/w15010206

[2] Kylyshkanov M, Gerassyova N, Sharipov R, Kuanysh A, Maldybayev G, Negim E-S, Baigenzhenov O, Bekbayeva L, Al Azzam K, & Balgimbayeva U. Innovative Adsorbent Materials for Efficient Silicon Extraction from Industrial Waters: A review. Kompleksnoe Ispolzovanie Mineralnogo Syra = Complex Use of Mineral Resources. 2025; 341(2):105–116. https://doi.org/10.31643/2027/6445.22

[3] Wang XJ, Goual L, Colberg PJS. Characterization and treatment of dissolved organic matter from oilfield produced waters. J. Hazard. Mater. 2012; 217:164–170.

[4] Fu F, Wang Q. Removal of heavy metal ions from wastewaters: A review. Journal of Environmental Management. 2011; 92(3):407-418. https://doi.org/10.1016/j.jenvman.2010.11.011

[5] Hubicki Z, Kolodynska D. Selective Removal of Heavy Metal Ions from Waters and Waste Waters Using Ion Exchange Methods. Ion Exch. Technol. 2012, 193-240. https://doi.org/10.5772/51040

[6] Ghosh P, Samanta AN, Ray S. Reduction of COD and removal of Zn2+ from rayon industry wastewater by combined electro-Fenton treatment and chemical precipitation. Desalination. 2011; 266(1-3):213-217. https://doi.org/10.1016/j.desal.2010.08.029

[7] Liu Q, Li Y, Chen H, et al. Superior adsorption capacity of functionalized straw adsorbent for dyes and heavy-metal ions. J. Hazard. Mater. 2020, 382. https://doi.org/10.1016/j.jhaz-mat.2019.121040

[8] Asere TG, Stevens CV, Du Laing G, Use of (modified) natural adsorbents for arsenic remediation: a review. Sci. Total Environ. 2019; 676:706–720. https://doi.org/10.1016/j.scitotenv.2019.04.237

[9] Xu H, Zhu S, Xia M, et al. Rapid and efficient removal of diclofenac sodium from aqueous solution via ternary core-shell CS@ PANI@ LDH composite: experimental and adsorption mechanism study. J. Hazard. Mater. 2021; 402. https://doi.org/10.1016/j.jhazmat.2020.123815 123815

[10] Xu H, Zhu S, Xia M, et al. Three-dimension hierarchical composite via in-situ growth of Zn/Al layered double hydroxide plates onto polyaniline-wrapped carbon sphere for efficient naproxen removal. J. Hazard. Mater. 2022; 423(B). https://doi.org/10.1016/j.jhazmat.2021.127192

[11] Xu Y, Zhang Q, Jiang G, et al. Activated Carbon Loaded with Ti3+ Self-Doped TiO2 Composite Material Prepared by Microwave Method. J. Mater. Eng. Perform. 2022; 31:2810–2822. https://doi.org/10.1007/s11665-021-06421-9

[12] Khan Z H, Gao M, Qiu W, et al. Mechanisms for cadmium adsorption by magnetic biochar composites in an aqueous solution. Chemosphere. 2020; 246. https://doi.org/10.1016/j.chemosphere.2019.125701125701.

[13] Khan A, Naeem A, Mahmood T, et al. Mechanistic study on methyl orange and congo red adsorption onto polyvinyl pyrrolidone modified magnesium oxide. Int. J. Environ. Sci. Technol. 2022; 19(4):2515–2528. https://doi.org/10.1007/s13762-021-03308-z

[14] Barakat M A. New trends in removing heavy metals from industrial wastewater. Arabian Journal of Chemistry. 2011;4(4):361-377.

[15] Guillaume Hopsort, Quentin Cacciuttolo, David Pasquier. Electrodialysis as a key operating unit in chemical processes: From lab to pilot scale of latest breakthroughs. Chemical Engineering Journal. 2024; 494:153111.

[16] Gmar S, Chagnes A, Lutin F, Muhr L. Application of Electrodialysis for the Selective Lithium Extraction Towards Cobalt, Nickel and Manganese from Leach Solutions Containing High Divalent Cations/li Ratio, Recycling. 2022; 7(2). https://doi.org/10.3390/recycling7020014

[17] Zimmermann P, Tekinalp O, Deng L, Wilhelmsen Ø, Burheim O S. Electrodialysis for Removal of Impurities in Silver Electrowinning, Meet. Abstr. 2023; MA2023-01:1608. https://doi.org/10.1149/ma2023-01241608mtgabs

[18] Kumar Y, Khalangre A, Suhag R, Cassano A. Applications of Reverse Osmosis and Nanofiltration Membrane Process in the Wine and Beer Industry. Membranes. 2025; 15:140.https://doi.org/10.3390/membranes15050140

[19] Charcosset C. Ultrafiltration, Microfiltration, Nanofiltration and Reverse Osmosis in Integrated Membrane Processes. In Integrated Membrane Systems and Processes; Basile A, Charcosset C, Eds. Wiley: Hoboken, NJ, USA. 2016, 1–22. ISBN 978-1-118-73908-2.

[20] Pati S, La Notte D, Clodoveo M L, Cicco G, Esti M. Reverse Osmosis and Nanofiltration Membranes for the Improvement of Must Quality. Eur. Food Res. Technol. 2014; 239:595–602.

[21] Poonguzhali E, Fathima Aadilah Mohamed Ali, Ashish Kapoor, Prabhakar S. Performance of membrane assisted solvent extraction with homologous solvents for the removal and recovery of phenol, Desalination and Water Treatment. 2022; 251:64-78. https://doi.org/10.5004/dwt.2022.28117

[22] Poonguzhali E, Ashish Kapoor, Prabhakar S. Membrane assisted process intensification and optimization for removal and recovery of phenol from industrial effluents, Separation and Purification Technology. 2023; 319:124026. https://doi.org/10.1016/j.seppur.2023.124026

[23] Sanika Bhokarikar, Poojitha P, Vijay Vaishampayan, Adithya Sridhar, Gurumoorthi P, Ashish Kapoor. Chapter Thirteen - Parameters affecting the efficiency of extraction systems in the food industries, Editor(s): Seid Mahdi Jafari, Sahar Akhavan-Mahdavi, In Unit Operation and Processing Equipment in the Food Industry, Extraction Processes in the Food Industry, Woodhead Publishing. 2024, 397-434. https://doi.org/10.1016/B978-0-12-819516-1.00010-7

[24] Ming Li, Chuanying Liu, Anting Ding, Chengliang Xiao, A review on the extraction and recovery of critical metals using molten salt electrolysis, Journal of Environmental Chemical Engineering. 2023; 11(3):109746. https://doi.org/10.1016/j.jece.2023.109746

[25] Yin T, Chen L, Xue Y, Zheng Y, Wang X, Yan Y, Zhang M, Wang G, Gao F, Qiu M. Electrochemical behavior and underpotential deposition of Sm on reactive electrodes (Al, Ni, Cu and Zn) in a LiCl-KCl melt, Int J. Min. Met. Mater. 2020; 27(12):1657–1665.

[26] Sun X, Chen Y, Liang L, Xie G, Peng Y. Research on Hydrocyclone Separation of Palygorskite Clay. Minerals. 2023; 13:1264. https://doi.org/10.3390/min13101264

[27] Baoyu Cui, Caie Zhang, Dezhou Wei, Shuaishuai Lu, Yuqing Feng. Effects of feed size distribution on separation performance of hydrocyclones with different vortex finder diameters, Powder Technology. 2017; 322:114-123. https://doi.org/10.1016/j.powtec.2017.09.010

[28] Aurélien Davailles, Eric Climent, Florent Bourgeois, Fundamental understanding of swirling flow pattern in hydrocyclones, Separation and Purification Technology. 2012; 92:152-160. https://doi.org/10.1016/j.seppur.2011.12.011

[29] Ghodrat M, Kuang SB, Yu AB, Vince A, Barnett GD, Barnett PJ. Numerical analysis of hydrocyclones with different conical section designs, Minerals Engineering. 2014; 62:74-84. https://doi.org/10.1016/j.mineng.2013.12.003

[30] Eldin Wee Chuan Lim, Yi-Ren Chen, Chi-Hwa Wang, Rome-Ming Wu. Experimental and computational studies of multiphase hydrodynamics in a hydrocyclone separator system, Chemical Engineering Science. 2010; 65(24):6415-6424. https://doi.org/10.1016/j.ces.2010.09.029

[31] Yin T, Xue Y, Yan Y, Ma Z, Ma F, Zhang M, Wang G, Qiu M. Recovery and separation of rare earth elements by molten salt electrolysis, Int J. Min. Met. Mater. 2021; 28(6):899–914.

[32] Irannajad M, Kamran Haghighi H. Removal of heavy metals from polluted solutions by zeolitic adsorbents: a review. Environmental Processes. 2021; 8:7-35. https://doi.org/10.1007/s40710-020-00476-x

[33] Bandura L, et al. Synthesis of zeolite-carbon composites using high-carbon fly ash and their ad-sorption abilities towards petroleum substances. Fuel. 2021; 283:119173. https://doi.org/10.1016/j.fuel.2020.119173

Crossref
DOI: 10.31643/2028/6445.02
Mining & Mineral Processing

Purification of metallic ions from technological solutions before sorption recovery of rhenium under JSC Almalyk MMC

[1]Azizova Kh.M., [2]Usmankulov O.N., [3]Kattaev N.T., [4]Kadirova Z.Ch., [5*]Yakubov M.M., [3]Akbarov Kh.I.

[1]Almalyk State Technical Institute, Almalyk, Uzbekistan
[2]Ministry of Mining Industry and Geology of the Republic of Uzbekistan, Tashkent, Uzbekistan
[3] National University of Uzbekistan named after Mirzo Ulugbek, Tashkent, Uzbekistan
[4] Uzbek-Japan Innovation Center of Youth, Tashkent, Uzbekistan
[5] National University of Science and Technology MISiS, Almalyk Branch, Uzbekistan

** Corresponding author email: yakubovmahmud51@gmail.com*

Received: *January 21, 2026*
Peer-reviewed: *February 27, 2026*
Accepted: *April 08, 2026*

ABSTRACT

In this article, rhenium's distinct physicochemical characteristics, which make it essential for petrochemistry, electrical technology, rocket and aviation engineering, and the manufacturing of catalysts and high-precision tools, account for the metal's rising demand. The main source of rhenium at JSC "Almalyk MMC" is the off-gases produced when molybdenum concentrates are roasted, where rhenium is mostly found as Re_2O_7. High selectivity and overall efficiency are ensured by optimizing the process parameters at each of the multiple subsequent technical phases involved in rhenium recovery. Perrhenate sorption is less efficient when organic molecules and Mn^{2+} and Cu^{2+} ions are present in the process fluids. Oxidative-precipitation techniques were used for the first purification: Mn ions were oxidized and precipitated using potassium permanganate, and Cu^{2}+ ions were selectively precipitated using an ammonium sulfide solution $(NH_4)_2S$. ICP-OES was used to assess the composition of the solutions, while SEM and EDS were used to examine the roasting gas-dust products. Using contemporary analytical methods, a thorough investigation of the relevant phases of selective purification was conducted for the first time at JSC "Almalyk MMC." It was shown that treating the solutions with KMnO4 and $(NH_4)_2S$ efficiently eliminates interfering elements without causing rhenium or molybdenum losses, thereby creating ideal conditions for the sorption of perrhenate ions later on. Manganese and copper concentrations dropped from 1.44 to 0.0039 and 2.68 to 0.0036 g/l, respectively, demonstrating the great purification process efficiency. Rhenium and molybdenum concentrations did not alter during these phases, suggesting that they were fully preserved.

Keywords: sorption, ICP-OES, SEM, EDS, oxidative-precipitation treatment, molybdenum, rhenium, and selective purification

Information about authors:

Azizova Kholida Mumin kizi — *PhD in Chemistry, Associate Professor in Almalyk State Technical Institute; Doctoral Student (DSc) in National University of Uzbekistan named after Mirzo Ulugbek, Tashkent, Uzbekistan. E-mail: azizovakholida@gmail.com; ORCID ID: https://orcid.org/0000-0003-4406-5941*

Usmankulov Orif Naziraliyevich — *PhD in Technical Sciences, Chief Specialist in the Ministry of Mining Industry and Geology of the Republic of Uzbekistan, Tashkent. E-mail: usmankulovorifjon@gmail.com; ORCID ID: https://orcid.org/0009-0003-8516-5065*

Kattaev Nuritdin Turayevich. — *Doctor of Chemical Sciences, Professor at the National University of Uzbekistan named after Mirzo Ulugbek, Tashkent. E-mail: ntkattaev@gmail.com; ORCID ID: https://orcid.org/0000-0002-0276-2717*

Kadirova Zukhra Chingizovna — *Doctor of Chemical Sciences, Professor in the Uzbek-Japan Innovation Center of Youth, Tashkent. E-mail: zuhra_kadirova@yahoo.com; https://orcid.org/0000-0002-2112-1886*

Yakubov Mahmud Mahamadjanovich — *Doctor of Technical Sciences, Professor at the National Research Technological University MISIS in Almalyk. E-mail: yakubovmahmud51@gmail.com; ORCID ID: https://orcid.org/0009-0008-8688-7066*

Akbarov Khamdam Ikramovich — *Doctor of Chemical Sciences, Professor at the National University of Uzbekistan named after Mirzo Ulugbek, Tashkent. E-mail: akbarov_kh@rambler.ru; ORCID ID: https://orcid.org/0000-0002-3225-2427*

Introduction

The unique physicochemical properties and high thermal stability of rhenium determine its wide application in rocket engineering, aviation, electrical engineering, petrochemistry, and in the production of catalysts and precision tools [[1], [2], [3], [4], [5]]. The primary industrial source of rhenium is the off-gases generated during the roasting of sulfide copper–molybdenum

concentrates (MoS_2), in which rhenium is predominantly present in the form of Re_2O_7 [[6], [7], [8], [9], [10], [11]]. Industrial recovery of rhenium involves several sequential technological stages, each requiring careful optimization of process parameters to ensure high selectivity and economic efficiency [[12], [13], [14], [15], [16]].

At JSC "Almalyk MMC," copper–molybdenum ores are processed by flotation [[17], [18], [19], [20]], producing sulfide copper and molybdenum concentrates. The initial processing stage includes oxidative roasting of molybdenum sulfide concentrates in electric tubular rotary furnaces at temperatures of 600–650 °C to convert sulfides before the subsequent leaching stage [21]. During roasting, molybdenum disulfide is oxidized to molybdenum trioxide according to the reaction:

$MoS_2 + 3.5O_2 \rightarrow MoO_3 + 2SO_2$

Simultaneously, rhenium sulfides are oxidized to volatile rhenium oxides, predominantly Re_2O_7:

$Re_2S_7 + 10.5O_2 \rightarrow Re_2O_7 + 7SO_2$

The off-gases generated during roasting contain sulfur dioxide and other volatile components, as well as minor amounts of sublimated oxides of rhenium and molybdenum [[22], [23]].

These gases undergo multi-stage purification using dry dust-collection systems followed by wet scrubbing units before being directed to sulfuric acid production [24]. As a result, acidic technological solutions enriched with rhenium are formed [[25], [26], [27], [28]]. During wet gas cleaning, dust particles are transferred into the scrubber slurry (cake), which is subsequently collected and stored as technogenic waste. However, the high acidity, complex chemical composition, and unfavorable physicochemical characteristics of this material, including high moisture content and poor filterability, complicate its comprehensive processing and limit its economic utilization.

Acidic scrubber solutions typically contain a range of impurity ions that may interfere with downstream hydrometallurgical processes. In particular, the presence of transition metals such as manganese, copper, and iron can influence solution chemistry, promote competing reactions, and reduce the efficiency of subsequent recovery stages. Therefore, preliminary purification represents an important step in preparing technological solutions for further processing.

Oxidative–precipitation methods are widely used in hydrometallurgy for the removal of interfering components due to their operational simplicity, technological reliability, and compatibility with strongly acidic media. Their application to complex technogenic solutions requires careful evaluation of purification efficiency and the behavior of valuable components during treatment.

This study aims to evaluate the effectiveness of oxidative precipitation purification for the targeted removal of interfering ions from acidic scrubber solutions before downstream recovery processes under the conditions of JSC "Almalyk MMC."

This study presents one of the first systematic assessments of oxidative precipitation purification performed under highly acidic industrial conditions (~300 g/L H_2SO_4), where the behavior of impurity ions differs substantially from that observed in conventional laboratory systems.

Selection and Characterization of Research Objects

Before the experimental work, the compositions of process gases, dust, and technological solutions formed during the roasting of molybdenum concentrates were analyzed to identify the primary sources of rhenium and associated impurity elements. Particular attention was given to the molybdenum-containing cake generated at the wet gas-cleaning stage, since its interaction with the scrubbing medium leads to the formation of acidic solutions subsequently subjected to purification.

The chemical composition of the molybdenum-containing cake is presented in Table 1. The analytical results indicate that the cake contains not only molybdenum and rhenium but also significant amounts of silicon, iron, copper, and other elements that may transfer into the liquid phase during wet gas treatment.

Table 1 - Chemical composition of molybdenum cake, %

Product (%)	Mo	Re	SiO_2	Fe	Cu	Zn	Au (g/t)	Ag (g/t)
Cake 1	41.1	0.025	26.14	4.92	0.01	1.7	17.6	48.76
Cake 2	39.8	0.08	24.1	4.06	0.02	1.5	18.2	42.00

The composition of gases and entrained dust produced during the roasting of molybdenum concentrate was also examined to better understand the origin of both valuable components and impurity ions in the scrubber solutions. Figure 1 shows a scanning electron microscope image of wet molybdenum dust, confirming the presence of fine particles capable of entering the scrubbing system and influencing the chemical composition of the resulting technological solutions.

Materials and Methods

Scrubber solutions collected from the industrial wet gas-cleaning system during the roasting of molybdenum concentrates at JSC “Almalyk MMC” were used as the primary research material. Prior to the experiments, the solutions were filtered through paper filters to remove suspended solids.

The technological solutions were characterized by a high sulfuric acid concentration (up to approximately 300 g/L), ensuring strongly acidic conditions throughout the experiments. The volumes of reagents used during purification were insufficient to cause significant dilution or neutralization; therefore, the solution remained strongly acidic during all treatment stages.

Purification Procedure

Selective purification was carried out in two sequential stages.

At the first stage, the pre-filtered solution was heated to 92 °C and treated with a 0.5 M potassium permanganate ($KMnO_4$) solution. The mixture was stirred using an electric mechanical stirrer at a speed of 200 rpm for 40 minutes to promote oxidation and precipitation of interfering ions. After completion of the reaction, the solution was cooled to room temperature and filtered to remove the formed precipitate.

At the second stage, the filtrate was treated with a 0.1 M ammonium sulfide ($(NH_4)_2S$) solution and stirred at 200 rpm for 20 minutes to facilitate the precipitation of copper ions. The resulting light-colored suspension was separated by paper filtration, yielding a clarified solution suitable for subsequent sorption processes.

Owing to the high initial sulfuric acid concentration (~300 g/L), the reagent volumes did not cause significant dilution or neutralization, and the solution remained strongly acidic throughout the purification process.

The purification procedure was repeated five times under identical conditions, and the reported results represent averaged values.

Analytical Methods

The morphology and elemental composition of solid particles were examined using scanning electron microscopy (SEM) coupled with energy-dispersive spectroscopy (EDS).

The chemical composition of the technological solutions before and after purification was determined by inductively coupled plasma optical emission spectrometry (ICP-OES).

Results

The analysis of off-gases and dust generated during molybdenum concentrate roasting confirmed their role as the primary source of rhenium and associated impurity elements entering the scrubber solutions (Table 2, Fig. 1).

Table 2 - Composition and characteristics of off-gases and dust generated during molybdenum concentrate roasting

Parameters of off-gases	Value	Unit
Oxygen flow rate V_0	565,8	m^3/h
Gas temperature T_r	140	°C
Dust loading z	3500	g/m^3
Dust particle size d, µm:	<5	20%
	5-10	22%
	10-20	24%
	20-40	16%

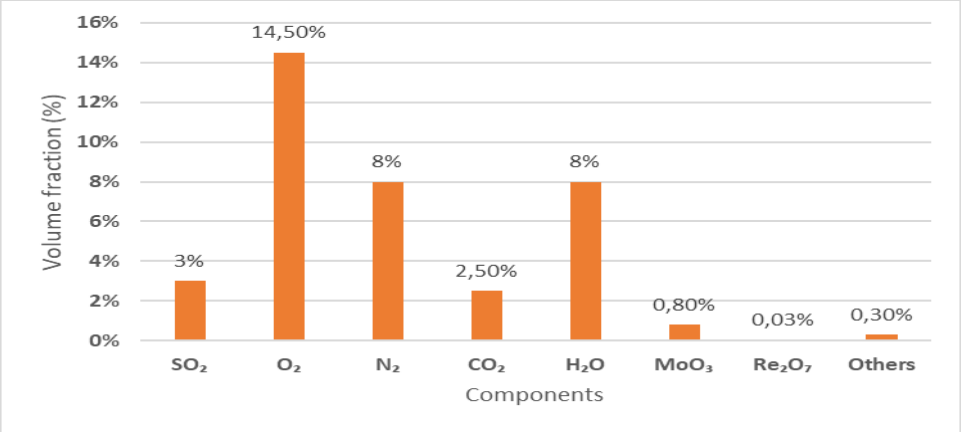

Fig. 1 - Composition of off-gases and dust contributing to the formation of scrubber solutions

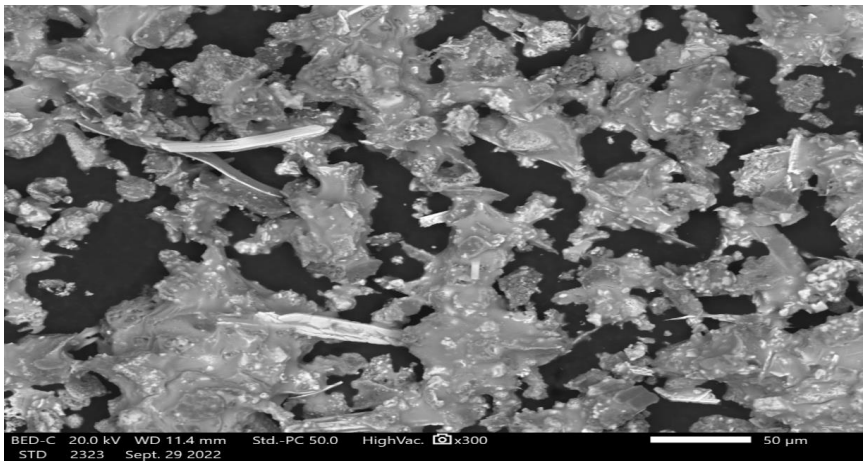

Fig. 2 - SEM image of wet molybdenum dust particles.

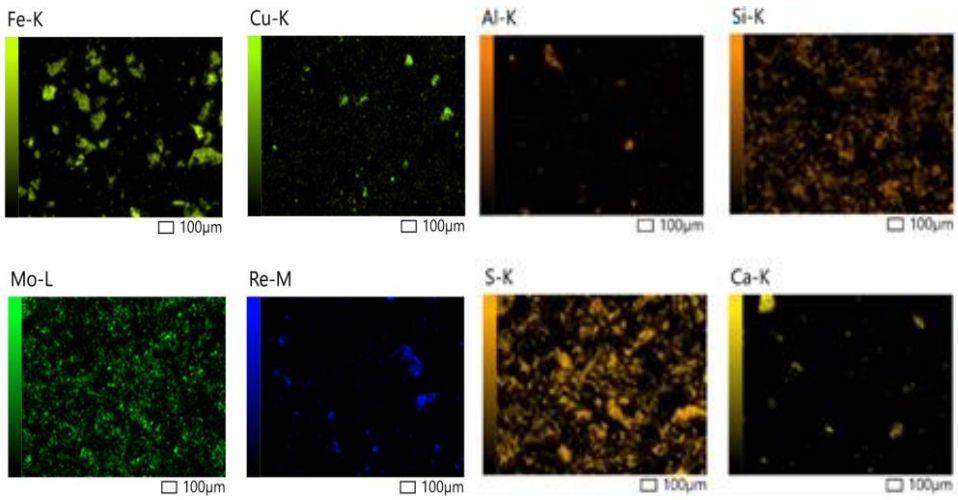

Fig. 3 - SEM images and EDS spectra of dust particles formed during molybdenum concentrate roasting.

SEM-EDS analysis revealed the presence of fine dust particles generated during the roasting of molybdenum concentrate. The particles exhibited heterogeneous morphology, indicating the entrainment of oxide phases from the high-temperature zone. Elemental spectra indicated the presence of Mo, S, O, Si, Fe, and trace amounts of rhenium, suggesting the transport of oxidized rhenium species into the dust phase. These observations support the role of roasting dust as a carrier of rhenium into the gas-cleaning system. These observations are consistent with the transfer of volatile rhenium species into the gas-cleaning system during concentrate roasting.

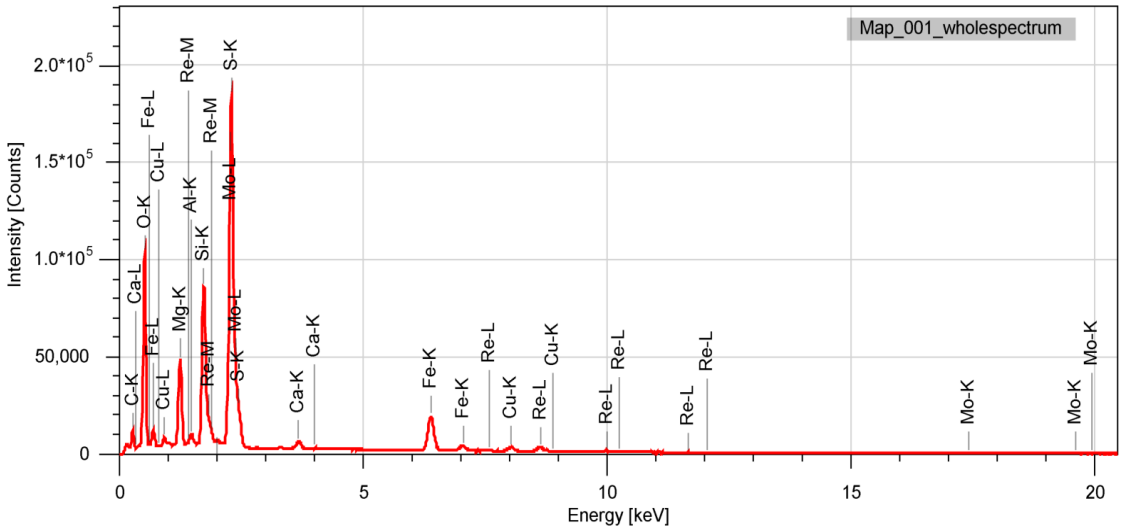

Fig. 4 - EDS spectra indicating the elemental composition of roasting dust particles.

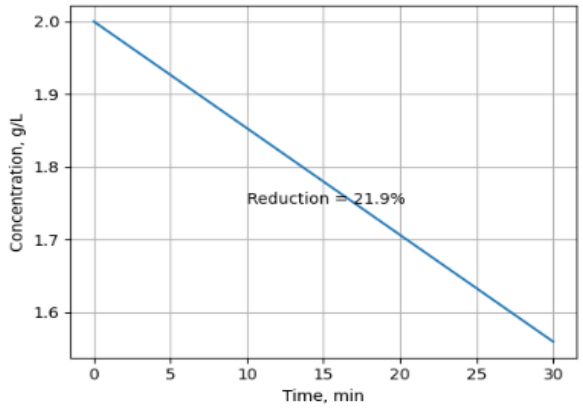

Fig. 5 - Changes in Fe^{3+} ion concentration during $KMnO_4$ treatment.

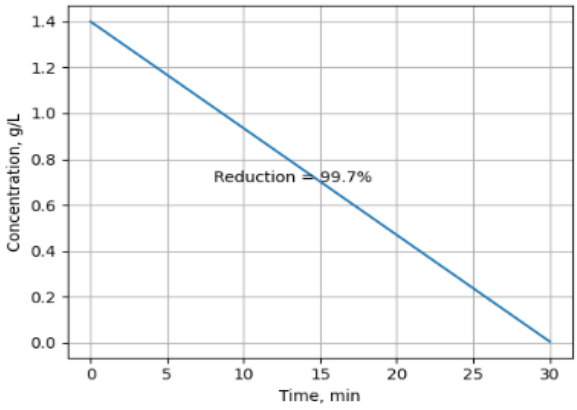

Fig. 6 - Changes in Mn^{2+} ion concentration during $KMnO_4$ treatment.

The presence of competing ions in strongly acidic technological solutions may negatively affect downstream recovery processes by occupying active sites of anion-exchange sorbents. Therefore, the removal or reduction of such components' during pretreatment is considered an important step in preparing solutions for further processing.

Scrubber solution samples were subjected to a two-stage oxidative–precipitation purification. Treatment with potassium permanganate resulted in the oxidation of Fe^{2+} to Fe^{3+}, while Mn^{2+} was converted into insoluble MnO_2, forming a colloidal precipitate that was subsequently removed by filtration. As a result, 21.9% of iron and 99.7% of manganese were removed (Figs. 5 and 6). The oxidation and precipitation processes can be described by the following reactions:

$$5Fe^{2+} + MnO_4^- + 8H^+ \rightarrow 5Fe^{3+} + Mn^{2+} + 4H_2O$$

$$3Mn^{2+} + 2MnO_4^- + 2H_2O \rightarrow 5MnO_2\downarrow + 4H^+$$

The limited removal of iron is attributed to the high stability of Fe^{3+} sulfate complexes in strongly acidic media, where iron predominantly remains in soluble form.

Equilibrium modeling was performed using Visual MINTEQ 3.1 to evaluate the speciation behavior of iron and manganese in strongly acidic sulfate media. The initial concentrations of the technological solution constituents (Table 4), together with the sulfuric acid concentration and temperature (25 °C), were used as input parameters. Modeling results (Fig. 7) indicate that under strongly acidic conditions, Fe^{3+} predominantly exists as soluble sulfate complexes ($FeSO_4^+$ and $Fe(SO_4)_2^-$), whereas Mn^{2+} is mainly stabilized as $MnSO_4$(aq). Under oxidizing conditions, manganese forms insoluble MnO_2, explaining the high degree of manganese removal observed experimentally.

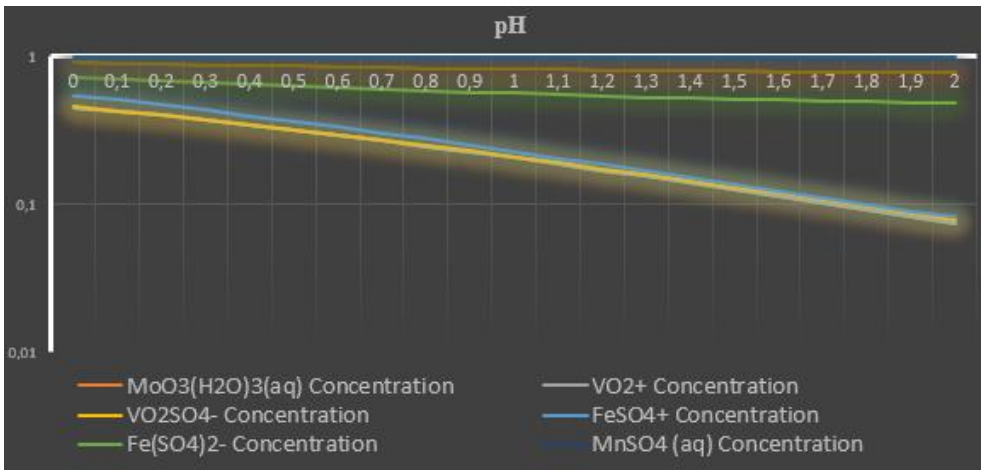

Fig. 7 - Distribution of iron and manganese species as a function of pH (0–2), calculated using Visual MINTEQ.

Table 4 - Elemental composition determined by ICP-OES (Thermo Scientific iCAP Pro)

Element	Initial solution (g/L)	Purified solution (g/L)
Nickel (Ni)	0.004	0.004
Iron (Fe)	2.01	1.57
Manganese (Mn)	1.44	0.0039
Rhenium (Re)	0.51	0.51
Molybdenum (Mo)	15.85	16.19
Vanadium (V)	0.019	0.019
Copper (Cu)	2.68	0.0036

At the second purification stage, treatment with ammonium sulfide precipitated Cu^{2+} ions as CuS, achieving a copper removal efficiency of approximately 95–100%, as confirmed by ICP-OES analysis and supported by equilibrium modeling.

The elemental composition of the initial and purified solutions was determined using ICP-OES (Thermo Scientific iCAP Pro, USA), and the results are presented in Table 4.

The results presented in Table 4 demonstrate a substantial reduction in the concentrations of major impurity ions following purification, particularly manganese and copper. Manganese concentration decreased from 1.44 g/L to 0.0039 g/L, while copper was reduced from 2.68 g/L to 0.0036 g/L, confirming the high efficiency of the oxidative–precipitation process.

The concentrations of rhenium and molybdenum remained essentially unchanged, indicating the absence of valuable metal losses during treatment. The slight increase in molybdenum concentration is within the analytical uncertainty of the ICP-OES method and does not indicate actual enrichment.

These findings confirm the effectiveness of oxidative precipitation treatment for removing interfering components from strongly acidic technological solutions while preserving valuable metals in the liquid phase.

Conclusion

Technological solutions obtained during the processing of molybdenum concentrates at JSC “Almalyk MMC” require preliminary purification to remove interfering components prior to downstream recovery stages. The results of this study demonstrate that oxidative precipitation treatment using potassium permanganate and ammonium sulfide effectively reduces the concentrations of major impurity ions, particularly copper and manganese. Copper concentration decreased from 2.68 g/L to 0.0036 g/L, while manganese was reduced from 1.44 g/L to 0.0039 g/L.

SEM-EDS analysis confirmed the presence of oxidized rhenium species and molybdenum-containing phases in the dust particles formed during concentrate roasting. The purification process did not result in detectable losses of rhenium and preserved valuable metals in the liquid phase.

These findings indicate that oxidative precipitation treatment represents an effective and technologically applicable approach for improving the chemical composition of strongly acidic process solutions by removing interfering ions while maintaining the stability of valuable components.

Conflict of interest. On behalf of all the authors, the corresponding author declares that there is no conflict of interest.

CRediT author statement: **Kh. Azizova:** conceptualization, designed the experimental methodology, writing – original draft; **O. Usmankulov:** writing -review and editing; **N. Kattaev:** writing -review and editing, literature review; **Z. Kadirova:** methodology and editing; **M. Yakubov:** writing – review and editing, supervision, methodology; **Kh. Akbarov:** writing - review and editing, data curation.

Cite this article as: Azizova KhM, Usmankulov ON, Kattaev NT, Kadirova ZCh, Yakubov MM, Akbarov KhI. Purification of metallic ions from technological solutions before sorption recovery of rhenium under JSC Almalyk MMC. Kompleksnoe Ispolzovanie Mineralnogo Syra = Complex Use of Mineral Resources. 2028; 344(1):18-27. https://doi.org/10.31643/2028/6445.02

Алмалық ТКМК АҚ жағдайында ренийді сорбциялық жолмен бөліп алу алдында технологиялық ерітінділерді металл иондарынан тазарту

[1]Азизова Х.М., [2]Усманқұлов О.Н., [3]Қаттаев Н.Т., [4]Қадырова З.Ш., [5]Якубов М.М., [3]Акбаров Х.И.

[1] Алмалық мемлекеттік техникалық институты, Алмалық, Өзбекстан
[2] Өзбекстан Республикасы Тау-кен өнеркәсібі және геология министрлігі, Ташкент, Өзбекстан
[3] Мирзо Ұлықбек атындағы Өзбекстан Ұлттық университеті, Ташкент, Өзбекстан
[4] Өзбек-Жапон жастар инновациялық орталығы, Ташкент, Өзбекстан
[5] Ұлттық ғылым және технологиялар университеті MISiS, Алмалық филиалы, Өзбекстан

Мақала келді: *21 қаңтар 2026*
Сараптамадан өтті: *27 ақпан 2026*
Қабылданды: *08 сәуір 2026*

АННОТАЦИЯ

Бұл мақалада ренийдің ерекше физикалық және химиялық қасиеттерін қарастырып, мұнай-химиясы, электр техникасы, зымыран және авиация техникасында, сондай-ақ катализаторлар мен жоғары дәлдіктегі құралдар өндірісі үшін аса маңызды ететін ерекше физика-химиялық қасиеттеріне байланысты осы металға деген сұраныстың артып келе жатқаны қарастырылады.«Алмалық ТКМК» АҚ -да ренийдің негізгі көзі молибден концентраттарын күйдіру кезінде түзілетін түтін газдар болып табылады, мұнда рений негізінен Re_2O_7 түрінде болады. Ренийді бөліп алу бірнеше техникалық кезеңдерден тұратындықтан, процестің әрбір сатысындағы параметрлерді оңтайландыру арқылы жоғары селективтілік пен жалпы тиімділікке қол жеткізіледі. Технологиялық ерітінділерде органикалық молекулалар мен Mn^{2+} және Cu^{2+} иондары болған кезде перренат сорбциясының тиімділігі төмен болады. Алғашқы тазарту үшін тотығу-тұндыру әдістері қолданылды: Mn иондары калий перманганатының көмегімен тотықтырылып тұндырылды, ал Cu^{2+} иондары аммоний сульфиді $(NH_4)_2S$ ерітіндісін пайдаланып селективті түрде тұндыру жүргізілді. Ерітінділердің құрамын бағалау үшін ICP-OES әдісі, ал күйдіру кезіндегі газ-тозаң өнімдерін зерттеу үшін SEM және EDS әдістері пайдаланылды. Заманауи аналитикалық әдістерді қолдана отырып, «Алмалық ТКМК» АҚ жағдайында селективті тазартудың тиісті кезеңдеріне алғаш рет жан-жақты зерттеу жүргізілді. Ерітінділерді $KMnO_4$ және $(NH_4)_2S$ реагенттерімен өңдеу рений мен молибденнің шығынынсыз кедергі келтіретін қоспаларды тиімді түрде жоятындығы, соның нәтижесінде кейінгі перренат иондарының сорбциясы үшін оңтайлы жағдайлар жасалатыны көрсетілді. Марганец пен мыс концентрациясы сәйкесінше 1,44-тен 0,0039 г/л-ға дейін және 2,68-ден 0,0036 г/л-ге дейін төмендеді, бұл тазарту процесінің жоғары тиімділігін дәлелдейді. Бұл фазаларда рений мен молибден концентрациясы өзген жоқ, бұл олардың толық сақталғанын көрсетеді.

Түйін сөздер: *сорбция, ICP-OES, SEM, EDS, тотығу-тұндыру арқылы өңдеу, молибден, рений, селективті тазарту.*

Азизова Холида Мумин қызы

Авторлар туралы мәлімет:
Химия ғылымдарының PhD докторы, Алмалық мемлекеттік техникалық институтының қауымдастырылған профессоры, Мирзо Ұлықбек атындағы Өзбекстан

	Ұлттық университетінің докторанты (DSc), Ташкент, Өзбекстан. E-mail: azizovakholida@gmail.com; ORCID ID: https://orcid.org/0000-0003-4406-5941
Усманқулов Ориф Назиралиевич	*Техника ғылымдарының PhD докторы, Өзбекстан Республикасы Тау-кен өнеркәсібі және геология министрлігінің бас маманы, Ташкент, Өзбекстан. E-mail: usmankulovorifjon@gmail.com; ORCID ID: https://orcid.org/0009-0003-8516-5065*
Қаттаев Нуритдин Тўраевич	*Химия ғылымдарының докторы, профессор, Мирзо Ұлықбек атындағы Өзбекстан Ұлттық университеті, Ташкент, Өзбекстан. E-mail: ntkattaev@gmail.com; ORCID ID: https://orcid.org/0000-0002-0276-2717*
Қадырова Зухра Шыңғысқызы	*Химия ғылымдарының докторы, профессор, Өзбек-Жапон жастар инновациялық орталығы, Ташкент, Өзбекстан. E-mail: zuhra_kadirova@yahoo.com; ORCID ID: https://orcid.org/0000-0002-2112-1886*
Якубов Махмуд Махамаджанұлы	*Техника ғылымдарының докторы, профессор, Ұлттық зерттеу технологиялық университеті MISIS-тің Алмалық қаласындағы филиалы, Өзбекстан. E-mail: yakubovmahmud51@gmail.com; ORCID ID: https://orcid.org/0009-0008-8688-7066*
Акбаров Хамдам Икрамұлы	*Химия ғылымдарының докторы, профессор, Мирзо Ұлықбек атындағы Өзбекстан Ұлттық университеті, Ташкент, Өзбекстан. E-mail: akbarov_kh@rambler.ru; ORCID ID: https://orcid.org/0000-0002-3225-2427*

Очистка технологических растворов от ионов металлов перед сорбционным извлечением рения в АО Алмалыкский ГМК

[1]Азизова Х.М., [2]Усманкулов О.Н., [3]Каттаев Н.Т., [4]Кадирова З.Ч., [5]Якубов М.М., [3]Акбаров Х.И.

[1]Алмалыкский государственный технический институт, Алмалык, Узбекистан
[2]Министерство горной промышленности и геологии Республики Узбекистан, Ташкент, Узбекистан
[3] Национальный университет Узбекистана имени Мирзо Улугбека, Ташкент, Узбекистан
[4]Узбекско-Японский молодежный центр инноваций, Ташкент, Узбекистан
[5] Национальный исследовательский технологический университет МИСИС, Алмалык, Узбекистан

Поступила: *21 января 2026*
Рецензирование: *27 февраля 2026*
Принята в печать: *08 апреля 2026*

АННОТАЦИЯ

В этой статье рассматриваются особые физико-химические характеристики рения, которые делают его незаменимым для нефтехимии, электротехники, ракетной и авиационной техники, а также для производства катализаторов и высокоточных инструментов, что объясняет растущий спрос на этот металл. Основным источником рения на АО "Алмалыкский ГМК" являются отходящие газы, образующиеся при обжиге молибденовых концентратов, где рений в основном содержится в виде Re_2O_7. Высокая селективность и общая эффективность обеспечиваются за счет оптимизации параметров процесса на каждом из множества последующих технических этапов, связанных с извлечением рения. Сорбция перрената менее эффективна, когда в технологических жидкостях присутствуют органические молекулы и ионы Mn^{2+} и Cu^{2+}. Для первой очистки были использованы методы окислительного осаждения: ионы марганца были окислены и осаждены с использованием перманганата калия, а ионы Cu^{2+} были выборочно осаждены с использованием раствора сульфида аммония $(NH_4)_2S$. ICP-OES использовали для оценки состава растворов, в то время как SEM и EDS использовались для изучения состава растворов. обжиг газопылевых продуктов. Впервые в условиях АО "Алмалыкский ГМК" с использованием современных аналитических методов было проведено тщательное исследование применимых стадий селективной очистки. Было показано, что обработка растворов $KMnO_4$ и $(NH_4)_2S$ эффективно устраняет мешающие элементы, не вызывая потерь рения и молибдена, что обеспечивает идеальные условия для последующей сорбции перренат-ионов. Концентрации марганца и меди снизились с 1,44 до 0,0039 и с 2,68 до 0,0036 г/л соответственно, что свидетельствует о высокой эффективности процесса очистки. Концентрации рения и молибдена не изменялись в течение этих фаз, что позволяет предположить, что они полностью сохранились.

Ключевые слова: сорбция, ICP-OES, SEM, EDS, окислительно-восстановительная обработка, молибден, рений и селективная очистка

Азизова Холида Мумин кизи	***Информация об авторах:*** *Кандидат химических наук, доцент Алмалыкского государственного технического института, Алмалыкский докторант Национального университета Узбекистана имени Мирзо Улугбека, Ташкент. azizovakholida@gmail.com; ORCID ID: https://orcid.org/0000-0003-4406-5941*
Усманкулов Ориф Назиралиевич	*Кандидат технических наук, главный специалист Министерства горной промышленности и геологии Республики Узбекистан, Ташкент. E-mail: usmankulovorifjon@gmail.com; ORCID ID: https://orcid.org/0009-0003-8516-5065*
Каттаев Нуритдин Тураевич.	*Доктор химических наук, профессор Национального университета Узбекистана имени Мирзо Улугбека, Ташкент. E-mail: ntkattaev@gmail.com; ORCID ID: https://orcid.org/0000-0002-0276-2717*

Кадирова Зухра Чингизовна	*Доктор химических наук, профессор, заместитель директора по науке Узбекско-Японский молодежный центр инноваций, Ташкент. E-mail: zuhra_kadirova@yahoo.com; ORCID ID: https://orcid.org/0000-0002-2112-1886*
Якубов Махмуджон Махамаджанович	*Доктор технических наук, профессор Национального исследовательского технологического университета "МИСиС" в Алмалыке. E-mail: yakubovmahmud51@gmail.com; ORCID ID: https://orcid.org/0009-0008-8688-7066*
Акбаров Хамдам Икрамович	*Доктор химических наук, профессор Национального университета Узбекистана имени Мирзо Улугбека, Ташкент. E-mail: akbarov_kh@rambler.ru; ORCID ID: https://orcid.org/0000-0002-3225-2427*

References

[1] Dobrzańska-Danikiewicz A D, & Wolany W. A rhenium review–from discovery to novel applications. Archives of Materials Science and Engineering. 2016; 82(2):70-78. https://doi.org/10.5604/01.3001.0009.7106

[2] Yagi R, & Okabe T H. Rhenium and its smelting and recycling technologies. International Materials Reviews. 2024; 69(2):142-177. https://doi.org/10.1177/09506608241229042

[3] Millensifer A, Sinclair T, Jonasson D, & Lipmann A. Rhenium. Critical metals handbook. 2014, 340-360. https://doi.org/10.1002/9781118755341.ch14

[4] Sengupta P, & Manna I. Advanced high-temperature structural materials in petrochemical, metallurgical, power, and aerospace sectors—An overview. Future landscape of structural materials in India. 2022, 79-131.

[5] Ganji D K, & Rajyalakshmi G. Influence of alloying compositions on the properties of nickel-based superalloys: a review. Recent Advances in Mechanical Engineering: Select Proceedings of NCAME. 2020, 537-555. https://doi.org/10.1007/978-981-15-1071-7_44

[6] Lessard J D, Gribbin D G, & Shekhter L N. Recovery of rhenium from molybdenum and copper concentrates during the Looping Sulfide Oxidation process. International Journal of Refractory Metals and Hard Materials. 2014; 44: 1-6. https://doi.org/10.1016/j.ijrmhm.2014.01.003

[7] Parmonov S, Sharipov K, Mirzavaliyev D, Makhmudova F, Askarova N, Toshkodirova R, ... & Kambarov A. The Technology of Obtaining Powders Used in the Production of Solid Alloys. New Materials, Compounds and Applications. 2024; 8(3):450-458. https://doi.org/10.62476/nmca83450

[8] Hofmann B J, Harms R G, Schwaminger S P, Reich R M, & Kühn F E. Reactivity of Re2O7 in aromatic solvents–Cleavage of a β-O-4 lignin model substrate by Lewis-acidic rhenium oxide nanoparticles. Journal of Catalysis. 2019; 373:190-200. https://doi.org/10.1016/j.jcat.2019.03.042

[9] Kühn F E, & Herrmann W A. Rhenium-oxo and rhenium-peroxo complexes in catalytic oxidations. Metal-Oxo and Metal-Peroxo Species in Catalytic Oxidations. 2001, 213-236.

[10] Hartmann T. Preparation, characterization and physical properties of new compounds in the system Ln2O3-ReO2–½ Re2O7 (Ln= lanthanides or yttrium). Doctoral dissertation, Technische Universität Darmstadt. 2003. https://doi.org/10.26083/tuprints-00000451

[11] Yagi R, & Okabe T H. Rhenium and its smelting and recycling technologies. International Materials Reviews. 2024; 69(2):142-177. https://doi.org/10.1177/09506608241229042

[12] Qiao H, Fang J, Wang X, & Wei C. Research progress on the recycling method of rhenium waste. Canadian Metallurgical Quarterly. 2025, 1-15. https://doi.org/10.1080/00084433.2025.2560195

[13] Liu Z, Shi S, Li Y L, Liu H, & Liu J. Advances and Challenges in Rhenium Recovery from Copper Smelting Dirty Acid: Solvent Extraction, Ion Exchange, and Adsorption. Journal of Sustainable Metallurgy. 2025, 1-19.

[14] Van Fan Y, Varbanov P S, Klemeš J J, & Nemet A. Process efficiency optimisation and integration for cleaner production. Journal of Cleaner Production. 2018; 174:177-183. https://doi.org/10.1016/j.jclepro.2017.10.325

[15] Yakubov M M, Yoqubov M M, Kholikulov D B, & Maksudhodjaeva M S. Depletion of converter slags to waste in the Vanyukov furnace during pyrometallurgical copper production at JSC Almalyk MMC. Kompleksnoe Ispolzovanie Mineralnogo Syra= Complex use of mineral resources. 2024; 331(4):60-68. https://doi.org/10.31643/2024/6445.39

[16] Bahrami A, Kashani R H, Kazemi F, & Ghorbani Y. Oxidation-reduction effects in the flotation of copper sulfide minerals and molybdenite–A proof of concept at industrial scale. Minerals Engineering. 2022; 180:107505. https://doi.org/10.1016/j.mineng.2022.107505

[17] Gerson A R, Smart R S C, Li J, Kawashima N, Weedon D, Triffett B, & Bradshaw D. Diagnosis of the surface chemical influences on flotation performance: Copper sulfides and molybdenite. International Journal of Mineral Processing. 2012; 106:16-30. https://doi.org/10.1016/j.minpro.2012.01.004

[18] Nazarov Y. Copper Super Concentrate Production Technology for Operating Copper–Molybdenum Processing Plants. Eurasian Mining. 2015; 1:25-30.

[19] Shamsuddin M. Roasting of sulfide minerals. In Physical Chemistry of Metallurgical Processes, Second Edition. 2021, 39-68. Cham: Springer International Publishing.

[20] Thomas K G, & Cole A P. Roasting developments–especially oxygenated roasting. In Gold ore processing. Elsevier. 2016, 373-392. https://doi.org/10.1016/B978-0-444-63658-4.00023-2

[21] Wei C, Qiao H, Fang J, Wang X, Wen J, & Tong P. Recovery of high-purity rhenium resources from W-Mo-Re alloy scraps by two-stage low-temperature oxidation volatilization. Process Safety and Environmental Protection. 2025; 197:107056. https://doi.org/10.1016/j.psep.2025.107056

[22] Elehinafe F B, Aondoakaa E A, Akinyemi A F, Agboola O, & Okedere O B. Separation processes for the treatment of industrial flue gases–effective methods for global industrial air pollution control. Heliyon. 2024; 10(11). https://doi.org/10.1016/j.heliyon.2024.e32428

[23] Wang Y, & Wang C. Recent advances of rhenium separation and enrichment in China: Industrial processes and laboratory trials. Chinese Chemical Letters. 2018; 29(3):345-352. https://doi.org/10.1016/j.cclet.2018.01.001

[24] Anderson C D, Taylor P R, & Anderson C G. Extractive metallurgy of rhenium: a review. Mining, Metallurgy & Exploration. 2013; 30(1): 59-73.

[25] Hori H, Otsu T, Yasukawa T, Morita R, Ishii S, & Asai T. Recovery of rhenium from aqueous mixed metal solutions by selective precipitation: A photochemical approach. Hydrometallurgy. 2019; 183:151-158. https://doi.org/10.1016/j.hydromet.2018.12.003

[26] Srivastava R R, Kim M S, Lee J C, & Ilyas S. Liquid–liquid extraction of rhenium (VII) from an acidic chloride solution using Cyanex 923. Hydrometallurgy. 2015; 157:33-38. https://doi.org/10.1016/j.hydromet.2015.07.011

[27] Kattaev N T, Tuygun B, Adinaeva D, Jumaev M, & Azizova K. A new granulated sorbent based on acrylonitrile: Synthesis and physico-chemical properties. In BIO Web of Conferences. EDP Sciences. 2024; 95:01043. https://doi.org/10.1051/bioconf/20249501043

[28] Laumola L. Characterization and treatment of waste gas emissions from process industry. 2020. https://urn.fi/URN:NBN:fi:aalto-202010255984

Crossref
DOI: 10.31643/2028/6445.03
Mining & Mineral Processing

Purification of lanthanum chloride solution through tertiary amine extraction: thermodynamic and graded assessment

[1] Zulkifli N., [1*] Shoparwe N., [1] Yusoff A.H., [2]Abdullah A.Z., [3] Ahmad M.N.

[1] Centre for Gold, Rare Earths and Materials (GREAT) Technopreneurship at Universiti Malaysia Kelantan, Jeli, Kelantan, Malaysia
[2] Universiti Sains Malaysia, Penang, Malaysia
[3] International Islamic University of Malaysia, Kuantan, Pahang, Malaysia

** Corresponding author's email: fazliani.s@umk.edu.my*

Received: *March 19, 2026*
Peer review: *March 26, 2026*
Received: *April 22, 2026*

ABSTRACT
Purification of lanthanum chloride from high-load zinc contaminants remains a major challenge in producing grade 5N lanthanum oxides. This study investigates the process of matrix-driven solvent extraction using tertiary amine N235 to treat a 1.41 M rare earth oxides (REO) industrial lanthanum chloride feed containing 3000 mg/L zinc. Thermodynamic modelling with Medusa Hydra and Langmuir isotherms revealed that the high chloride activity (> 4 M) of the matrix induced significant changes in coordination towards the extractable $[ZnCl_4]^{2-}$ complex. This transition has a spontaneous Gibbs free energy of -14.68 kJ/mol. While the two-stage counter-current flow sheet meets the industry target of less than 50 mg/L zinc, the five-stage configuration achieves a four-log reduction to 0.23 mg/L, effectively achieving 99.999% purity. This reagent's lean approach, using water-induced stripping, offers a sustainable and mathematically validated framework for ultra-high purity rare earth finishes.

Keywords: lanthanum chloride, solvent extraction, zinc, N235, McCabe-Thiele.

Information about the author:

Zulkifli N. *PhD candidate at the Centre for Gold, Rare Earths and Materials Technopreneurship (GREAT), Faculty of Bioengineering and Technology, Universiti Malaysia Kelantan, Jeli 17600 Kelantan, Malaysia. Email: norazihan.zulkifli@gmail.com; ORCID ID: https://orcid.org/ 0009-0009-4772-0578*

Shoparwe N. *Associate Professor at Gold, Rare Earth and Material Technopreneurship Centre (GREAT), Faculty of Bioengineering and Technology, Universiti Malaysia Kelantan, Jeli 17600 Kelantan, Malaysia. Email: fazliana.s@umk.edu.my; ORCID ID: https://orcid.org/ 0000-0002-4329-2459*

Yusofff A.H. *Associate Professor at Gold, Rare Earth and Material Technopreneurship Centre (GREAT), Faculty of Bioengineering and Technology, Universiti Malaysia Kelantan, Jeli 17600 Kelantan, Malaysia. Email: hafidz.y@umk.edu.my; ORCID ID: https://orcid.org/0000-0003-0229-886X*

Abdullah A.Z. *Professor at the School of Chemical Engineering, Engineering Campus, Universiti Sains Malaysia, 14300 Nibong Tebal, Penang, Malaysia. Email: chzuhairi@usm.my*

Ahmad M.N. *Associate Professor at the Sustainable Computational Nanotechnology and Chemistry Research Group (SuNCoM), Department of Chemistry, Faculty of Science, International Islamic University Malaysia, 25200 Kuantan, Pahang, Malaysia. Email: mnorazmi@iium.edu.my; ORCID ID: https://orcid.org/ 0000-0001-5742-0346*

Introduction

Rare earth elements (REEs), from lanthanum (La) to lutetium (Lu), are essential in modern technologies such as communications, defence, medicine, and clean energy due to their magnetic, catalytic, and fluorescent properties. Global demand has soared with the shift to a high-tech, low-carbon economy, yet supply chains remain vulnerable, especially for ultra-high (5N, 99.999%) lanthanum oxide (La_2O_3) used in optical lenses, capacitors, and photocatalysts [1]. Impurities such as Zn severely degrade performance, disrupting dielectric properties or the lattice structure [[2], [3], [4]].

Purifying industrial lanthanum chloride ($LaCl_3$) solutions, often near saturation yet contaminated with thousands of ppm Zn, is a key bottleneck in hydrometallurgy [[5], [6]]. Conventional methods, such as sulphide precipitation, generate hazardous gases and fail to meet sub-ppm targets. Ion exchange suits only low-concentration, low-flow REE solution rates [[7], [8]]. Solvent extraction using organo-phosphonic acids, such as D2EHPA/PC-88A/Ionquest 801, incurs high cost [[9], [10], [11]. Tertiary amines such as N235 show promise for

Table 1 - A performance benchmark of the matrix-driven N235 system against literature-reported organophosphorus and solvating extractants for zinc removal

Extractant	Impurity	Extraction			Stripping		Ref
		Medium	D_{Zn}	Stages	Reagent	Stages	
DEHPA di-2-ethylhexyl phosphoric acid	Zn + Mn	Cl^- Zn-C battery leach liquor	9	1+3	6M HCl	1+3	[18]
Cyanex 923 trialkyl phosphine oxides	Zn + Fe	Steel pickle liquor Cl^-	5 - 100	3	0.8M HNO_3	1	[19]
D2EHPA + Cyanex 302 2-ethylhexyl phosphonic acid mono-2-ethylhexyl ester + bis(2,4,4-trimethylpentyl) monothiophosphinic acid	Zn $ZnSO_4[CS(NH_2)_2]$	Zn SO_4^{2-} solution	20 - 80	n/r	0.45M thiourea acid	2	[20]
N503 N, N-di(1-methylheptyl) acetamide	Fe/Zn $[CH3CONR2H]ZnCl_3$	Spent pickle solution Cl^-	278.92	4	0.4M HCl		[21]
N1953 primary amine	Zn RNH_3ZnCl_3	Spent pickle solution Cl^-		3	H_2SO_4 -> 5.39M Zn		[22]
Aliquat 336 quaternary ammonium salt	Zn From 17 g/L	Spent pickle solution Cl^-					[23]
TOA tri-n-octylamine	Zn	Spent pickle solution Cl^-		5	2M HNO_3		[24]
P507+P204 2-ethylhexyl phosphonic acid mono-2-ethylhexyl ester + di-2-ethylhexyl phosphoric acid	Zn	Spent acid Cl^-		84.7% E-Zn	H_2SO_4		[25]
Cyanex 272, bis(2,4,4-trimethylpentyl) phosphinic acid	Zn	Cobalt-Zn Cl^-		15	H_2SO_4		[26]

other metal separation, such as mini actinides and REE [12], molybdenum recovery from copper leach [13], but require a complexing agent such as tartaric acid to form extractable anionic species [13][14]. Despite advances in zinc recovery from secondary sources [[15], [16], [17] no reagent-free framework leverages high-salinity $LaCl_3$ matrices for deep purification in concentrated REE streams.

Existing research, summarised in Table 1, mostly studies Zn removal from spent pickle solution of Cl^- basis and the stripping with acid, overlooking matrix-induced coordination shifts, limiting scalability from 99.9% industrial feed to 5N high-tech grades. This study harnesses chloride activity in $LaCl_3$ as a self-salting agent for Zn removal via N235-based solvent extraction, achieving <50 ppm and enabling 5N purity.

Experimental section

Chemicals and reagents

Aqueous feed is an industrial-grade solution of lanthanum chloride. The chemical properties are summarised in Table 2. This solution is characterised by a Total Rare Earth Oxide (TREO) concentration of 260 g/L (1.41 mol/L) and a base acidity of 0.012 mol/L (pH 1.92). A critical feature of this feed is a significantly high zinc concentration of 3000 mg/L, which represents the main impurity barrier to achieving high-purity-grade lanthanum.

To establish a thermodynamic basis for zinc removal, the stability of various zinc chloride complexes has been modelled using the Medusa Hydra software, as presented in Figure 1. The coordination sphere is evaluated as a function of chloride activity to confirm the self-salting potential of the matrix.

Table 2 - Characteristics of $LaCl_3$ industrial solution

Acidity	REO	La2O3 /REO	CeO2 /REO	Pr6Nd1 1 /REO	Nd2O 3 /REO	Sm2O 3 /REO	Eu2O 3 /REO	Tb4O 7 /REO	Tm2O 3 /REO	Y2O 3 /RE O	Yb2O 3 /REO	Fe	Zn
(mol/L)	(mol/L)	(%)	(%)	(%)	(%)	(%)	(%)	(%)	(%)	(%)	(%)	(ppm)	(ppm)
0.012	1.41	99.9	0.011	0.00	0.00	0.00	0.00	0.00	0.00	0.00	0.00	1.44	3000

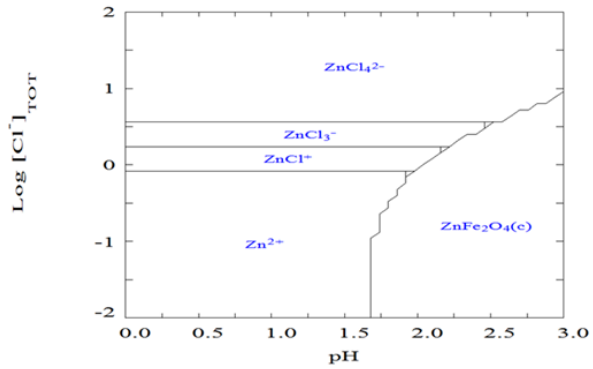

Figure 1 - Zinc species dominance diagram as a function of pH activity and chloride volume in the high Cl, high Zn $LaCl_3$ system

The dominance of the anionic species $[ZnCl_4]^{2-}$ at chloride levels above 4 M, naturally provided by a 1.41 M $LaCl_3$ matrix, supports a very high selectivity compared to conventional low-salinity environments.

At the industrial feed acidity (pH 1.9) and high chloride activity ($[Cl^-]$ 4.23M, or log $[Cl^-]$ 0.63), the system is in the predominance field of the anionic tetrachloride-zincate complex $[ZnCl_4]^{2-}$. The quantitative transformation of Zn^{2+} to the anionic tetrachloride-zincate complex $[ZnCl_4]^{2-,}$ is represented by Equation 1.

$$Zn^{2+}(aq) + 4Cl^{-}(aq) = [ZnCl_4]^{2-}(aq) \quad (1)$$

The organic phase is prepared using tri-iso-octylamine (N235) (industrial grade, 98.5%) as the extractor, diluted in sulfonated kerosene (Escaid 110) (industrial grade, 99.8%). Isopropanol (IPA) (industrial grade, 99%) has been used as a polar modifier to stabilise mixtures. Although previous literature often used iso-butanol, this study strategically chose short-chain alcohol IPAs over iso-butanol to minimise overall viscosity and prioritise mass transfer kinetics.

The organic mixture has been pre-treated with an alkaline wash using an 8 wt.% sodium carbonate solution to remove impurities. This is followed by protonation with 4.5 M hydrochloric acid to form a substituted quaternary ammonium cation, as shown in Equation 2

$$R_3N(org) + H(^{+}aq) + Cl(^{-}aq) \rightleftharpoons (R_3NH^{+}Cl^{-})(org) \quad (2)$$

where R represents the octyl chain.

Extraction occurs when the anionic complex $[ZnCl_4]^{2-}$ has a strong affinity for the protonated amine carrier $R_3NH^{+}Cl$-. This causes the target species to be separated into organic phases through the formation of stable ion pairs as described in Equation 3.

$$2(R_3NH^{+}Cl^{-})(org) + [ZnCl_4]^{2-}(aq) \rightleftharpoons ([R_3NH]_2[ZnCl_4])(org) + 2Cl(^{-}aq) \quad (3)$$

This is unlike the extracted zinc with primary amine N1953 as RNH_3ZnCl_3 and tri-n-octylamine (TOA) as $R_3NHZnCl_3$[24].

Extraction and Analysis Procedures

Batch extraction tests were conducted in a 250 mL borosilicate glass beaker using an IKA RW20 digital overhead mixer at 700 RPM at an ambient temperature of 25 ± 2°C. For isotherm extraction studies, the aqueous-to-organic (A/O) ratio ranges from 1:5 to 5:1. The sample is equilibrated for 15 minutes to ensure thermodynamic equilibrium [18].

After phase discharge, aqueous fines were analysed for zinc using Inductively Coupled Plasma Optical Emission Spectrometry (ICP-OES). The concentration of metals in the organic phase is determined by mass balance. The organic phase is then stripped by contacting it with 0.1 M hydrochloric acid (HCl) and deionized water to assess the stripping efficiency. After separation, the aqueous phase was analysed for zinc, lanthanum, and total rare earth oxides (TREO). Zinc is measured using atomic absorption spectroscopy (AAS) while REO and lanthanum are determined by ICP-OES. The concentration of metals in the organic phase (C_{org}) is determined by the mass equilibrium as in Equation 4.

$$C_{org} = \frac{(C_{init} - C_{equil}) \times V_{aq}}{V_{org}} \quad (4)$$

Where C_{init} and C_{equil} are the initial aqueous and equilibrium concentrations, and V_{aq} and V_{org} are the aqueous and organic phase volumes, respectively. The refining purity target has been set at a zinc concentration of <50 ppm to meet stringent industry specifications.

The distribution ratio, D_{Zn}, which measures the zinc equilibrium distribution between the organic and aqueous phases, has been calculated using Equation 5.

$$D_{Zn} = [Zn]_{organic}/[Zn]_{aqueous} \quad (5)$$

To assess the loading capacity and equilibrium behaviour, the initial Zn concentration was varied from 10 to 2000 mg/L. The resulting data were fitted to the Langmuir adsorption isotherm model as Equation 6

$$q_e = \frac{q_m K_L C_e}{1 + K_L C_e} \quad (6)$$

where q_m (mg/g) is the amount of Zn extracted per unit of extractor mass, C_e (mg/L) is the equilibrium concentration in the aqueous phase, q_m is the maximum load capacity, and KL is the Langmuir constant.

The spontaneity of the extraction process was evaluated by calculating the standard Gibbs free energy (ΔG°) from the equilibrium constant (K_c) derived from the Langmuir model, as given in Equation 7.

$$\Delta G° = -RTln(K_C) \quad (7)$$

This calculation provides a rigorous thermodynamic assessment of coordination shifts in the $LaCl_3$ matrix.

From the isotherm, the McCabe-Thiele construction method will be used to determine the number of stages required to achieve 5N purity.

As in any continuous solvent extraction system, the loaded organics must be efficiently stripped to recover the extracted product. The barren organic matter is then regenerated and recycled back to the beginning of the system, repeating the process. In REE recovery through a continuous solvent extraction system, strong acids such as HCl are used to remove the extracted elements. The water is used to wash away the waste acids, produce a barren organic backing, and is then treated, ready for extraction. In this study, 0.1 M HCl and water were compared for their ability to strip the zinc loaded at N235 at an A/O of 0.5-10.

Results and Discussions

Distribution Coefficient: Extraction Rate

The distribution ratio (D_{Zn}) in this $LaCl_3$ matrix exceeded 150 at low A/O, significantly surpassing the DEHPA benchmark (D_{Zn}=45 in Cl^- leach). This demonstrates N235's superior affinity for $[ZnCl_4]^{2-}$ at low A/O ratios, as shown in Figure 2 (a). D_{Zn} drops dramatically from over 20 to under 5 when the A/O increases from 0.25 to 1.0 with 7% v/v N235. Higher concentrations (40% to 99% extraction at A/O=2)

a)

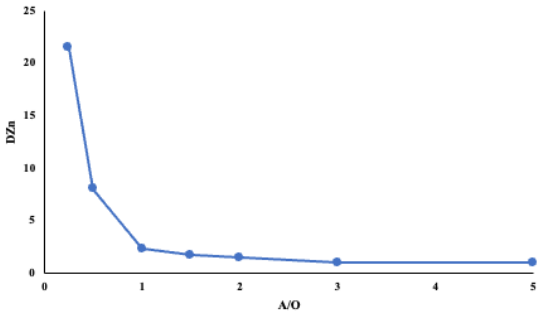

b)

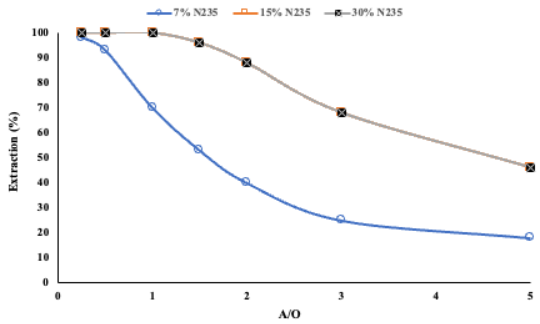

Figure 2 – Zn extraction from La chloride, a) the effect of A/O on the distribution ratio, and b) the effect of N235 concentration and A/O on the extraction efficiency

further exacerbate this effect. Interestingly, the D_{Zn} values for 15% and 30% N235 are identical across the higher A/O range (1.5 to 5.0). This indicates that beyond a 15% concentration, the extraction is no longer limited by extractant availability but is instead governed by the aqueous speciation of the $[ZnCl_4]^{2-}$ complex. This supports the "matrix-driven" hypothesis, where the 1.41 M $LaCl_3$ environment dictates the maximum possible formation of

extractable anionic species, as illustrated in Figure 2 (b).

Table 3 summarises D_{Zn} values across N235 concentrations (7-30% v/v) and A/O ratios (0.25-2.0), confirming peak extraction efficiency (>150) under optimal, low A/O conditions and highlighting

the system's robustness across industrial operating windows. These data validate 7% v/v N235 as the cost-effective choice for continuous modelling, balancing high D_{Zn} with minimal reagent use.

Table 3 - Distribution coefficients (D_{Zn}) for N235 extraction from $LaCl_3$ matrix

N235 (v/v%)	A/O 0.25	A/O 0.5	A/O 1.0	A/O 2.0	Extraction % (A/O=2)
7%	>150	85	18	5	40%
15%	220	140	45	22	90%
30%	280	195	75	45	90%

The higher polarity of isopropanol effectively dissolves the large ion pair complex $(R_3NH^+)_2ZnCl_4^{2-}$, preventing third phase formation and maintaining a sharp interface even at maximum zinc loading.

The distribution ratio (D_{Zn}) in this REE matrix exceeds 150. This D_{Zn} >150 in concentrated $LaCl_3$ exceeds DEHPA benchmarks (D_{Zn}=45) and Cyanex 923 (3 stages), due to $[ZnCl_4]^{2-}$ stability vs cation exchange limits of phosphonic at high salinity [27].

Equilibrium Modelling and Thermodynamic Evaluation

Extraction data have been analysed to fit the Langmuir isothermal model. The linearised Hanes-Wool shape was used as Equation 8.

$$\frac{x}{y} = \frac{1}{q_m}x + \frac{1}{q_m K_L} \quad (8)$$

The extraction balance has been carefully modelled to assess the process efficiency for handling a 3000 ppm zinc load. The data show a strong correlation with Langmuir Isotherms, as illustrated in Figure 3.

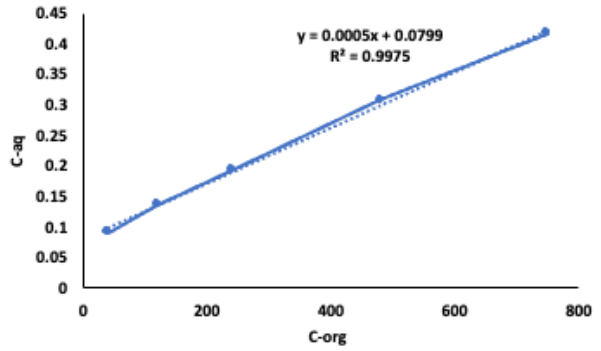

Figure 3 - Plot of the Hanes-Woolf of the linearised Langmuir fit

The linear regression analysis yields an R^2 value of 0.9975, indicating a good fit. The maximum loading capacity (q_m) has been determined to be 2222 mg/L, indicating that the N235 system is well-suited for high-impurity industrial flows. Furthermore, a standard Gibbs free energy (ΔG) of -14.68 kJ/mol confirms that the extraction is thermodynamically spontaneous. This is in line with the extraction of Zn using DEHPA in the Zn-C battery chloride leach solution, where ΔH was -245.59 kJ/mol and 100% extraction in one stage.

Multi-Stage Simulation for 5N Purity

The McCabe-Thiele diagram for the industrial feed containing 3000 ppm Zn is shown in Figure 4(a). The concentration profile is shown in Figure 4(b).

a)

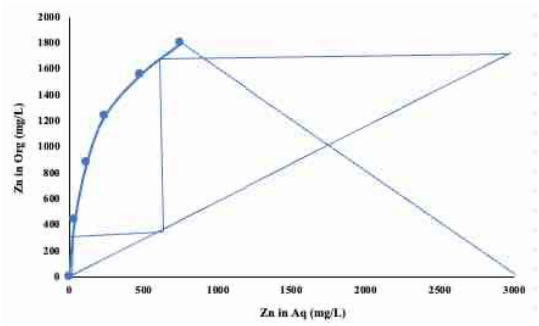

b)

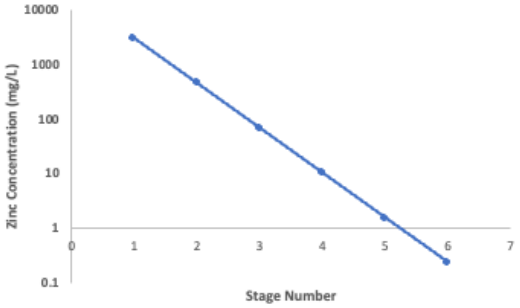

Figure 4 – $LaCl_3$ Zn extraction with 15% N235 at A/O 1.25 a) McCabe-Thiele construction, and b) stage concentration profile

The $LaCl_3$ purification circuit's main goal is to reduce zinc pollution from 3000 mg/L to <50 mg/L. The McCabe-Thiele construction shows that a 2-stage counter-current extraction with an A/O ratio of 1:25 is enough to meet this commercial threshold. This 2-stage configuration is highly efficient and reagent-lean, unlike other systems that need 3 stages, such as Cyanex 923.

The concentration profile provides a deeper scientific insight into the system's ultimate limits of purification. Although two stages are sufficient for bulk removal, linear developments on the logarithmic scale indicate that the N235 carrier does not experience loading inhibition at the trace level. As seen in the profile, the zinc concentration

decreases exponentially across 5 stages. By the final stage, the concentration reached < 0.5 ppm, indicating that the matrix-driven self-salting effect was sufficient to bridge the gap from the 99.9% industrial grade to the 99.999% high purity threshold required for advanced optical and electronics applications. By extending the circuit to 5 stages, the system can achieve a 4-log reduction, reaching 0.23 mg/L Zn. This confirms that the same matrix-driven self-salting mechanism used for bulk recovery can be scaled to produce 5N (99.999) grade lanthanum, offering a versatile flow sheet that can be adjusted to meet the purity requirements of the final application.

Extractor Stripping and Regeneration

The stripping study evaluated the comparative efficiency of deionised water and 0.1 M HCl across varying A/O ratios (Figure 5a) and stripping stages (Figure 5b), using the McCabe-Thiele construction.

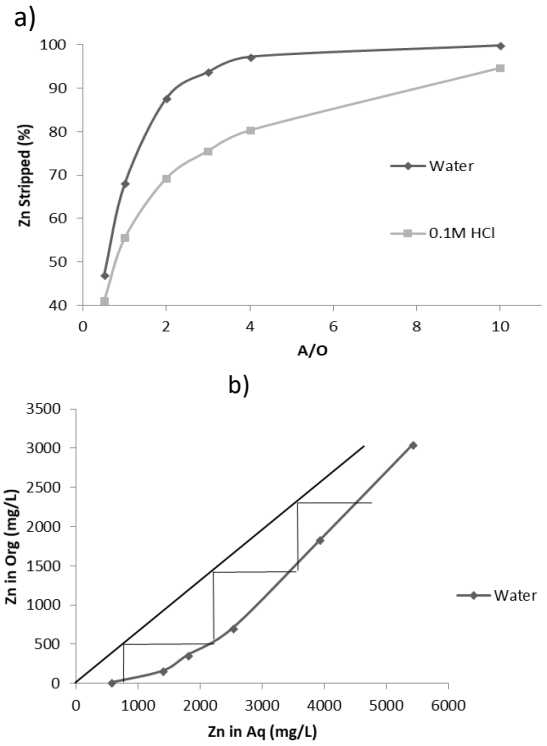

Figure 5 - Zn stripping with water a) efficiency at different A/O, and b) McCabe Thiele diagram at A/O 1.3

The results show that water is a superior stripping agent, achieving almost quantitative efficiency (about 100%) at 10 A/O. This significantly outperforms the 92% efficiency observed with 0.1 M HCl. Water stripping (100% at A/O 10) surpasses HCl (92%) and thiourea systems, disrupting $[ZnCl_4]^{2-}$ without complexing. This high efficiency is attributed to the water-induced separation mechanism. When the concentration and acidity of chloride decrease during contact with pure water, the complex balance of ion pairs shifts back towards the aqueous phase.

Although recent studies have successfully used thiourea in hydrochloric acid media to remove zinc, such a system relies on the formation of a strong and stable complex to attract the metal into the aqueous phase.

The McCabe-Thiele construction shows that a three-stage counter-current stripping process at an A/O ratio of 1:3 is sufficient to completely strip the zinc from the organic phase. The absence of a high chloride background destabilizes the $[ZnCl_4]^{2-}$ complex, causing it to decompose into Zn^{2+} cations, which are insoluble in the organic phase.

While previous studies reported a two-stage stripping process, the three-stage stripping process with water in this study resulted in a more concentrated zinc strip liquor with a higher O/A ratio and more favorable stripping chemistry.

Figure 6 summarises the complete extraction and stripping mechanism. It depicts the transition from the aqueous matrix to the organic phase, followed by the next stage of green stripping using deionised water. This water-induced separation is the main sustainable feature of the proposed flow sheet.

Flowsheet

The process flow sheet is depicted in Figure 7. The successful integration of extraction and stripping circuits demonstrates that the continuous counter-current solvent extraction process is technically superior and environmentally friendly [[28], [27][29]]. It meets the 5N purity requirements of the high-purity lanthanum application.

Conclusion

The study successfully demonstrated a high-efficiency solvent extraction flow sheet for deep purification of industrial-grade lanthanum chloride solutions, specifically addressing continuous 3000 ppm zinc jamming. By investigating the chemical mechanisms, it was established that the high chloride activity ($[Cl^-]$ about 4.23 M) of the 1.41 M $LaCl_3$ matrix drives the displacement of quantitative coordination. This transforms the hydrated zinc cation into an anionic tetrachloride-zincate complex ($[ZnCl_4]^2$-), which is then selectively partitioned into the organic phase N235 via ionic pairing.

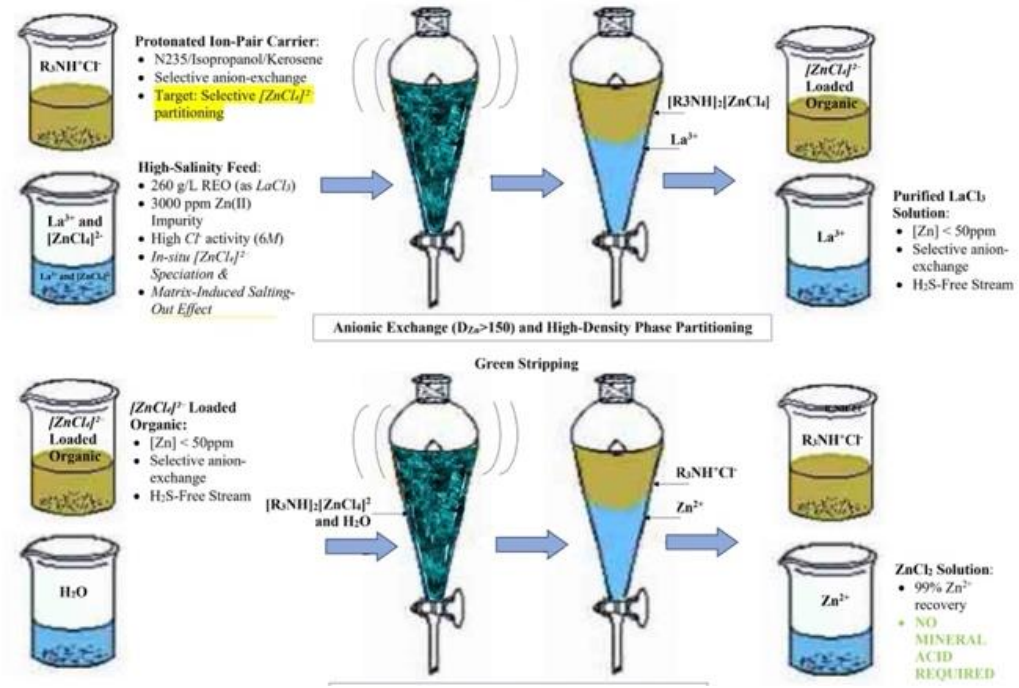

Figure 6 – Schematic diagram for Zn partition from concentrated $LaCl_3$ solution through N235 solvent extraction and water stripping

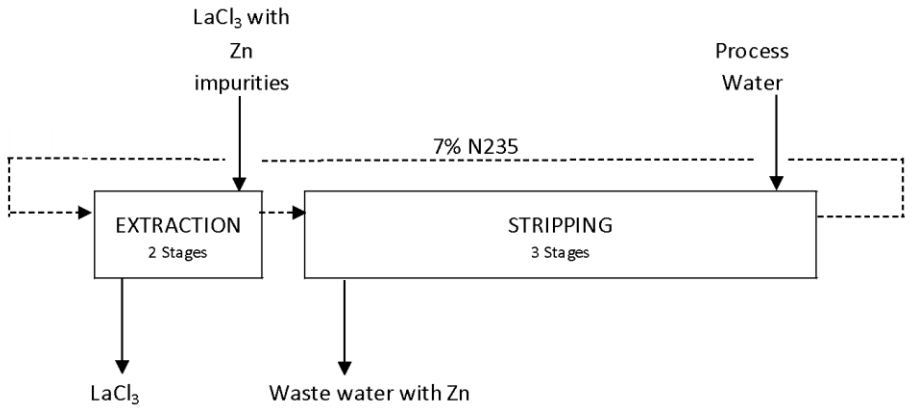

Figure 7 - Flow sheet for continuous counter-current zinc extraction with N235 in $LaCl_3$ and stripping with water

Thermodynamic evaluations using Langmuir isotherms confirmed that the process was very spontaneous (ΔG = -14.68 kJ/mol). The system's robustness under high-load industrial flows is confirmed by a maximum loading capacity of 2222 mg/L. Furthermore, a five-stage counter-current simulation shows that the self-salting effect of this matrix is sufficient to reduce the zinc concentration to < 0.5 ppm. This bridges the gap from 99.9% purity to the 99.999% (5N) threshold required for advanced optical and electronic applications.

Finally, this research provides a sustainable, lean reagent alternative to traditional purification methods, complementing the cycle of recovery-to-purification recently emphasised in this journal by offering a high-purity aqueous finishing stage that operates at ambient temperature. Future work would focus on the organic stability and coextraction of Fe.

Conflict of interest. On behalf of all authors, the corresponding author states that there is no conflict of interest.

CRediT author's statement: **N. Zulkifli:** Conceptualization, Methodology, Formal analysis, Writing – Original Draft; **N. Shoparwe**: Supervision, Writing – Review & Editing; **A.H. Yusoff**: Supervision, Validation; **A.Z. Abdullah**: Supervision, Methodology support; **M.N. Ahmad**: Supervision, Review & Editing.

Acknowledgment. This work is supported by a GREAT grant from the Universiti Malaysia Kelantan Research Fund, grant No. R/FRGS/A1300/01702A/007/2023/01193.

Cite this article as: Zulkifli N, Shoparwe N, Yusoff MA, Abdullah AY, Ahmad MN. Purification of lanthanum chloride solution through tertiary amine extraction: thermodynamic and graded assessments. Kompleksnoe Ispolzovanie Mineralnogo Syra = Complex Use of Mineral Resources. 2028; 344(1):28-37. https://doi.org/10.31643/2028/6445.03

Лантан хлориді ерітінділерін үшінші деңгейлі амин экстракциясы арқылы тазарту: термодинамикалық және кезеңдік бағалау

[1] Zulkifli N., [1*] Shoparwe N., [1] Yusoff A.H., [2]Abdullah A.Z., [3] Ahmad M. N.

[1]Universiti Malaysia Kelantan, Малайзиядағы Алтын, Сирек Жер және Материалдар Технокәсіпкерлік Орталығы (GREAT), Малайзия
[2] Universiti Sains Malaysia, Пенанг, Малайзия
[3] Малайзия Халықаралық Ислам Университеті, Куантан, Паханг, Малайзия

Мақала келді: *19 наурыз 2026*
Сараптамадан өтті: *26 наурыз 2026*
Қабылданды: *22 сәуір 2026*

ТҮЙІНДЕМЕ

Лантан хлоридін мырыш құрамы жоғары мырыш қоспаларынан тазарту 5N класты лантан оксидтерін өндіруде басты мәселе болып қала береді Бұл зерттеу құрамында 3000 мг/л мырыш бар 1,41 М сирек кездесетін жер оксидтері (СЖО) концентрациясы бар өндірістік лантан хлоридінің шикізатын өңдеу үшін N235 үшіншілік аминін пайдаланып, матрицалық еріткішті экстракциялау процесін зерттейді. Medusa Hydra және Langmuir изотермаларын қолдана отырып, термодинамикалық модельдеу матрицаның жоғары хлоридті белсенділігі (> 4 М) экстракцияланатын $[ZnCl_4]^{2-}$ кешеніне қарай координацияда айтарлықтай өзгерістер тудыратынын көрсетті. Бұл ауысудың өздігінен пайда болатын Гиббстің бос энергиясы -14,68 кДж/моль құрайды. Екі сатылы қарсы ток ағыны схемасы 50 мг/л-ден төмен мырыштың өндірістік мақсатына сай болса, бес сатылы конфигурация төрт логарифмдік төмендетуді 0,23 мг/л-ге дейін қамтамасыз етеді, бұл тиімді түрде 99,999% тазалыққа қол жеткізеді. Бұл реагенттің үнемді тәсілі, су арқылы алынған стриппингті пайдаланып, өте жоғары тазалықты сирек кездесетін жер элементтерін өңдеу үшін тұрақты және математикалық тұрғыдан расталған негіз ұсынады.

Түйін сөздер: Ерітінді экстракция, мырыш, лантан хлориді, N235, McCabe-Thiele.

Авторлар туралы ақпарат:

Zulkifli N. — *Алтын, сирек жер және материалдар технологиясы орталығында (GREAT) PhD кандидаты, биоинженерия және технология факультеті, Universiti Malaysia Kelantan, Джели 17600 Келантан, Малайзия. Email: norazihan.zulkifli@gmail.com; ORCID ID: https://orcid.org/ 0009-0009-4772-0578*

Shoparwe N. — *Алтын, сирек жер және материалдық технологиялар орталығының (GREAT) доценті, биоинженерия және технология факультеті, Universiti Malaysia Kelantan, Джели 17600 Келантан, Малайзия. Email: fazliana.s@umk.edu.my; ORCID ID: https://orcid.org/ 0000-0002-4329-2459*

Yusofff A.H. — *Алтын, сирек жер және материалдық технологиялар орталығының (GREAT) доценті, биоинженерия және технология факультеті, Universiti Malaysia Kelantan, Джели 17600 Келантан, Малайзия. Email: hafidz.y@umk.edu.my; ORCID ID: https://orcid.org/0000-0003-0229-886X*

Abdullah A.Z. — *Химиялық инженерия мектебінің профессоры, Инженерлік кампусы, Universiti Sains Malaysia, 14300 Нибонг Тебал, Пенанг, Малайзия. Email: chzuhairi@usm.my*

Ahmad M.N. — *Малайзия Халықаралық Ислам Университетінің Ғылым факультеті, Химия кафедрасының Тұрақты есептеу нанотехнологиясы және химиясын зерттеу тобының (SuNCoM) доценті, 25200 Куантан, Паханг, Малайзия. Email: mnorazmi@iium.edu.my; ORCID ID: https://orcid.org/ 0000-0001-5742-0346*

Очистка растворов хлорида посредством третичной аминной экстракции: термодинамическая и этапная оценка

[1] Zulkifli N., [1*] Shoparwe N., [1] Yusoff A.H., [2]Abdullah A.Z., [3] Ahmad M. N.

[1] Центр технопредпринимательства в области золота, редкоземельных элементов и материалов (GREAT) Universiti Malaysia Kelantan, Джели, Келантан, Малайзия
[2] Universiti Sains Malaysia, Пенанг, Малайзия
[3] Международный Исламский университет Малайзии, Куантан, Паханг, Малайзия

Поступила: *19 марта 2026*
Рецензирование: *26 марта 2026*
Принята в печать: *22 апреля 2026*

АННОТАЦИЯ

Очистка лантана от загрязнителей с высокой нагрузкой цинка остаётся одной из основных задач при производстве оксидов лантана 5N класса. В данном исследовании изучается процесс экстракции растворителя с помощью матричного растворителя с использованием третичного амина N235 для обработки промышленной подачи оксидов редкоземельных элементов (REO) с содержанием 3000 мг/л цинка. Термодинамическое моделирование с помощью изотерм Медузы Гидры и Лангмюра показало, что высокая хлоридная активность (> 4 М) матрицы вызывала значительные изменения координации в направлении экстрируемого комплекса $[ZnCl_4]^{2-}$. Этот переход имеет спонтанную свободную энергию Гиббса -14,68 кДж/моль. В то время как двухступенчатый противотоковой расходный лист достигает отраслевой цели — менее 50 мг/л цинка, пятиступенчатая конфигурация достигает четырёхлогадичного сокращения до 0,23 мг/л, фактически достигая чистоты 99,999%. Бережливый подход этого реагента, использующий водяное удаление, предлагает устойчивую и математически валидированную основу для покрытия из редкоземельных материалов сверхвысокой чистоты.

Ключевые слова: Экстракция растворителя, цинк, хлорид лантана, N235, McCabe-Thiele.

Информация об авторах:

Zulkifli N. *Кандидат наук в Центре технологического предпринимательства в области золота, редких земель и материалов (GREAT), факультет биоинженерии и технологий, Universiti Malaysia Kelantan, Джели 17600 Келантан, Малайзия. Email: norazihan.zulkifli@gmail.com; ORCID ID: https://orcid.org/ 0009-0009-4772-0578*

Shoparwe N. *Доцент Центра технологического предпринимательства в области золота, редких земель и материалов (GREAT), факультет биоинженерии и технологий, Universiti Malaysia Kelantan, Джели 17600 Келантан, Малайзия. Email: fazliana.s@umk.edu.my; ORCID ID: https://orcid.org/ 0000-0002-4329-2459*

Yusofff A.H. *Доцент Центра технологического предпринимательства в области золота, редких земель и материалов (GREAT), факультет биоинженерии и технологий, Universiti Malaysia Kelantan, Джели 17600 Келантан, Малайзия. Email: hafidz.y@umk.edu.my; ORCID ID: https://orcid.org/0000-0003-0229-886X*

Abdullah A.Z. *Профессор Школы химического машиностроения Инженерного кампуса Universiti Sains Malaysia, 14300 Нибонг Тебал, Пенанг, Малайзия. Email: chzuhairi@usm.my*

Ahmad M.N. *Доцент исследовательской группы по устойчивым вычислительным нанотехнологиям и химии (SuNCoM), кафедра химии, факультет естественных наук, Международный исламский университет Малайзии, 25200 Куантан, Паханг, Малайзия. Email: mnorazmi@iium.edu.my; ORCID ID: https://orcid.org/ 0000-0001-5742-0346*

References

[1] Shahbaz A. A systematic review on leaching of rare earth metals from primary and secondary sources. Minerals Engineering. 2022; 84:107632. https://doi.org/10.1016/j.mineng.2022.107632

[2] Balaram V. Rare earth elements, resources, applications, extraction technologies, chemical characterization and global trade – A comprehensive review. Treatise on Geochemistry (Third edition). 2024, 193–233. https://doi.org/10.1016/B978-0-323-99762-1.00041-3

[3] Alnoman RB. Ion-imprinted chelating resin for targeted adsorption of lanthanum ions: synthesis, characterization, and application. J Chem Technol Biotechnol. 2025; 100:717-731. https://doi.org/10.1002/jctb.7810

[4] Alcaraz L, Rodríguez-Largo O, Álvarez-Montes M, López FA, & Baudín C. Effect of lanthanum content on physicochemical properties and thermal evolution of spent and beneficiated spent FCC catalysts. Ceramics International. 2022; 48(12):17691–17702. https://doi.org/10.1016/j.ceramint.2022.03.039

[5] Zulkifli N, Shoparwe NF, Yusof AH, Abdullah AZ, & Ahmad MN. From Light to Heavy: Addressing the Gap in Rare Earth Element Extraction at Lynas' Advanced Materials Plant. Journal of Bioengineering and Technology Malaysia (MJBeT). 2024; 1(2):113–120. https://doi.org/10.1007/s12598-024-03019-710.70464/mjbet.v1i2.1470

[6] Merroune A, Ait BJ, Berrada M, Essakhraoui M, Achiou B, Mazouz H, & Beniazza R. A comprehensive study of rare earth element solvent extraction technologies from different acidic media: Current challenges and future perspectives. Journal of Industrial Chemistry and Engineering. 2024; 139:1–17. https://doi.org/10.1016/j.jiec.2024.04.042

[7] Zulkifli N, Shoparwe N, Yusof AH, Abdullah, AZ, & Ahmad MN. Ion exchange of lanthanum chloride and Lewatit Monoplus S 108 H resin. Malaysian Journal of Bioengineering and Technology (MJBeT). 2025; 2(3):115-128. https://doi.org/10.70464/mjbet.v2i3.1710

[8] Yu Y, Wang M, Zhang Q, Feng Z, Xu Y, Yang G, & Yang Z. Application of temperature regulation of complex stability constants in removal of key impurities from lanthanum oxide. Journal of Rare Earths 2025. https://doi.org/10.1016/j.jre.2025.05.021

[9] Li S, Wang H, Wang S, Xie F, & Sun X. Selective indium extraction from zinc oxide dust seepage by microwave-assisted solvent extraction with P507 and stripping with HCl: Thermodynamics and kinetics. Hydrometallurgy. 2025; 235:106483. https://doi/org.10.1016/j.hydromet.2025.106483

[10] Munshi B. Integrated hydromining and advanced hydrometallurgical strategies for sustainable zinc recovery from legacy tailings. 2025. https://doi/10.13140/RG.2.2.33997.29923

[11] Zulkifli N, Shoparwe NF, Yusof AH, Abdullah AZ, & Ahmad MN. Flow sheet design and modelling for high-purity praseodymium and neodymium through solvent extraction. Kompleksnoe Ispolzovanie Mineralnogo Syra = Complex Use of Mineral Resources. 2026; 342(3):111–122. https://doi/org.10.31643/2027/6445.35

[12] Suzuki H & Ban Y. Extraction behavior of small actinides and rare earth elements with NTA amide extractors. Journal of Nuclear Science and Technology. 2025; 62(2):157–166. https://doi.org/10.1080/00223131.2024.2402366

[13] Utta B, Dreisinger D, Moser M, Jakovljevic B, & Moya L. Extraction of molybdenum (VI) solvent from sulfuric acid solution by FENTAMINE™ TA0810. Journal of Water Process Engineering. 2026; 81:109333. https://doi.org/10.1016/j.jwpe.2025.109333

[14] Jiang T, Wang P, Liao C, Liu Z, Zhang W, Chen F, & Liu F. A new insight into the synergistic mechanism of germanium extraction through tertiary amine systems: The protonation process and behavior of tartaric acid. Journal of Environmental Chemical Engineering. 2026; 14(1):120982. https://doi.org/10.1016/j.jece.2025.120982

[15] Wang Z, Song Y, Yin N, Shi J, Lang S, & Wang Y. Extraction for separation of Zn and Cu in cyanide gold extraction wastewater by hydrophobic deep eutectic solvent. Journal of Sustainable Metallurgy. 2025; 11(4):4284–4297. https://doi.org/10.1007/s40831-025-01252-7

[16] Berkinbaeva AN, Surkova T Yu, Dosymbayeva ZD, Umirbekova NS, Kebekbaeva AA, & Kyussubayeva NA. Investigation of zinc leaching from clinker by pretreatment of raw materials by ultra-high frequency (microwave) radiation. Kompleksnoe Ispolzovanie Mineralnogo Syra = Complex Use of Mineral Resources. 2026; 339(4):5–13. https://doi.org/10.31643/2026/6445.35

[17] Koishina GM, Zholdasbay EE, Kurmanseitov MB, Tazhiev EB, & Argyn AA. A study of the behavior of zinc and related metal impurities in the waste chlorination baking process. Kompleksnoe Ispolzovanie Mineralnogo Syra = Complex Use of Mineral Resources. 2021; 318(3):71–80. https://doi.org/10.31643/2021/6445.30

[18] Abdelraheem MTO, Level A, Taner HA, & Agacayak T. Extraction of manganese and zinc solvents from Zn–C battery chloride leaching solution applied with DEHPA in benzene melters. Journal of Sustainable Metallurgy. 2024; 10(2):557–565. https//doi.org/10.1007/s40831-024-00810-9

[19] Hu S, Xu C, Srinivasakannan C, Tan X, Ni S, Zhang J, Li X, Zhang H, & Li S. Recovery of zinc and iron from hot-galvanized braided pickled liqueur using solvent extraction. Journal of Molecular Fluids. 2022; 362:119741. https://doi.org/10.1016/j.molliq.2022.119741

[20] Noah NFM, Othman N, Kahar INS, & Suliman SS. Potential use of D2EHPA/Cyanex 302 synergy in kerosene systems for reactive extraction: Zinc recovery and organic phase regeneration. Chemical Engineering and Processing – Process Intensification. 2022; 176:108976. https://doi.org/10.1016/j.cep.2022.108976

[21] Zheng X, Zhang J, Shen J, Jiang X, Guo J, Lei Y, Zhang H, & Li S. Extraction and recovery of zinc from spent pickling solution: Experimental design and mechanism analysis. Journal of Molecular Liquids. 2024; 404:125007. https://doi.org/10.1016/j.molliq.2024.125007

[22] Hu S, Zhang H. Tan X, Ni S, & Li S. Extraction of zinc from spent pickle liquor using primary amine extraction system. Hydrometallurgy. 2024; 224:106259. https://doi.org/10.1016/j.hydromet.2023.106259

[23] Wang Y, He Y, Yin S, Long H, & Li S. Research on extraction of zinc from spent pickling solution using Aliquat 336. Hydrometallurgy. 2020; 193:105322. https://doi.org/10.1016/j.hydromet.2020.105322

[24] Xu C, Zhou J, Yin S, Wang Y, Zhang L, Hu S, Li X, & Li S. Solvent extraction and separation of zinc-iron from spent pickling solution with tri-n-octylamine. Separation and Purification Technology. 2021; 278:119579. https://doi.org/10.1016/j.seppur.2021.119579

[25] Zheng X, Zhang J, Shen J, Guo J, Jiang X, Lei Y, & Li S. Synergistic extraction of zinc from spent acid using P507-P204: A novel approach for efficient separation. Journal of Environmental Chemical Engineering. 2024; 12(6):114515. https://doi.org/10.1016/j.jece.2024.114515

[26] Zou X, Meng X, Jiang Y, Dong X, & Li S. Closed-Loop Process of Extracting and Separating Zinc Impurities from Industrial Cobalt Products—Pilot Test Study. Minerals. 2024; 14(11):1127. https://doi.org/10.3390/min14111127

[27] Udawattha DS, & Alam S. Predicting the distribution coefficient in the solvent extraction of rare earth elements. Separation and Purification Technology. 2025; 377:134382. https://doi.org/10.1016/j.seppur.2025.134382

[28] Dewulf B, Riaño S, & Binnemans K. Separation of heavy rare earth elements by non-aqueous solvent extraction: Flow sheet construction and mixer-settler test. Separation and Purification Technology. 2022; 290:120882. https://doi.org/10.1016/j.seppur.2022.120882

[29] Binnemans K & Jones PT. Twelve principles of spherical hydrometallurgy. Journal of Sustainable Metallurgy. 2023; 9(1):1–25. https://doi.org/10.1007/s40831-022-00636-3

Crossref
DOI: 10.31643/2028/6445.04
Mining & Mineral Processing

Qualitative Analysis of the Circuits of Au-Tonomous Inverters with Shut-off Valves

[1]Toshov J.B., [2*]Zheldikbayeva A.T., [3]Sarsenbayev Y., [2]Smagulova K.K., [1]Umarov Sh., [1]Pulatov A., [2]Abdykenov Y.K.

[1] Tashkent State Technical University named after Islam Karimov, Tashkent, Uzbekistan
[2] Abylkas Saginov Karaganda Technical University, Karaganda, Kazakhstan
[3] Satbayev University, Almaty, Kazakhstan

** Corresponding author email: aisaule89@mail.ru*

Received: *May 17, 2025*
Peer-reviewed: *June 2, 2025*
Accepted: *April 24, 2026*

ABSTRACT
The article presents the results of a qualitative analysis of circuits of autonomous current and voltage inverters with cut-off valves. The influence of the charge on the switching capacitor in parallel and series equivalent circuits on the restoration of the switching properties of the thyristors in the inverter power circuit is studied. It is shown that, due to the energy periodically accumulated in the inductive elements of the load, the voltage across the switching capacitor in the cut-off state is higher than in a conventional parallel autonomous current inverter. This ensures increased switching stability of the inverter. Consequently, the circuit of an autonomous current inverter with cut-off valves remains operational in valve converters for variable-frequency electric drives and maintains performance during sudden load surges and short circuits, since the voltage on the switching capacitor does not depend on the load voltage. Thus, the charge on the switching capacitor is preserved even when the load voltage drops sharply between thyristor commutations.

Keywords: autonomous current inverter, inductive load, valve frequency converter, variable-frequency electric drive, cut-off valves, commutation capacitor charge.

Information about authors:

Toshov Javokhir Buriewicz — *Doctor of Technical Sciences, Professor, Islam Karim Tashkent State Technical University, 100095, Almazar district, Universitetskaya street 2, Tashkent, Uzbekistan. E-mail: j.toshov@tdtu.uz; ORCID ID: https://orcid.org/0000-0003-4278-1557*

Zheldikbayeva Aisaule Takenovna — *PhD student of the Department of Automation of manufacturing processes, Abylkas Saginov Karaganda Technical University, 100027, Ave. Nursultan Nazarbayev, 56, Karaganda, Kazakhstan. E-mail: aisaule89@mail.ru; ORCID ID: https://orcid.org/0009-0005-1325-5576*

Sarsenbayev Yerlan — *PhD, Associate Professor, Head of Department of Power Engineering, Satbayev University, 050013, Satbayev str. 22, Almaty, Kazakhstan. E-mail: y.sarsenbayev@satbayev.university; ORCID ID: https://orcid.org/0000-0002-8887-1171*

Smagulova Karshiga Kanatovna — *Ph.D., Acting Associate Professor of the Department of Automation of manufacturing processes, Abylkas Saginov Karaganda Technical University, 100027, Ave. Nursultan Nazarbayev, 56, Karaganda, Kazakhstan. E-mail: smagulovakk@mail.ru; ORCID ID: https://orcid.org/0000-0001-6834-8490*

Umarov Shukhrat — *Doctor of Technical Sciences, Professor of the department Electrical machines and drivers engineering, Islam Karim Tashkent State Technical University, 100095, Almazar district, Universitetskaya street 2, Tashkent, Uzbekistan. E-mail: shumarov1951@mail.ru; ORCID ID: https://orcid.org/0000-0002-9262-4683*

Pulatov Abror — *Ph.D., Associate Professor, Head of the department Electrical machines and drivers engineering, Islam Karim Tashkent State Technical University, 100095, Almazar district, Universitetskaya street 2, Tashkent, Uzbekistan. E-mail:abrorobidovich@mail.ru; ORCID ID: https://orcid.org/0000-0002-2641-571X*

Abdykenov Yerzhan Kanatuly — *PhD student of the Department of Automation of manufacturing processes, Abylkas Saginov Karaganda Technical University, 100027, Ave. Nursultan Nazarbayev, 56, Karaganda, Kazakhstan. E-mail: erzhan_aiu@mail.ru; ORCID ID: https://orcid.org/0009-0008-0095-576X*

Introduction

In modern industry, variable-frequency electric drives based on valve converters play a critical role in ensuring energy efficiency, precise speed control, and operational reliability of technological processes. However, traditional autonomous current inverters (ACI) using thyristors encounter significant challenges in achieving reliable forced commutation, particularly under variable or shock loads, low operating frequencies, and during overloads or short circuits. In conventional parallel ACI circuits, the voltage across the commutation capacitor depends directly on the load voltage. This

often results in insufficient reverse bias for thyristor turn-off, leading to commutation failures and reduced operational stability [[1], [2], [3], [4]].

These limitations are especially pronounced in high-power applications in mining, metallurgy, and transport sectors, where sudden load changes are common and high commutation reliability is essential. Although various auxiliary commutation circuits have been proposed in the literature, many of them still suffer from strong dependence on load parameters, require oversized capacitors, or exhibit limited overload capability.

A promising approach to overcome these drawbacks is the use of cut-off valves (auxiliary diodes or thyristors), which decouple the commutation capacitor from the load during critical intervals. This allows independent charging of the capacitor and retention of a higher voltage.

Despite numerous studies devoted to modeling and simulation of ACI [[2], [5], [6]], a detailed qualitative analysis of the influence of cut-off valve circuits on commutation processes — particularly the charge dynamics of the switching capacitor in series and parallel equivalent circuits under real operating conditions, including overloads — remains insufficiently addressed. This research gap motivates the present study, which performs a physico-mathematical qualitative analysis of such circuits.

This study aims to conduct a qualitative analysis of autonomous inverter circuits with cut-off valves and to evaluate the effect of the switching capacitor charge on the restoration of thyristor switching properties, thereby enhancing the stability and reliability of inverters for variable-frequency electric drives.

The experimental part

Theoretical Analysis and Equivalent Circuits.

In quasi-steady-state mode, the capacitors in the power circuit of an autonomous current inverter (ACI) act as the primary source for compensating the reactive power of the load and restoring the blocking properties of the thyristors, thereby maintaining the reactive energy balance:

$$Q_{\text{н}} = Q_{\delta} \qquad (1)$$

where: Q_{δ} - is the reactive power required to restore the thyristors' blocking capability;

$Q_{н}$- is the reactive power of the load.

Figures 1 and 2 illustrate that the voltage waveform across the capacitors in a conventional ACI without cut-off valves is nearly sinusoidal, whereas in circuits with cut-off valves, it approaches a trapezoidal shape. Reducing the capacitance value leads to steeper voltage fronts and enrichment of the load voltage with higher harmonics. This redistribution of reactive energy significantly affects commutation stability [[7], [8], [9], [10]].

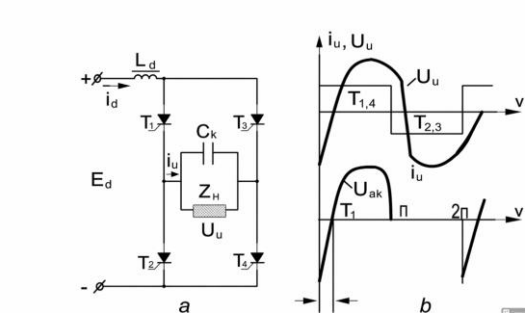

Figure 1 - Scheme (a) and time diagrams (b) of a single-phase ACI

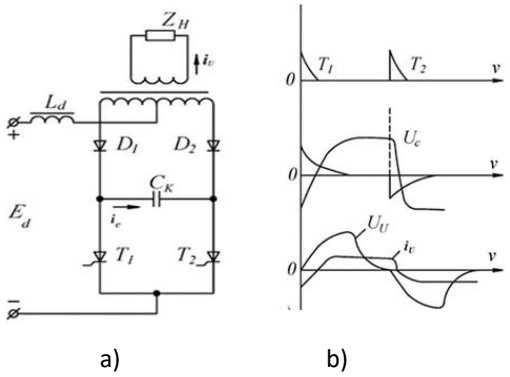

Figure 2 - Scheme (a) and time diagrams (b) of a single-phase ACI with OV

A detailed analysis of the single-phase bridge circuit with cut-off valves (Fig. 3) shows that at the instant of commutation (t = 0), the reverse voltage across the outgoing thyristors is higher due to the energy stored in the load inductance. This enables the cut-off diodes (or thyristors) to maintain the charge on the switching capacitor independently of the instantaneous load voltage.

Equivalent circuits (series and parallel) were derived, and analytical expressions describing the capacitor voltage and current during the recharge intervals were obtained. The structure of the single-phase ACI with DC cut-off is illustrated in Figure 4.

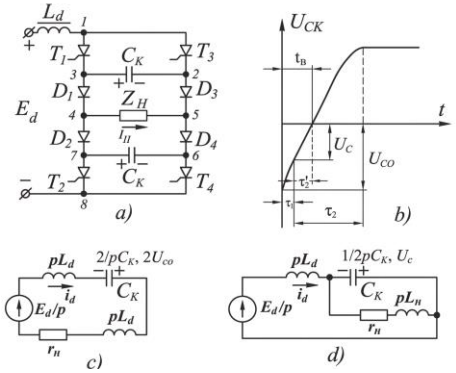

Figure 3 - ACI with S: circuit (a); time diagram of the capacitor voltage (b); replacement circuits (c, d).

Detailed Operation of the ACI with Cut-off Valves

Consider the operation of a single-phase bridge ACI with cut-off valves in quasi-steady-state mode (Fig. 3). At the instant t = 0, when thyristors T3 and T2 are turned on by the control system, thyristors T1 and T4 are instantly reverse-biased and turn off. However, the cut-off diodes do not conduct immediately because the absolute value of the capacitor voltage exceeds the load voltage. The capacitor discharge occurs through the series LC circuit (contour 1-2-3-4-5-6-7-8, see equivalent circuit in Fig. 3c).

When the capacitor voltage reaches zero, the cut-off diodes open, and the load current and capacitor voltage change polarity. The interval for restoring the blocking properties of the outgoing thyristors ends when the capacitor voltage reaches a certain negative value.

To investigate the influence of the switching capacitor charge in series and parallel equivalent circuits, the cut-off diodes were replaced with controlled thyristors, allowing a deliberate delay in their turn-on. This makes it possible to adjust the duration of the series and parallel recharge intervals.

Under simplifying assumptions, the system of equations describing the circuit behavior was derived as follows:

$$\tau_1 < \tau_{11} < (\tau_1 + \tau_2) \qquad (2)$$

For the case of replacing cut-off diodes with thyristors, under the simplifying assumption $i_d(\mathrm{t}) = I_d = const$, the following system of calculation expressions can be obtained for a single-phase ACI with cut-off thyristors:

$$U'_{11} = r_н I_d$$

$$\tau_2 = \frac{\left[\pi - arctg\left(\frac{\Omega_1}{6_1}\right)\right]}{\Omega_1}$$

$$U_{11} = r_н I_d + \frac{[2\Omega_1 L_H I_d \cdot \exp(-6_1\tau_2)]}{\sin\Omega_1\,\tau_2}\tau_1 = C\left(\frac{U_{11}}{I_d - r_н}\right)$$

where:

$$6_1 = \frac{r_н}{2L_H}\ ; \quad \Omega_1 = \left[\frac{1}{(2L_H C) - 6_1^2}\right]^{\frac{1}{2}}. \qquad (3)$$

$$U_{11} = |U_{C0}| = |u_C(\tau_1 + \tau_2)|$$

$$U'_{11} = u_C(\tau_1) = u_н(\tau_1) = u_н(0)$$

Here, τ_1 is characterized as the moment of transition from a serial to a parallel recharge circuit of a switching capacitor Sk.

Suppose the switching on of the cut-off thyristors is delayed relative to the moment t=0 until $u_C(\tau_{11}) = 0$. is obtained. Then, in the interval τ_{11}, a sequential replacement circuit of the charge Cк operates. If you enter the intervalτ_{21} for a parallel circuit, then you can write the inequality:

$$\tau_{11} + \tau_{21} \neq \tau_1 + \tau_2$$

Under the above assumptions, the system of calculation ratios for ACI with cut-off thyristors has the form:

$$U_{11}^1 = 0\,,$$

$$\tau_{21} = \frac{\pi}{2\Omega_1}\,,$$

$$U_{11} = r_H\ I_d + 2\Omega_1 L_H I_d * exp\,(-6_1\,\tau_{21})\,,$$

(4)

$$\tau_{11} = C * U_{11}/\,I_d\,.$$

In the circuit with cut-off thyristors$t_{B1} = \tau_{11}$,, and in the circuit with cut-off diodes$t_B = \tau_1 + \tau_2'$ Obviously, in the latter case, it is necessary to have the expression U_c (t) on the recharge interval in a parallel circuit, and then the value of τ_2' ' is found from the solution of the equation:

$$U_c(\tau_2') = 0. \qquad (5)$$

Analysis of the obtained expressions reveals the following key advantages of ACI circuits with cut-off valves:

a) Due to the energy stored in the load inductance, the voltage across the switching capacitor in the cut-off state is higher than in a conventional parallel ACI at the moment of commutation.

b) The capacitor voltage is independent of the load voltage and operating frequency, which ensures reliable operation of the inverter in variable-frequency drives, even at low frequencies.

c) The charge on the switching capacitor is preserved even during sharp decreases in load voltage between commutations. This provides stable switching under sudden load surges and short-circuit conditions.

d) The use of cut-off thyristors allows controlled variation of the ratio between series and parallel recharge durations, offering additional flexibility in circuit design.

Complete decoupling of the commutation circuit from the load circuit in a single-phase ACI is achieved only when cut-off valves are used [[11], [12]].

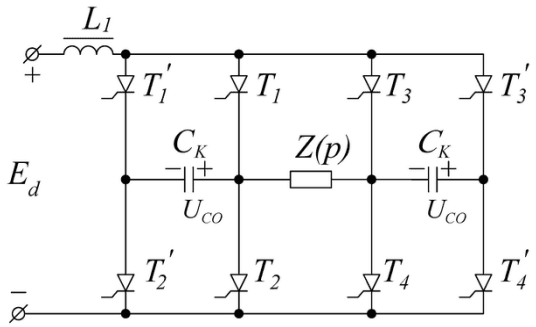

Figure 4 - Single-phase ACI circuit with DC cut-off.

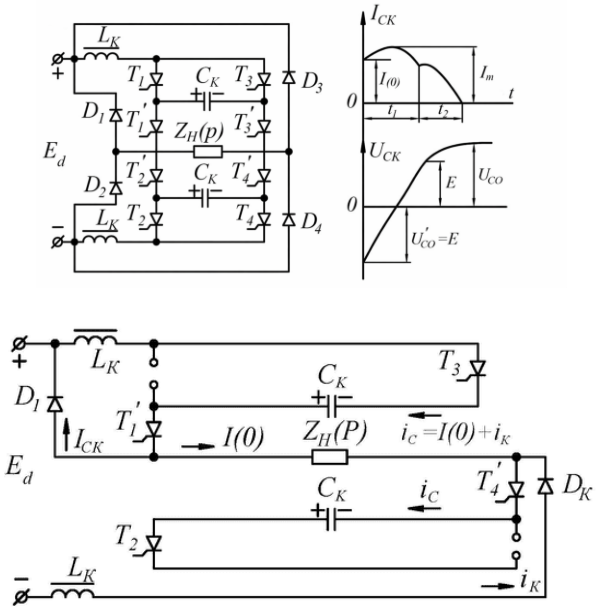

Figure 5 - Single-phase bridge ACI with cut-off valves: (a) circuit diagram; (b) switching circuit through D1 and Dк; (c) switching circuit through D2 and D3; (d) time diagrams.

Compensation of the reactivity of the load in the AIS is carried out due to the reactive current valves and the capacitance of the filter C_{ϕ} connected to the power source E_d or due to inter-phase interactions. It will be shown below that the separation of the $L_{\text{к}}$ From the $C_{\text{к}}$ circuit is possible in a single-phase AIS only in the presence of OF [[13], [14]].

Let's consider the operation of a single-phase bridge circuit of an AI with an OV (Fig. 5).

Discussion of the results

The qualitative analysis demonstrates that the introduction of cut-off valves (diodes or auxiliary thyristors) fundamentally improves the commutation process in autonomous current inverters. The main advantage arises from the decoupling of the switching capacitor recharge circuit from the load during critical intervals. As a result, the voltage across the capacitor at the moment of thyristor turn-off is significantly higher than in conventional parallel autonomous current inverters (ACI), which directly enhances switching stability.

Interpretation of the results shows that the voltage on the commutation capacitor becomes largely independent of the instantaneous load voltage and operating frequency. This property is particularly valuable for variable-frequency electric drives operating at low speeds or under fluctuating loads, where traditional circuits often lose commutation reliability.

Comparison with previous research confirms the obtained findings. In conventional ACI schemes, commutation depends heavily on load parameters, which frequently leads to failures during overloads and short circuits [[15], [16]]. The analyzed circuits with cut-off valves successfully overcome this limitation, which is consistent with earlier reports on auxiliary commutation techniques [[17], [18], [19], [20]]. The observed increase in stored energy from the load inductance further supports the higher reverse bias voltage, aligning with theoretical expectations for forced-commutated thyristor inverters.

Limitations of the study

The present work is based on qualitative theoretical analysis and idealized equivalent circuits, assuming ideal circuit elements. In real devices, losses, parasitic parameters, and non-ideal thyristor recovery characteristics exist, which may quantitatively affect the predicted commutation margins. No new laboratory experiments on a physical prototype were conducted in this study; validation relied on analytical consistency and data from previously published works.

Future research plans

The next stage of the research should include detailed numerical simulation using SPICE or MATLAB/Simulink models with real thyristor parameters, followed by experimental testing on a scaled laboratory prototype under controlled overload and short-circuit conditions. Quantitative comparison of commutation margins, efficiency, and harmonic distortion with conventional circuits will provide stronger practical recommendations for industrial implementation, particularly in mining and other heavy industries.

Conclusion

The conducted qualitative analysis has shown that the use of shut-off valves in autonomous inverter circuits provides a significant improvement in commutation stability and overall operating reliability. Owing to the decoupling of the commutation capacitor from the load circuit, the capacitor is able to retain its maximum voltage between switching intervals, which makes the commutation process substantially less dependent on load conditions. This feature is especially important under variable load operation, overloads, and short-circuit modes, where conventional inverter circuits may experience a deterioration of switching performance. The study confirms that the proposed circuit solutions create more favorable conditions for restoring the blocking properties of thyristors and ensuring stable inverter operation over a wider range of operating regimes. Therefore, inverter circuits with shut-off valves can be considered a promising technical solution for valve frequency converters used in adjustable-speed electric drives, particularly in high-power industrial applications characterized by severe and rapidly changing load conditions. In addition, the identified operating principles may be extended to the development of both current-source and voltage-source inverter systems with enhanced reliability and improved dynamic characteristics. Future research may be directed toward detailed quantitative evaluation, simulation-based verification, and experimental validation of the proposed circuit approaches under real operating conditions.

Conflict of interest. On behalf of all the authors, the corresponding author declares that there is no conflict of interest.

CRediT author statement:

J. Toshov, Y. Abdykenov: Conceptualization, Methodology, Software. **K. Smagulova, A. Zheldikbayeva**: Data curation, Writing draft preparation. **Y. Sarsenbayev, Sh. Umarov**: Visualization, Investigation. **A. Pulatov**: Supervision. **A. Zheldikbayeva**: Software, Validation. **J. Toshov**: Reviewing and Editing.

Cite this article as: Toshov JB, Zheldikbayeva AT, Sarsenbayev Y, Smagulova KK, Umarov Sh, Pulatov A, Abdykenov YK. Qualitative Analysis of the Circuits of Au-Tonomous Inverters with Shut-off Valves. Kompleksnoe Ispolzovanie Mineralnogo Syra = Complex Use of Mineral Resources. 2028; 344(1):38-45. https://doi.org/10.31643/2028/6445.04

Сөндіру клапандары бар автономды инверторлық схемасының сапалық талдауы

[1]Тошов Ж.Б., [2]Желдикбаева А.Т.,[3]Сарсенбаев Е.А.,[2]Смагулова К.К., [1]Умаров Ш.Б., [1]Пулатов А.А., [2]Абдыкенов Е.К.

[1] Ислам Кәрім атындағы Ташкент Мемлекеттік Техникалық Университеті, Ташкент, Өзбекстан
[2]Ә. Сағынов атындағы Қарағанды техникалық университеті, Қарағанды, Қазақстан
[3] Сәтбаев университеті, Алматы, Қазақстан

Мақала келді: *17 мамыр 2025*
Сараптамадан өтті: *2 маусым 2025*
Қабылданды: *24 сәуір 2026*

ТҮЙІНДЕМЕ

Мақалада ажыратқыш (сөндіру) клапандары бар автономды ток және кернеу инверторларының схемаларын сапалық талдау нәтижелері келтірілген. Параллель және тізбекті эквивалентті схемалардағы коммутациялық конденсатордың зарядының инвертордың қуат тізбегіндегі тиристорлардың коммутациялық қасиеттерін қалпына келтіруге әсері зерттелген. Жүктеменің индуктивті элементтерінде мезгіл-мезгіл жинақталатын энергияның арқасында ажыратылған күйдегі коммутациялық конденсатордағы кернеу әдеттегі параллельді автономды ток инверторына қарағанда жоғары болатыны көрсетілген. Бұл инвертордың коммутациялық тұрақтылығын арттырады.

	Нәтижесінде ажыратқыш клапандары бар автономды ток инверторының схемасы айнымалы жиілікті электр жетектеріне арналған вентильді түрлендіргіштерде жұмыс істейді және кенеттен жүктеме секірістері мен қысқа тұйықталулар кезінде де өзінің жұмыс қабілеттілігін сақтайды, өйткені коммутациялық конденсатордағы кернеу жүктеме кернеуіне тәуелді емес. Сонымен, коммутациялық конденсатордың заряды тиристорларды ауыстыру аралығында жүктеме кернеуі күрт төмендеген кезде де сақталады.
	Түйін сөздер: автономды тоқ инверторы, ажыратқыш клапандар, коммутациялық конденсатор, коммутациялық тұрақтылық, айнымалы жиілікті электр жетегі.
Тошов Жавохир Буриевич	***Авторлар туралы ақпарат:*** *Техника ғылымдарының докторы, Ислам Кәрім атындағы Ташкент Мемлекеттік Техникалық Университетінің профессоры, 100095, Алмазар ауданы, Университетская көшесі 2, Ташкент, Өзбекстан. E-mail: j.toshov@tdtu.uz;ORCID ID: https://orcid.org/0000-0003-4278-1557*
Желдикбаева Айсауле Такеновна	*Әбілқас Сағынов атындағы Қарағанды техникалық университеті, Өндірістік процестерді автоматтандыру кафедрасының PhD докторанты, 100027, Нұрсұлтан Назарбаев даңғ. 56, Қарағанды, Қазақстан. E-mail: aisaule89@mail.ru; ORCID ID: https://orcid.org/0009-0005-1325-5576*
Сарсенбаев Ерлан Алиаскарович	*PhD, доцент, Сәтбаев Университеті, Энергетика кафедрасының меңгерушісі, 050013, Сәтбаев көшесі, 22, Алматы, Қазақстан. E-mail: y.sarsenbayev@satbayev.university; ORCID ID: https://orcid.org/0000-0002-8887-1171*
Смагулова Каршыга Канатовна	*PhD докторы, Әбілқас Сағынов атындағы Қарағанды техникалық университеті, Өндірістік процестерді автоматтандыру кафедрасының PhD доценті, 100027, Нұрсұлтан Назарбаев даңғ. 56, Қарағанды, Қазақстан. E-mail: smagulovakk@mail.ru; ORCID ID: https://orcid.org/0000-0001-6834-8490*
Омаров Шухрат Бадретдинович	*Техника ғылымдарының докторы, Электр машиналары және жүргізушілер техникасы кафедрасының профессоры, Ислам Кәрім атындағы Ташкент Мемлекеттік Техникалық Университеті, 100095, Алмазар ауданы, Университетская көшесі 2, Ташкент Өзбекстан. E-mail: shumarov1951@mail.ru; ORCID ID: https://orcid.org/0000-0002-9262-4683*
Пулатов Аброр Абидович	*Ph.D., доцент, Электр машиналары және жүргізушілер техникасы кафедрасының меңгерушісі, Ислам Кәрім атындағы Ташкент Мемлекеттік Техникалық Университеті, 100095, Алмазар ауданы, Университетская көшесі 2, Ташкент, Өзбекстан. E-mail: abrorobidovich@mail.ru; ORCID ID: https://orcid.org/0000-0002-2641-571X*
Абдыкенов Ержан Канатулы	*Әбілқас Сағынов атындағы Қарағанды техникалық университеті, Өндірістік процестерді автоматтандыру кафедрасының PhD докторанты, 100027, Нұрсұлтан Назарбаев даңғ. 56, Қарағанды, Қазақстан. E-mail: erzhan_aiu@mail.ru; ORCID ID: https://orcid.org/0009-0008-0095-576X*

Качественный анализ схем автономных инверторов с запорными клапанами

[1]Тошов Ж.Б., [2]Желдикбаева А.Т.,[3]Сарсенбаев Е.А.,[2]Смагулова К.К., [1]Умаров Ш.Б., [1]Пулатов А.А., [2]Абдыкенов Е.К.

[1] Ташкентский государственный технический университет имени Ислама Карима, Ташкент, Узбекистан
[2] Карагандинский технический университет имени А. Сагинова, Караганда, Казахстан
[3] Satbayev University, Алматы, Казахстан

Поступила: *17 мая 2025*
Рецензирование: *2 июня 2025*
Принята в печать: *24 апреля 2026*

АННОТАЦИЯ

В статье представлены результаты качественного анализа схем автономных инверторов тока и напряжения с запорными (отсечными) вентилями. Исследовано влияние величины заряда коммутирующего конденсатора в параллельных и последовательных схемах замещения на восстановление коммутационных свойств тиристоров силовой цепи инвертора. Показано, что благодаря энергии, периодически накапливаемой в индуктивных элементах нагрузки, напряжение на коммутирующем конденсаторе в отключённом состоянии выше, чем в обычном параллельном автономном инверторе тока. Это обеспечивает повышение коммутационной устойчивости инвертора. В результате схема автономного инвертора тока с запорными вентилями сохраняет работоспособность в вентильных преобразователях для частотно-регулируемых электроприводов и остаётся работоспособной при внезапных бросках нагрузки и коротких замыканиях, поскольку напряжение на коммутирующем конденсаторе не зависит от напряжения нагрузки. Таким образом, заряд коммутирующего конденсатора сохраняется даже при резком снижении напряжения нагрузки в промежутках между коммутациями тиристоров.

Ключевые слова: автономный инвертор тока, запорные вентили, коммутирующий конденсатор, коммутационная устойчивость, частотно-регулируемый электропривод.

Тошов Жавохир Буриевич	***Информация об авторах:*** *Доктор технических наук, профессор Ташкентского государственного технического университета имени Ислама Карима, 100095, Алмазарский район, улица Университетская 2, Ташкент, Узбекистан. E-mail: j.toshov@tdtu.uz; ORCID ID: https://orcid.org/0000-0003-4278-1557*
Желдикбаева Айсауле Такеновна	*PhD докторант кафедры Автоматизации производственных процессов, Карагандинский технический университет имени А. Сагинова, 100027, пр. Нурсултана Назарбаева, 56, Караганда, Казахстан. E-mail: aisaule89@mail.ru; ORCID ID: https://orcid.org/0009-0005-1325-5576*
Сарсенбаев Ерлан Алиаскарович	*PhD, Доцент, заведующий кафедрой энергетики, Satbayev University, 050013, ул. Сатбаева. 22, Алматы, Казахстан. E-mail: y.sarsenbayev@satbayev.university; ORCID ID: https://orcid.org/0000-0002-8887-1171*
Смагулова Каршыга Канатовна	*Доктор PhD, доцент кафедры Автоматизации производственных процессов, Карагандинский технический университет имени А. Сагинова, 100027, пр. Нурсултана Назарбаева, 56, Караганда, Казахстан. E-mail: smagulovakk@mail.ru; ORCID ID: https://orcid.org/0000-0001-6834-8490*
Омаров Шухрат Бадретдинович	*Доктор технических наук, профессор кафедры Электрические машины и приводное оборудование, Ташкентский государственный технический университет имени Ислама Карима, 100095, Алмазарский район, улица Университетская 2, Ташкент, Узбекистан. E-mail: shumarov1951@mail.ru; ORCID ID: https://orcid.org/0000-0002-9262-4683*
Пулатов Аброр Абидович	*Ph.D., доцент, заведующий кафедрой Электрические машины и приводное оборудование, Ташкентский государственный технический университет имени Ислама Карима, 100095, Алмазарский район, улица Университетская 2, Ташкент, Узбекистан. E-mail: abrorobidovich@mail.ru; ORCID ID: https://orcid.org/0000-0002-2641-571X*
Абдыкенов Ержан Канатулы	*PhD докторант кафедры Автоматизации производственных процессов, Карагандинский технический университет имени А. Сагинова, 100027, пр. Нурсултана Назарбаева, 56, Караганда, Казахстан. E-mail: erzhan_aiu@mail.ru; ORCID ID: https://orcid.org/0009-0008-0095-576X*

References

[1] Volkov AV, Kosenko AI. Issledovanie energeticheskikh parametrov asinkhronnogo elektroprivoda na baze avtonomnogo invertora toka [Investigation of the energy parameters of an asynchronous electric drive based on an autonomous current inverter]. Electrotechnical and Computer Systems. 2011; 3(79):40-42. (In Russ).

[2] Umarov Sh, Sapaev Kh, Mirsaidov M, Ruzmatov A. Ensuring design reliability of three phase parallel inverter with cut-off valves by improving the efficiency of its mathematical modeling. Meterials of compliance with AIP Conf. Proc. 2023; 2552(1). https://doi.org/10.1063/5.0111343

[3] Egorov AN, Semenov AS, Fedorov OV. Prakticheskiy opyt ispolzovaniya pribora POWER FLEX 7000 v gornodobyvayushchey promyshlennosti [Practical experience of using the POWER FLEX 7000 device in the mining industry]. NSTU Publishing House. 2017; 4:86-93. (In Russ).

[4] Rakhmonov IU, Ushakov VYa, Niyozov NN, Kurbonov NN. Prognozirovanie elektropotrebleniya s pomoshchyu neyronnykh setey c LSTM [Forecasting electricity consumption by LSTM neural network. Bulletin of the Tomsk Polytechnic University. Geo Assets Engineering]. 2023; 334(12):125–133. (In Russ.). https://doi.org/10.18799/24131830/2023/12/4407

[5] Cahyana Y, Verrell C, Kriswanda D, Aulia GA, Yusra NA, Marta H, Sukri N, Safarov JE, Sultanova ShA. Properties comparison of oxidized and heat moisture treated (HMT) starch-based biodegradable films. Polymers. 2023; 15(9):2046. https://doi.org/10.3390/polym15092046

[6] Rakhmonov IU, Ushakov VYa, Niyozov NN, Kurbonov NN. Prognozirovanie elektropotrebleniya na osnove metoda glavnykh komponent (PCA) [Forecasting electricity consumption using the principal component analysis method. Bulletin of the Tomsk Polytechnic University]. Geo Assets Engineering. 2024; 335(12):198–209. (In Russ.) https://doi.org/10.18799/24131830/2024/12/4731

[7] Zhu S, Liu K, Qin L, et al. 'Global assessment of the asymptotic stability of three-phase inverters with saturation', electron energy analysis. 2018; 11(9):1556-1565.

[8] Mekhtiyev A, Dunayev P, Neshina Y, Alkina A, Aimagambetova R, Mukhambetov G, et al. Power supply via fiber-optical conductor for sensors of mine working monitoring system. Eastern-European Journal of Enterprise Technologies. 2023; 5(5(125)): 15–23. https://doi.org/10.15587/1729-4061.2023.289775

[9] Chen SL, Gerner FM, Tien CL. General film condensation correlations, Exp. Heat Transfer. 1987; 1:93–107. http://dx.doi.org/10.1080/08916158708946334

[10] Toshov ZhB, Rahutin MG, Toshov BR, Baratov BN. Tracking prevention in roller cone bit drilling. Eurasian Mining. 2024; 1:62–66. https://doi.org/10.17580/em.2024.01.15

[11] Kubín M, Hirš J, Plášek J. Experimental analysis of steam condensation in vertical tube with small diameter. Int. J. Heat Mass Transfer. 2016; 94:403-410.

[12] Rabatuly M, Myrzathan SA, Toshov JB, Nasimov J, Khamzaev A. Views on drilling effectiveness and sampling estimation for solid ore minerals. Kompleksnoe Ispolzovanie Mineralnogo Syra = Complex Use of Mineral Resources. 2026; 336(1):5-14. https://doi.org/10.31643/2026/6445.01

[13] Roetzel W. Laminar film condensation in tubes; calculation of local film resistance and local adiabatic mixing temperature, Int. J. Heat Mass Transfer. 1973; 16:2297–2304. http://dx.doi.org/10.1016/0017-9310(73)90015-X

[14] Seban RA, Hodgson JA. Laminar film condensation in a tube with upward vapor flow, Int. J. Heat Mass Transfer. 1982; 25:1291–1300. http://dx.doi.org/10.1016/0017-9310(82)90123-5

[15] Chen SL, Gerner FM, Tien CL. General film condensation correlations, Exp. Heat Transfer. 1987; 1:93–107. http://dx.doi.org/10.1080/08916158708946334

[16] Toshov JB, Eshkuvatov LM, Smagulova KK, Zheldikbayeva AT, Rabatuly M, Tashbayev NN, Madaminova G. Study of Steam Condensation on Vertical Finned Tubes. Kompleksnoe Ispolzovanie Mineralnogo Syra = Complex Use of Mineral Resources. 2026; 338(3):21-28. https://doi.org/10.31643/2026/6445.25

[17] Liao Y, Guentay S, Suckow D, Dehbi A. Reflux condensation of flowing vapor and non-condensable gases counter-current to laminar liquid film in a vertical tube, Nuclear Eng. Des. 2009; 239:2409–2416.

[18] Rabatuly M, Demin VF, Kenetaeva AA, Steflyuk YuYu, Toshov JB. Evaluation of modern methods and techniques for calculating parameters during coal bed degassing. Kompleksnoe Ispolzovanie Mineralnogo Syra = Complex Use of Mineral Resources. 2025; 334(3):110-120. https://doi.org/10.31643/2025/6445.33

[19] Toshov JB, Fozilov DM, Yelemessov KK, Ruziev UN, Abdullayev DN, Baskanbayeva DD, Bekirova LR. Povysheniye stoykosti zub'yev burovykh dolot za schet izmeneniya tekhnologii ikh izgotovleniya [Increasing the durability of drill bit teeth by changing their manufacturing technology]. Obrabotka metallov (tekhnologiya, oborudovaniye, instrumenty) [Metal processing (technology, equipment, tools)]. 2024; 26(4):112–124. (In Russ.). http://dx.doi.org/10.17212/1994-6309-2024-26.4-112-124

[20] Oumayma Boukria, El Mestafa El Hadrami, Aysha Sameen, Amna Sahar, Sipper Khan, Jasur Safarov, Shakhnoza Sultanova, Françoise Leriche, Abderrahmane Aït-Kaddour. Biochemical, physicochemical and sensory properties of yoghurts made from mixing milks of different mammalian species: a review. Foods. 2020; 9(11):1722.

Crossref
DOI: 10.31643/2028/6445.05
Mining & Mineral Processing

Biogenic Amine Determination by High-Performance Liquid Chromatography Using a Sol-Gel-Immobilized 2-Hydroxy-5-nitrobenzaldehyde-2,4-dinitro phenyl hydrazone Solid-Phase Extractant

[*1]Abdassalam Abdelhafiz Tameem, [1]Salam Salhin Mohamed, [1]Afiyah S. Alnaas, [2] Eny Kusrini

[1]Sirte University, Sirte, Libya
[2]Universitas Indonesia, Depok 16424, West Java, Indonesia

** Corresponding author email: salam1961@su.edu.ly*

Received: *March 4, 2026*
Peer-reviewed: *April 14, 2026*
Accepted: *April 29, 2026*

ABSTRACT

This study focuses on the solid phase extraction of biogenic amines (BAs) using a sol-gel adsorbent immobilized with a hydrazone ligand, named 2-hydroxy-5-nitrobenzaldehyde-2,4-dinitrophenylhydrazone. The hydrazone compound was synthesized and characterized through Fourier Transform Infrared Spectroscopy (FT-IR) and Nuclear Magnetic Resonance (NMR) spectroscopy. The efficiency of the sorbent material for extracting BAs was evaluated using the solid phase extraction (SPE) method. Key experimental parameters affecting BA extraction, including pH, equilibrium time, ligand concentration, and biogenic amine (BA) concentration, were systematically investigated. The results indicated a strong recovery of BAs from aqueous samples, demonstrating a significant affinity between the sol-gel matrix containing the hydrazone ligand and the target analytes. The findings demonstrate that incorporating the hydrazone ligand resulted in a marked enhancement of extraction efficiency at a concentation of 17×10^{-3} M. Notably, the method exhibited high selectivity for aliphatic biogenic amines such as putrescine (PUT), cadaverine (CAD), and spermidine (SPD). This extraction method was successfully applied to food samples, yielding good recovery rates.

Keywords: HPLC, SPE, extraction, Bas, Sol-Gel.

Information about authors:

Abdassalam Abdelhafiz Tameem — *Faculty of Education, Sirte University, Sirte, Libya. Email: salam1961@su.edu.ly*

Salam Salhin Mohamed — *Faculty of Science, Sirte University, Sirte, Libya. Email: salam_salhin@su.edu.ly*

Afiyah S. Alnaas — *Faculty of Education, Sirte University, Sirte, Libya. Email: salam_salhin@su.edu.ly*

Eny Kusrini — *Department of Chemical Engineering; Green Product and Fine Chemical Engineering Research Group; Advanced Materials Research Center, Faculty of Engineering, Universitas Indonesia, Depok 16424, West Java, Indonesia. Email: eny.k@ui.ac.id*

Introduction

Biogenic amines (BAs) are low-molecular-weight nitrogenous compounds primarily formed through the decarboxylation of amino acids, as well as through amination and transamination reactions during metabolic processes. This decarboxylation removes the α-carboxyl group, yielding the corresponding amine [1]. BAs can have aliphatic, aromatic, or heterocyclic structures and are found in various food products, biological fluids, and environmental samples. The study of BAs is significant because they serve as biomarkers in toxicological risk assessments and indicators of food quality [2].

The toxicological effects of BAs vary significantly, with toxicity values largely dependent on the efficiency of detoxification mechanisms for each compound. Food products that undergo natural fermentation, such as cheese, soybean products, and alcoholic beverages, are particularly susceptible to BAs due to the presence of contaminating microflora that exhibit amino acid decarboxylase activity [3]. Numerous studies have reported the presence of BAs in various contexts, including human tissues [3], plants [4], and food products like fish and seafood [[5], [6]], meat products [[7], [8]], bean products [9], fruits and vegetables [[10], [11]], and beverages [[12], [13]]. Notable biogenic amines, such as histamine, tyramine, putrescine, cadaverine, spermidine, and spermine, are significant due to their physiological activity and potential adverse health effects at high concentrations [14]. Therefore, accurately determining the levels of

biogenic amines is crucial for food quality control, clinical analysis, and environmental monitoring.

Several analytical methods, including liquid-liquid extraction (LLE), liquid-phase microextraction (LPME), solid-phase extraction (SPE) [15], and solid-phase microextraction (SPME) [16], as well as techniques such as spectrophotometry [17], capillary electrophoresis [18], gas chromatography [19], and high-performance liquid chromatography (HPLC) [20], have been developed for this purpose. Among these, HPLC is particularly favored for its high sensitivity, selectivity, and compatibility with a wide range of analytes. However, directly measuring biogenic amines can be challenging due to their high polarity, lack of strong chromophores, and low concentrations in complex matrices [21]. Therefore, an effective sample preparation step is often necessary to enhance detection limits and minimize matrix interferences. The SPE method has emerged as a widely used sample preparation technique due to its simplicity, high enrichment capability, and low solvent consumption. The effectiveness of this method largely depends on the type of sorbent material used [22]. Recently, the development of selective and chemically modified sorbents has garnered significant attention. Notably, sol–gel technology offers considerable advantages for sorbent preparation, including high chemical and thermal stability, controllable porosity, and the ability to immobilize functional organic ligands within an inorganic framework [[23], [24]]. This study aimed to extract biogenic amines (BAs) using a solid-phase method with a sol-gel adsorbent that had been modified with the hydrazone ligand 2-hydroxy-5-nitrobenzaldehyde-2,4-dinitro phenyl hydrazone. The amounts of these amines were then measured with high-performance liquid chromatography (HPLC).

Experimental part

Materials

2,4-Dinitrophenylhydrazine (DNPH) (Aldrich), 2-Hydroxy-5-nitrobenzaldehyde (Fluka), cadaverine (CAD) dihydrochloride, histamine (HIS) dihydrochloride, putrescine (PUT) dihydrochloride, β-phenylethylamine (PEA) dihydrochloride, spermidine (SPD) trihydrochloride, tryptamine (TRY) hydrochloride, and tyramine (TYR) hydrochloride were all obtained from Sigma-Aldrich. Dansyl chloride (Dns-Cl) (Fluka), hydrochloric acid (Across), L-glutamic acid monosodium monohydrate (Across), sodium hydroxide (Across), sodium hydrogen carbonate (Across), sulfuric acid (Across), tetraethoxysilane (TEOS) (Sigma-Aldrich), and tris(hydroxymethyl)aminomethane (Tris) (Sigma-Aldrich) were also used. All chemicals and reagents were used as received without further purification.

Instruments

Elemental analysis (CHN) of the ligand and its sorbent material were carried out using a Perkin–Elmer 240011 elemental analyzer. Infrared analysis was performed on a Perkin–Elmer 2000 FT–IR unit using a KBr system. The structure of the ligand was further confirmed by H NMR using a Bruker 400 MHz spectroscopy. Thermogravimetric analyses (TGA) were carried out using a Perkin–Elmer Thermo Gravimetric Analyzer TGA 7 under nitrogen gas, scanning rate of 10 °C/min. A Perkin-Elmer Lambda 35 (dual beam) spectrophotometer was used to record the spectra of the ligand and sorbent material. A Perkin Elmer 200-series HPLC unit consisting of a pump, vacuum degasser, auto sampler, diode array detector, and C_{18} ODS Hypersil column (250 × 4.5 mm, 5 µm) was used. The mobile phase was acetonitrile: water: methanol: (60: 25: 15) at a flow rate of 1.0 mL min^{-1}.

Synthesis of 2-hydroxy-5-nitrobenzaldehyde-2,4-dinitrophenylhydrazone

The ligand was synthesized as previously reported by Tameem et al. [25]. A solution containing 0.0057 M (1.6 g) of DNPH in 30 mL of ethanol was thoroughly mixed with 0.0081 M (1.35 g) of 2-hydroxy-5-nitrobenzaldehyde in 10 mL of ethanol. An orange solid precipitate formed, which was then filtered and dried overnight in an oven at 70 °C. The yield was 2.65 g (94%), with a melting point of 300 °C (Figure 1).

Preparation of the sorbent

The sorbent was prepared as previously reported [25]. The ligand was physically immobilized in the silica sol–gel matrix by stirring a mixture of TEOS (3.28 mL), ethanol (4.56 mL), and HCl (0.36 mL, 4 M) in a 50 mL beaker for 15 minutes to create a sol solution. An appropriate amount (0.017 g) of the hydrazone ligand (L), dissolved in 10 mL of THF, was added to the sol solution and stirred vigorously for 45 minutes. After homogenization, the mixture was aged in an oven at 60 ºC for 2 days. The sol-gel product was then soaked in water for 1 day for conditioning and subsequently dried at 60 ºC. A blank sorbent was prepared similarly, without the ligand.

Extraction of biogenic amine

The extraction process of BAs was conducted according to our previously reported method [[25], [26]] using a batch extraction technique. A 25 mg sorbent was placed in a glass vial with 1 mL of a BAs standard mixture (100 mg L-1) and 4 mL of 0.1 M Tris buffer (pH 8-10). The vial was then shaken mechanically at room temperature for 30 minutes. After the equilibrium period, the mixture was processed as previously described [25]. The percentage of extraction was calculated using the following equation:

$$\%E = \frac{C_0 - C}{C_0} \times 100$$

where, C_0 and C are the BA concentration (mg. L^{-1}) in the solution before and after extraction, respectively.

Results and discussion

Extraction of biogenic amine

The extraction process of BAs was conducted according to our previously reported method [[25], [26]] using a batch extraction technique. A 25 mg sorbent was placed in a glass vial with 1 mL of a BAs standard mixture (100 mg L-1) and 4 mL of 0.1 M Tris buffer (pH 8-10). The vial was then shaken mechanically at room temperature for 30 minutes. After the equilibrium period, the mixture was processed as previously described [25]. The percentage of extraction was calculated using the following equation:

$$\%E = \frac{C_0 - C}{C_0} \times 100$$

where, C_0 and C are the BA concentration (mg. L^{-1}) in the solution before and after extraction, respectively.

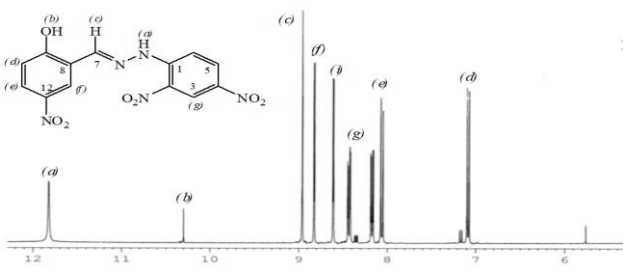

Figure 1 - HNMR of 2-Hydroxy-5-nitrobenzaldehyde-2,4-dinitrophenylhydrazone

Characterization of sol-gel sorbent

Solid UV-Vis analysis

The FTIR analysis did not provide conclusive evidence of hydrazones in the gel matrix, as the spectra of the blank and the sorbent were too similar. This lack of distinction is likely due to the very small amounts of ligand present in the network, a challenge noted by other researchers [[27], [28]]. Subsequently, solid-state UV-Visible analysis was conducted. A comparison was made between the free ligand and its corresponding sol-gel sorbent using solid-state UV-Vis spectroscopy in the 200 to 800 nm range. The free ligand exhibited a maximum absorption (λ_{max}) at 382 nm, which displayed a red shift compared to the sol-gel sorbent, which had a λmax of 381 nm (Figure 2). The notable difference between the spectra of the blank and the sorbent provides strong evidence for the successful incorporation of the hydrazone ligand into the sol-gel network. This slight shift may be attributed to intermolecular interactions between the ligand and silica, which could alter the characteristics of the absorption spectra [[27], [28]]

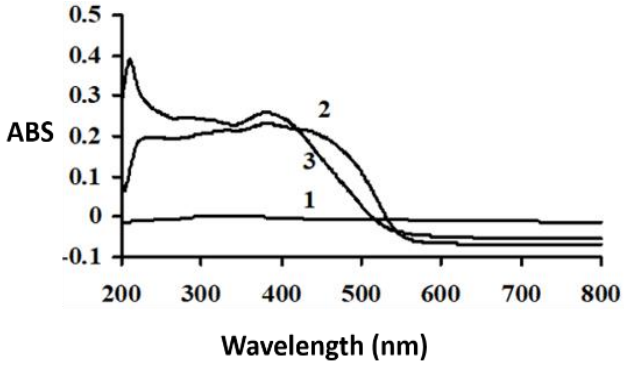

Figure 2 - UV-Vis spectra of (1) the blank sol-gel sorbent, (2) free ligand (2) and (3) sol-gel sorbent

HPLC conditions

An earlier HPLC method [25] was utilized to separate BA using a three-solvent mobile phase mixture: methanol (MeOH) (0.0 - 20%), water (20 - 40%), and acetonitrile (ACN) (50 - 70%). The flow rate was maintained between 0.8 and 1.4 mL min^{-1} at ambient temperature. The optimal separation occurred at a flow rate of 1.0 mL min^{-1} with a mobile phase composition of 60:25:15 (v/v/v) (ACN:H_2O:MeOH). Under these conditions, dansylated amines were detected at 254 nm, and all components of BA were eluted in under 18 minutes. To assess the linearity of the response, a standard mixture of BA was prepared, ranging from 0.001 to

50 mg L^{-1}, and injected. Calibration graphs for each BA were created by plotting the peak area against concentration

Optimized parameters for extraction

The effect of pH

The study examined the impact of sample pH on extraction efficiency. It was determined that the optimal pH range for the quantitative extraction of BA lies between 8 and 11 (Figure 3). Within this range, the sorbent achieved extraction efficiencies close to 100%, particularly for SPD, followed by CAD and His. Deprotonation occurs at the N-H amino group [[26], [29]], enhancing delocalization resonance and creating additional charge interactions between the protic BA and the N-H group. This finding underscores the significant role of ligand polarity in the interaction between the studied sorbent material and amines within this pH range [26]. Conversely, the low extraction efficiency observed in acidic conditions may result from the high ionization potential of BA at lower pH levels or repulsion between the protic BA and the protic (N-H) group on the ligand. Additionally, the sorbent material contains a ligand with an extra polar OH group, which may enhance electrostatic interactions with BA.

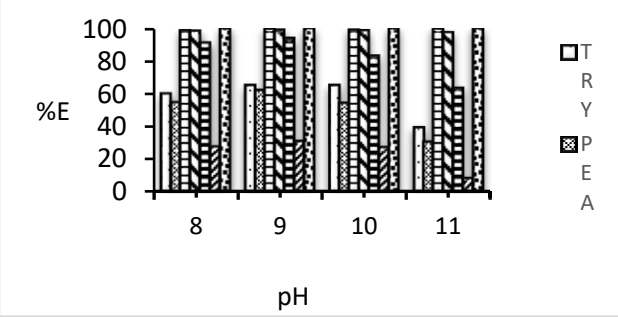

Figure 3 - Effect of pH on the extraction of BA (20 mg L^{-1}).

Effect of contact time

The effect of contact time on the extraction efficiency was studied by shaking the BA mixture with the adsorbent, ranging from 5 to 60 min at optimum pH 9. Good extraction (%E > 70 %) was observed after 5 min of contact time for all studied amines (Figure 4). The process was maximized after 30 min of contact time, especially for SPD, CAD, and PUT. No significant effect on extraction was observed after this. Therefore, 30 min contact time was chosen for subsequent studies [30].

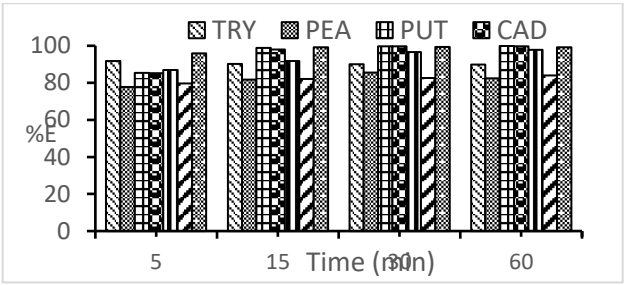

Figure 4 - Effect of contact time on the extraction of BA (20 mg L^{-1}); pH 9.

Effect of ligand concentration in the sol - gel network

The effect of the concentration of the immobilized ligand on the extraction efficiency of BAs was also examined. A 25 mg sample of the adsorbent with varying ligand concentrations ranging from 8.5 to 68 × 10^{-3} M was used to extract 20 mg L^{-1} BAs from an aqueous solution at the optimal pH of 9. More than 80% of BA was extracted when 17 × 10^{-3} M of the ligand was used (Figure 5). Increasing the ligand concentration beyond this point did not further enhance extraction efficiency. In contrast, no extraction was observed in the absence of the ligand (Blank sol-gel). These results indicate that the addition of the hydrazone ligand significantly improved extraction efficiency [31].

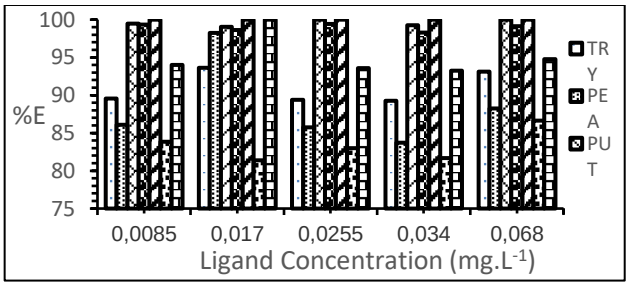

Figure 5 - Effect of ligand concentration on the extraction of BA, pH 9, contact time 30 min.

Effect of biogenic amine

Five different concentrations (5.0-500 mg L^{-1}) of BAs were used to evaluate the extraction efficiency and capacity of the sorbent. It was found that at lower concentrations (5 mg L^{-1}), most of the studied BAs, including SPD, TRY, P

UT, CAD, and HIS were extracted efficiently (100% extraction) (Figure 6). The sorbent demonstrated high extraction efficiency for SPD even at 500 mg L-1. However, a decrease in extraction efficiency was observed at concentrations higher than 200 mg L^{-1}. Among the BAs, the aromatic

compounds (HIS, TYR, PEA) were extracted the least effectively within this concentration range [33].

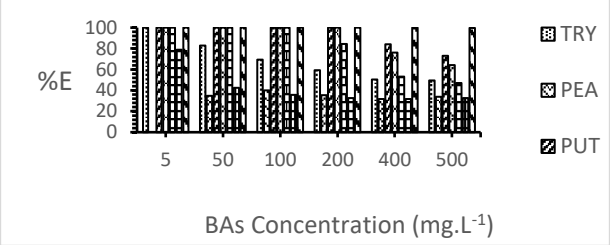

Figure 6 - Effect of biogenic amine (BA) concentration on the extraction.

Capacity of sorbents

The capacity of the sorbent material was found to be dependent on the initial concentration of these analytes in the solution (Figure 7). As the concentration of SPD, PUT, CAD, and HIS increase, the capacity value of the sorbent also increases (PUT > HIS > SPD > CAD). The highest value of the capacity was found for PUT (0.0023 - 0.220 mmol g^{-1}). The capacity of this sorbent is slightly inferior when compared to the sorbents based on silica gel immobilized aliphatic amines and imprinted organic – inorganic hybrid (e.g., 0.1 - 3.1 mmol g^{-1}) but higher than the sorbents based on the immobilized ligands such as crown ethers (0.0016 – 033 and 0.0038 – 0.00086 mmol g^{-1}) [[34], [35]].

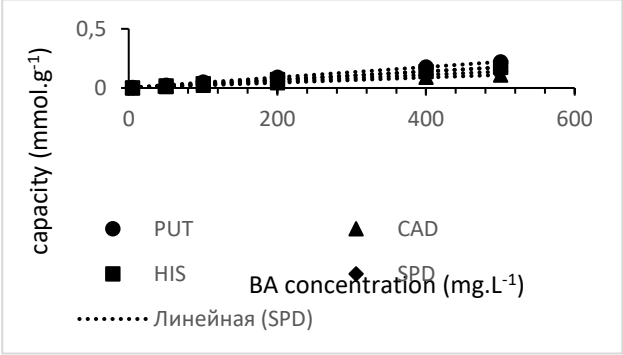

Figure 7 - The capacity of sorbent (mmol g^{-1}) with different concentrations of BA.

Adopted extraction conditions

The adopted extraction conditions were: pH, 9; contact time, 30 min; ligand concentration, 17×10^{-3} M; sorbent mass, 25 mg; and room temperature, 25 °C.

Extraction of BA from food samples

The proposed method was applied for the extraction and determination of biogenic amines (BAs) in ketchup. Table 1 presents the recovery results. Representative chromatograms of the unspiked sample extract (Figure 8) and the spiked sample (5 mg L^{-1} BA) before and after extraction (Figure 9) are included. The effectiveness of the sorbent in removing BA from the sample matrices is evident. All food samples achieved satisfactory recoveries of over 85% for the spiked 5 mg L^{-1} BA. Additionally, good recoveries were observed for putrescine (PUT), cadaverine (CAD), and spermidine (SPD). These high recovery rates for PUT, CAD, and SPD from food matrices suggest that this method can be successfully applied for determining these BAs in various foods [[36], [37], [38]].

Table 1 - Recoveries (%) of BA from spiked (5 mg L^{-1} BA) ketchup food sample.

	BA						
	TRY	PEA	PUT	CAD	HIS	TYR	SPD
%E	93.7	85.6	100	100	90.1	88.0	99.0
±SD	1.9	2.0	1.3	0.1	0.3	0.8	0.0

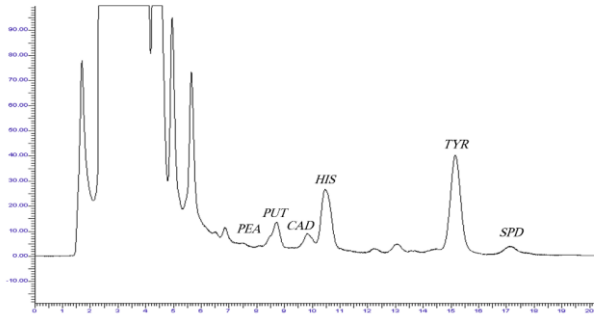

Figure 8 - Chromatogram of ketchup extract. Peak identification.

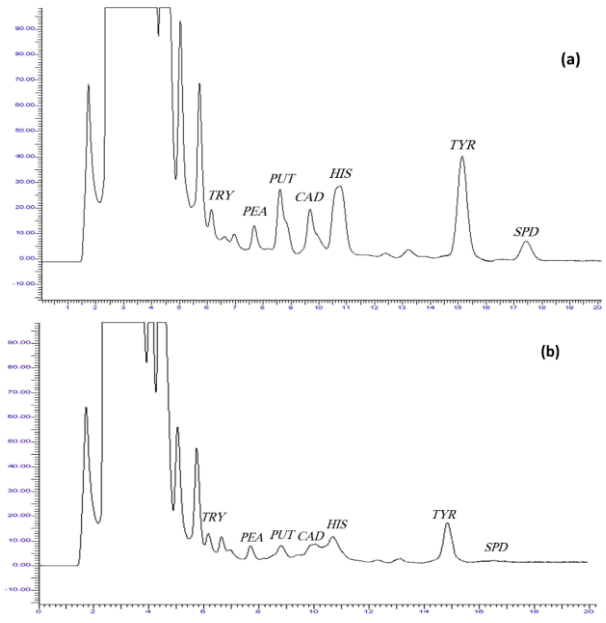

Figure 9 - Chromatogram of ketchup extract, spiked with 5 mg L^{-1} BA, (a) Before extraction and (b) after extraction.

Conclusion

The hydrazone ligand, synthesized and immobilized within a sol-gel matrix, was evaluated for its performance in solid-phase extraction (SPE) of biogenic amines (BAs). Derived from 2-hydroxy-5-nitrobenzaldehyde-2,4-dinitrophenylhydrazone, this sorbent demonstrated marked selectivity towards aliphatic biogenic amines, including putrescine (PUT), cadaverine (CAD), and spermidine (SPD). The enhanced extraction efficiency stems from the strong interaction between the hydrazone-containing sol-gel matrix and the target analytes. This approach proved effective for extracting biogenic amines from ketchup samples. Furthermore, hydrazone compounds offer a significant advantage over crown ether-based sorbents by enabling straightforward single-step synthesis at ambient temperature [[25], [38]].

Conflicts of interest. Authors declare no conflict of interest.

CRediT author statement: **A.A. Tameem:** Conceptualization, Methodology, Software. **S.S. Mohamed**: Data curation, Writing draft preparation. **A.S. Alnaas**: Visualization, Investigation. **E. Kusrini**: Reviewing and Editing

Cite this article as: Abdassalam Abdelhafiz Tameem, Salam Salhin Mohamed, Afiyah S Alnaas, Eny Kusrini. Biogenic Amine Determination by High-Performance Liquid Chromatography Using a Sol-Gel-Immobilized 2-Hydroxy-5-nitrobenzaldehyde-2,4-dinitro phenyl hydrazone Solid-Phase Extractant. Kompleksnoe Ispolzovanie Mineralnogo Syra = Complex Use of Mineral Resources. 2028; 344(1):46-54. https://doi.org/10.31643/2028/6445.05

Иммобилизацияланған 2 гидрокси-5 нитробензальдегид 2,4-динитрофенилгидразонды қатты фазалы экстрагентті золь гелін қолдана отырып жоғары өнімді сұйық хроматография арқылы биогенді аминдерді анықтау

[*1]Abdassalam Abdelhafiz Tameem, [1]Salam Salhin Mohamed, [1]Afiyah S. Alnaas, [2] Eny Kusrini

[1]Сирт университеті, Сирт, Ливия
[2]Индонезия университеті, Депок 16424, Батыс Ява, Индонезия

Мақала келді: *4 наурыз 2026*
Сараптамадан өтті: *14 сәуір 2026*
Қабылданды: *29 сәуір 2026*

ТҮЙІНДЕМЕ

Бұл зерттеу иммобилизацияланған 2-гидрокси-5-нитробензальдегид-2,4-динитрофенилгидразон деген атауы бар гидразон лигандымен золь-гель адсорбентін қолданып биогенді аминдерді (БА) қатты фазалы экстракциялауға арналған . Гидразон қосылысы ИК және ЯМР спектроскопиясы арқылы синтезделіп, сипатталды. Қатты фазалы экстракциялау (ҚФЭ) әдісін қолдану арқылы биогенді аминдердің экстракциясына сорбциалық материалдың тиімділігі бағаланды . Биогенді аминдердің экстракциясына әсер ететін негізгі эксперименттік параметрлер: соның ішінде pH, тепе-теңдік уақыты, лиганд концентрациясы және ҚФЭ концентрациясы жүйелі түрде зерттелді. Нәтижелер сулы үлгілерден биогенді аминдердің жоғары дәрежеде қалпына келтірілгенін көрсетті, бұл гидразон лигандтары бар золь-гель матрицасы мен нысаналы аналиттер арасындағы айтарлықтай жақындықты көрсетті. Айта кетсек бұл әдіс путресцин (PUT), кадаврин (CAD) және спермидин (SPD) сияқты алифатты биогенді аминдерге жоғары селективтілік көрсетті. Жақсы экстракция көрсеткіштерін қамтамасыз ету арқылы бұл әдісі тағам үлгілеріне сәтті қолданылды.

Түйін сөздер: ЖӨСХ, ҚФЭ, экстракция, биогенді аминдер , золь -гель.

Авторлар туралы ақпарат:

Abdassalam Abdelhafiz Tameem — *Білім беру факультеті, Сирт университеті, Сирт, Ливия. Email: salam1961@su.edu.ly*

Salam Salhin Mohamed — *Ғылым факультеті, Сирт университеті, Сирт, Ливия. Email: salam_salhin@su.edu.ly*

Afiyah S. Alnaas — *Білім беру факультеті, Сирт университеті, Сирт, Ливия. Email: salm@su.edu.ly*

Eny Kusrini — *Химиялық инженерия кафедрасы; Жасыл өнім және ұсақ химиялық инженерияны зерттеу тобы; Озық материалдарды зерттеу орталығы, Инженерия факультеті, Индонезия университеті, 16424 депосы, Батыс Ява, Индонезия. Email: eny.k@ui.ac.id*

Определение биогенных аминов методом высокоэффективной жидкостной хроматографии с использованием твердофазного экстрагента на основе золь-геля, иммобилизованного на 2-гидрокси-5-нитробензальдегиде и 2,4-динитрофенилгидразоне

[*1]Abdassalam Abdelhafiz Tameem, [1]Salam Salhin Mohamed, [1]Afiyah S. Alnaas, [2] Eny Kusrini

[1]Университет Сирте, Сирте, Ливия
[2]Университет Индонезии, Депок 16424, Западная Ява, Индонезия

Поступила: *4 марта 2026*
Рецензирование: *14 апреля 2026*
Принята в печать: *29 апреля 2026*

АННОТАЦИЯ

Данное исследование посвящено твердофазной экстракции биогенных аминов (БА) с использованием золь-гелевого адсорбента, иммобилизованного гидразоновым лигандом, названным 2-гидрокси-5-нитробензальдегид-2,4-динитрофенилгидразоном. Гидразоновое соединение было синтезировано и охарактеризовано с помощью ИК-спектроскопии и ЯМР-спектроскопии. Эффективность сорбционного материала для экстракции биогенных аминов оценивалась с использованием метода твердофазной экстракции (ТФЭ). Были систематически исследованы ключевые экспериментальные параметры, влияющие на экстракцию биогенных аминов , включая pH, время достижения равновесия, концентрацию лиганда и концентрацию биогенных аминов. Результаты показали высокую степень извлечения биогенных аминов из водных образцов, демонстрируя значительное сродство между золь-гелевой матрицей, содержащей гидразоновый лиганд, и целевыми аналитами. Примечательно, что метод показал высокую селективность по отношению к алифатическим биогенным аминам, таким как путресцин (PUT), кадаверин (CAD) и спермидин (SPD). Данный метод экстракции был успешно применен к образцам пищевых продуктов, обеспечив хорошие показатели извлечения.

Ключевые слова: ВЭЖХ, ТФЭ, экстракция, биогенные амины, золь-гель.

Информация об авторах:

Abdassalam Abdelhafiz Tameem — *Педагогический факультет, Университет Сирте, Сирт, Ливия. Email: salam1961@su.edu.ly*

Salam Salhin Mohamed — *Факультет естественных наук, Университет Сирте, Сирт, Ливия. Email: salam_salhin@su.edu.ly*

Afiyah S. Alnaas — *Факультет образования, Университет Сирте, Сирт, Ливия. Email: salm@su.edu.ly*

Eny Kusrini — *Кафедра химической инженерии; Группа исследований экологически чистых продуктов и тонкой химической инженерии; Центр исследований передовых материалов, инженерный факультет, Университет Индонезии, Депок 16424, Западная Ява, Индонезия. Email: eny.k@ui.ac.id*

References

[1] Ekegren T, Gomes-Trolin C. Determination of polyamines in human tissues by precolumnderivatization with 9-fluo[renylmethyl chloroformate and high-performance liquid chromatography. Analytical Biochemistry. 2005; 338:179-185. https://doi.org/10.1016/j.ab.2004.11.040

[2] Walters D R. Polyamines and plant disease. Phytochemistry. 2003; 64:97-107. https://doi.org/10.1016/s0031-9422(03)00329-7

[3] Tsai Y-H, Lin C-Y, Chang S-C, Chen H-C, Kung H-F, Wei C-I, Hwang D-F. Occurrence of histamine-forming bacteria in salted mackerel in Taiwan. Food Microbiology. 2005; 22:461-467. https://doi.org/10.1016/j.fm.2004.11.003

[4] Auerswald L, Morren C, Lopata A L. Histamine levels in seventeen species of fresh and processed South African seafood. Food Chemistry. 2006; 98;231-239. https://doi.org/10.1016/j.foodchem.2005.05.071

[5] Özogul F, Özogul Y. Biogenic amine content and biogenic amine quality indices of sardines (Sardinapilchardus) stored in modified atmosphere packaging and vacuum packaging. Food Chemistry. 2006; 99:574-578. https://doi.org/10.1016/j.foodchem.2005.08.029

[6] Gençcelep H, Kaban G, Aksu Mİ, Öz F, Kaya M. Determination of biogenic amines in sucuk. Food Control. 2008; 19:868-872. https://doi.org/10.1016/j.foodcont.2007.08.013

[7] Kalač P, Krausová P. A review of dietary polyamines: Formation, implications for growth and health and occurrence in foods. Food Chemistry. 2005; 90:219-230. https://doi.org/10.1016/j.foodchem.2004.03.044

[8] Chiacchierini E, Restuccia D, Vinci G. Evaluation of two different extraction methods for chromatographic determination of bioactive amines in tomato products. Talanta. 2006; 69:548-555. https://doi.org/10.1016/j.talanta.2005.10.027

[9] Adão RC, Glória MBA. Bioactive amines and carbohydrate changes during ripening of 'Prata' banana (Musa acuminate x M. balbisiana). Food Chemistry. 2005; 90:705-711. https://doi.org/10.1016/j.foodchem.2004.05.020

[10] Valero D, Martínez-Romero D, Serrano M. The role of polyamines in the improvement of the shelf life of fruit. Trends in Food Science & Technology. 2002; 13;228-234. https://doi.org/10.1016/S0924-2244(02)00134-6

[11] Soleas G J, Carey M, Goldberg D M. Method development and cultivar-related differences of nine biogenic amines in Ontario wines. Food Chemistry. 1999; 64:49-58. https://doi.org/10.1016/S0308-8146(98)00092-2

[12] Vidal-Carou MC, Lahoz-Portolés F, Bover-Cid S, Mariné-Font A. Ion-pair highperformance liquid chromatographic determination of biogenic amines and polyamines in wine and other alcoholic beverages. Journal of Chromatography A. 2003; 998:235-241. https://doi.org/10.1016/S0021-9673(03)00610-1

[13] Stratton J E, Hutkins R W, Taylor S L. Biogenic amines in Chinese and otherfermented foods: A review. Journal of Food Protection. 1991; 54:460-470. https://doi.org/10.4315/0362-028X-54.6.460

[14] Santos M H S. Biogenic amines: their importance in foods. International Journal of Food Microbiology. 1996; 29: 213-231. https://doi.org/10.1016/0168-1605(95)00032-1

[15] Valero D, Martínez-Romero D, Serrano M. The role of polyamines in the improvement of the shelf life of fruit. Trends in Food Science & Technology. 2002; 13:228-234. https://doi.org/10.1016/S0924-2244(02)00134-6

[16] Anli RE, Vural N, Yilmaz S, Vural ŸH. The determination of biogenic amines in Turkish red wines. Journal of Food Composition and Analysis. 2004; 17:53-62. https://doi.org/10.1016/S0889-1575(03)00104-2

[17] Soleas GJ, Carey M, Goldberg D M. Method development and cultivar-related differences of nine biogenic amines in Ontario wines. Food Chemistry. 1999; 64:49-58. https://doi.org/10.1016/S0308-8146(98)00092-2

[18] Sano M, Nishino I. Assay for spermidine synthase activity by micellar electrokinetic chromatography with laser-induced fluorescence detection. Journal of Chromatography B. 2007; 845:80-83. https://doi.org/10.1016/j.jchromb.2006.07.052

[19] Kvasnička F, Voldřich M. Determination of biogenic amines by capillary zone electrophoresis with conductometric detection. Journal of Chromatography A. 2006; 1103:145-149. https://doi.org/10.1016/j.chroma.2005.11.005

[20] Landete J M, de las Rivas B, Marcobal A, Muñoz R. Molecular methods for the detection of biogenic amine-producing bacteria on foods. International Journal of Food Microbiology. 2007; 117:258-269. https://doi.org/10.1016/j.ijfoodmicro.2007.05.001

[21] Marcobal A, Polo M C, Martín-Álvarez P J, Moreno-Arribas M V. Biogemic amine content of red Spanish wines: comparison of a direct ELISA and an HPLC method for the determination of histamine in wines. Food Research International. 2005; 38:387-394. https://doi.org/10.1016/j.foodres.2004.10.008

[22] Shakila R J, Vasundhara T S, Kumudavally K V. A comparison of the TLC desitometry and HPLC method for the determination of biogenic amines in fish and fishery products. Food Chemistry. 2001; 75:255-259. https://doi.org/10.1016/S0308-8146(01)00173-X

[23] Soufleros E H, Bouloumpasi E, Zotou A, Loukou Z. Determination of biogenic amines in Greek wines by HPLC and ultraviolet detection after dansylation and examination of factors affecting their presence and concentration. Food Chemistry. 2007; 101;704-716. https://doi.org/10.1016/j.foodchem.2006.02.028

[24] Yongmei L, Xin L, Xiaohong C, Mei J, Chao L, Mingsheng D. A survey of biogenic amines in Chinese rice wines. Food Chemistry. 2007; 100:1424-1428. https://doi.org/10.1016/j.foodchem.2005.11.035

[25] Abdassalam A T, Saad B, Makahleh A, Salhin A, Saleh M I. A4-hydroxy-N-[(E)-(2-hydroxyphenyl)methylidene] benzohydrazide-based sorbent material for the extraction-HPLC determination of biogenic amines in food samples. Talanta. 2010; 82:1385-1391. https://doi.org/10.1016/j.talanta.2010.07.004

[26] Chanbasha B, Weishan W, Ahmad M, Abdassalam AT, Abdussalam S, Bahruddin S, Hian K L. Hydrazone-based ligands for micro-solid phase extraction-high performance liquid chromatographic determination of biogenic amines in orange juice. Journal of Chromatograph A. 2011; 1218:4332– 4339. https://doi.org/10.1016/j.chroma.2011.04.073

[27] Oana Stamatoiu, Alexej Bubnov, Isabela Ţârcomnicu, Mircea Iovu. Synthesis and spectral characterisation of new amido-ether Schiff bases. Journal of Molecular Structure. 2008; 886:187–196. https://doi.org/10.1016/j.molstruc.2007.11.025

[28] Monfared, Hassan Hosseini, Pouralimardan, Omid and Janiak, Christoph. Synthesis and Spectral Characterization of Hydrazone Schiff Bases Derived from 2,4-Dinitrophenylhydrazine. Crystal Structure of Salicylaldehyde-2,4-Dinitrophenylhydrazone. Zeitschrift für Naturforschung B. 2007; 62(5):717-720. https://doi.org/10.1515/znb-2007-0515

[29] Runmo W, Yu Z, Yaqun W, Ze Y. Aromatic conjugated organic small molecules achieve ultra-stable NH4+ deprotonation storage. Chemical Engineering Journal. 2025; 522:168029. https://doi.org/10.1016/j.cej.2025.168029

[30] Tu W, Zeng S, Bai Y, Zhang X, Dong H, Zhang X P. Theoretical Insights into NH_3 Absorption Mechanisms with Imidazolium-based Protic Ionic Liquids. Industrial Chemistry & Materials. 2023; 1:262-270. https://doi.org/10.1039/d2im00041e

[31] Soad S, Abd E-H, Magda E, Khaled M, Adel E I. Cost-effective, green HPLC determination of losartan, valsartan and their nitrosodiethylamine impurity: application to pharmaceutical dosage forms. R Soc Open Sci. 2022; 9(6):20250. https://doi.org/10.1098/rsos.220250

[32] Bhushan R, Kumar V. Synthesis of chiral hydrazine reagents and their application for liquid chromatographic separation of carbonyl compounds via diastereomer formation. Journal of Chromatography A. 2008; 1190:86-94. https://doi.org/10.1016/j.chroma.2008.02.084

[33] Mehta M, Mehta D, Mashru R. Recent application of green analytical chemistry: eco-friendly approaches for pharmaceutical analysis. Futur J Pharm Sci. 2024; 10:83. https://doi.org/10.1186/s43094-024-00658-6

[34] Mahmoud A A, Ashraf AM. A systematic review of layered double hydroxide-based materials for environmental remediation of heavy metals and dye pollutants. Inorganic Chemistry Communications. 2023; 148:110325. https://doi.org/10.1016/j.inoche.2022.110325

[35] Scott ED, Wen-Tau TC, Houk KN, Peng L. Development of Chiral Bis-hydrazone Ligands for the Enantioselective Cross-Coupling Reactions of Aryldimethylsilanolates. The Journal of Organic Chemistry. 2014; 80(1):313-366. https://doi.org/10.1021/jo502388r

[36] Rampazzo G, Depau G, Pagliuca G, Zironi E, Serraino A, Savini F, Gazzotti T. A Rapid LC-MS/MS Method for Quantification of Biogenic Amines in Meat: Validation and Application for Food Safety Monitoring. Methods Protoc. 2025; 8(5):106. https://doi.org/10.3390/mps8050106

[37] Jindal D P, Bedi V, Jit B, Karkra N, Guleria S, Bansal R, Palusczak A, Hartmann R W. Synthesis and study of some new N-substituted imide derivatives as potential anticancer agents. II Farmaco. 2005; 60:283-290. https://doi.org/10.1016/j.farmac.2005.01.011

[38] Ramanathan K, Kamalasanan MN, Malhotra B D, Pradhan D R, Chandra S. Immobilization and characterization of lactate dehydrogenase on TEOS derived sol-gel films. Journal of Sol-Gel Science and Technology. 1997; 10:309-316. https://doi.org/10.1023/A:1018329518938

Crossref
DOI: 10.31643/2028/6445.06
Metallurgy and Metallurgical Engineering

Investigation of the Structure and Composition of TiN and CrN Coatings as a Function of Deposition Parameters

[1]Kenzhegulov A.K., [1,2*]Smailov K.M., [1]Mamaeva A.A., [1]Bakhytuly N., [1]Uskenbayeva A.M., [1]Alibekov Zh. Zh.

[1] Institute of Metallurgy and Ore Beneficiation JSC, Satbayev University, Almaty, Kazakhstan
[2] Al-Farabi Kazakh National University, Almaty, Kazakhstan

** Corresponding author email: k.smailov@satbayev.university*

Received: *January 31, 2026*
Peer-reviewed: *February 8, 2026*
Accepted: *May 29, 2026*

ABSTRACT

Addressing corrosion and wear in assemblies, components, machine parts, and equipment operating in aggressive environments under severe wear conditions remains a pressing challenge and continues to draw focused scientific attention. This work aimed to investigate how the key magnetron sputtering parameters (working pressure, plasma current, and process-gas flow rates) affect the surface morphology, microstructure, and composition of TiN and CrN films deposited under different conditions. Microstructural analysis revealed that, across the investigated parameter window, the films exhibit a columnar cross-sectional architecture and a smooth surface morphology with no visible defects, showing no pronounced differences between the deposition regimes. After 30 min of deposition, the film thickness ranged from 0.17 to 0.46 µm for TiN and from 0.59 to 3.46 µm for CrN, depending on the sputtering conditions. The results demonstrate that plasma current and working pressure have a strong effect on film thickness and chemical composition, whereas variations in the working-gas flow rate exert a coupled influence on thickness, microstructure, and the stoichiometry of TiN and CrN layers. Elemental analysis further indicates that increasing the pressure to 0.65 Pa increases oxygen incorporation in the films. During chromium sputtering, raising the plasma current to 1.5 A leads to film delamination. For TiN, a balanced regime with a moderate N2 flow is preferable, providing a reasonable growth rate and a composition close to stoichiometric. For CrN, the range of stable operating conditions is substantially broader, and the process parameters have a more pronounced impact on its structure and composition. These findings can support the design of TiN/CrN wear-resistant multilayer coatings produced by magnetron sputtering for protecting machine parts and equipment against wear and corrosion.

Keywords: working chamber pressure, plasma discharge current, nitrogen flow rate, film elemental composition, film thickness.

Information about authors:

Kenzhegulov Aidar Karaulovich — *PhD, Head of Metal Science Laboratory of the Institute of Metallurgy and Ore Beneficiation JSC, Satbayev University, Shevchenko str., 29/133, 050010, Almaty, Kazakhstan. Email: a.kenzhegulov@satbayev.university; ORCID ID: https://orcid.org/0000-0001-7001-2654*

Smailov Kenzhegali Mamanovich — *Doctoral student, Al Farabi Kazakh National University; Junior Researcher at the Chemical Analytical Laboratory of the Institute of Metallurgy and Ore Beneficiation JSC,Satbayev University, 050010, Shevchenko str., 29/133, Almaty, Kazakhstan. Email: k.smailov@satbayev.university; ORCID ID: https://orcid.org/0000-0002-9277-5254*

Mamaeva Axaule Alipovna — *Associate professor, Candidate of Physical and Mathematical Sciences, Leading Researcher at the Metal Science Laboratory of the Institute of Metallurgy and Ore Beneficiation JSC, Satbayev University, Shevchenko str., 29/133, 050010, Almaty, Kazakhstan. Email: ak78@mail.ru; ORCID ID: https://orcid.org/0000-0002-9659-8152*

Bakhytuly Nauryzbek — *PhD, Head of Laboratory of Physical Methods of Analysis of the Institute of Metallurgy and Ore Beneficiation JSC, Satbayev University, Shevchenko str., 29/133, 050010, Almaty, Kazakhstan. Email: n.bakhytuly@satbayev.university; ORCID ID: https://orcid.org/0000-0003-3087-0616*

Uskenbayeva Alma Muratbekovna — *PhD, Senior Researcher at the Metal Science Laboratory of the Institute of Metallurgy and Ore Beneficiation JSC, Satbayev University, Shevchenko str., 29/133, 050010, Almaty, Kazakhstan. Email: almauskenbaeva@mail.ru; ORCID ID: https://orcid.org/0000-0002-0540-5651*

Alibekov Zhasulan Zhanuzakovich — *PhD, Lead Engineer at the Metal Science Laboratory of the Institute of Metallurgy and Ore Beneficiation JSC, Satbayev University, Shevchenko str., 29/133, 050010, Almaty, Kazakhstan. Email: zh.alibekov@satbayev.university; ORCID ID: https://orcid.org/0000-0003-3213-5420*

Introduction

The durability of parts and components operating in aggressive environments under intense friction and wear (mechanical engineering, transport, chemical and petrochemical industries, power generation, and related sectors) remains a critical challenge. Premature failure of such components under service conditions can lead to substantial economic losses [1]. Improving the tribological and corrosion performance of contacting surfaces largely determines their service life, operational safety, and reliability [[2], [3], [4], [5]]. For this reason, enhancing the tribo-corrosion behaviour of frictional surfaces continues to be a key focus of scientific research.

One of the most effective approaches to addressing this challenge is surface engineering through the deposition of coatings with high wear resistance, hardness, and corrosion resistance [[6],[7][8]]. Metal-nitride coatings are widely employed for these purposes because they combine features typical of covalent compounds with those of ionic crystals. The incorporation of nitrogen alters bond energy, expands the crystal lattice, increases interatomic distances, and raises the lattice parameter, imparting distinctive physical and chemical properties to these compounds [[9], [10]].

Metal–nitride coatings can be produced by chemical vapour deposition (CVD), physical vapour deposition (PVD), and related methods. Selecting an appropriate deposition route is crucial because it directly affects coating microstructure and performance. In practice, metal-nitride coatings are predominantly fabricated by PVD processes; among them, magnetron sputtering (MS) is one of the most frequently used techniques. MS enables control over coating structure and composition by adjusting process parameters such as working pressure, plasma discharge current, reactive-gas flow rate, substrate bias, and others [11].

Pressure governs the energy and transport of species, thereby affecting film densification and porosity; discharge current/power controls the growth rate and the degree of ionization; the nitrogen flow rate regulates nitride stoichiometry and the onset of the target “poisoning” regime; substrate bias intensifies ion bombardment, increasing density and adhesion while promoting the build-up of residual stresses; and temperature determines adatom mobility and crystallinity [[12], [13]]. For multilayer coatings (e.g., TiN/CrN), these parameters additionally control interfacial sharpness, bilayer periodicity, and stress partitioning, which collectively define the mechanical, tribological, and corrosion performance.

For nitride coatings (TiN, CrN, TiAlN/CrAlN), the key requirements are the optimization of working pressure and nitrogen flow together with strict composition control to ensure high density, hardness, corrosion resistance, and thermal stability. For carbonitrides and multicomponent/multilayer systems (TiCN, TiAlCrN, AlCrSiN, TiN/CrN), additional critical factors include regulating carbon-containing gases, distributing power between targets, and controlling architectural parameters (layer period, interface sharpness, and the balance of residual stresses).

Among PVD-derived metal-nitride coatings, titanium nitride (TiN) and chromium nitride (CrN) attract sustained interest because they offer a favourable combination of high hardness, strong adhesion, wear resistance, corrosion resistance, and thermal stability, making them versatile for a wide range of applications [[9], [14]]. However, quantitative “parameter → structure/composition” relationships for individual TiN and CrN coatings remain under active investigation. Several studies have examined how sputtering conditions (pressure, gas flow, current density, ionization) affect composition, microstructure, and residual stresses in TiN and CrN films. At low pressure and moderate plasma currents, TiN typically forms a NaCl-type cubic structure with a preferred (111) or (200) orientation. For example, study [15] showed that increasing the working pressure from 2 mTorr to 9 mTorr changes grain orientation and increases oxygen incorporation in TiN coatings. Increasing the nitrogen fraction during titanium sputtering (nitrogen and argon flow rates: 9.0 and 51 sccm) while reducing pressure to 2 Pa has been reported to decrease vacancy concentration and increase coating density, as demonstrated by Wei B. and co-workers [16].

For CrN. Bai H. and others [9] demonstrated that both the deposition method and sputtering parameters affect nitrogen content and defect population in CrN coatings and, consequently, their mechanical behaviour. The authors of [17] reported that residual stress and hardness depend strongly on the sputtering regime. The authors found that increasing the deposition pressure from 2 to 4. 5. and 7 mTorr reduced film deformation and increased the oxygen content. The pronounced effect of substrate bias was attributed to enhanced ionization of film-forming species. In [18]. the influence of MS parameters on the tribological

performance of CrN coatings was examined. Thin CrN films were deposited at pressures of 0.4 and 4 Pa; after testing, the coating synthesized at 0.4 Pa exhibited less surface damage due to its higher film density, and its hardness was higher by 5 GPa.

Overall, studies on TiN and CrN deposition indicate that controlling MS parameters enables tuning of composition (metal-to-nitrogen ratio and oxygen incorporation), microstructure (grain size and texture), and, consequently, key properties such as hardness and wear resistance. This knowledge underpins the design of multilayer coating systems and the optimization of deposition regimes for practical applications (e.g., tooling and mechanical engineering). In this context, the present work investigates the structure and composition of TiN and CrN films as a function of magnetron sputtering parameters (pressure, plasma current, and working-gas flow rate) to support the subsequent design of TiN/CrN multilayer coatings.

Experimental part

TiN and CrN films were deposited by direct-current magnetron sputtering (DCMS) in a high-vacuum system developed by the authors, employing two separate magnetrons (APEL-MRE100 and MKE-95/100; Applied Electronics, Tomsk, Russian Federation). A 99 mm diameter VT1-0 titanium target (VostokMetService, Ust-Kamenogorsk, Kazakhstan) and a 75 mm diameter ERKh-1 chromium target (Ural Metall Export–Kazakhstan, Astana, Kazakhstan) were used. Polished p-type single-crystal Si(100) substrates (SW GmbH, Schramberg, Germany) with dimensions of 10 × 10 mm were mounted inside the chamber on a 200 mm-diameter substrate holder. The chamber was evacuated to a base pressure of 5×10^{-3} Pa using diffusion and rotary pumps (2NVR-60D; Vakuummash, Kazan, Russian Federation). The chamber pressure was monitored with a Televac CC-10 vacuum gauge (The Fredericks Company, USA). The substrates were then ion-cleaned at 0.3 Pa with a plasma current of 40 mA and an accelerating voltage of 2.5 kV for 20 min using an APEL-IS-21CELL ion source (Applied Electronics, Tomsk, Russia). After ion etching, the cleaned substrates were positioned opposite the corresponding magnetrons for TiN and CrN deposition.

The following deposition parameters were maintained throughout: substrate bias −100 V, deposition time 30 min, target-to-substrate distance 300 mm, and argon flow rate 1.3 L/h. Argon and nitrogen flow rates were regulated using RRG-12 flow controllers (Eltochpribor, Moscow, Russia). For TiN deposition, the plasma current was varied between 0.5 and 2 A, the working pressure between 0.3 and 0.65 Pa, and the nitrogen flow rate between 0.08 and 0.11 L/h. For CrN deposition, the plasma current ranged from 0.5 to 1.5 A, the working pressure from 0.3 to 0.65 Pa, and the nitrogen flow rate from 0.08 to 0.2 L/h.

Film thickness and morphology were evaluated by scanning electron microscopy (SEM) using a JXA-8230 microscope (JEOL, Tokyo, Japan) equipped with an energy-dispersive X-ray spectroscopy (EDS) system for elemental analysis.

Graphs and figures were prepared using OriginPro SR1 10.1.0.178 and CorelDRAW 25.0.0.230.

Results and Discussion

Microstructural analysis confirmed that, under the investigated conditions, the deposited films exhibit a columnar cross-sectional morphology and a smooth microstructure without visible defects. Depending on the sputtering parameters, after 30 min of deposition, the TiN and CrN thicknesses ranged from 0.17 to 0.46 μm and from 0.59 to 3.46 μm, respectively. Under identical magnetron sputtering conditions, the CrN deposition rate was approximately 3.5 times higher than that of TiN. The effects of the individual MS parameters on TiN and CrN films are discussed below.

Effect of Working Pressure in the MS Chamber

Based on the preceding results, the working pressure during titanium and chromium sputtering was set to 0.45 and 0.65 Pa while maintaining a nitrogen flow rate of 0.08 L/h. The thicknesses of TiN and CrN films synthesized at 0.65 Pa were lower than those obtained at 0.3 and 0.45 Pa. At elevated pressure (0.65 Pa), the TiN and CrN growth rates decrease due to an increased frequency of collisions in the plasma, which reduces the kinetic energy and mean free path of the sputtered species. This trend is consistent with previous reports [[15],[18]]. During titanium sputtering, increasing the pressure from 0.45 to 0.65 Pa decreased the TiN deposition rate from 0.16 to 0.13 μm/min, whereas during chromium sputtering, the CrN deposition rate decreased from 0.50 to 0.38 μm/min.

SEM examination of the surface morphology of TiN and CrN films deposited at 0.45 and 0.65 Pa revealed a smooth, uniform surface, with only occasional, randomly distributed nuclei. Figure 1 summarizes the surface morphology and EDS-derived composition. The left-hand images (×250)

show a dense and homogeneous microstructure without pronounced defects. Both titanium nitride and chromium nitride surfaces exhibit a similar, uniform contrast, indicating good film continuity. The small number of micron-sized nuclei observed on the TiN and CrN surfaces may be associated with droplet-phase formation or microdroplets, a phenomenon occasionally reported for magnetron sputtering processes [[19], [20]]. Their low areal density suggests stable deposition conditions. Notably, the surface morphology did not change appreciably with variations in pressure, plasma current, or nitrogen flow rate; therefore, only cross-sectional images are discussed in the following sections.

The right-hand plot in Fig. 1 shows the chemical composition of the films as a function of working pressure. Elemental analysis indicates that increasing the pressure to 0.65 Pa increases the oxygen content to 26.45 at.% in CrN and to 10.32 at.% in TiN, which may adversely affect tribological performance. The increase in oxygen content with increasing pressure has been reported by many researchers [[15], [17], [18]]. This effect is commonly attributed to the incorporation of residual gases during film growth and to the pronounced affinity of Cr for oxygen.

On the basis of the pressure-dependent results, subsequent deposition experiments were conducted at 0.45 Pa. However, given the relatively low nitrogen content in CrN films, a higher nitrogen flow rate during chromium sputtering is required to promote nitride formation.

Effect of Magnetron Sputtering Plasma Discharge Current

To examine the influence of the MS plasma discharge current on the structure and composition of TiN and CrN films, films were deposited on Si substrates at a chamber pressure of 0.45 Pa with a nitrogen flow rate of 0.08 L/h and an argon flow rate of 1.3 L/h for 30 min.

During titanium sputtering, plasma currents below 0.5 A led to deviations of TiN from stoichiometry due to changes in the discharge zone, whereas currents above 2.0 A caused overheating of the magnetron housing. Similar behaviour has been reported in [[21],[22]]. Figure 2 presents a cross-sectional SEM image and the dependence of the TiN deposition rate and film thickness on the plasma current. The cross-section clearly reveals the “film-substrate” interface. The film exhibits a dense microstructure without cracks or visible defects. Thickness uniformity across the cross-section confirms stable deposition conditions and efficient mass transport of species to the substrate. As shown in the right panel of Fig. 2, increasing the plasma current results in an approximately linear rise in deposition rate from 5 to 15 nm/min, leading to a film thickness of ~0.5 µm. The chemical composition of TiN films as a function of plasma current is summarized in Table 1, where reducing the current is accompanied by changes in the titanium and nitrogen contents. Because the film deposited at 2 A exhibited a composition closest to stoichiometric, and given that titanium has a lower sputtering yield than chromium, the plasma current for titanium sputtering was fixed at 2 A in subsequent experiments.

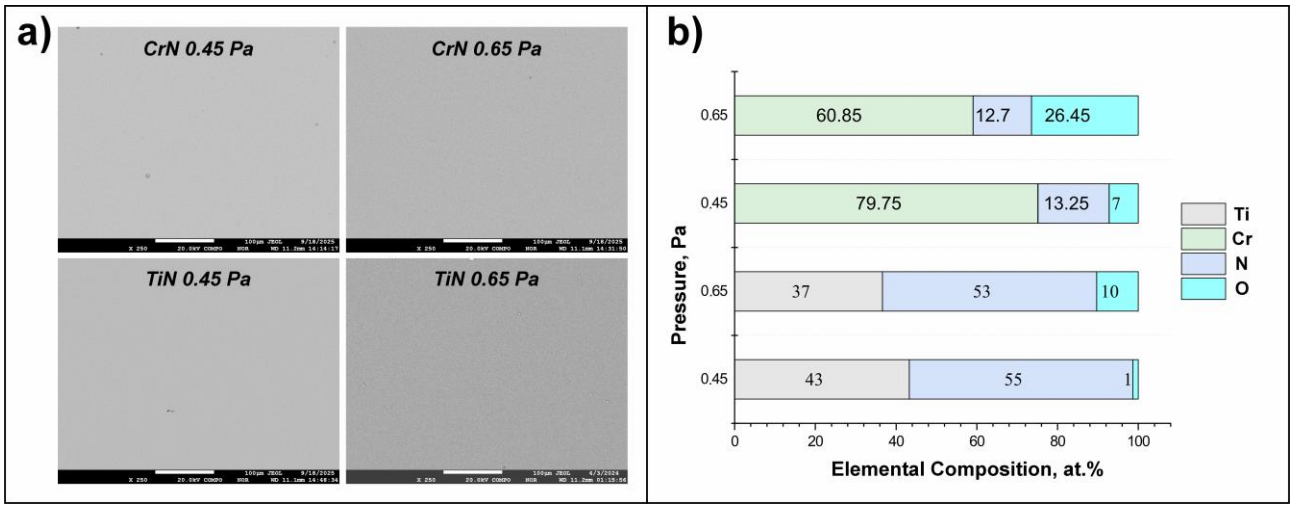

Figure 1 - Surface morphology (a) and chemical composition (b) of TiN and CrN films as a function of working pressure

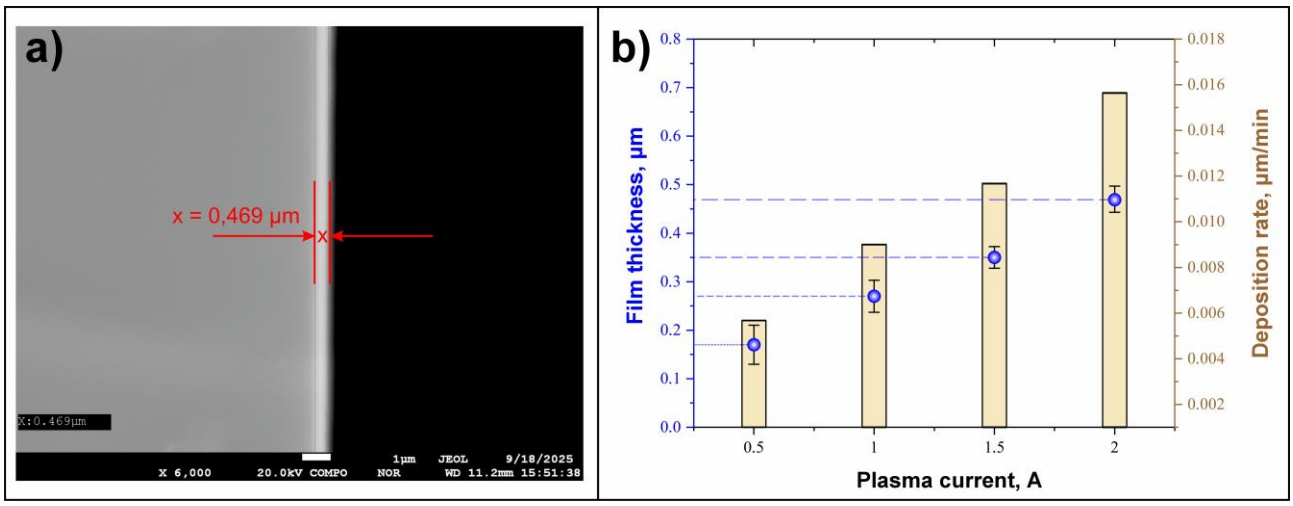

Figure 2 - Cross-sectional SEM image of the TiN film at 2 A (a) and the dependence of deposition rate and film thickness on plasma current (b)

Table 1 - Chemical composition of TiN films deposited at plasma currents from 0.5 to 2 A

Sample	Plasma current, A	Ti	N	O
7-1	2	43.25	55.4	1.35
7-2	1.5	43.1	53.8	3.1
7-3	1	39.5	59.3	1.2
7-4	0.5	32.2	62.5	5.3

During chromium sputtering, plasma currents above 1.5 A led to film delamination, which is attributed to an excessively high deposition rate and the build-up of residual stresses. This can degrade the adhesion durability of the CrN film, ultimately leading to delamination, as also reported in [[9], [17], [23]].

Figure 3 provides cross-sectional SEM images of the CrN film and shows the dependence of deposition rate and film thickness on plasma current. The deposition rate increased from 0.02 to 0.11 µm/min as the plasma current was raised, resulting in film thicknesses ranging from 0.5 to 3.46 µm. The higher growth rate can be explained by the intensification of ion-plasma processes, including a greater probability of ionization of sputtered species and an increased deposition efficiency [24]. The relatively small thickness scatter, shown as error bars, indicates good reproducibility of the deposition process.

Table 2 summarizes the composition of CrN films deposited at plasma currents from 0.5 to 1.5 A in 0.5 A increments. Elemental analysis shows that increasing the plasma current markedly reduces the oxygen content in the film, while the chromium fraction increases. At the lower current of 0.5 A, oxygen from residual chamber gases is incorporated into the growing film. Raising the current to 1.0-1.5 A increases the density of energetic ions in the plasma, thereby promoting nitridation [[25], [26]]. As a result, the chromium and nitrogen contents increase, whereas the oxygen level decreases.

Based on the current-dependent deposition results, a plasma current of 2 A was selected for titanium sputtering and 1 A for chromium sputtering as the working regimes for subsequent experiments.

Effect of Nitrogen Flow Rate during MS

The influence of nitrogen flow rate on the stoichiometry of individual TiN and CrN films was examined at a constant argon flow rate of 1.3 L/h.

For TiN films, the nitrogen flow rate was varied between 0.08, 0.18, 0.36, and 0.54 L/h. Under these conditions, a decrease in the TiN deposition rate was observed with increasing nitrogen flow (Fig. 4). This behaviour can be attributed to a reduction in the effective sputtering yield of the titanium target caused by the formation of a TiN compound film on the target surface; in addition, the density and kinetic energy of titanium species reaching the substrate decrease due to a higher collision frequency in the gas phase [[27], [28]]. In other words, the process transitions from a metallic mode to a reactive regime. Figure 4 shows the deposition rate as a function of nitrogen flow rate together with the corresponding TiN film compositions. As the nitrogen flow increases, the titanium fraction decreases, whereas the nitrogen content rises.

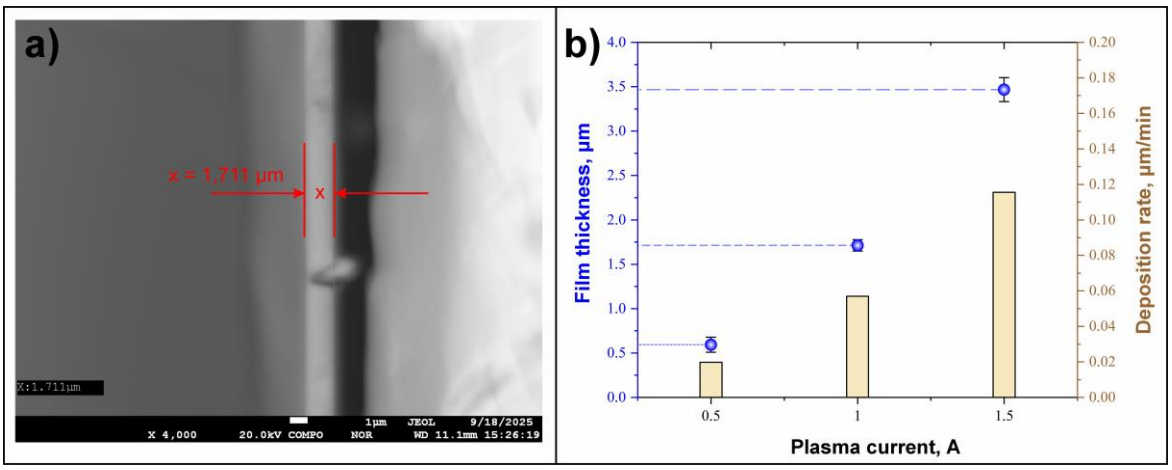

Figure 3 - Cross-sectional SEM image of the CrN film at 1 A (a) and the dependence of deposition rate and film thickness on plasma current (b)

Table 2 - Chemical composition of CrN films deposited at plasma currents from 0.5 to 2 A

Sample	Plasma current, A	Cr	N	O
1	0.5	60.5	12.69	26.81
3	1	79.75	13.03	7.22
2	1.5	81.3	12.66	6.04

Across all regimes, the nitrogen content was in the range of 44-56 at.% and titanium in the range of 36-47 at.%. Based on the composition data, 0.08 L/h is the optimal nitrogen flow rate for forming TiN.

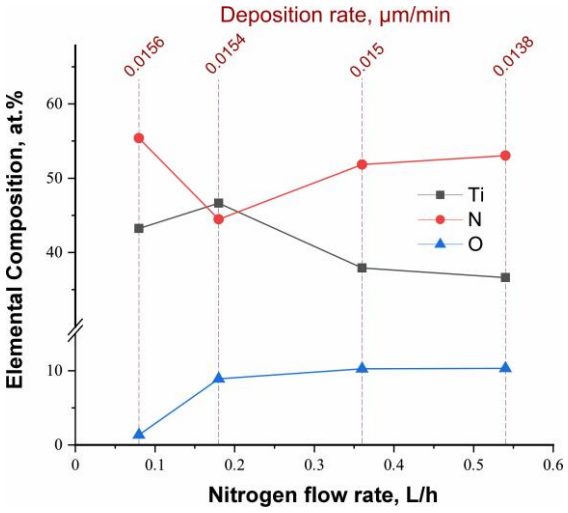

Figure 4 - Elemental composition and deposition rate of TiN films as a function of nitrogen flow rate

For CrN layers, the nitrogen flow rate was varied at 0.08, 0.12, 0.18, 0.22, and 0.26 L/h. As in the TiN case, increasing the nitrogen flow initially reduced the CrN deposition rate, after which the rate levelled off. However, unlike TiN, CrN films exhibited a substantially higher growth rate (0.055–0.057 µm/min), consistent with the higher sputtering yield of chromium [29]. Elemental analysis (Fig. 5) shows that increasing the nitrogen flow decreases the chromium content from ~80 to ~67 at.% while simultaneously increasing the nitrogen fraction to ~25 at.%. This behaviour indicates a transition from a metallic or nitrogen-deficient Cr(N) state toward a nitride phase approaching CrN; nevertheless, even at the maximum nitrogen flow, the composition remains shifted toward metal-rich stoichiometry. The elevated oxygen content (up to ~21 at.% at intermediate N2 flow) suggests a tendency of CrN films toward oxygen contamination, which may be associated with the high chemical reactivity of chromium [[30], [31], [32], [33]].

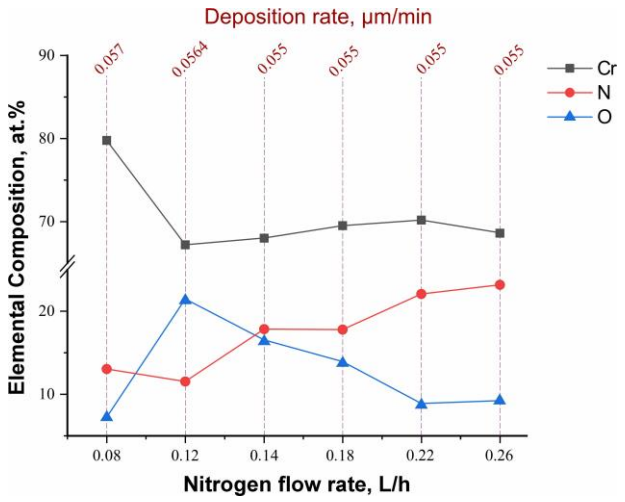

Figure 5 - Elemental composition and deposition rate of CrN films as a function of nitrogen flow rate

Thus, optimizing the nitrogen flow rate is a key lever for controlling both the deposition rate and the stoichiometry of TiN and CrN coatings. For TiN, a balanced regime with a moderate N_2 flow is preferable, providing a reasonable growth rate together with a composition close to stoichiometric. For CrN, the range of stable operating conditions is substantially broader, indicating higher process robustness during reactive magnetron deposition.

Conclusions

The present work investigated the structure and composition of TiN and CrN films as a function of key magnetron sputtering parameters (pressure, plasma current, and process-gas flow rates) to support the design of TiN/CrN multilayer coatings. The main conclusions are as follows:

- The experiments showed that plasma current and working pressure strongly affect film thickness and chemical composition, whereas variations in the working-gas flow rate exert a coupled influence on thickness, microstructure, and layer stoichiometry.
- For TiN deposition, a near-optimal regime was identified at a working pressure of 0.45 Pa, with titanium sputtered at an N2 flow rate of 0.08 L/h and a plasma current of 2 A.
- For CrN deposition, a working pressure of 0.45 Pa, a plasma current of 1 A, and an N2 flow rate of 0.22 L/h were found to be optimal; however, the N2 flow rate requires further refinement.

Further studies will focus on a more detailed assessment of film properties under the identified operating regimes and on evaluating the behaviour of these layers within a TiN/CrN multilayer architecture.

Conflicts of interest. On behalf of all authors, the corresponding author states that there is no conflict of interest.

CRediT author statement: **A. Kenzhegulov**: Conceptualization, Methodology, Software; **K. Smailov**: Data curation, Writing draft preparation; **A. Mamaeva and N. Bakhytuly**: Visualization, Investigation; **A. Kenzhegulov**: Supervision; **A. Uskenbayeva**: Software, Validation; **Zh.Zh. Alibekov**: Reviewing and Editing.

Formatting of funding sources. This research was funded by the Science Committee of the Ministry of Science and Higher Education of the Republic of Kazakhstan (Grant No. AP26101617).

Cite this article as: Kenzhegulov AK, Smailov KM, Mamaeva AA, Bakhytuly N, Uskenbayeva AM, Alibekov ZhZh. Investigation of the Structure and Composition of TiN and CrN Coatings as a Function of Deposition Parameters. Kompleksnoe Ispolzovanie Mineralnogo Syra = Complex Use of Mineral Resources. 2028; 344(1):55-64. https://doi.org/10.31643/2028/6445.06

TiN және CrN жабындарының құрылымы мен құрамын тұндыру параметрлеріне байланысты зерттеу

[1] Кенжеғұлов А.К., [1,2] Смаилов К.М., [1] Мамаева А.Ә., [1] Бахытұлы Н., [1] Ускенбаева А.М., [1] Алибеков Ж.Ж.

[1] Металлургия және кен байыту институты АҚ, Сәтбаев университеті, Алматы, Қазақстан
[2] Әл-Фараби атындағы Қазақ ұлттық университеті, Алматы, Қазақстан

Мақала келді: *31 қаңтар 2026*
Сараптамадан өтті: *8 ақпан 2026*
Қабылданды: *29 мамыр 2026*

Агрессивті ортада және қарқынды тозу жағдайында жұмыс істейтін тораптар, құрамдас бөлшектер, машиналар мен жабдық элементтерінің коррозиясы мен тозуы мәселесін шешу өзекті және ерекше ғылыми назар аударатын нысан болып табылады. Бұл жұмыстың мақсаты әртүрлі шарттарда тұндырылған TiN және CrN қабықшаларының морфологиясына, микроқұрылымына және құрамына магнетрондық тозаңдатудың негізгі параметрлерінің (қысым, плазма тогы, жұмыс газдарының ағыны) әсерін зерттеу. Нәтижесінде микроқұрылымдық талдау зерттелген жағдайларда көлденең қимасында бағаналы құрылымы және тегіс беті морфологиялы, көрінетін ақаулары жоқ қабықшалардың қалыптасатынын, олардың микроқұрылымы көрінетін ақаулардан бос және шашырау жағдайларынан айтарлықтай айырмашылық көрсетпейтінін анықтады. Тозаңдату параметрлеріне байланысты, 30 минуттық тұндыру кезінде TiN және CrN қабықшаларының қалыңдығы сәйкесінше 0,17–0,46 мкм-ге дейін және 0,59–3,46 мкм -ге дейін аралығында болды. Жүргізілген жұмыс нәтижелеріне сүйене отырып, плазмалық ток пен қысым қабықша қалыңдығына мен химиялық құрамына елеулі ықпал ететінін, ал жұмыс газы ағынының өзгеруі TiN және CrN қабаттарының қалыңдығына, құрылымына және құрамының стехиометриясына кешенді әсер ететініні анықталды. Элементтік талдау нәтижелері қысымды 0,65 Па-ға дейін арттыру қабықшалардағы оттегі мөлшерін өсетінін көрсетті.

	Хромды тозаңдату кезінде плазма тогын 1,5 А-ға дейін ұлғайту қабықшаның қабыршақтануына әкеледі. TiN қабықшалары үшін өсу жылдамдығын қабылдауға болатын деңгейді сақтай отырып, стехиометрияға жақын құрамды қамтамасыз ететін N_2 ағынының орташа мәндеріндегі компромистік режим қолайлы. CrN үшін тұрақты режимдер диапазоны едәуір кең және құрылым мен құрамға үлкен әсер етеді. Алынған нәтижелер машиналар мен жабдық бөлшектерін тозу мен коррозиядан қорғауға қолданылатын магнетрондық тозаңдату әдісімен көпқабатты тозуға төзімді TiN/CrN жабын жүйелерін жобалау кезінде пайдалы болуы мүмкін.
	Түйін сөздер: камераның жұмыс қысымы, плазмалық разряд тогы, азот ағынының жылдамдығы, қабықшаның элементтік құрамы, қабықшаның қалыңдығы.
Кенжеғұлов Айдар Қарауылұлы	***Авторлар туралы ақпарат:*** *PhD, Металлургия және кен байыту институты АҚ, Сәтбаев университеті, Материалтану зертханасының меңгерушісі, 050010, Шевченко көш., 29/133, Алматы, Қазақстан. Email: a.kenzhegulov@satbayev.university; ORCID ID: https://orcid.org/0000-0001-7001-2654*
Смаилов Кенжеғали Маманұлы	*Докторант, Әл-Фараби атындағы Қазақ Ұлттық университеті; Аналитикалық химия зертханасының ғылыми қызметкері, Металлургия және кен байыту институты АҚ, Сәтбаев университеті, 050010, Шевченко көш., 29/133, Алматы, Қазақстан. Email: k.smailov@satbayev.university; ORCID ID: https://orcid.org/0000-0002-9277-5254*
Мамаева Ақсәуле Әліпқызы	*Қауымдастырылған профессор, Физика-математика ғылымдарының кандидаты, жетекші ғылыми қызметкер, Металлургия және кен байыту институты АҚ, Сәтбаев университеті, 050010, Шевченко көш., 29/133, Алматы, Қазақстан. Email: ak78@mail.ru; ORCID ID: https://orcid.org/0000-0002-9659-8152*
Бахытұлы Наурызбек	*PhD, Металлургия және кен байыту институты АҚ, Сәтбаев университеті, Физикалық әдіспен талдау зертханасының меңгерушісі, 050010, Шевченко көш., 29/133, Алматы, Қазақстан. Email: n.bakhytuly@satbayev.university; ORCID ID: https://orcid.org/0000-0003-3087-0616*
Ускенбаева Алма Мұратбековна	*PhD, Металлургия және кен байыту институты АҚ, Сәтбаев университеті, Материалтану зертханасының аға ғылыми қызметкері, 050010, Шевченко көш., 29/133, Алматы, Қазақстан. Email: almauskenbaeva@mail.ru; ORCID ID: https://orcid.org/0000-0002-0540-5651*
Алибеков Жасұлан Жанұзақұлы	*Металлургия және кен байыту институты АҚ, Сәтбаев университеті, Материалтану зертханасының жетекші инжинері, 050010, Шевченко көш., 29/133, Алматы, Қазақстан. Email: zh.alibekov@satbayev.university; ORCID ID: https://orcid.org/0000-0003-3213-5420*

Исследование структуры и состава покрытий TiN и CrN в зависимости от параметров осаждения

[1] Кенжегулов А.К., [1,2] Смаилов К.М., [1] Мамаева А.А., [1] Бахытулы Н., [1] Ускенбаева А.М., [1] Алибеков Ж.Ж.

[1] АО Институт металлургии и обогащения, Satbayev University, Алматы, Казахстан
[2] Казахский национальный университет имени аль-Фараби, Алматы, Казахстан

Поступила: *31 января 2026*
Рецензирование: *8 февраля 2026*
Принята в печать: *29 мая 2026*

АННОТАЦИЯ

Решение проблемы коррозии и износа узлов, компонентов, деталей машин и оборудовании, работающих в условиях агресиной среди и интенсивного износа, является актульным и является объектом особого научного внимания. Целью настоящей работы являлась исследование влияния основных параметров магнетронного распыления (давление, ток плазмы, поток рабочих газов) на морфологию, микроструктуру и состав пленок TiN и CrN, осажденных в разных условиях. В результате, микроструктурный анализ показал, что при исследованных режимах формируются пленки с колонной структурой по поперечному сечению и гладкой поверхностной морфологией микроструктура котрого без видимых дефектов и существенно не отличающегося от режимов напыления. В зависимости от параметров распыления при 30 минутной осаждении толщина пленок было в пределах от 0,17 до 0,46 мкм и от 0,59 до 3,46 мкм для TiN и CrN, соответственно. По результатам проведённых работ установлено, что ток плазмы и давление существенно влияют на толщину и химический состав пленок, тогда как изменение потока рабочего газа оказывает комплексное влияние на толщину, структуру и стехиометрию состава слоёв TiN и CrN. Результаты элементного анализа показали, что при увеличении давления до 0,65 Па возрастает содержание кислорода в пленках. В случае распылении хрома повышения тока плазмы до 1,5 А приводит к отслоению пленки. Для плеок TiN предпочтителен компромиссный режим с умеренным потоком N2, обеспечивающий приемлемую скорость роста и близкую к стехиометрической композицию. Для CrN диапазон стабильных режимов существенно шире и проявялет большего влияние на структуру и состав. Полученные результаты могут быть полезны при проектировании многослойной системы износостойкого покрытия TiN/CrN методом магнетронного распыления, которые используется для защиты от износа и коррозии деталей машин или оборудовании.

	Ключевые слова: рабочее давление камеры, ток разряда плазмы, скорость потока азота, элементный состав пленки, толщина пленки.
Кенжегулов Айдар Караулович	***Информация об авторах:*** *PhD, заведующий лабораторией металловедения АО Институт металлургии и обогащения, Satbayev University, ул. Шевченко, 29/133, 050010, Алматы, Казахстан. Email: a.kenzhegulov@satbayev.university; ORCID ID: https://orcid.org/0000-0001-7001-2654*
Смаилов Кенжегали Маманович	*Докторант, Казахский национальный университет им. аль-Фараби; Научный сотрудник Химико-аналитической лаборатории, АО Институт металлургии и обогащения, Satbayev University, 050010, ул. Шевченко, 29/133, Алматы, Казахстан. Email: k.smailov@satbayev.university; ORCID ID: https://orcid.org/0000-0002-9277-5254*
Мамаева Аксауле Алиповна	*Ассоцированный профессор, кандидат физико-математических наук, ведущий научный сотрудник, АО Институт металлургии и обогащения, Satbayev University, ул. Шевченко, 29/133, 050010, Алматы, Казахстан. Email: ak78@mail.ru; ORCID ID: https://orcid.org/0000-0002-9659-8152*
Бахытулы Наурызбек	*PhD, заведующий лабораторией физических методов анализа АО Институт металлургии и обогащения, Satbayev University, ул. Шевченко, 29/133, 050010, Алматы, Казахстан. Email: n.bakhytuly@satbayev.university; ORCID ID: https://orcid.org/0000-0003-3087-0616*
Ускенбаева Алма Муратбековна	*PhD, старший научный сотрудник лоборатории металловедения АО Институт металлургии и обогащения, Satbayev University, ул. Шевченко, 29/133, 050010, Алматы, Казахстан. Email: almauskenbaeva@mail.ru; ORCID ID: https://orcid.org/0000-0002-0540-5651*
Алибеков Жасулан Жанузакович	*Ведущий инженер лобратории металловедения АО Институт металлургии и обогащения, Satbayev University, ул. Шевченко, 29/133, 050010, Алматы, Казахстан. Email: zh.alibekov@satbayev.university; ORCID ID: https://orcid.org/0000-0003-3213-5420*

References

[1] Wang Z, Chen X, Gong Y, He X, Wei Y, Li H. Tribocorrosion behaviours of cold-sprayed diamond–Cu composite coatings in artificial sea water. Surface Engineering. 2018; 34:392-398. https://doi.org/10.1080/02670844.2017.1376821

[2] Mamaeva A, Kenzhegulov A, Panichkin A, Kshibekova B, Bakhytuly N. Deposition of carbonitride titanium coatings by magnetron sputtering and its effect on tribo-mechanical properties. Kompleksnoe Ispolzovanie Mineralnogo Syra = Complex Use of Mineral Resources. 2022; 321(2):65-78. https://doi.org/10.31643/2022/6445.19

[3] Muradova S, Negim E-S, Makhmetova A, Ainakulova D, Mohamad N. An overview of the current state and the advantages of using acrylic resins as anticorrosive coatings. Kompleksnoe Ispolzovanie Mineralnogo Syra = Complex Use of Mineral Resources. 2023; 327(4):90-98. https://doi.org/10.31643/2023/6445.44

[4] Shan L, Zhang YR, Wang YX, Li JL, Jiang X, Chen JM. Corrosion and wear behaviors of PVD CrN and CrSiN coatings in seawater. Transactions of Nonferrous Metals Society of China (English Edition). 2016; 26:175-184. https://doi.org/10.1016/S1003-6326(16)64104-3

[5] Kenzhaliyev B, Berkinbayeva A, Baltabekova Z, Moldabayeva G, Smailov K, Saulebekkyzy S, Tolegenova N, Karim D, Omirbek T. Investigation of phase transformations in technogenic raw materials under microwave treatment for enhanced zinc leaching. Processes. 2025; 13:1099. https://doi.org/10.3390/pr13041099

[6] Totolin V, Pejaković V, Csanyi T, Hekele O, Huber M, Rodríguez Ripoll M. Surface engineering of Ti6Al4V surfaces for enhanced tribocorrosion performance in artificial seawater. Materials & Design. 2016; 104:10-18. https://doi.org/10.1016/j.matdes.2016.04.080

[7] Ultarakova A, Karshyga Z, Lokhova N, Yessengaziyev A, Kassymzhanov K, Mukangaliyeva A. Studies on the processing of fine dusts from the electric smelting of ilmenite concentrates to obtain titanium dioxide. Materials. 2022; 15:8314. https://doi.org/10.3390/ma15238314

[8] Sabergaliyev M, Yeligbayeva G, Khassanov D, Muradova S, Orazalin Z, Ainakulova D, Sharipov R, Negim E-S. Modified bitumen-polymer mastic to protect metal coatings from corrosion. Kompleksnoe Ispolzovanie Mineralnogo Syra = Complex Use of Mineral Resources. 2024; 331(4):12-20. https://doi.org/10.31643/2024/6445.35

[9] Bai H, Li J, Gao J, Ni J, Bai Y, Jian J, Zhao L, Bai B, Cai Z, He J, et al. Comparison of CrN coatings prepared using high-power impulse magnetron sputtering and direct current magnetron sputtering. Materials. 2023; 16(18):6303. https://doi.org/10.3390/ma16186303

[10] Goyenola C, Gueorguiev GK, Stafström S, Hultman L. Fullerene-like CSx: A first-principles study of synthetic growth. Chemical Physics Letters. 2011; 506:86-91. https://doi.org/10.1016/j.cplett.2011.02.059

[11] Tang J-F, Lin C-Y, Yang F-C, Chang C-L. Effects of nitrogen-argon flow ratio on the microstructural and mechanical properties of AlCrN coatings prepared using high power impulse magnetron sputtering. Surface & Coatings Technology. 2020; 386:125484. https://doi.org/10.1016/j.surfcoat.2020.125484

[12] Margono M, Darmadi DB, Gapsari F, Widodo TD, Kozin M, Puranto P, et al. Optimized deposition parameters for titanium nitride coatings: Enhancing mechanical properties of Al 6011 substrates via DC sputtering. Mechanical Engineering for Society and Industry. 2024; 4(2):252-262.

[13] Bakhytuly N, Kenzhegulov A, Nurtanto M, Aliev A, Kuldeev E. Microstructure and tribological study of TiAlCN and TiTaCN coatings. Kompleksnoe Ispolzovanie Mineralnogo Syra = Complex Use of Mineral Resources. 2023; 327(4):99-110. https://doi.org/10.31643/2023/6445.45

[14] Kenzhaliyev B, Kenzhegulov A, Mamaeva A, Panichkin A, Kshibekova B, Alibekov Z, Fischer D. Tribological characteristics of multilayer TiN/TiCN coatings compared to TiN coatings. Journal of Materials Engineering and Performance. 2025; 34(9):25810-25819. https://doi.org/10.1007/s11665-025-11182-w

[15] Ohya S, Chiaro B, Megrant A, Neill C, Barends R, Chen Y, Kelly J, Low D, Mutus J, O'Malley P, et al. Sputtered TiN films for superconducting coplanar waveguide resonators. 2013. https://doi.org/10.48550/arXiv.1306.2966

[16] Wei B, Liang H, Zhang D, Qi Z, Shen H, et al. Magnetron sputtered TiN thin films toward enhanced performance supercapacitor electrodes. Materials for Renewable and Sustainable Energy. 2018; 7:11. https://doi.org/10.1007/s40243-018-0117-9

[17] Elo R, Jacobson S, Kubart T. Tailoring residual stresses in CrNx films on alumina and silicon deposited by high-power impulse magnetron sputtering. Surface and Coatings Technology. 2020; 397:125990. https://doi.org/10.1016/j.surfcoat.2020.125990

[18] Ruden-Muñoz A, Restrepo-Parra E, Sequeda F. CrN coatings deposited by magnetron sputtering: mechanical and tribological properties. DYNA. 2015; 82(191):147-155. https://doi.org/10.15446/dyna.v82n191.43292

[19] Vereschaka A, Milovich F, Andreev N, Sotova C, Alexandrov I, Muranov A, et al. Investigation of the structure and phase composition of the microdroplets formed during the deposition of PVD coatings. Surface and Coatings Technology. 2022; 441:128574. https://doi.org/10.1016/j.surfcoat.2022.128574

[20] Yu X, Ma L, Liu Y, Yang ZZ, Meng H. Reducing surface defects of CrxOy film in mid-frequency dual-magnetron sputtering. Advanced Materials Research. 2011; 291:219-222. https://doi.org/10.4028/www.scientific.net/AMR.291.219

[21] Soshina TO, Mezentseva DS. Vliyaniye tekhnologicheskikh parametrov protsessa impul'snogo magnetronnogo raspyleniya na strukturu i fazovyy sostav pokrytiy na osnove TiN [Influence of technological parameters of the pulsed magnetron sputtering process on the structure and phase composition of TiN-based coatings]. Vestnik Yugorskogo gosudarstvennogo universiteta = Bulletin of Yugra State University. 2023; 1(68):111-119. (in Russ.).

[22] Tetsuji S, et al. Development of electromagnetic acceleration plasma arcjet generators for titanium nitride reactive spray coatings. Quarterly Journal of the Japan Welding Society. 2001; 19(3):465-471.

[23] Zin V, Montagner F, Deambrosis SM, Mortalò C, Litti L, Meneghetti M, Miorin E. Mechanical and tribological properties of Ta-N and Ta-Al-N coatings deposited by reactive high power impulse magnetron sputtering. Materials. 2022; 15(9):3354. https://doi.org/10.3390/ma15093354

[24] Jiang X, Herrasti P, Sundgren JE, Greene JE. The influence of ionization on the growth kinetics of transition-metal nitride films deposited by reactive sputtering. Surface and Coatings Technology. 2021; 410:126904. https://doi.org/10.1016/j.surfcoat.2021.126904

[25] Borowski P, Myśliwiec J. Recent advances in magnetron sputtering: From fundamentals to industrial applications. Coatings. 2025; 15(8):922. https://doi.org/10.3390/coatings15080922

[26] Zin V, Montagner F, Deambrosis SM, Miorin E, Comisso N, Rancan M, Paradisi E, Mortalò C. High power impulse magnetron sputtering plasma nitriding of biomedical grade CoCrMo alloy. Materials & Design. 2025; 252:113802. https://doi.org/10.1016/j.matdes.2025.113802

[27] Lee JH, Nathanael AJ, Hong SI. Effect of nitrogen flow rate on the structure and properties of TiN thin films deposited onto β-type Ti-15Mo-3Nb-3Al-0.2Si alloy substrates by reactive magnetron sputtering. Advanced Materials Research. 2012; 557-559:1998-2001. https://doi.org/10.4028/www.scientific.net/AMR.557-559.1998

[28] Yermakhanova AM, Baiserikov BM, Kenzhegulov AK, Meiirbekov MN, Zhumadilov BY. Study on methods to improve the mechanical properties of aramid/epoxy composites. Journal of Elastomers & Plastics. 2023; 55(2):331-346. https://doi.org/10.1177/00952443221147645

[29] Feng J, Shi Z, Zhao Y, Wang J, Yang X, Zhao M. Surface performance of nano-CrN/TiN multi-layered coating on the surface of Ti alloy. Materials. 2023; 16(24):7707. https://doi.org/10.3390/ma16247707

[30] Du JW, Yan XY, Chen L, Yue J, Du Y. Enhancing corrosion behavior of CrN coating through oxygen incorporation: Experimental and theoretical analyses. Ceramics International. 2024; 50(15):27380-27388. https://doi.org/10.1016/j.ceramint.2024.05.037

[31] Bakhytuly N, Smailov K, Kenzhegulov A, Kudabayeva M, Yessengaziyev A, Karim D, & Arynbayev T. Deposition Methods of Multilayer Hard Coatings for Improving Tribological Performance: A Mini-Review. Kompleksnoe Ispolzovanie Mineralnogo Syra = Complex Use of Mineral Resources. 2026; 343(4):16–33. https://doi.org/10.31643/2027/6445.37

[32] Berkinbayeva A, Saulebekkyzy S, Kenzhaliyev B, Smailov K, Yessengaziyev A, Nurtazina N, Karim D, Birlikzhan Y. Sodium Percarbonate for Eco-Efficient Cyanide Detoxification in Gold Mining Tailings. Metals. 2025; 15(10):1162. https://doi.org/10.3390/met15101162

[33] Kenzhaliyev B, Berkinbayeva A, Smailov K, Baltabekova Z, Saulebekkyzy S, Tolegenova N, Yessengaziyev A, Bakhytuly N, Tugambay S. Microwave Pre-Treatment for Efficient Zinc Recovery via Acid Leaching. Materials. 2025; 18:2496. https://doi.org/10.3390/ma18112496

Crossref
DOI: 10.31643/2028/6445.07
Metallurgy and Metallurgical Engineering

Modelling and Solving Problems of Sustainable Efficiency of Technological Processes in Metallurgy

*** Kazhikenova S.Sh., Shaikhova G.S., Shaltakov S.N., Shaltakova A.N.**

Abylkas Saginov Karaganda Technical University, Kazakhstan

** Corresponding author email: sauleshka555@mail.ru*

Received: *January 20, 2026*
Peer-reviewed: *February 25, 2026*
Accepted: *May 4, 2026*

ABSTRACT

Through a comparative analysis, this study investigates the development, simulation, and application of mathematical models for integrated analysis of copper rod production in order to improve product quality, reduce costs, and minimize risks. The purpose of this article is achieved by creating mathematical descriptions of real processes, which are then used to conduct computer experiments. In contrast to the traditional molecular dynamic methods, this study used information technology to obtain the characteristics of the flow field in technological equipment. The novelty lies in: integration of thermomechanical modeling with an optimization algorithm; introduction of a criterion minimizing mechanical property variation; consideration of reduction and redistribution effects on roll wear; possibility of adaptive real-time control. An information analysis of the profiles of copper melt flow velocities in a wide range of temperatures in the Copper Rod Production Plant Kazkat is presented. Information Technology fulfils the need to address the problem of determining the optimal values of temperature, rolling speed, and other parameters to achieve the best quality and productivity of copper rod production processes. Based on these findings, this study proposes the optimization directions for the temperature field profile in the rolling rolls, which leads to a decrease in roll wear and an increase in the uniformity of the wire rod structure, focusing on improving microstructural properties.

Keywords: simulation, copper, computer modelling, melt, information technology, numerical method.

Information about authors:

Kazhikenova Saule Sharapatovna — *Doctor of Technical Sciences, Higher Mathematics Department, Abylkas Saginov Karaganda Technical University, Nazarbayev str., 56, 100000, Karaganda, Kazakhstan. Email: sauleshka555@mail.ru; ORCID ID: https://orcid.org/0000-0002-6937-1577*

Shaikhova Gulnazira Serikovna — *Candidate of Technical Sciences, Higher Mathematics Department, Abylkas Saginov Karaganda Technical University, Nazarbayev str., 56, 100000, Karaganda, Kazakhstan. Email: shaikxova_2011@mail.ru; ORCID ID: https://orcid.org/0000-0002-2036-3023*

Shaltakov Sagyndyk Nagashibaevich — *PhD, Department of Physics, Abylkas Saginov Karaganda Technical University, Nazarbayev str., 56, 100000, Karaganda, Kazakhstan. Email: sagyndyk613@mail.ru; ORCID ID: https://orcid.org/0000-0002-1186-1178*

Shaltakova Ainura Nigmatollovna — *Master, Abylkas Saginov Karaganda Technical University, Nazarbayev str., 56, 100000, Karaganda, Kazakhstan. Email: ainurashatakova@gmail.com*

Introduction

The economic growth of Kazakhstan is providing local enterprises with the necessary goods and materials produced at the national level that meet high-quality standards and scientific algorithms for theoretical research. In the mining and metallurgical industry, there is a need to create high-quality products that meet the needs of the market, as well as the creation of scientific algorithms for the study of metals with different physical properties and inhomogeneities. Simulations of technological processes in metallurgical production, such as process modeling in metallurgical production, is aimed at solving production problems with molten systems for approaching sustainable efficiency.

Contribution [1] combines molecular dynamic methods, the properties of Al, and the matrix composite.

This study presents a new technology for low-carbon hydrogen metallurgy based on hydrogen instead of carbon and a method for producing pig iron for a reducing smelting furnace [2].

This article focuses on the simulations of technological processes in metallurgical production. The study presents a new technology associated with copper staves. The method of mathematical modelling and analysis of slag crust in the bosh was conducted [3]. The solutions to numerous problems

and technical indicators associated with the copper slag crust were investigated.

This study is concerned with microstructure evolution in high stacking fault metals and alloys, «it is relevant to the high-temperature extrusion of aluminum alloys» [4].

Recommendations are proposed for technological optimization and the use of technologies to create an integrated low-carbon metallurgical system, storage technologies, and carbon cycling technologies [5].

The purpose of this article is to provide local enterprises with the necessary goods and materials produced at the national level that meet high-quality standards and scientific algorithms for theoretical research for the production of «titanium sponge from concentrates of the Satbaevskoye deposit in Kazakhstan. The article uses an innovative approach for obtaining titanium slag from low-grade Kazakhstan ilmenite concentrates characterized by a high content of refractory components» [6].

To experiment, the water model of the oxygen with recommendations for technological optimization and the use of technologies to create an integrated metallurgical system, storage technologies, carbon cycling technologies, and the effects of a new retaining wall device are proposed for innovative research [7].

One of the most resource-intensive and strategically important industries is the production of copper rods, which have various physical and chemical characteristics. This trend is the demand of society for high-quality materials with high-performance properties. To solve the corresponding technological problems, it is necessary to use mathematical modelling tools and informatization, cognitive tools, which make it possible to study the static or dynamic characteristics of the object under study [[8], [9]]. The purpose of this article is to simulate technological processes in metallurgical production, as process modeling in metallurgical production is aimed at solving production problems with molten systems for approaching sustainable efficiency.

To experiment with recommendations for technological optimization and the use of technologies to create an integrated metallurgical system, technologies for creating retaining walls for innovative research are proposed for the development of the metallurgical industry [10]. Modeling of technological processes in metallurgical production is aimed at solving production problems using various microstructures to achieve sustainable efficiency [11].

The solution of production problems at modern metallurgical enterprises is carried out using the Recommendation for Technological Optimization, aimed at an analytical solution based on differential equations proposed in [12].

Recommendations are offered on the use of technologies for the purpose of technological optimization of production, storage technologies, cycling technologies, modelling [[13], [14], [15], [16], [17], [18]].

Theoretical framework

Particular attention should be paid to intensifying work on the creation of a new copper smelter that meets modern environmental requirements [[19], [20]]. The importance of the metallurgical industry and non-ferrous metallurgy for the economy at present can hardly be overestimated - the bulk of all spheres of production enjoy the results of metallurgical production. Metallurgy is of great importance for the development of national production and ensuring the modernization of the economies of countries, their integration into the world economy [[21], [22], [23], [24], [25], [26]].

The above technologies use high-quality scientific and technical problems [[27], [28]]. The study of various areas made it possible to design the most optimal option for cognitive studies on intellectual results [[29], [30], [31]].

There is a movement of convective flows or thermodynamic flows, where the bulk force divides the flow into the bottom layer and the main flow. The main flow moves upwards, and the denser lower layer descends, creating circulation and mixing of the medium, as when heated from below [[32], [33], [34]].

Mathematical modelling is a powerful tool for achieving a competitive advantage in the production of copper rods. Kazakhstan has significant copper reserves, which makes the production and export of copper rod a key area for the development of the mining industry. This study fulfils the need for determining the optimal values of temperature, rolling speed, and other parameters to achieve the best quality and productivity of copper rod production processes. Mathematical modelling of the copper rod process aims to optimize the temperature field profile, which leads to an increase in the uniformity of the wire rod structure at the Copper Rod Production Plant Kazkat. The production of copper at modern metallurgical enterprises is

carried out using the following technologies: SCR, SMS Contirod, UPCAST Outokumpu.

The production scheme of copper rods is presented in Figure 1.

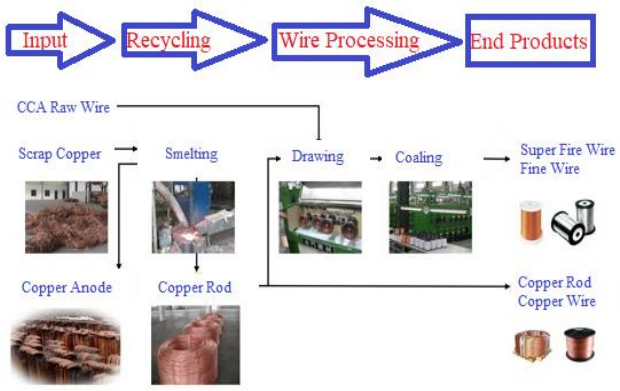

Figure 1 - Production scheme of copper rods

At present, the copper industry in the country is represented by the production of copper concentrate products. Half of the exported materials fall on the share of ore concentrates and metals, which occupy the most important place in the list of products exported from the country [[27], [35], [36]].

It is well known that the approximation of hydrodynamic equations leads to nonlinear systems of algebraic equations. Consequently, their numerical solution is associated with significant computational difficulties. In this regard, various approaches to the construction of operator-splitting schemes for the Navier–Stokes equations in the sense of weak approximation were considered.

Let us outline the general principle for constructing splitting schemes for the Navier–Stokes equations. In a bounded domain $\Omega \in R^3$, we consider a system of nonlinear stationary equations subject to prescribed boundary conditions. In addition, a temperature model of a heterogeneous melt is formulated with specified initial and boundary conditions.

Monitoring and analyzing melt motion constitute the central problem of this study. It is assumed that the external forces acting on the melt under boundary conditions are known, and that the initial velocity field is specified in the case of unsteady flow. The physical and mathematical model of melt motion is formulated in a coordinate system in which the computational domain associated with the melt remains fixed.

The metal melt moved along the inclined chute of the metallurgical equipment. This study aims to address obtaining high-quality products with ever-increasing demand from machine builders while minimizing the costs of their production. The modelling framework is based on the fundamental principles of continuum mechanics and thermodynamics. The motion of the molten copper is described using the Navier–Stokes equations for incompressible viscous flow (1)-(3):

Continuity equation:

$$\nabla \cdot \vartheta = 0 \tag{1}$$

Momentum conservation equation:

$$\rho\left(\frac{\partial \vartheta}{\partial t} + (\vartheta \cdot \nabla)\vartheta\right) = \mu \nabla^2 \vartheta - \nabla p + \rho f \tag{2}$$

Energy equation (with thermal conductivity)

$$\rho c_p \left(\frac{\partial T}{\partial t} + \vartheta \cdot \nabla T\right) = \theta \nabla^2 T \tag{3}$$

For steady-state flow conditions:

$$\frac{\partial \vartheta}{\partial t} = 0$$

with initial boundary conditions:

$$\vartheta\big|_{t=0} = \vartheta_0(x), t\big|_{t=0} = t_0(x),\ \vartheta\big|_S = 0, t\big|_S = 0\,, \tag{4}$$

where:

ϑ — velocity vector of the melt;

ρ — density;

ρ — pressure;

μ — dynamic viscosity;

f — gravitational acceleration vector;

c_p — specific heat capacity;

θ — thermal conductivity.

Let the metal melt move along the inclined chute of metallurgical equipment. The physical and mathematical model of this technological process is built under the assumption that the length of the trough is infinite, the metal melt moves along the axis of the trough in such a way that the velocity function ω depends only on the variable x, y whereas, the pressure function depends on the variable z. Such motions are called steady-state motions. As a result, we obtain a model with isothermal motion of the melt, in which density ρ and viscosity μ are constant. Hence, the metal melt moves along the inclined chute of metallurgical equipment, as given in Navier-Stokes equations form (5). The change in pressure is negligible from

section to section, keeping the same value in a given section. Such motions are called steady-state motions. Thus, based on (5), we obtain the following equation (6).

$$\begin{cases} -\frac{1}{\rho}\frac{\partial p}{\partial x}=0, \\ -\frac{1}{\rho}\frac{\partial p}{\partial y}=0, \\ \omega\frac{\partial \omega}{\partial z}=-\frac{1}{\rho}\frac{\partial p}{\partial z}+\xi\left(\frac{\partial^2\omega}{\partial x^2}+\frac{\partial^2\omega}{\partial y^2}+\frac{\partial^2\omega}{\partial z^2}\right), \\ \frac{\partial \omega}{\partial z}=0. \end{cases} \quad (5)$$

$$\frac{dp}{dz}=\lambda\left(\frac{\partial^2\omega}{\partial x^2}+\frac{\partial^2\omega}{\partial y^2}\right). \quad (6)$$

The right side of (6) depends of x, y coordinates, the left side depends of z coordinate. Let us the main statements of hydrodynamics:

$$\frac{dp}{dz}=-\frac{\Delta p}{\lambda},$$

λ is the chute length.

When the melt flows through an inclined trough, there is a movement of convective flows or thermodynamic flows, where the bulk force divides the flow into the bottom layer and the main flow. Internal friction forces slow down the movement of the atoms of the lower layer. This deceleration is transferred from one layer to another along the entire flow to the surface of the copper melt; there is a free surface of the metal melt. So, the pressure will be equal to the atmospheric pressure.

This study aims to address the angle of inclination, which is equal to Θ, a volumetric force, and is equal to $F_z=\lambda\sin\Theta=\frac{\Delta p}{\ell}$. So

$$\lambda\left(\frac{\partial^2\omega}{\partial x^2}+\frac{\partial^2\omega}{\partial y^2}\right)+\rho\lambda\sin\Theta=0. \quad (7)$$

$$\omega=0 \;\; y=0,\; \frac{\partial\omega}{\partial y}=0,\; y=\lambda_1,\; \frac{\partial\omega}{\partial x}=0,\; x=\lambda_2. \quad (8)$$

Calculations were constructed for industrial equipment at the Copper Rod Production Plant Kazkat. We obtained data from industrial partners or public repositories.

Production of copper rods requires a constant search for technical solutions aimed at reducing harmful impurities and oxygen to the lowest possible concentrations. The study of various areas made it possible to design the most optimal option for copper rods using modern Continuous Casting and Rolling Technology. We conduct cognitive studies on intellectual results with existing measures of copper melt velocities. As a result, the problem of decision-making is solved using the proposed cognitive measure of similarity to check its applicability.

Modern achievements in this area have led to the production of high-quality copper at the Copper Rod Production Plant Kazkat, in Figure 2. The technological scheme of the equipment is shown in Figure 3.

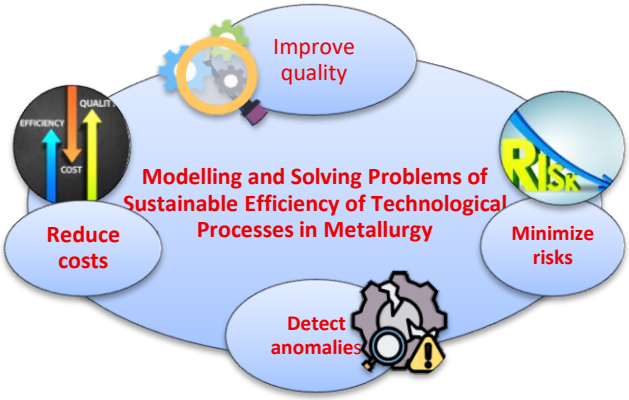

Figure 2 - Theoretical framework

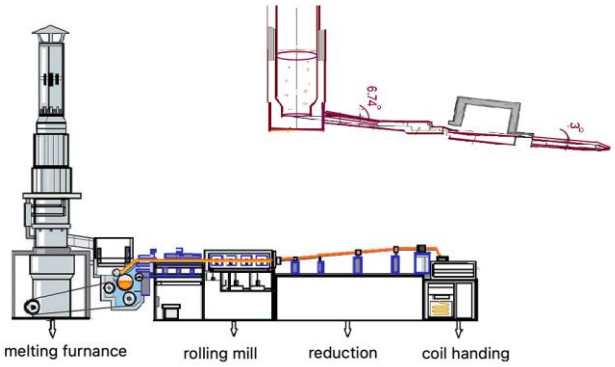

Figure 3 - Technological scheme of SCR Plant Kazkat, measurements are given in [mm]

Numerical Modelling

Using Equations (9) – (11), we calculated the numerical values of the melt flow parameters for the Copper Rod Production Plant Kazkat business perimeter for the lower chute with an inclination angle of 3º, as shown in Fig. 4:

$$S=\frac{\lfloor \lambda r-\sigma(r-h)\rfloor}{2}, \quad (9)$$

λ is arc length, σ is chord, $h-$ is segment arrow:

$\sigma = 80[\text{mm}], \quad h = 16[\text{mm}],$

$$\lambda \approx \sqrt{\sigma^2 + \left(\frac{15h^2}{3}\right)} = \sqrt{80^2 + \left(15 \cdot \frac{16^2}{3}\right)} = 87.6[mm^2]. \quad (10)$$

$$S = \frac{\left[87{,}6 \cdot \frac{104}{2} - 80\left(\frac{104}{2} - 16\right)\right]}{2} = 1675.2[mm^2]. \quad (11)$$

The average flow velocity of the copper melt is equal to $\upsilon_{middle} = 0.42\left[\frac{m}{s}\right]$.

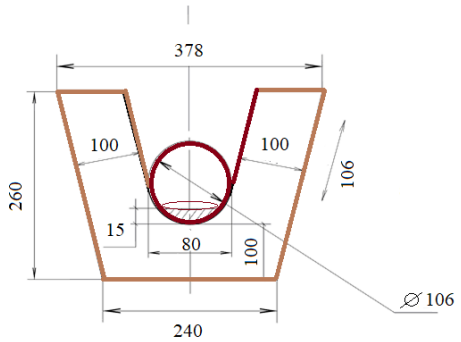

Figure 4 - Section of lower chute (measurements given in [mm])

The governing Navier–Stokes equations (5)–(6) were discretized using the finite volume approach.

$$\frac{\partial}{\partial t}\int_V \rho\phi dV + \iint_S \rho\phi\vec{u}\cdot\vec{n}dS = \iint_S \Gamma\nabla\phi\cdot\vec{n}dS + \int_V S_\phi dV \quad (12)$$

ϕ is a general transported variable (e.g., velocity component or energy),

Γ is the diffusion coefficient,

S_ϕ is the source term,

$\vec{n}$ n is the outward unit normal vector on the surface.

Spatial discretization of the convective terms was performed using a second-order upwind scheme (13) to achieve higher-order accuracy and reduce numerical diffusion. Time integration was performed using a second-order implicit scheme (14), which ensures enhanced temporal accuracy and improved stability characteristics of the numerical solution.

$$\phi_f = \phi_P + \nabla\phi_P \cdot \left(\vec{r}_f - \vec{r}_P\right), \quad (13)$$

P denotes the upstream control volume, $\vec{r}_f, \vec{r}_P$ are position vectors of the face center and cell center, respectively.

The transient term is discretized using the second-order backward differencing formula (BDF2):

$$\left(\frac{\partial\phi}{\partial t}\right)^{n+1} = \frac{3\phi^{n+1} - 4\phi^n + \phi^{n-1}}{2\Delta t}, \quad (14)$$

which yields second-order temporal accuracy $0\left(\Delta t^2\right)$.

The scheme is implicit because the unknown value ϕ^{n+1} appears in the discretized equation and is obtained by solving the resulting algebraic system.

In the calculations of the numerical scheme $\Delta x = \Delta y = 0{,}02$ we used constant time step sizes $\Delta t = 0{,}001$. Calculated profiles of flow velocities υ and u are shown in Fig. 5.

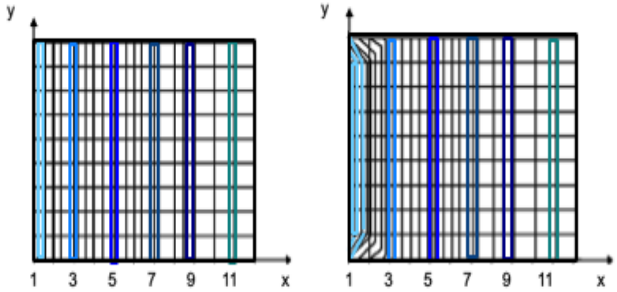

a) b)

Figure 5 - (a) transverse υ and (b) longitudinal u melt flow velocity profiles

A structured computational grid with local refinement in the near-wall regions was employed to ensure accurate resolution of boundary layer phenomena. The mesh was selectively refined in areas with high velocity and pressure gradients to improve predictions of wall shear stresses and heat transfer, while maintaining a reasonable overall cell count and computational cost. A structured grid with local refinement near walls was used.

Three grid levels were tested:

- 1.2×10^5 cells
- 3.8×10^5 cells
- 9.5×10^5 cells

Grid independence was achieved when the variation in mean velocity was below 2%.

The simulation and application of mathematical parameters include movement of convective flows or thermodynamic flows, the bulk force, and internal friction forces when the melt flows in an inclined trough.

The temperature dependence of the dynamic viscosity was described by the Arrhenius-type equation:

$$\mu_{model}(T) = A\exp\left(\frac{Q}{RT}\right) \quad (15)$$

$A = 3.2 \times 10^{-4}$Pa·s
$Q = 39{,}000$J/mol
$R = 8.314$J/(mol·K)

The strength of the relationship between the experimental data and the values calculated using (15) was evaluated using the coefficient of nonlinear multiple correlation (16), together with an assessment of its statistical significance using the Fisher criterion (17).

The coefficient of nonlinear multiple correlation was determined as:

$$R = \sqrt{1 - \frac{(n-1)\sum_{i=1}^{n}\left(y_{\exp,i} - y_{calc,i}\right)^2}{(n-k-1)\sum_{i=1}^{n}\left(y_{\exp,i} - \bar{y}_{\exp}\right)^2}} \quad (16)$$

$$F = \frac{R^2}{1-R^2}\frac{n-m-1}{m}, \quad (17)$$

$y_{\exp.i}$ experimental value

$y_{calc.i}$ calculated value,

$\bar{y}_{\exp.i}$ mean experimental value,

n number of experimental data points,

m number of independent variables in the regression model.

Let us construct an algorithm for calculating the viscosity of a copper melt and establish the dependence of viscosity on temperature. The results are presented in Table 1 and Figure 6.

Table 1 - Calculated and experimental data [37] of the viscosity

T	μ_{exp}	μ_{calc}	Δ (model–exp)	Relative Error (%)
T_m =1355	4.5	4.24	-0.26	-5.8
1395	4.2	4.10	-0.10	-2.4
1435	4.0	3.97	-0.03	-0.8
1475	3.5	3.85	-0.00	0.00
1515	3.75	3.74	-0.01	-0.03
1555	3.65	3.63	-0.02	-0.05
1595	3.55	3.53	-0.02	-0.06
1635	3.45	3.44	-0.01	-0.03
MAPE	-	-		1.34

The correlation coefficient R=0.986626 is high, therefore, and shows the correctness and adequacy of our verification of theoretical results.

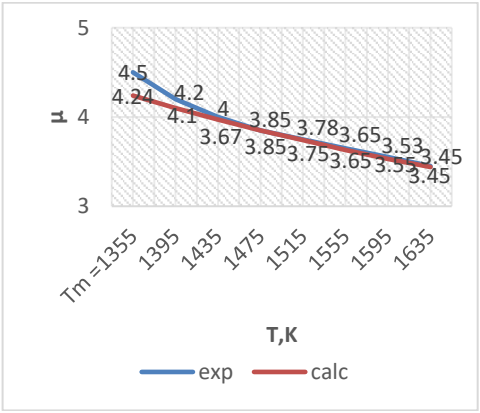

Figure 6 – The copper viscosity as a function of temperature

Comparison between the proposed model and experimental viscosity data of liquid copper in the temperature range 1355–1635 K demonstrates excellent agreement, R^2 = 0.91, MAPE = 1.34%. The maximum deviation 5.8% occurs near the melting temperature, likely due to structural fluctuations and the assumption of constant activation energy. In In the range 1435–1635 K, the model accuracy remains within 1%, confirming its suitability for engineering
calculations.

The coefficient of determination is calculated using the standard formula for model validation:

$$R^2 = 1 - \frac{SS_{res}}{SS_{tot}},$$

$SS_{res} = \sum\left(\mu_{\exp} - \bar{\mu}_{model}\right)^2$ Is the sum of squared residuals,

$SS_{tot} = \sum\left(\mu_{\exp} - \bar{\mu}_{\exp}\right)^2$ is the total sum of squares, representing the total variance of the experimental data.

$\bar{\mu}_{\exp}$ is the mean experimental viscosity.

R	R^2	SS_{res}	SS_{tot}	$\bar{\mu}_{\exp}$
0.986626	0.91	0.0795	0.842	3.869mPA

Results and Discussion

The copper flow velocity distribution profiles at 1355 K, 1395 K, 1435 K, 1475 K, 1515 K, 1555 K, 1595 K, and 1635 K are presented in Figures 7 – 14 and Tables 2-9.

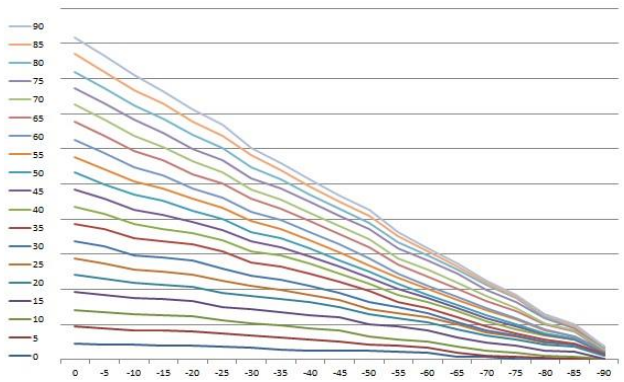

Figure 7 - Velocity isolines at 1355 K

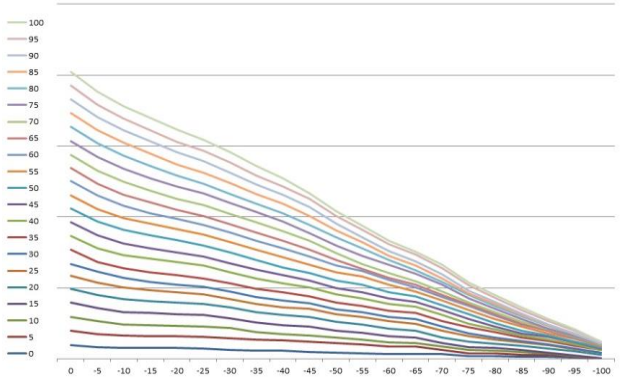

Figure 8 - Velocity isolines at 1395 K

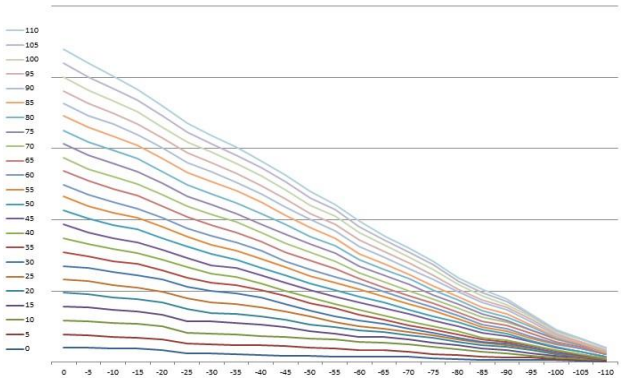

Figure 9 - Velocity isolines at 1435 K

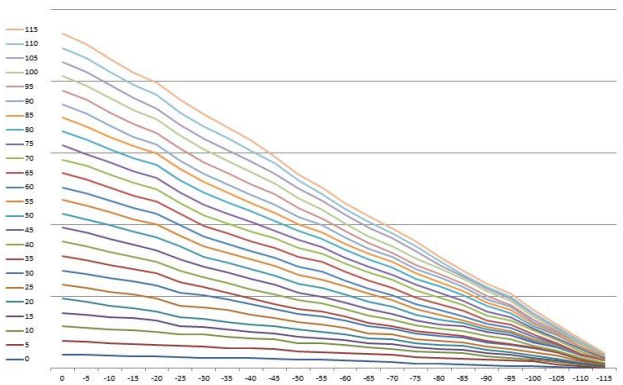

Figure 10 - Velocity isolines at 1475 K

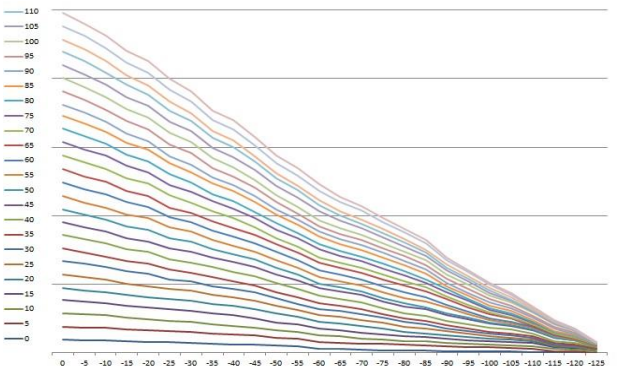

Figure 11 - Velocity isolines at 1515 K

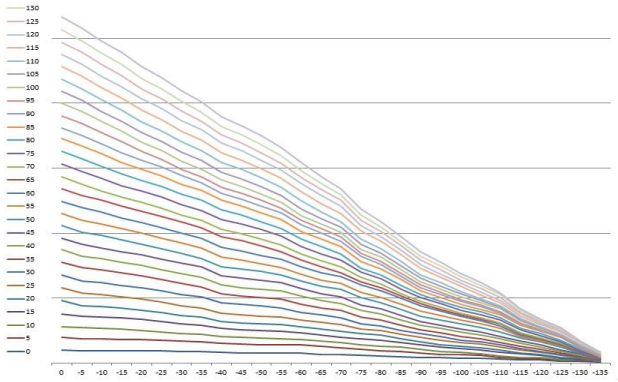

Figure 12 - Velocity isolines at 1555 K

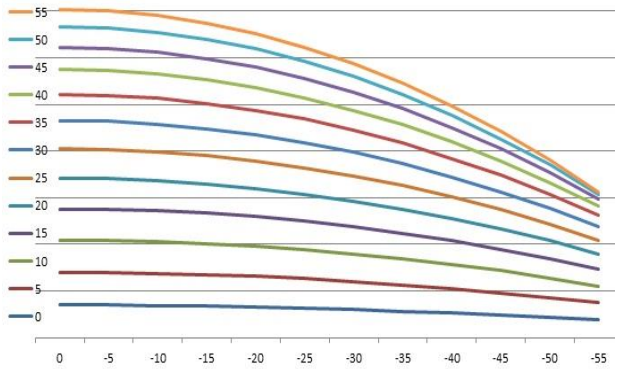

Figure 13 - Velocity isolines at 1595 K

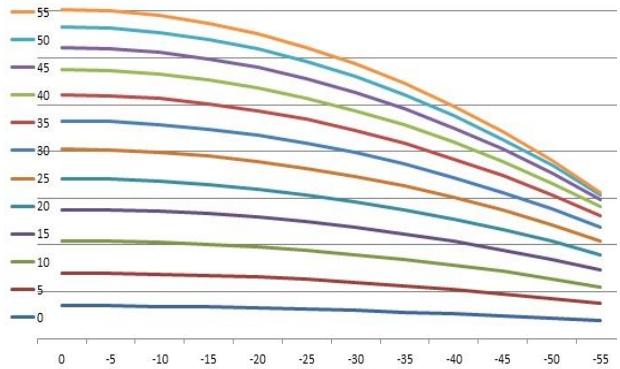

Figure 14 - Velocity isolines at 1635 K

Table 2 - Data from numerical calculations of the copper melt motion at 1355 K

y / x	0.00	-10.00	-20.00	-30.00	-40.00	-50.00
0.00	0.4021	0.3963	0.3774	0.3461	0.3032	0.2471
10.00	0.3932	0.3900	0.3722	0.3400	0.2972	0.2412
20.00	0.3773	0.3711	0.3520	0.3210	0.2783	0.2223
30.00	0.3461	0.3402	0.3213	0.2913	0.2471	0.1923
40.00	0.3030	0.2973	0.2783	0.2470	0.2051	0.1484
50.00	0.2472	0.2410	0.2220	0.1910	0.1480	0.0922

Table 3 - Data from numerical calculations of the copper melt motion at 1395 K

y / x	0.00	-10.00	-20.00	-30.00	-40.00	-50.00
0.00	0.4422	0.4342	0.4142	0.3801	0.3324	0.2711
10.00	0.4341	0.4280	0.4073	0.3732	0.3250	0.2642
20.00	0.4142	0.4070	0.3872	0.3520	0.3053	0.2442
30.00	0.3801	0.3730	0.3523	0.3190	0.2710	0.2105
40.00	0.3320	0.3250	0.3051	0.2712	0.2243	0.1623
50.00	0.2710	0.2640	0.2440	0.2101	0.1620	0.1023

Table 4 - Data from numerical calculations of the copper melt motion at 1435 K

y / x	0.00	-10.00	-20.00	-30.00	-40.00	-50.00
0.00	0.4823	0.4742	0.4511	0.4142	0.3620	0.2962
10.00	0.4740	0.4670	0.4440	0.4072	0.3555	0.2880
20.00	0.4513	0.4440	0.4232	0.3851	0.3330	0.2660
30.00	0.4140	0.4070	0.3850	0.3490	0.2964	0.2290
40.00	0.3620	0.3550	0.3333	0.2960	0.2442	0.1770
50.00	0.2962	0.2883	0.2660	0.2290	0.1770	0.1120

Table 5 - Data from numerical calculations of the copper melt motion at 1475 K

y / x	0.00	-10.00	-20.00	-30.00	-40.00	-50.00
0.00	0.5231	0.5137	0.4901	0.4500	0.3940	0.3210
10.00	0.5140	0.5070	0.4820	0.4420	0.3859	0.3131
20.00	0.4900	0.4820	0.4590	0.4181	0.3610	0.2890
30.00	0.4500	0.4420	0.4178	0.3780	0.3210	0.2490
40.00	0.3939	0.3860	0.3610	0.3213	0.2660	0.1920
50.00	0.3209	0.3128	0.2890	0.2490	0.1920	0.1210

Table 6 - Data from numerical calculations of the copper melt motion at 1515 K

y / x	0.00	-10.00	-20.00	-30.00	-40.00	-50.00
0.00	0.5659	0.5630	0.5300	0.4870	0.4260	0.3470
10.00	0.5560	0.5550	0.5210	0.4780	0.4170	0.3390
20.00	0.5301	0.5280	0.4958	0.4522	0.3910	0.3129
30.00	0.4870	0.4850	0.4520	0.4091	0.3469	0.2690
40.00	0.4260	0.4240	0.3910	0.3469	0.2882	0.2081
50.00	0.3470	0.3450	0.3131	0.2689	0.2080	0.1310

Table 7 - Data from numerical calculations of the copper melt motion at 1555 K

y / x	0.00	-10.00	-20.00	-30.00	-40.00	-50.00
0.00	0.6111	0.6002	0.5721	0.5250	0.4589	0.3752
10.00	0.6002	0.5920	0.5633	0.5159	0.4503	0.3660
20.00	0.5720	0.5630	0.5362	0.4880	0.4223	0.3372
30.00	0.5253	0.5159	0.4882	0.4420	0.3753	0.2903
40.00	0.4590	0.4501	0.4221	0.3750	0.3092	0.2253
50.00	0.3750	0.3660	0.3370	0.2900	0.2250	0.1410

Table 8 - Data from numerical calculations of the copper melt motion at 1595 K

y / x	0.00	-10.00	-20.00	-30.00	-40.00	-50.00
0.00	0.6011	0.6432	0.6130	0.5631	0.4922	0.4023
10.00	0.6430	0.6340	0.6028	0.5530	0.4822	0.3922
20.00	0.6132	0.6030	0.5740	0.5230	0.4521	0.3620
30.00	0.5633	0.5532	0.5230	0.4733	0.4020	0.3110
40.00	0.4920	0.4822	0.4520	0.4022	0.3330	0.2412
50.00	0.4021	0.3920	0.3622	0.3110	0.2410	0.1511

Table 9 - Data from numerical calculations of the copper melt motion at 1635 K

y / x	0.00	-10.00	-20.00	-30.00	-40.00	-50.00
0.00	0.6988	0.6880	0.6560	0.6020	0.5270	0.4301
10.00	0.6880	0.6772	0.6450	0.5910	0.5160	0.4190
20.00	0.6560	0.6449	0.6131	0.5590	0.4840	0.3871
30.00	0.6020	0.5909	0.5591	0.5060	0.4301	0.3331
40.00	0.5270	0.5160	0.4842	0.4302	0.3562	0.2580
50.00	0.4300	0.4190	0.3870	0.3330	0.2580	0.1620

The physical picture is: when the melt flows through an inclined trough, there is a movement of convective flows or thermodynamic flows, where the bulk force divides the flow into the bottom layer and the main flow. The main flow moves upwards, and the denser lower layer descends, creating circulation and mixing of the medium, as when heated from below. Internal friction forces slow down the movement of the atoms of the lower layer. When the melt flows in an inclined trough, this deceleration is transferred to the surface of the copper melt [8].

The simulation and application of mathematical models for integrated analysis of copper rod production may show manufacturing abnormalities, production efficiency, and reliability.

We have developed a mathematical model for calculating the melt flow rate profile at different temperatures in process equipment, starting from the melting point of copper. We built graphs of isolines of the flow velocities of melted copper in the

technological equipment Copper Rod Production Plant Kazkat. Calculations showed the heterogeneity of the structure of the copper melt near the melting point. Calculations showed that the number of contours at low temperatures, such as 1355 K, is smaller. It was also analytically established that the number of contours at higher temperatures, such as 1595 K, is smaller. This is due to the thermal weakening of the metal properties of the copper melt, which is the cause of structural defects in the production of copper rod.

By analysing early, simulation and application of mathematical models improve decision-making, resource allocation, and operational expenses for process optimization and quality control. The recommended approach to the issues and technological processes for increased efficiency and profitability.

Verification of the melting parameters with manufacturing parameters at Plant Kazkat shows fulfils to optimize the temperature field profile, which leads to an increase in the uniformity of the wire rod from $0.62\left[\frac{m}{s}\right]$ to $0.05\left[\frac{m}{s}\right]$. Therefore, it is important to take into account that the minimum flow rate of the melt will be at the bottom of the trough, the highest flow rate will be at the surface of the melt. The melting parameters with manufacturing parameters at Plant Kazkat include movement of equations (5) and (6).

Let us calculate the number of isolines at the specified temperatures. The maximum isoline value of the velocity profiles of the copper melt movement at Plant Kazkat equipment at the specified temperatures was 28 at 1555 K, and are presented in Figure 15.

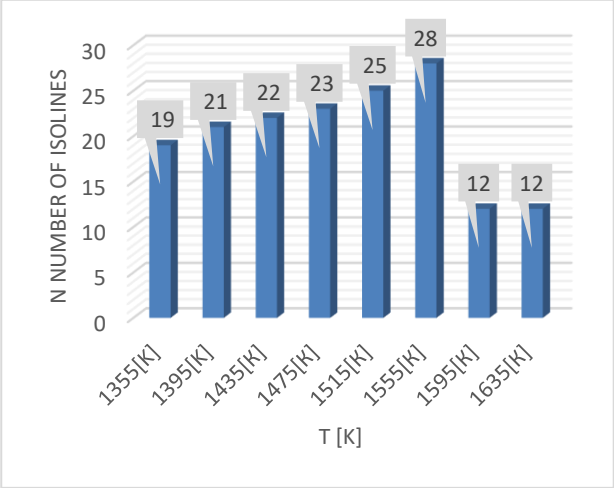

Figure 15 - The isoline value

The numerical methods show that the average value of the mathematical model velocity is approximately equal to the average velocity of the copper melt flow $v = 0.4\left[\frac{m}{s}\right]$.

Mathematical and numerical modelling of the copper rod process aims to optimize the temperature field profile. The technological temperature field profile at Plant Kazkat equipment was in the range of 1425-1553 K and shows the correctness and adequacy of our verification of theoretical results.

Below is an example calculation demonstrating the reduction in tensile strength variation and the increase in ductility. We compare 10 batches before and 10 batches after optimization in Table 10.

Table 10 - Batches before and after optimization

Batch No	Tensile Strength σ_u, MPa		Similar Example for Ductility δ, %	
	Before optimization	After optimization	Before optimization	After optimization
1	560	538	21.8	22.6
2	525	542	22.1	22.9
3	545	540	21.5	22.7
4	530	536	22.3	22.8
5	555	544	21.7	22.5
6	520	539	22.0	22.9
7	548	541	21.6	22.6
8	535	537	22.2	22.7
9	562	543	21.4	22.8
10	528	540	21.9	22.6
Mean value	540.8	540.0	21.85	22.71

Calculation of the standard deviation presented at equation (18)

$$s = \sqrt{\frac{\sum(x_i - \bar{x})^2}{n-1}} \qquad (18)$$

Standard deviation before optimization s_1 and after optimization s_2 is equal to

$$s_1 \approx 14.8 \text{ MPa}, \; s_2 \approx 2.7 \text{ MPa}.$$

Technological spread $\pm 2s_1 = \pm 29.6$ MPa.
Technological spread $\pm 2s_2 = \pm 5.4$ MPa.
So, variance comparison (F-test):

$$F = \frac{s_1^2}{s_2^2}; F = \frac{14.8^2}{2.7^2}; \; F \approx \frac{219}{7.3} \approx 30.$$

Critical value for n=10 at 95% confidence is 3.18.
Since:

$$F = 30 > 3.1.$$

The difference in variances is statistically significant.

Calculation of ductility increase

$$\frac{22.71 - 21.85}{21.85} - 100\% = 3.9\%$$

Ductility increased by approximately 4%.

As a result of implementing the optimization model, the standard deviation of tensile strength decreased from 14.8 MPa to 2.7 MPa, corresponding to a reduction in technological variation from ±29.6 MPa to ±5.4 MPa. The F-test confirmed statistical significance at a 95% confidence level.

The average elongation increased from 21.85% to 22.71%, corresponding to 39% increase in ductility.

In practice, the following groups of methods are commonly used for wire rod rolling process optimization:

- Empirical technological schedules;
- Regression-based statistical models;
- Finite Element Method (FEM) simulations;
- Machine learning approaches;
- The proposed integrated optimization model.

Advantages of the proposed integrated model combine: physical–mathematical description of deformation; thermal balance modeling; optimization algorithms; statistical validation (Table 11).

Quantitative performance comparison of the proposed integrated model is presented in Table 12.

Table 11 - Advantages of the proposed integrated model

Criterion	Empirical	Regression	FEM	ML	Integrated Model
Accounts for process physics	–	±	+	–	+
Temperature modeling	–	±	+	±	+
Real-time applicability	+	+	–	+	+
Roll wear prediction	–	–	+	±	+
Adaptability	–	±	–	+	+
Industrial applicability	+	+	±	±	+

Table 12 - Quantitative performance comparison

Indicator	Empirical	Regression	Integrated Model
Tensile strength variation	±25–30 MPa	±18–20 MPa	±8–12 MPa
Increase in elongation	0–1%	1–2%	3–5%
Roll wear reduction	0–5%	5–8%	15–25%
Scrap reduction	up to 1%	1–2%	2–3%

Table 13 - Initial assumptions for a medium-capacity plant

Annual production volume	$Q = 120.000 t/year$
Average product value	$C_p = 8.500 USD/t$
Baseline defect rate	$d_o = 2.5\%$
Expected reduction in defect rate	$\Delta d = 1.0\%$
Annual energy consumption for melting and casting	$E_o = 45.000 MWh$
Specific energy consumption, MWh/t	$e_{spec} = 0.52 MWh/t$
Expected energy savings	3%
Estimated implementation cost (software integration, training, system calibration)	$I = 450.000 USD$
Annual loss due to defects before optimization	$L_0 = 25.5 millionUSD$
Economic effect after optimization (defect reduction by 1%)	$\Delta L = Q \Delta d C_p = 10.2 millionUSD/year$
Annual energy savings:	$E_S = 0.03 \bullet 45.000 = 1.350 MWh$
Assuming an electricity cost of	$C_e = 110 USD/MWh$
Annual energy savings	$S_e = 1.350 \cdot 110 \approx 148.500 USD/year$
Reduction in roll maintenance costs if annual roll maintenance costs	$C_m = 1.2 millionUSD/year$
The model reduces wear-related costs by 15%	$S_m = 0.15 \cdot 1.2 \approx 180.000 USD/year$
Total annual economic benefit	$S_{total} \approx 10.53 millionUSD/year$
Return on investment (ROI)	$ROI = \frac{S_{total} - I}{I} \cdot 100\% \approx \approx 2240\%$
Payback period	$T_{payback} = \frac{I}{S} \cdot 100\% \approx 0.5 monts$

Unlike empirical and regression-based approaches, the proposed model provides a comprehensive thermomechanical description of the rolling process and enables multi-objective

optimization. Compared with finite element modeling, the model has significantly lower computational complexity and is suitable for real-time industrial applications. This ensures reduced mechanical property variation, lower roll wear, and improved stability of wire rod quality.

To evaluate the feasibility of implementing the proposed viscosity-based optimization model in copper wire rod production, a quantitative economic analysis was performed.

The implementation of the proposed model demonstrates (Table 13):

- Extremely high return on investment (>2000%);
- Payback period of less than one month;
- Significant reduction in defect-related losses;
- Measurable energy savings;
- Extended roll service life.

Even under more conservative assumptions, a defect reduction of 0.3–0.5%, the payback period remains within several months, confirming strong industrial feasibility.

Conclusions

A mathematical and computer model and the numerical integration algorithm for calculating the melt flow rate profile at different temperatures in process equipment, starting from the melting point of copper, were developed.

The validation of theoretical results, mathematical model, and the numerical integration algorithm show the recommended approach to the issues and technological processes for increased efficiency and profitability. The proposed model fulfils to optimize the temperature field profile, integration of thermomechanical modeling with an optimization algorithm; introduction of a criterion minimizing mechanical property variation; consideration of reduction and redistribution effects on roll wear; possibility of adaptive real-time control.

The technological temperature field profile at Plant Kazkat equipment was in the range of 1425-1553 K, and the best melting occurred at 1555 K.

The strength of the relationship between the experimental data and the values calculated using it was evaluated using the coefficient of nonlinear multiple correlation, together with an assessment of its statistical significance. The correlation coefficient R=0.952734 is high, therefore, and shows the correctness and adequacy of our verification of theoretical results.

The numerical calculations show that the average elongation increased from 21.85% to 22.71%, corresponding to 3.9% increase in ductility. Comparison between the proposed model and experimental viscosity data of liquid copper in the temperature range 1355–1635 K demonstrates excellent agreement R^2 = 0.91, MAPE = 1.34%. The maximum deviation 5.8% occurs near the melting temperature, likely due to structural fluctuations and the assumption of constant activation energy. In In the range 1435–1635 K, the model accuracy remains within 1%, confirming its suitability for engineering
calculations.

Unlike empirical and regression-based approaches, the proposed model provides a comprehensive thermomechanical description of the rolling process and enables multi-objective optimization, has significantly lower computational complexity, and is suitable for real-time industrial applications.

This ensures reduced mechanical property variation, lower roll wear, and improved stability of wire rod quality. The implementation of the proposed model demonstrates extremely high return on investment (>2000%); payback period of less than one month; a significant reduction in defect-related losses; measurable energy savings; extended roll service life.

Conflicts of interest. The authors declare that they have no conflicts of interest in this work.

CRediT author statement: **S. Kazhikenova**: Conceptualisation, Methodology, Software; **G. Shaikhova**: Data curation, Writing draft preparation; **S. Shaltakov**: Visualisation, Investigation, Validation; **A. Shaltakova**: Reviewing and Editing.

Acknowledgements.

This work was supported by the Ministry of Science and Education of the Republic of Kazakhstan [grant numbers AP23486482, 2024-2026].

Cite this article as: Kazhikenova SSh, Shaikhova GS, Shaltakov SN, Shaltakova AN. Modeling and Solving Problems of Sustainable Efficiency of Technological Processes in Metallurgy. Kompleksnoe Ispolzovanie Mineralnogo Syra = Complex Use of Mineral Resources. 2028; 344(1):65-78. https://doi.org/10.31643/2028/6445.07

Металлургиядағы технологиялық процестердің тұрақты тиімділігі мәселелерін модельдеу және шешу

Кажикенова С.Ш., Шаихова Г.С., Шалтаков С.Н., Шалтакова А.Н.

Әбілқас Сағынов атындағы Қарағанда техникалық университеті, Қазақстан

Мақала келді: *20 қаңтар 2026*
Сараптамадан өтті: *25 ақпан 2026*
Қабылданды: *4 мамыр 2026*

ТҮЙІНДЕМЕ

Мақалада өнім сапасын жақсарту, шығындар мен тәуекелдерді азайту мақсатында мыс илемдік өндірісін интеграциалық талдау үшін модельдеу және математикалық модельдерді құру әдістері қарастырылды. Жүргізілген зерттеу мақсаты нақты процестердің математикалық сипаттамаларын жасау арқылы жүзеге асады, олар кейін компьютерлік тәжірибелер жүргізу үшін қолданылады. Дәстүрлі молекулалық динамикалық әдістерден айырмашылығы, бұл зерттеуде ақпараттық технологияны пайдалану арқылы ағын өрісінің сипаттамаларын технологиялық жабдықтар пайдаланды. Жаңалық келесіде: термомеханикалық модельдеуді оңтайландыру алгоритмімен интеграциялау, критерийлерді енгізу, механикалық қасиеттердің өзгеруін азайту, аударылу кезінде тозуын азайту, нақты уақыт режимінде бейімделгіш басқару мүмкіндігі Kazkat мыс таяқшаларын өндіру зауытында мыс балқыту ағынының кең ауқымдағы жылдамдықтарының профилдерінің ақпараттық талдауы ұсынылған. Ақпараттық технологияларды қолдана отырып, мыс таяқшаларын өндіру процестерінде ең жақсы сапа мен өнімділікке қол жеткізу үшін оңтайлы температура мәндерін, илемдеу жылдамдығын және басқа да параметрлерді анықтау мәселелері шешілді. Осы нәтижелерге сүйене отырып, орамдардағы температура өрісінің профилін оңтайландыру бойынша бағыттар ұсынылды, бұл роликтің тозуын азайтуға және сым таяқшасы құрылымының біркелкілігін арттыруға әкеледі, микроқұрылымды жақсартуға назар аударады.

Түйін сөздер: модельдеу, мыс, компьютерлік модельдеу, балқыту, ақпараттық технологиялар, сандық әдіс.

Авторлар туралы ақпарат:

Кажикенова Сауле Шарапатовна — *Техникалық ғылымдар докторы, Жоғары математика факультеті, Әбілқас Сағынов атындағы Қарағанда техникалық университеті, Назарбаев көшесі., 56, 100000, Қарағанда, Қазақстан. Email: sauleshka555@mail.ru; ORCID ID: https://orcid.org/0000-0002-6937-1577*

Шаихова Гүлназира Сериковна — *Техникалық ғылымдар кандидаты, Жоғары математика кафедрасы, Әбілқас Сағынов атындағы Қарағанда техникалық университеті, Назарбаев көшесі., 56, 100000, Қарағанда, Қазақстан. Email: shaikxova_2011@mail.ru; ORCID ID: https://orcid.org/0000-0002-2036-3023*

Шалтаков Сағындық Нағашибаевич — *PhD, Физика кафедрасы, Әбілқас Сағынов атындағы Қарағанда техникалық университеті, Назарбаев көшесі, 56, 100000, Қарағанда, Қазақстан. Email: sagyndyk613@mail.ru; ORCID ID: https://orcid.org/0000-0002-1186-1178*

Шалтакова Айнура Нигматолловна — *Магистр, Әбілқас Сағынов атындағы Қарағанда техникалық университеті, Назарбаев көшесі, 56, 100000, Қарағанда, Қазақстан. Email: ainurashatakova@gmail.com*

Моделирование и решение задач устойчивой эффективности технологических процессов в металлургии

Кажикенова С.Ш., Шаихова Г.С., Шалтаков С.Н., Шалтакова А.Н.

Карагандинский технический университет имени Абылкаса Сагинова, Караганда, Казахстан

Поступила: *20 января 2026*
Рецензирование: *25 февраля 2026*
Принята в печать: *4 мая 2026*

АННОТАЦИЯ

В статье рассмотрены методы применения, моделирования и создания математических моделей для интегрированного анализа производства медной катанки с целью повышения качества продукции, снижения затрат и минимизации рисков. Цель проводимых исследований достигается путем создания математических описаний реальных процессов, которые затем используются для проведения компьютерных экспериментов. В отличие от традиционных методов молекулярной динамики, применены информационные технологии для получения характеристик поля потока в технологическом оборудовании. Новизна заключается в: интеграции термомеханического моделирования с алгоритмом оптимизации; введение критерия, минимизирующего вариацию механических свойств; рассмотрение влияния перераспределения уменьшения на износ переворота; Возможность адаптивного управления в реальном времени. Представлен информационный анализ профилей скоростей течения расплава меди в широком диапазоне температур на заводе

	Казкат по производству медной катанки. С помощью информационных технологий решены задачи определения оптимальных значений температуры, скорости проката и других параметров для достижения наилучшего качества и производительности процессов производства медной катанки. На основании проведенных исследований предложены направления оптимизации профиля температурного поля в валках, что приводит к снижению износа рулона и увеличению равномерности структуры катанки, с акцентом на улучшение микроструктуры.
	Ключевые слова: Моделирование, медь, компьютерное моделирование, расплав, информационные технологии, численный метод.
Кажикенова Сауле Шарапатовна	***Информация об авторах:*** *Доктор технических наук, Кафедра высшей математики, Карагандинский технический университет имени Абылкаса Сагинова, ул. Назарбаева, 56 100000, Караганда, Казахстан. Email: sauleshka555@mail.ru; ORCID ID: https://orcid.org/0000-0002-6937-1577*
Шаихова Гулназира Сериковна	*Кандидат технических наук, Кафедра высшей математики, Карагандинский технический университет имени Абылкаса Сагинова, ул. Назарбаева, 56 100000, Караганда, Казахстан. Email: shaikxova_2011@mail.ru; ORCID ID: https://orcid.org/0000-0002-2036-3023*
Шалтаков Сагындык Нагашибаевич	*PhD, Кафедра физики, Карагандинский технический университет имени Абылкаса Сагинова, ул. Назарбаева, 56 100000, Караганда, Казахстан. Email: sagyndyk613@mail.ru; ORCID ID: https://orcid.org/0000-0002-1186-1178*
Шалтакова Айнура Нигматолловна	*Магистр, Карагандинский технический университет имени Абылкаса Сагинова, ул. Назарбаева, 56 100000, Караганда, Казахстан. Email: ainurashatakova@gmail.com*

References

[1] Sun H, Li N, Zhu Y, Liu K. A Model for Direct Effect of Graphene on Mechanical Property of Al Matrix Composite. Metals. 2023; 13:1351. https://doi.org/10.3390/met13081351 .

[2] Dvoynikov M V, Minaev Y D. Mathematical Model of Non-pressurized Flow for Calculating Killing of Gas Wells with Abnormally Low Reservoir Pressures. International Journal of Engineering. 2025: 38(7):1677-1684. https://doi.org/10.5829/ije.2025.38.07a.18

[3] Liu D, Zhang W, Xue Z, Song C, Chen, L. Simulation and Validation of Thickness of Slag Crust on the Copper Stave in the High-Temperature Area of Blast Furnace. Metals. 2024; 14:19. https://doi.org/10.3390/met14010019

[4] Heydari M, Osanloo M. A New Comprehensive Model for Integrating Environmental, Economic, and Social Performance of Deep and Large-scale Open-Pit Copper Mines. International Journal of Engineering. 2024; 37(1): 1-13. https://doi.org/10.5829/ije.2024.37.01a.01

[5] Lajevardi M, Nikbakht M, Boyer O, Tavakkoli-Moghaddam R. Designing a Model to Optimize the Operations of the Production Processes in Industry 4.0. International Journal of Engineering. 2024; 37(10): 2080-2090. https://doi.org/10.5829/ije.2024.37.10a.18

[6] Myrzakulov MK, Dzhumankulova SK, Yelemessov KK, Barmenshinova MB, Martyushev NV, Skeeba VY, Kondratiev VV, Karlina AI. Analysis of the Effect of Fluxing Additives in the Production of Titanium Slags in Laboratory Conditions. Metals. 2024; 14:1320. https://doi.org/10.3390/met14121320

[7] Zhang Z, Shao P, Shi S. Physical Simulation of Gas—Liquid Mass Transfer Behavior in Oxygen Bottom Blowing Copper Furnace. Metals. 2024; 14:1362. https://doi.org/10.3390/met14121362

[8] Kazhikenova SSh. The unique solvability of stationary and non-stationary incompressible melt models in the case of their linearization. Archives of Control Sciences. 2021; 2:307-332. https://doi.org/10.24425/acs.2021.137420

[9] Kazhikenova SSh, Shaltakov SN, Nussupbekov B. Difference melt model. Archives of Control Sciences. 2021; 31(3):607-627. https://doi.org/10.24425/acs.2021.138694

[10] Picella F, Loiseau JCh, Lusseyran F, Robinet JCh, Cherubini S, Pastur L. Successive bifurcations in a fully three-dimensional open cavity flow. Journal of Fluid Mechanics. 2018; 844:855-877. https://doi.org/10.1017/jfm.2018.169

[11] Yan X, Wei L, Lei Y, Xin X, Yanbin W, Gang Zh, Juntao L, Qingyan X. Numerical Simulation of Meso-Micro Structure in Ni-Based Superalloy During Liquid Metal Cooling. Proceedings of the 4th World Congress on Integrated Computational Materials Engineering. The Minerals, Metals & Materials Series. 2017; 249-259. https://doi.org/10.1007/978-3-319-57864-4_23

[12] Barannyk TA. Barannyk AF, Yuryk II. Exact Solutions of the Nonliear Equation. Ukrains'kyi Matematychnyi Zhurnal. 2017; 69(9):1180-1186. http://umj.imath.kiev.ua/index.php/umj/article/view/1768

[13] Buslaev G V, Konoplyannikov A V. Mathematical Modeling of a Hydro-mechanical System with a Positive Displacement Motor and Hydraulic Thruster to Optimize the Drilling Process for Extended-reach Drilling Wells. International Journal of Engineering. Transactions A: Basics. 2026; 39(5):1077-1087. https://doi.org/10.5829/ije.2026.39.05b.03

[14] Felipe A, Sevilla R, Hassan O. A conservative degree adaptive HDG method for transient incompressible flows. International Journal of Numerical Methods for Heat & Fluid Flow. 2025; 35(1):300-329. https://doi.org/10.1108/HFF-09-2024-0651

[15] Skorokhodov SL, Kuzmina NP. Analytical-numerical method for solving an Orr–Sommerfeld-type problem for analysis of instability of ocean currents. Zh Vychisl Mat Mat Fiz. 2018; 58(6);1022–1039. https://doi.org/10.7868/S0044466918060133

[16] Bakirova E, Iskakova N, Kadirbayeva Z. Numerical implementation for solving the boundary value problem for impulsive integro-differential equations with parameter. Journal of Mathematics, Mechanics and Computer Science. 2023; 119(3):19–29. https://doi.org/10.26577/JMMCS2023v119i3a2

[17] Zou Q, Lei H. The Cauchy problem for compressible Navier–Stokes equations with shear viscosity and large data. Z Angew Math Phys. 2018; 66:2305–2341. https://doi.org/10.1007/s00033-015-0522-1

[18] Carvalho MP, Scalon VL, Padilha A. Analysis of CBS numerical algorithm execution to flow simulation using the finite element method. Ingeniare Revista chilena de Ingenier´ıa. 2009; 17(2):166–174. https://doi.org/10.4067/S0718-33052009000200005

[19] Ali FH, Almensoury MF, Hashim AS, Al-Amir QR, Hamzah HK, Hatami M. Nanofluid natural convection of hot concentric cylinder in oval-shaped porous cavity at different eccentricity. International Journal of Numerical Methods for Heat & Fluid Flow 2024; 34(5):2146-2176. https://doi.org/10.1108/HFF-08-2023-0494

[20] Peng YJ, Zhao L. Global Convergence to Compressible Full Navier–Stokes Equations by Approximation with Oldroyd-Type Constitutive Laws. J. Math. Fluid Mech. 2022; 24:29. https://doi.org/10.1007/s00021-022-00669-4

[21] Ranjan KK, Kumar S, Tyagi A, Sharma A. An adaptive wavelet Galerkin scheme for solving contact problems based on elliptic variational inequalities of the first kind. Engineering Computations. 2019; 36(4):1258-1281. https://doi.org/10.1108/EC-07-2018-0294

[22] Mao C, Zhou B, Xue S. The actuation performance of a piezoelectric laminated plate actuator via Galerkin method. Multidiscipline Modeling in Materials and Structures 2022; 18(5):900-918. https://doi.org/10.1108/MMMS-05-2022-0086

[23] Deng L, Liang J, Zhang Y, Zhou H, Huang Z. Efficient numerical simulation of injection mold filling with the lattice Boltzmann method. Engineering Computations. 2017; 34(2):307-329. https://doi.org/10.1108/EC-01-2016-0023

[24] Oztop HF, Gür M, Selimefendigil F, Coşanay H. Analysis of melting of phase change material inserted a block via impinging turbulent slot jet. International Journal of Numerical Methods for Heat & Fluid Flow. 2023; 33(10):3467-3491. https://doi.org/10.1108/HFF-03-2023-0109

[25] Yang J, Zhang T. Stability and convergence of iterative finite element methods for the thermally coupled incompressible MHD flow. International Journal of Numerical Methods for Heat & Fluid Flow. 2020; 30(12):5103-5141. https://doi.org/10.1108/HFF-11-2019-0821

[26] Papon EA, Haque A, Sharif MAR. Numerical study for the improvement of bead spreading architecture with modified nozzle geometries in additive manufacturing of polymers. Rapid Prototyping Journal. 2021; 3:518-529. https://doi.org/10.1108/RPJ-05-2019-0142

[27] Baron A. Determination of hydraulic resistance of channels using spectral geometry methods. Fluid Dyn Res. 2021; 53:065508. https://doi.org/10.1088/1873-7005/ac44fa

[28] Liu Y, Peng Y, Qu X. Mechanism of and Key Technologies for Copper Bonding in the Hot Rolling of SCR Continuous Casting and Rolling. Appl Sci. 2021; 22:11023. https://doi.org/10.3390/app112211023

[29] Chepushtanova TA, Yessirkegenov MI, Nikoloski A, Merkibayev YS, Altmyshbayeva AZh.Development of an Enhanced Method for Copper Extraction from Sulfuric Acid Solutions. Kompleksnoe Ispolzovanie Mineralnogo Syra= Complex Use of Mineral Resources. 2025; 334(3):99-109. https://doi.org/10.31643/2025/6445.32

[30] He H, Chen J, Zhang S, Liao M, Li L, He W, Chen Y, Chen S. Fabrication and surface treatment of fine copper lines for HDI printed circuit board with modified full-additive method. Circuit World. 2017; 43(3):131-138. https://doi.org/10.1108/CW-02-2017-0004

[31] Al-Zadi MSA, Haghighat H. Experimental evaluation and FE simulation of the asymmetrical rolling process of bimetal rods. Aircraft Engineering and Aerospace Technology. 2025; 97(4):488-497. https://doi.org/10.1108/AEAT-10-2024-0302

[32] Guan J, Luo S, Kan X, Chen C, Wang, Q. Preparation of copper/binder composites and fused filament fabrication process. Rapid Prototyping Journal. 2025; 31(5):925-933. https://doi.org/10.1108/RPJ-12-2023-0436

[33] Sharabian E, Khorasani M, Gulizia S, Ghasemi AH, MacDonald E, Downing D, Rolfe B, Brandt M, Leary M. Numerical simulation and analytical modelling of temperature and morphology of melt pool in electron beam powder bed fusion of copper. Rapid Prototyping Journal. 2025; 31(1):127-144. https://doi.org/10.1108/RPJ-03-2024-0141

[34] Assael MJ, Kalyva AE, Antoniadis KD, Banish RM, Egry I, Wu J, Kaschnitz E, Wakeham WA. Reference Data for the Density and Viscosity of Liquid Copper and Liquid Tin. J. Phys. Chem. Ref. Data. 2010; 39(3). https://doi.org/10.1063/1.3467496

[35] Kenzhaliyev BK, Imangalieva LM, Manapova AI, Azlan MN. Kaolinite clays as a source of raw materials for the aluminum industry of the Republic of Kazakhstan. Kompleksnoe Ispolzovanie Mineralnogo Syra = Complex Use of Mineral Resources. 2021; 319(4):5-12. https://doi.org/10.31643/2021/6445.34

[36] Shaik MB, Nasina V, Mamilla RS. Experimental investigation into nano-finishing of pure copper built using atomic diffusion additive manufacturing. Rapid Prototyping Journal. 2025; 31(5):998-1013. https://doi.org/10.1108/RPJ-12-2023-0438

[37] Zheng J, Li G, Teng X, Qiu Z. Analysis and Research of Molten Copper Sloshing in Mould of Anode Based on VOF Method. IOP Conf. Ser.: Mater. Sci. Eng. 2019; 711:21-22. https://doi.org/10.1088/1757-899X/711/1/012031

Crossref
DOI: 10.31643/2028/6445.08
Metallurgy and Metallurgical Engineering

Development of a methodology for microstructural and thermal verification of the quality of an industrial Ti-10V-2Fe-3Al triple vacuum arc remelted ingot

[1]Mamutova A.T., [2*]Chepushtanova T.A., [3]Mishra B.

[1] Ust-Kamenogorsk Titanium and Magnesium Plant JSC, Kazakhstan
[2]Satbayev University, Almaty, Kazakhstan
[3]Worcester Polytechnic Institute, USA, Worcester

** Corresponding author email: t.chepushtanova@satbayev.university*

Received: *March 5, 2026*
Peer-reviewed: *March 16, 2026*
Accepted: *May 6, 2026*

ABSTRACT

The article is devoted to the development of a methodology for microstructural and thermal verification of the quality of an industrial Ti-10V-2Fe-3Al triple vacuum arc remelted ingot produced by UK TMP JSC. It was established that all zones of the ingot demonstrate a two-stage thermal evolution characteristic of the β-metastable Ti-10V-2Fe-3Al alloy: decomposition of the metastable β phase (≈520–570 °C) and an endothermic α→β phase transformation (≈950–1120 °C). It was found that the enthalpy of the exothermic decomposition of the β matrix increases by approximately 60–80% in the lower zone of the ingot. The width of the phase transition (ΔT) correlates with an increase in microsegregation. It was also determined that the enthalpy of the endothermic α→β transformation decreases from the bottom part of the ingot toward the steady-state crystallization zone (Middle-1), which correlates with a reduction in the microsegregation parameters obtained from SEM–EDS profiles (ΔC_max, σC, L_{corr}). Thus, thermal analysis confirms the absence of a pronounced vertical gradient of structural stability and can be used as a validating criterion for the integral electrode quality index. For the first time, a quantitative correlation between SEM–EDS profiles and DSC–DTG characteristics has been proposed. Thermal analysis is suggested as an independent validator of microsegregation. An approach to the quantitative evaluation of microsegregation based on SEM–EDS profiles using the parameters ΔC_max, σC, L_{corr}, and $\Delta CO_{(local)}$ has been developed. Additionally, the use of an integral chemical index I_{chem}, and a critical threshold I^{crit}_{chem} is proposed for electrode quality control using thermal analysis results.

Keywords: Ti-10V-2Fe-3Al triple-remelt alloy, vacuum arc melting, DSC–DTG and SEM–EDS analyses, α/β phase transformations, thermal decomposition analysis.

Information about authors:

Mamutova Assem Tlekovna — *President of Titanium and Magnesium Plant JSC, Ust-Kamenogorsk, Kazakhstan, PhD student of the Mining and Metallurgical Institute, Satbayev University, Almaty, Kazakhstan. Email: a.mamutova@satbayev.university*

Chepushtanova Tatyana Aexandrovna — *Candidate of Technical Sciences, PhD, Professor, Head of Laboratory 'Metallurgical processes, heat engineering and powder metallurgy, Mining and Metallurgical Institute, Satbayev University, Almaty, Kazakhstan. Email: T.Chepushtanova@satbayev.university*

Mishra Brajendra — *Professor and MPI Director of Mechanical and Materials Engineering, Worcester Polytechnic Institute, USA, Worcester. Email: bmishra@wpi.edu*

Introduction

In industrial titanium metallurgy, vacuum arc remelting (VAR) remains the fundamental technology for producing large ingots, while triple VAR is used as a method to reduce inclusions, stabilize the molten pool, and improve chemical homogeneity [1]. However, even with multiple remelting cycles, risks of crystallization defects persist: macrosegregation, local segregation channels, "hot top" defects, inhomogeneity of the solidification zone, and variations in molten pool depth—factors that cannot be completely eliminated solely by increasing the number of remelts. Studies on VAR defects emphasize that the evolution of macrosegregation during different stages of triple VAR remains a distinct scientific problem requiring a combination of experimental and modeling approaches [[2], [3]].

A modern trend is the control of structure and segregation through melting regimes and pool management: melt depth, mushy zone width, thermal gradients, and solidification rate. These aspects are actively developed in numerical VAR

models, including multilevel and multiscale approaches [4].

The quality of a VAR ingot is determined not only by chemical composition but also by the trajectory of heat and mass transfer and arc/gap stability, which influence the pool profile and solidification conditions. Therefore, methods that "read" quality through structural-chemical markers (microsegregation, oxygen-enriched zones, α/β morphology) and link them to thermal signals of phase transformations and melting are becoming increasingly important [[5], [6]].

Control of the VAR process and ingot quality today relies on electrode gap control, melt pool modeling, and structure prediction. Arc gap control and melting stability are widely discussed. For Ti-10V-2Fe-3Al (Ti-1023), it has been shown that automatic electrode gap regulation (via maintaining average voltage and using specific pulse/polarity modes) significantly affects remelting stability and indirectly influences homogeneity and defect formation. This research direction is important as it links VAR "process maps" with industrial ingot quality [[7], [8], [9]].

VAR modeling as a tool for segregation prevention is considered a source of critical data. Models have evolved from axisymmetric to 3D/multiscale (arc → pool → solidification → grain structure). Key references include multiscale 3D VAR models (process-oriented coupling of arc/pool/solidification), multiscale modeling of microstructure formation in Ti-6Al-4V, and models validated for Ti-10V-2Fe-3Al aiming to reproduce pool profiles and solidification behavior [[4], [10]].

Additionally, modern solidification simulation approaches (e.g., CAFE methods) demonstrate that modeling is becoming a practical tool for selecting process parameters, although experimental validation remains necessary to confirm real homogeneity.

Macrosegregation and its persistence remain among the most critical defects, as they can survive subsequent heat treatment and degrade properties. For triple VAR, it is emphasized that repeated remelting does not always guarantee elimination of macrosegregation without process optimization [[11], [12], [13]].

Channel segregation and its relation to processing are also highly relevant. In industrial ingots, channel segregation typically appears in characteristic zones (often 1/4–3/4 of the radius), with morphology correlated to pool profile and steady/transient remelting regions [[14], [15], [16]]. These defects may be associated with local oxide particles, directly linking to oxygen enrichment and α_2-phase risks.

From a technological perspective, microsegregation of β-stabilizers (Fe, V) and oxygen should be considered as "hidden" quality markers. For Ti-1023, Fe microsegregation is critical due to the risk of β-flecks and property degradation. SEM–EDS is widely used to quantify these effects, including diffusion and homogenization behavior of Fe. This confirms that SEM–EDS profiles are not merely illustrative but serve as a quantitative quality control tool. Oxygen plays a separate role, affecting phase equilibria (β-transus), promoting local strengthening or embrittlement zones, and being difficult to accurately assess without spatial resolution beyond bulk chemical analysis [[17], 18], [19]].

Thermal analysis using high-temperature analyzers is also a universal tool for quality control of Ti alloys, particularly for determining β-transus and phase transformations via DSC/STA. DSC is widely used for evaluating β-transus, composition effects, oxygen influence, and thermokinetics. Literature emphasizes that DSC can be faster and more objective than purely metallographic methods. Thermal analysis allows evaluation of melting intervals, phase transitions, and heating rate effects. For Ti alloys, phase transformations and melting behavior are sensitive to processing conditions and material state (including heating rate effects). Some studies demonstrate the determination of liquidus/solidus temperatures using DTA as a classical approach for obtaining technologically significant temperatures [[20], [21], [22]].

This work proposes the development of a methodology for microstructural and thermal verification of the quality of an industrial Ti-10V-2Fe-3Al triple VAR ingot through metrological coupling of spatial chemical heterogeneity (SEM–EDS profiles) and thermokinetic analysis (STA/DSC/TG), as well as the introduction of the Ichemcrit criterion as a decision-making tool for rejection or correction of triple remelting parameters and charge preparation.

Initial materials

The object of the study was a triple vacuum arc remelted (VAR) ingot of Ti-10V-2Fe-3Al, produced by vacuum arc melting in accordance with the customer's specification: Al — 2.60–3.40%, V — 9.00–11.00%, Fe — 1.60–2.20%, O — max. 0.13%.

The objects of investigation for SEM–EDS and DSC/DTG analyses were three electrode zones: samples taken from the “top”, “middle 1”, “middle 2”, and “bottom” regions of the ingot.

Technology for the production of titanium ingots in a vacuum arc furnace (VAR)

The triple vacuum arc remelted Ti-10V-2Fe-3Al alloy was produced on an industrial scale at *Ust-Kamenogorsk Titanium and Magnesium Plant JSC*. The VAR furnace configuration used for producing the Ti-10V-2Fe-3Al alloy is shown in Figure 1.

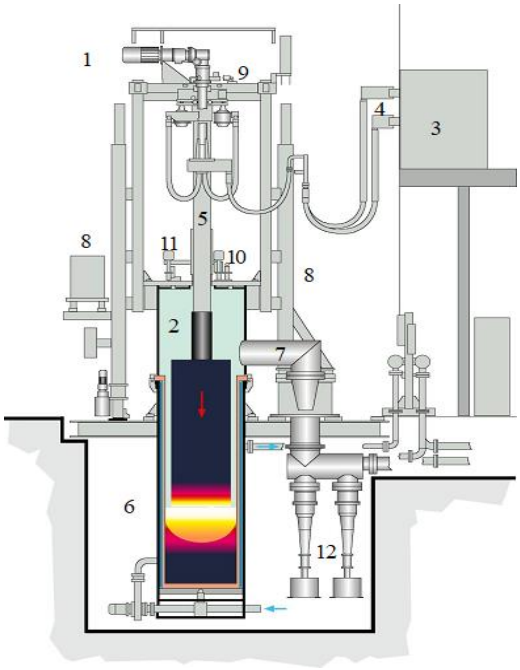

Legend for the schematic: 1 – electrode feed drive; 2 – furnace chamber; 3 – melting power supply; 4 – busbars and cables; 5 – plunger-type electrode holder; 6 – water jacket with mold (crystallizer); 7 – vacuum duct; 8 – rotating column; 9 – coordinate adjustment system; 10 – load cell system; 11 – TV camera system; 12 – oil booster pumps.

Figure 1 – Schematic of the VAR furnace

The industrial Ti-10V-2Fe-3Al alloy ingot was produced by triple vacuum arc remelting (VAR). Multiple remelting was applied to minimize macrosegregation, improve chemical homogeneity, and stabilize the molten pool depth.

The main technological parameters for each remelting stage are presented below:

1st remelting: mass of melted metal – 4.5 t; melting time – 7 h 40 min; electrode area – 500 mm²; 2nd remelting: mass – 4.4 t; time – 10 h; electrode area – 600 mm²; 3rd remelting: mass – 4.4 t; time – 21 h 40 min; electrode area – 680 mm².

The density of titanium was taken in the range of 4.67–4.75 g/cm³.

The first remelting was carried out in a mold with a diameter of 620 mm. The mass melting rate was 9.90 kg/min (1st electrode), 7.49 kg/min (2nd electrode), and 7.96 kg/min (3rd electrode). The formation of a residual disk with a height of at least 40 mm ensured melt pool stability and controlled solidification.

A key technological parameter was cooling under residual pressure in the VAR chamber: 10 hours after the first and second remelting stages and 8 hours after the third. The average voltage in the steady-state phase was 29.8–33.3 V with a solenoid coil operation periodicity of ±3 s, ensuring arc stability and thermal regime control.

The calculated electrode composition was identical for all remelting stages: Al – 3.25%, V – 9.7%, Fe – 1.95%, O – 0.105%, C – 0.011%.

The selected processing conditions ensured process reproducibility and minimization of macrosegregation.

Research methodology, sampling, and homogeneity control strategy

To assess structural and chemical homogeneity, samples were taken from four characteristic zones along the ingot height: “top”, “middle 1”, “middle 2”, and “bottom”. Additionally, each ingot was divided into three sections with transverse cuts performed: at a distance of 40 mm from the top, from the central steady-state zone, and at a distance of 40 mm from the bottom.

This approach made it possible to analyze the vertical distribution of elements and identify potential zones of non-steady crystallization.

The chemical composition of all studied samples meets the specification requirements for Ti-10V-2Fe-3Al, confirming the effectiveness of triple VAR in terms of macrochemical homogeneity. Further analysis of structure and elemental distribution was carried out using SEM–EDS and DSC/DTG methods to identify microsegregation, local oxygen enrichment, and to perform thermal verification.

The study employed scanning electron microscopy (SEM) and energy-dispersive spectroscopy (EDS) using a JEOL JSM-7000 system.

Thermal analysis was performed using a STA 449 Jupiter NETZSCH thermal analyzer with heating up to 2000 °C.

For SEM–EDS investigations, key magnifications were selected to reflect the technological relationship of structure formation within the ingot:

– 500× — general structure, primary phase distribution;
– 1000–2000× — morphology of α plates;
– 5000× — local features, dispersed particles, segregation zones.

Thus, the study focused on identifying: vertical chemical gradients (increase of V or Fe upward or downward); distribution of β-stabilizers during remelting; presence of oxygen or carbon segregation; oxygen enrichment in the upper part due to interaction with residual gas in VAR; and oxygen accumulation at α-phase boundaries as an early stage of α_2–Ti_3Al formation.

SEM–EDS Analysis Results

As a result of analyzing the morphological evolution of the α/β structure, the following features along the ingot height were identified.

"Top" zone. At magnifications of ×3000–5000, thin parallel stepped layers, individual loose fragments, and isolated fine particles are observed. According to EDS data, Ti dominates (TiKα peak ~4.5 keV), with pronounced V and Al peaks, as well as elevated carbon content. The surface is generally smooth with minor defects; the increased carbon content is likely associated with the final stage of remelting and surface-related processes.

"Bottom" zone. Clusters of rounded and irregularly shaped particles are identified between the matrix steps, morphologically corresponding to non-metallic inclusions (oxide or slag fragments). Pronounced layering and the presence of large defects are observed, indicating structure formation under unstable initial remelting conditions and possible dendritic segregation. The Ti content is ~83.5–84 wt.%, while V and Al concentrations are close to nominal values, and no pronounced vertical gradient of β-stabilizers is detected. The carbon content is lower than in the top zone, confirming its predominantly surface-related nature in the upper section.

"Middle-1" zone. The structure is characterized by the most uniform lamellar morphology: α plates are well-bonded and aligned, the surface is relatively smooth, and the number of inclusions is minimal. The chemical composition is stable and closest to the nominal composition of Ti-10V-2Fe-3Al. Low carbon content and the absence of pronounced oxygen peaks indicate minimal gas saturation and oxide defects. This zone corresponds to a steady-state remelting regime and uniform formation of the α/β structure.

"Middle-2" zone. A layered and split structure is observed, with the presence of oxide phases and film-like inclusions. EDS data confirm the presence of local structural defects. Since the "middle-1" zone reflects a stable crystallization regime and the highest structural homogeneity, the SEM–EDS results for this sample are presented in Figures 2–4.

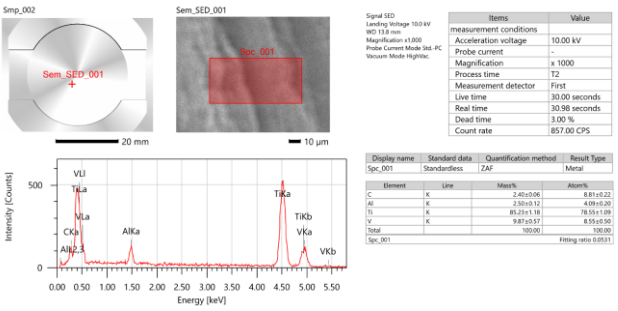

Figure 2 – SEM elemental analysis results over the surface area of the "middle 1" zone

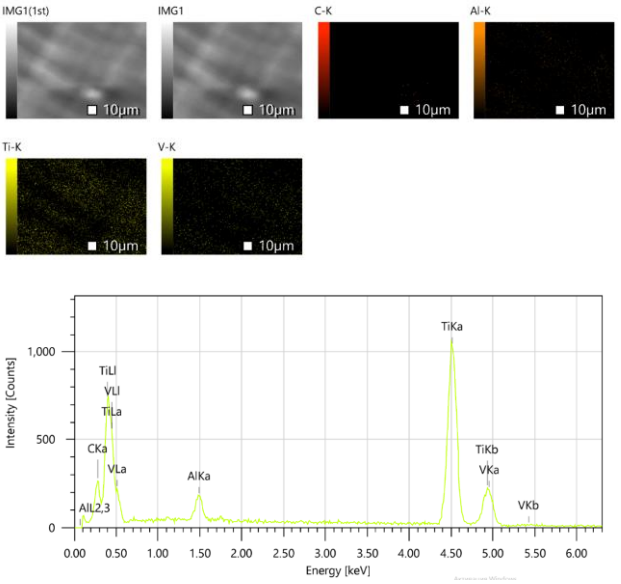

Figure 3 – EDS mapping results of the "middle 1" zone

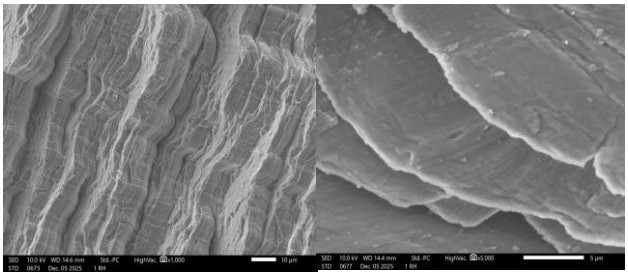

Figure 4 – SEM micrographs of the "middle 1" zone

As a result of analyzing the vertical distribution of Al–V–Ti, no pronounced chemical gradient along

the ingot height was identified. This confirms the high efficiency of triple VAR, which ensures melt homogenization and suppression of segregation, positively affecting phase stability, uniformity of the α/β structure, and reproducibility of mechanical properties.

SEM–EDS data show that the V content in all studied zones (top, bottom, middle-1) is within ~9.3–9.9 wt.%, Al — 2.5–3.1 wt.%, while the slight increase in Ti from the top to middle-1 falls within the measurement error. No significant vertical segregation of β-stabilizers was detected.

Thus, the Ti-10V-2Fe-3Al ingot is characterized by complete chemical uniformity along its height. The variation in the concentrations of the main alloying elements does not exceed 1–1.5% (Al and V — within ±0.5–1.0%, Ti — ~83–86%), which, for an industrial ingot weighing 4.5 t, indicates the high quality of the performed triple VAR process.

Macrohomogeneity in V and Al is confirmed by SEM–EDS: triple VAR effectively suppresses macrosegregation of β-stabilizers along the ingot height. Microdefects are distributed according to technological zones: bottom — non-metallic inclusions/layering (initial remelting stage, interaction with the baseplate/crucible); middle-1 — minimal defects (steady-state regime); middle-2 — film-like/oxide inclusions (local disturbances in charge preparation/purity); top — surface reactivity and elevated carbon content (final stage/surface processes).

Development of a methodology for electrode quality control based on SEM–EDS profiles

The obtained SEM–EDS profiles of V, Fe, Al, and O distribution along scan lines in the “top”, “middle 1”, “middle 2”, and “bottom” zones make it possible to transition from qualitative assessment to a quantitative electrode quality criterion based on microsegregation parameters.

The following diagnostic indicators are proposed: the maximum deviation of β-stabilizer concentrations (V, Fe) from the mean value along the scan line, $\Delta C_{max} = \max |C_i - \bar{C}|$; the standard deviation of concentration:

$$\delta C = \sqrt{\frac{1}{n}\sum_{i=1}^{n}(Ci - \bar{C})^2} \quad (1)$$

the correlation length L_{cor} – the characteristic size of chemically heterogeneous regions, determined from the autocorrelation function of the profile (the distance at which the correlation coefficient decreases to 1/e); local oxygen enrichment:

$$\Delta C_0^{(loc)} = C_{0,\,loc} - \overline{C_0} \quad (2)$$

For the central zone of the ingot (“middle-1”), the values of ΔC_{max} and σC are minimal, and L_{corr} is small, corresponding to fine-scale, statistically averaged microsegregation. In the lower part of the ingot, these parameters increase, reflecting the formation of more extended chemically heterogeneous regions. Based on these quantities, an integral index of chemical heterogeneity is introduced:

$$Ichem = a_1\frac{\Delta C_{max}}{\bar{C}} + a_2\frac{\delta C}{\bar{C}} + a_3\frac{\Delta Lcorr}{Lref} + a_4\frac{\Delta C_O}{\overline{C_{O,ref}}} \quad (3)$$

where a_i are weighting coefficients (determined empirically), and L_{ref} и $C_{O,ref}$ – are normalization parameters.

A threshold value I_{chem}^{crit} (critical chemical inhomogeneity index) is defined. If the condition $I_{chem} \le I^{crit}_{chem}$ is satisfied, the electrode is considered compliant with homogeneity requirements; if the threshold is exceeded, adjustment of the triple VAR regime or rejection of the billet is required.

Thus, the proposed index transforms SEM–EDS analysis from a descriptive tool into a quantitative method of incoming quality control. Incorporation of this criterion into the charge preparation protocol enables closure of the technological chain “briquette → electrode → ingot” and ensures reproducible alloy structure under industrial conditions.

Results of thermal analysis (differential scanning calorimetry) DSC/DTG

Thermal analysis by DSC/DTG provides information that is not accessible through SEM/XRD analysis, namely: the temperatures at which structural transformations begin, thermal markers of phase rearrangements, high-temperature anomalies, temperature indicators of local microzones/defects that manifest only at elevated temperatures, as well as the solidus–liquidus interval of alloys.

The aim of the thermal analysis using differential scanning calorimetry (DSC/DTG) was to determine the thermo-microstructural properties of the triple VAR Ti-10V-2Fe-3Al ingot, including the identification of temperature transformation gradients along the ingot height.

Figure 5 presents the results of the thermal analysis, including DSC/DTG thermograms of the Ti-10V-2Fe-3Al ingot.

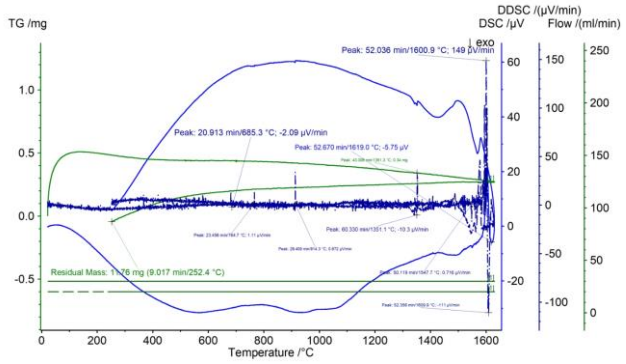

a - “middle 1” zone

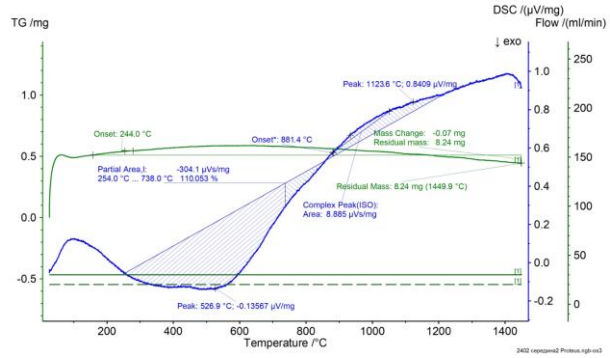

b - “middle 2” zone

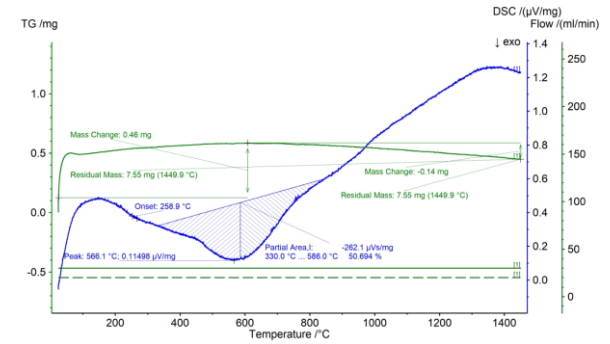

c – “top” zone

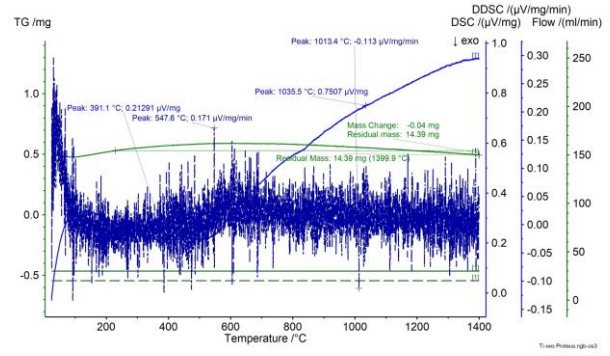

d – “bottom” zone

Figure 5 – DSC/DTG thermograms along the height of the Ti-10V-2Fe-3Al ingot for different zones

Table 1 presents the results of the thermal analysis of the zones of the industrial Ti-10V-2Fe-3Al ingot.

Table 1 – Summary thermal analysis of the zones of the industrial Ti-10V-2Fe-3Al ingot (triple VAR)

Zone	T, peak (°C)	Phase interpretation	Structural mechanism and diagnostic significance
Middle-1	685.3	Stage-wise decomposition of metastable β	Precipitation of dispersed α/ω phases; reflects initial microsegregation of β-stabilizers
	764.7	α coarsening	Redistribution of V and Fe; indicator of β-matrix homogeneity
	914.3	Onset of α→β transformation	Dissolution of secondary α; marker of transition toward the β-region
	1352.2	β stabilization	Completion of solid-state homogenization; indicator of steady-state remelting
	1495.8	Solidus	Onset of partial melting of segregated domains; sensitive indicator of microsegregation
	1547.7	Main melting stage	Increase in liquid phase fraction; reflects compositional distribution
	1610	Liquidus	Completion of melting; melting interval ΔT characterizes chemical homogeneity
Middle-2	526.9	Decomposition of metastable β	Precipitation of ω/early α; indicator of local heterogeneity
	975	Onset of precipitate dissolution	α→β transition; degree of phase stability
	1123	Peak of α→β transformation	Stabilization of β-matrix; reflects structural energy rearrangement
Top	566.1	Solid-state β decomposition	Dispersed α precipitation; influence of final remelting stage
	975	α→β transition	Dissolution of precipitates; uniformity of phase structure
	1449	Upper limit of solid-state region	Stabilization before melting; absence of premature partial melting
Bottom	547.6	Enhanced β decomposition	Intensive α/ω precipitation
	975	Onset of α→β	Phase dissolution; broader transformation range
	1013.4	Multi-stage α→β transformation	Non-uniform dissolution; presence of local compositional domains
	1399.9	End of solid-state region	β stabilization; absence of melting up to 1400 °C

It was established that all zones of the ingot exhibit a characteristic two-stage thermal evolution typical of the β-metastable Ti-10V-2Fe-3Al alloy: decomposition of the metastable β phase (≈520–570 °C) and the endothermic α→β transformation (≈950–1120 °C). The analysis of the zones revealed the following:

The “middle-1” zone is characterized by the smoothest transitions and minimal staging, confirming a steady-state crystallization regime during triple VAR.

The “bottom” zone exhibits additional staging (≈1013 °C) and more pronounced exothermic effects, indicating increased microsegregation formed during the initial stage of remelting.

Only in the “middle-1” zone, the solidus (≈1496 °C) and liquidus (≈1610 °C) temperatures were identified, which made it possible to evaluate the melting interval and confirm the absence of macrosegregation along the ingot height.

Figure 6 shows the dependence of the relative enthalpy of phase transformations on the ingot height.

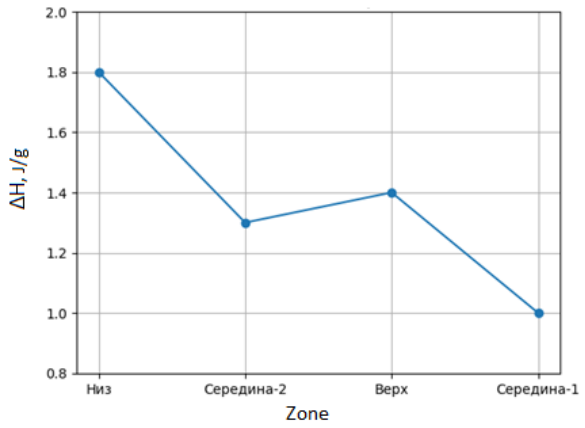

Figure 6 – Dependence of the relative enthalpy of phase transformations on the ingot height

It was established that the enthalpy of the exothermic decomposition of the β-matrix increases by approximately 60–80% in the lower zone of the ingot. The width of the phase transformation interval ΔT correlates with increasing microsegregation. The minimum values of ΔH and ΔT in the “middle-1” zone confirm a steady-state crystallization regime.

The thermograms demonstrate a clear dependence of the energetics of phase transformations on the position along the ingot height: the middle-1 zone shows minimum enthalpy and narrow transitions → maximum homogeneity; the bottom zone shows increased ΔH and broadened transitions → macro- and microsegregation, ΔH values for endothermic transformations along the ingot height Table 2.

Table 2 – ΔH values for endothermic transformations along the ingot height

Zone	ΔH, J/g	T_{α→β} onset, °C	T_{max α→β}, °C	$T_{solidus}$, °C	$T_{liquidus}$, °C
Bottom	1.7	~975	1013.4	—	—
Middle-2	1.4	~975	1123	—	—
Top	1.3	~975	—	—	—
Middle-1	1.0	914.3	1352.2	1495.8	1610

The “bottom” zone exhibits the maximum relative enthalpy of the endothermic transition ($\Delta H_{en}d_o$ ≈ 1.7 J/g), which is associated with a more pronounced staging of the α→β transformation and increased microsegregation of β-stabilizers.

The “middle-2” zone is characterized by a pronounced α→β transition peak at 1123 °C ($\Delta H_{en}d_o$ ≈ 1.4 J/g), reflecting active dissolution of precipitates and redistribution of alloying elements.

The “top” zone shows a less pronounced endothermic effect ($\Delta H_{en}d_o$ ≈ 1.3 J/g), corresponding to a more uniform phase structure after the final stage of remelting.

The “middle-1” zone demonstrates the minimum $\Delta H_{en}d_o$ ≈ 1.0 J/g and a smooth transformation behavior. It is also the only zone where the melting interval (1495.8–1610 °C) is recorded, allowing evaluation of the solidus–liquidus range and confirming high chemical homogeneity.

The enthalpy of the endothermic α→β transition decreases from the lower part of the ingot toward the steady-state crystallization zone (middle-1), correlating with a reduction in microsegregation parameters obtained from SEM–EDS (ΔC_{max}, σC, Lcorr).

An increase in microsegregation directly correlates with a rise in the enthalpy of phase transformations and a widening of temperature

intervals, confirming the consistency between SEM–EDS and DSC/DTG approaches.

Thus, thermal analysis confirms the absence of a pronounced vertical gradient in structural stability and can be used as a validation criterion for the integral electrode quality index.

Thermal verification (DSC)

To validate the I_{chem} index (which integrates the contribution of β-stabilizers and oxygen), a thermal component is introduced:

– presence/intensity of the β-phase decomposition transition (≈520–570 °C), staging/broadening of the α→β transformation (≈950–1123 °C), and the appearance of an additional marker (~1013.4 °C) as an indicator of large-scale heterogeneity (L_{corr}↑);

– for the "middle-1" zone — control of the solidus–liquidus interval as an integral indicator of homogeneity;

– confirmation of SEM–EDS results using DSC–DTG data: the higher the macro- and microsegregation (ΔC_{max}, σC, Lcorr), the wider the melting interval $\Delta T\_melt = T_{liquidus} - T_{solidus}$ due to the presence of local compositions with different melting temperatures. The observation of a well-defined solidus–liquidus pair and the absence of premature melting in other zones within 1400–1450 °C confirm the absence of severe macrosegregation and the correctness of the triple VAR regime.

A "thermal indicator" has been developed: the number of stages/peaks in the α→β transition range, the transition width ΔT, and the presence of early melting or expansion of ΔT_{melt}.

Thus, SEM–EDS determines the cause (spatial profile of chemical inhomogeneity), while DSC–DTG captures the consequence (thermodynamic and kinetic response of the structure). The integration of these methods enables the transition from qualitative assessment to a verifiable quality control protocol for industrial electrodes and ingots.

Conclusion

Thus, for the first time, a quantitative correlation between SEM–EDS profiles and DSC characteristics has been proposed. Thermal analysis is suggested as an independent validator of microsegregation.

Triple vacuum arc remelting ensures high chemical homogeneity of the main alloying elements (Ti, V, Al, Fe), as confirmed by SEM–EDS through the absence of a pronounced vertical gradient.

The results of thermal analysis (DSC/TG) confirm the SEM–EDS findings regarding the absence of a significant gradient along the ingot height. It has been established that the intensification and staging of β-phase decomposition and α→β transformation effects are characteristic of the lower zone of the ingot, which is consistent with increased microsegregation parameters (ΔC_{max}, σC, Lcorr).

A methodology for microstructural and thermal verification of the quality of an industrial Ti-10V-2Fe-3Al triple VAR ingot has been developed using DSC–DTG and SEM–EDS analyses. This approach is based on quantitative evaluation of microsegregation through SEM–EDS profiles using the parameters ΔC_{max}, σC, Lcorr, ΔC_o (local), as well as the application of the integral index I_{chem} and the threshold I^{crit}_{chem} for electrode quality control.

Conflict of interest. On behalf of all the authors, the corresponding author declares that there is no conflict of interest.

CRediT author statement: **A. Mamutova**: Conceptualization, Methodology, experiments, Funding; **T. Chepushtanova**: Data curation, Writing draft preparation, Investigation; **B. Mishra**: Supervision, Reviewing and Editing.

Acknowledgement. The research was carried out with the financial support of the agreement № 1090-ТМК from 02.11.2025 / 11-168 from 19.11.2025 г. of Ust-Kamenogorsk Titanium and Magnesium Plant JSC.

Cite this article as: Mamutova AT, Chepushtanova TA, Mishra B. Development of a methodology for microstructural and thermal verification of the quality of an industrial Ti-10V-2Fe-3Al triple vacuum arc remelted ingot. Kompleksnoe Ispolzovanie Mineralnogo Syra = Complex Use of Mineral Resources. 2028; 344(1):79-89. https://doi.org/10.31643/2028/6445.08

Ti-10V-2Fe-3Al титан қорытпасының үш мәрте вакуумды-доғалық қайта балқыту арқылы алынған өнеркәсіптік құймасының сапасын микрокұрылымдық және термиялық верификациялау әдістемесін әзірлеу

[1]Мамутова А.Т., [2]Чепуштанова Т.А., [3]Mishra B.

[1] Өскемен титан-магний комбинаты АҚ, Қазақстан
[2] Сәтбаев университеті, Алматы, Қазақстан
[3] Вустер политехникалық институты, Вустер, АҚШ

Мақала келді: *5 наурыз 2026*
Сараптамадан өтті: *16 наурыз 2026*
Қабылданды*: 6 мамыр 2026*

ТҮЙІНДЕМЕ

Мақала «Өскемен титан-магний комбинаты» АҚ-да алынған Ti-10V-2Fe-3Al қорытпасының үш мәрте вакуумды-доғалық қайта балқытудан кейінгі өнеркәсіптік құймасының сапасын микрокұрылымдық және термиялық верификациялау әдістемесін әзірлеуге арналған. Құйманың барлық аймақтары β-метатұрақты Ti-10V-2Fe-3Al қорытпасына тән екі сатылы термиялық эволюция сипаттамасын көрсететіні анықталды: метастабильді β фазаның ыдырауы (≈520–570 °C) және эндотермиялық α→β фазалық қайта құрылуы (≈950–1120 °C). β-матрицаның экзотермиялық ыдырау энтальпиясы құйманың төменгі аймағында шамамен 60–80%-ға артатыны анықталды. Фазалық ауысу ені ΔT микросегрегацияның артуымен корреляцияланады. Эндотермиялық α→β ауысуының энтальпиясы құйманың түбінен тұрақты күйдегі кристалдану аймағына (Middle-1) дейін төмендейтіні анықталды, бұл SEM-EDS профильдеріне сәйкес микросегрегация параметрлерінің төмендеуімен корреляцияланады (ΔC_max, σC, Lcorr). Бұл SEM–EDS профильдері бойынша алынған микросегрегация параметрлерінің (ΔC_max, σC, Lcorr) төмендеуімен сәйкес келеді. Қортындылай келе, алғаш рет SEM–EDS профильдері мен DSC–DTG сипаттамалары арасында сандық корреляция ұсынылды, ал термиялық талдауды микросегрегацияның тәуелсіз валидаторы ретінде пайдалану ұсынылды SEM–EDS профильдері негізінде микросегрегацияны ΔCmax, σC, L_{corr} және ΔCO(лок.) параметрлері арқылы сандық бағалау тәсілі әзірленді. Сонымен қатар, термиялық талдау нәтижелері негізінде электродтардың сапасын бақылау үшін интегралдық көрсеткіш $I_{che}m$ және шекті мән I^{crit}_{chem} қолдану ұсынылды.

Түйін сөздер: Ti-10V-2Fe-3Al үш мәрте қайта балқытылған қорытпасы, вакуумды-доғалық балқыту, DSC–DTG және SEM–EDS талдаулары, α/β фазалық ауысулар, термиялық ыдырауды талдау.

Информация об авторах:

Мамутова Асем Тлековна — *Өскемен титан-магний комбинаты АҚ президенті, Өскемен; докторант, Тау-кен металлургия институты, Сәтбаев университеті, Алматы, Қазақстан. Email: a.mamutova@satbayev.university*

Чепуштанова Татьяна Александровна — *Профессор, техника ғылымдарының кандидаты, PhD докторы, Металлургиялық процестер, жылутехника және ұнтақты металлургия» зертханасының меңгерушісі, МиОПИ кафедрасы, Тау-кен металлургия институты, Satbayev University, Алматы, Қазақстан. Email: t.chepushtanova@satbayev.university*

Mishra Brajendra — *Профессор, PhD, NSF ресурстарды алу және қайта өңдеу орталығының директоры, Вустер политехникалық институты, Вустер, АҚШ. Email: bmishra@wpi.edu*

Разработка методики микроструктурной и термической верификации качества промышленного слитка Ti-10V-2Fe-3Al тройного вакуумно-дугового переплава

[1]Мамутова А.Т., [2]Чепуштанова Т.А., [3]Mishra B.

[1] АО Усть-Каменогорский титано-магниевый комбинат, Казахстан
[2]Satbayev University, Алматы, Казахстан
[3] Вустерский политехнический институт, Вустер, США

Поступила: *5 марта 2026*
Рецензирование: *16 марта 2026*
Принята в печать: *6 мая 2026*

АННОТАЦИЯ

Статья посвящена разработке методики микроструктурной и термической верификации качества промышленного слитка Ti-10V-2Fe-3Al тройного вакуумно-дугового переплава АО УК ТМК. Установлено, что все зоны слитка демонстрируют характерную для β-метастабильного сплава Ti-10V-2Fe-3Al двухстадийную термическую эволюцию: распад метастабильной фазы β (≈520–570 °C), эндотермическая α→β перестройка (≈950–1120 °C). Установлено, что энтальпия экзотермического распада β-матрицы увеличивается на ~60–80% в нижней зоне слитка. Ширина фазового перехода ΔT коррелирует с увеличением

	микросегрегации. Установлено, что значение энтальпии эндотермического α→β перехода уменьшается от нижней части слитка к зоне установившейся кристаллизации (Середина-1), что коррелирует со снижением параметров микросегрегации по SEM-EDS профилям (ΔC_max, σC, L_{corr}). Таким образом, термический анализ подтверждает отсутствие выраженного вертикального градиента структурной стабильности и может использоваться как валидирующий критерий интегрального индекса качества электрода. Таким образом, впервые предложена количественная корреляция SEM-EDS профилей с DSC-DTG характеристиками, предложено термический анализ использовать как независимый валидатор микросегрегации. Разработан подход к количественной оценке микросегрегации по профилям SEM–EDS через параметры ΔCmax, σC, L_{corr} и ΔCO(лок.) и предложено использовать интегральный показатель I_{chem} и порог I^{crit}_{chem} для контроля качества электродов с помощью результатов термического анализа.
	Ключевые слова: сплав тройного переплава Ti-10V-2Fe-3Al, вакуумно-дуговая плавка, DSC-DTG и SEM–EDS анализы, α/β- фазовые переходы, анализ термического разложения.
Мамутова Асем Тлековна	***Информация об авторах:*** *Президент АО Усть-Каменогорского титано-магниевого комбината, Усть-Каменогорск; докторант, Горно-металлургический институт, Satbayev University, Алматы, Казахстан. Email: a.mamutova@satbayev.university*
Чепуштанова Татьяна Александровна	*Профессор, кандидат технических наук, доктор PhD, заведующая лабораторией Металлургические процессы, теплотехника и порошковая металлургия, кафедра МиОПИ, Горно-металлургический институт, Сәтбаев университеті, Алматы, Қазақстан. Email: t.chepushtanova@satbayev.university*
Mishra Brajendra	*Профессор, PhD, директор Центра извлечения и переработки ресурсов NSF, Вустерский политехнический институт, Вустер, США. Email: bmishra@wpi.edu*

References

[1] Banerjee D, Williams JC. Perspectives on titanium science and technology. Acta Materialia. 2013; 61(3): 844-879. https://doi.org/10.1016/j.actamat.2012.10.043

[2] Lutjering G, Williams JC. Titanium. Springer. 2007. https://doi.org/10.1007/978-3-540-73036-1

[3] Peters M, Kumpfert J, Ward CH, and Leyens C. Titanium Alloys for Aerospace Applications. Adv. Eng. Mater. 2003; 5:419-427. https://doi.org/10.1002/adem.200310095

[4] Kolli RP, Devaraj A. A Review of Metastable Beta Titanium Alloys. Metals (MDPI). 2018; 8(7):506. https://doi.org/10.3390/met8070506

[5] Banerjee D, Williams JC. Perspectives on Titanium Science and Technology. Acta Mater. 2013; 61:844–879. https://doi.org/10.1016/j.actamat.2012.10.043

[6] Mamutova AT, Chepushtanova TA, Mishra B. Thermodynamic prediction of the technological conditions for producing the Ti-10V-2Fe-3Al alloy by vacuum arc remelting. The Mining Journal of Kazakhstan. 2026; 1(249):55-60. https://doi.org/10.48498/minmag.2026.249.1.006

[7] Jing Z, Liu R, Geng N, Wang Y, Sun Y. Simulation of Solidification Structure in the Vacuum Arc Remelting Process of Titanium Alloy TC4 Based on 3D CAFE Method. Processes. 2024; 12(4):802. https://doi.org/10.3390/pr12040802

[8] Liu X, Zhang Y, Li H, Wang J, Chen L. The morphology features, formation mechanism and elimination of channel segregation in industrial-scale Ti–Nb ingots produced by vacuum arc remelting. Journal of Materials Research and Technology. 2023; 23:2781–2793. https://doi.org/10.1016/j.jmrt.2023.11.009

[9] Liu H, Wang L, Zhang Z. Effects of homogenization heat treatment on Fe microsegregation in Ti-1023 titanium alloy. Materials. 2023; 16(14):4892.

[10] TA Instruments. Determination of beta transus temperature in titanium alloys by DSC. TA Application Note TA131. 2018.

[11] Xumei Yang, Hongzhen Guo, Zhanglong Zhao, Yongquan Ning, Shichong Yuan, Shewei Xin. Quantitative analysis of the effect of deformation temperature on microstructure evolution and mechanical property of isothermally forged BT25y titanium alloy. Procedia Engineering. 2017; 207:2167-2172. https://doi.org/10.1016/j.proeng.2017.10.976

[12] Boyer RR. An Overview on the Use of Titanium in the Aerospace Industry. Materials Science and Engineering: A. 1996; 213:103-114. https://doi.org/10.1016/0921-5093(96)10233-1

[13] Zhao Q, et al. High-strength titanium alloys for aerospace engineering applications: A review on melting-forging process. Materials Science and Engineering A. 2022; 845:143260. https://doi.org/10.1016/j.msea.2022.143260

[14] Guo Jie, Huang Liqing, Wu Jingyang, LI Junjie, Wang Jincheng, Fan Kai. Evolution of Macrosegregation During Three-Stage Vacuum Arc Remelting of Titanium Alloys. Acta Metall Sin. 2024; 60(11):1531-1544. https://doi.org/10.11900/0412.1961.2022.00544

[15] Semiatin SL, Bieler TR. Effect of texture and slip mode on the anisotropy of plastic flow and flow softening during hot working of Ti-6Al-4V. Metallurgical and Materials Transactions A. 2001; 32:1787–1799. https://doi.org/10.1007/s11661-001-0155-1

[16] Semiatin SL, Seetharaman V, and Weiss I. in Advances in the Science and Technology of Titanium Alloy Processing, I Weiss, R Srinivasan, PJ Bania, D Eylon, and SL Semiatin, eds, TMS, Warrendale, PA. 1997, 3–73.

[17] Lütjering G. Influence of processing on microstructure and mechanical properties of (α+β) titanium alloys. Materials Science and Engineering A. 1998; 243:32–45. https://doi.org/10.1016/S0921-5093(97)00778-8

[18] Qinyang Zhao, Qiaoyan Sun, Shewei Xin, Yongnan Chen, Cong Wu, Huan Wang, Jianwei Xu, Mingpan Wan, Weidong Zeng, Yongqing Zhao. High-strength titanium alloys for aerospace engineering applications: A review on melting-forging process. Materials Science and Engineering A. 2022; 845:143260. https://doi.org/10.1016/j.msea.2022.143260

[19] Xiaoli Zhao, Shujun Li, Man Zhang, Yandong Liu, Timothy Sercombe, Shaogang Wang, Yulin Hao, Rui Yang, Lawrence E. Murr. Comparison of the microstructures and mechanical properties of Ti–6Al–4V fabricated by selective laser melting and electron beam melting. Materials & Design. 2016; 95:21-31. https://doi.org/10.1016/j.matdes.2015.12.135

[20] Qiu C, Adkins NJE, Attallah MM. Microstructure and tensile properties of selectively laser-melted and HIPed Ti-6Al-4V. Materials Science and Engineering A. 2013. https://doi.org/10.1016/j.msea.2013.04.099

[21] Boivineau M, Cagran C, Doytier D, Eyraud V, Nadal M-H, Wilthan B, Pottlacher G. Thermophysical Properties of Solid and Liquid Ti-6Al-4V (TA6V) Alloy. International Journal of Thermophysics. 2006; 27(2):507–529. https://doi.org/10.1007/PL00021868

[22] Joakim Karlsson, Anders Snis, Håkan Engqvist, Jukka Lausmaa. Characterization and comparison of materials produced by Electron Beam Melting (EBM) of two different Ti–6Al–4V powder fractions. Journal of Materials Processing Technology. 2013; 213(12):2109-2118. https://doi.org/10.1016/j.jmatprotec.2013.06.010

Crossref
DOI: 10.31643/2028/6445.09
Earth and Planetary Sciences: Earth-Surface Processes

Assessment of the mineral composition, microstructure, and energy properties of the sample from the Shargun coal field based on instrumental analysis methods

[1] Sharopov Kh., [2] Makhmarezhabov D., [3*]Rabatuly M., [1] Daminov T., [3] Beisembay D.S., [3]Satbek B.A.

[1] Islam Karim Tashkent State Technical University, Tashkent, Uzbekistan
[2] National Quality Assurance Agency for Education under the Administration of the President of the Republic of Uzbekistan, Tashkent, Uzbekistan
[3]Abylkas Saginov Karaganda Technical University, Karaganda, Kazakhstan

** Corresponding author email: mukhammedrakhym@mail.ru*

Received: *March 5, 2026*
Peer-reviewed: *March 18, 2026*
Accepted: *May 8, 2026*

ABSTRACT
In this scientific article, the material composition and microstructure of the sample obtained from the Shargun coal deposit were studied based on complex instrumental methods. Based on the conducted research, the elemental composition was determined using an AL-NP-5010A X-ray fluorescence spectrometer, and microscopic analyses were carried out with an increase of up to 1600 times. The spectrometric analysis showed that the high intensities of silicon and aluminum are due to the high proportions of kaolin and quartz, which are aluminosilicates. Also, the detection of iron, calcium, and sulfur indicated the presence of additional sulfides in the iron and carbonate phases. Based on the results of microscopic analyses, it was established that the coal sample has a heterogeneous and porous structure, and the mineral inclusions within the organic matrix are located in a dispersed and clustered state, characterized by micro porousness. At the same time, the proportion of the mineral phase area according to the morphometric assessment was 18-27%, and the micro-porousness coefficient was in the range of 0.12-0.20. It was observed that the angular shape of the particles and the polydisperse granulometric composition correspond to the Rosin distribution. From the integral analysis of the obtained results, it was established that the high content of aluminosilicates and iron oxides increases the susceptibility to ash formation and slagging processes. Also, the presence of porous microstructures and microcracks made it possible to increase the reactivity of the process of heat treatment and gasification.

Keywords: spectrometric analysis, Microscopic analysis, granulometric composition, fluorescent spectrometer, Shargun coal.

Information about authors:

Sharopov Khusanjon Ne'mat ogli — *PhD student of the Mining Department of Islam Karim Tashkent State Technical University, 100095, Almazar district, Universitetskaya street 2, Tashkent, Uzbekistan. E-mail: sharopovhusanjon@gmail.com; ORCID ID: https://orcid.org/0009-0001-2042-3057*

Makhmarezhabov Dilmurod Bakhtiyarovich — *DSc, Associate Professor, Chief Inspector of the National Quality Assurance Agency for Education under the Administration of the President of the Republic of Uzbekistan, 100100, Bobur Street, 30, Tashkent, Uzbekistan. E-mail: dmahmarejabov@mail.ru; ORCID ID: https://orcid.org/0000-0002-7708-6485*

Rabatuly Mukhammedrakhym — *Ph.D., Associate Professor, Department of Development of Mineral Deposits of Abylkas Saginov Karaganda Technical University, 100027, Ave. Nursultan Nazarbayev, 56, Karaganda, Kazakhstan. E-mail: mukhammedrakhym@mail.ru; ORCID ID: https://orcid.org/0000-0002-7558-128X*

Daminov Temurbek Zokir ogli — *PhD student of the Mining Department of Islam Karim Tashkent State Technical University, 100095, Almazar district, Universitetskaya street 2, Tashkent, Uzbekistan. E-mail: daminov.temurbek@tdtu.uz; ORCID ID: https://orcid.org/0009-0007-2798-2752*

Beisembay Daryn Sagyntaiuly — *Master's student, Department of Development of Mineral Deposits of Abylkas Saginov Karaganda Technical University, 100027, Ave. Nursultan Nazarbayev, 56, Karaganda, Kazakhstan. E-mail: sagynta1evv09@gmail.com; ORCID ID: https://orcid.org/0009-0002-4225-487X*

Satbek Balgynbek Aybaruly — *Master's student, Department of Development of Mineral Deposits of Abylkas Saginov Karaganda Technical University, 100027, Ave. Nursultan Nazarbayev, 56, Karaganda, Kazakhstan. E-mail: balgynbekoff@gmail.com; ORCID ID: https://orcid.org/0009-0006-6408-8445*

Indroduction

The modernization of Uzbekistan's energy sector has become one of the country's foremost policy priorities, with particular emphasis on ensuring energy security and the smart use of domestic fuel and raw material resources. The Energy Strategy of the Republic of Uzbekistan until 2030 identifies two key strategic objectives: the gradual improvement of energy efficiency and the reduction of the environmental impact of energy production [1].

This strategy, revised in 2026, places special emphasis on the efficient use of local fuel resources

- including the country's existing coal reserves - through comprehensive processing, increased energy output, and the adoption of waste-free technologies for extracted coal minerals. When coal is used as an energy source, several properties are critically important: its thermic value, ash content, mineral composition, and the concentration of harmful impurities. A thorough scientific investigation of the material composition of coal raw materials, therefore, forms the practical foundation for implementing the national energy strategy [2].

The Shargun coal mine is one of the most significant domestic fuel sources, situated in the southern part of the Republic. Its coal is intended for use in thermal power plants (TPPs), various local industrial enterprises, and centralized district heating systems. Similarly, the Angren coal mine, located in the Kurama and Chatkal mountain ranges, serves as the primary fuel source for Angren TPP JSC. The material composition of coal from both the Shargun and Angren deposits directly influences a range of key technological parameters during combustion:

1) Melting temperature and degree of slag formation;

2) Fouling and deposit buildup in the heat-transfer sections of boilers;

3) Accelerated corrosion of equipment components;

4) Emissions of CO_2 and other harmful gases into the atmosphere;

5) Overall energy efficiency.

One of the central challenges in achieving the energy efficiency targets set out in the national strategy [3] is balancing increased energy output with environmental sustainability. Meeting these goals requires accurate quantification of key elemental constituents in coal - including silicon, calcium, sulfur, aluminum, and iron - alongside the implementation of appropriate processing technologies [4]. For example, sulfur content in coal minerals has a direct bearing on environmental performance, while aluminum and silicon are primary contributors to ash and slag-related problems.

Within the framework of Uzbekistan's 2030 strategy, expanding electricity generation capacity and optimizing the role of coal in the national fuel mix are both explicit objectives. Achieving these aims requires scientifically grounded analysis of coal quality and the application of optimized enrichment and processing technologies. In this context, modern analytical methods - particularly X-ray fluorescence spectrometry (XRF) - enable rapid and accurate determination of coal's material composition using standard laboratory equipment.

In this study, the material composition of a Shargun coal sample was analyzed using an AL-NP-5010A X-ray fluorescence spectrometer. The results carry direct practical relevance to the goals of the national energy strategy: improving energy efficiency, ensuring environmental sustainability, and advancing waste-free coal processing technologies. The findings provide a scientific basis for refining and optimizing coal enrichment methods.

Experimental part

The subjects of this study are representative brown coal samples of grade B-1 obtained from two deposits: the Shargun coal deposit in the Surkhandarya region, located in the south of Uzbekistan, and the Angren coal deposit in the Tashkent region. Both deposits play a significant role in the republic's solid fuel and energy system, serving as primary fuel sources for local heating networks, thermal power plants, and industrial enterprises [5].

Prior to analysis, all coal samples were prepared under laboratory conditions to ensure their representativeness. Sample preparation followed established standard procedures (Fig. 1), encompassing drying, crushing, screening, grinding, and mixing stages [6].

The samples were dried to a constant mass at temperatures between 70°C and 100°C, eliminating the influence of residual moisture on sample weight and ensuring the required analytical accuracy [7]. The dried samples were subsequently ground to a particle size of 0.074 mm, as this fine fraction optimizes the interaction between X-rays and the sample surface, improving measurement reliability [8].

An AL-NP-5010A X-ray fluorescence spectrometer and associated laboratory equipment were used to determine the elemental composition of the coal samples. XRF analysis is a modern analytical method for the in-depth investigation of elemental composition in solid materials. The method is based on the excitation of atoms within the analyzed samples under the influence of radiation and the emission of a characteristic secondary fluorescence spectrum, the intensity of which is proportional to the elemental concentration. The XRF method is widely used for the rapid and comparatively high-precision determination of the oxide composition of coal and mineral raw materials.

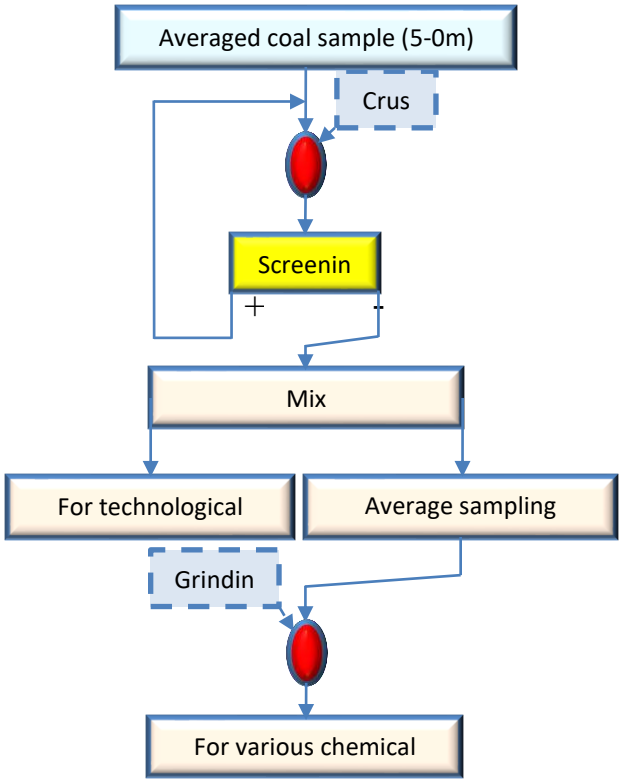

Figure 1 - Sample preparation scheme for research

The analysis was carried out at an accelerating voltage of 45 kV and a current of 300 μA, providing optimal energy conditions for the detection of various elements in the coal. Based on the analysis results, the major elements with high probability of occurrence were identified: silicon, aluminum, calcium, iron, and sulfur - elements that govern the mineral composition and ash-forming properties of the coal. The elevated concentrations of Si and Al indicate the presence of clay minerals, which serve as the primary factor responsible for increased ash yield during coal combustion. Since iron compounds may occur in the form of oxides or sulfides, they raise the risk of slag formation on the steam boiler surfaces at TPPs and accelerate the corrosion process. Sulfur content, in turn, is the principal cause of the formation of harmful combustion by-products [9].

The analytical data reported here were obtained under scientific project AL-9124093979, 'Development of Coal Enrichment and Gas Production Technology for the Construction Materials Industry'. These results constitute a preliminary analytical report on the mineral-chemical composition of Shargun coal and provide a scientific basis for evaluating its energy efficiency and industrial applicability.

Results and Discussion

X-ray fluorescence spectrometric analysis of the Shargun coal sample was performed using an AL-NP-5010A spectrometer, and the material and mineralogical-chemical composition was determined from well-resolved spectral peaks. The results are summarized in Tables 1 and 2. The highest spectral intensities corresponded to silicon (Si), with characteristic peaks at approximately 1.74 keV and intensities of 7,000–8,000 cps, indicating the predominance of aluminosilicate mineral phases. Aluminum (Al) peaks were recorded at approximately 1.49 keV with intensities of 4,500–5,500 cps, confirming the presence of aluminosilicate clay minerals such as kaolinite - $Al_2Si_2O_5$ $(OH)_4$ and $(K_{0.75}$ $(H_3O)_{0.25})$ Al_2 (Si_3Al) O_{10} $((H_2O)_{0.75}$ $(OH)_{0.25})_2$ [10].

Table 1 - Elemental composition of the Shargun coal sample (XRF analysis)

T/r	Elements	I (cps)	Quantity, %
1	Carbon (C)	6703.0	40.585
2	Nitrogen (N)	5080.0	30.758
3	Oxygen (O)	3576.0	21.652
4	Aluminium (Al)	87.0	0.527
5	Silicon (Si)	25.00	0.151
6	Phosphorus (P)	19.00	0.115
7	Sulphur (S)	18.00	0.109
8	Sodium (Na)	522.00	3.161
11	Calcium (Ca)	33.00	0.200
12	Iron (Fe)	149.00	0.902
13	Gallium (Ga)	13.00	0.079
14	Germanium (Ge)	12.00	0.073
15	Arsenic (As)	32.00	0.194
16	-	-	-

Table 2 - Elemental composition of the Angren coal sample (XRF analysis)

T/r	Elements	B-1	
		I (cps)	Quantity, %
1	Carbon (C)	6621	47.2
2	Oxygen (O)	5257	37.5
3	Aluminium (Al)	698	5
4	Silicon (Si)	464	3.3
5	Phosphorus (P)	347	2.5
6	Sulphur (S)	262	1.9
7	Iron (Fe)	209	1.5
8	Calcium (Ca)	167	1.1

A spectral peak in the energy range of approximately 2.30-2.35 keV, recorded at a moderate intensity of 2,000-3,000 cps, is attributed to sulfur (S). This finding indicates the presence of sulfide minerals such as pyrite (FeS_2) and provides scientific justification for the formation of SO_2 during coal combustion [11].

Iron (Fe) peaks were detected at approximately 6.4 keV, with intensities in the range of 1,500-2,500 cps. The presence of iron-bearing minerals in the coal is a key factor promoting slagging and deposit formation in thermal equipment during combustion [12].

Calcium (Ca) peaks were recorded at 3.69 keV at low-to-medium intensities of 1,000-1,800 cps, indicating the presence of carbonate minerals such as calcite ($CaCO_3$) and dolomite ($CaMg(CO_3)_2$). Calcium compounds exert a significant influence on coal combustion behavior and ash mineralogy, particularly in determining ash melting temperature and slagging tendency [13]. Furthermore, the relatively high intensities of Low-energy peaks (1-3 keV) compared to the overall spectrum indicate that the mineral fraction of the coal is substantial relative to its organic fraction, which is characteristic of brown coal.

A comprehensive interpretation of the XRF results confirms that the elevated intensities of Si and Al reflect the predominance of aluminosilicate minerals in the Shargun coal sample, while the detection of Fe and S signals the presence of pyrite (FeS_2) and related sulfide phases. These characteristics collectively increase ash yield during combustion, promote slagging, and reduce the operational efficiency of TPP steam boiler units [14]. The low intensity of heavy metal peaks in the high-energy spectral region further indicates that metallic components are present only at trace levels, with aluminosilicate phases dominating the mineral fraction [15].

Based on the obtained spectral data, it can be concluded that the Shargun coal sample is a relatively high-ash fuel, and its direct use requires optimization of combustion and processing parameters. The high concentrations of Si and Al reduce heat exchange efficiency when the coal is used directly as fuel in thermal power plants and industrial applications. The presence of sulfur and its conversion into toxic gases during combustion poses environmental risks - providing scientific justification for the implementation of gas purification technologies prior to atmospheric discharge.

The XRF analysis results for the sample obtained from the Angren coal deposit (Table 2) show that this coal differs significantly from Shargun coal in terms of its chemical and mineralogical composition.

The carbon content of the sample is 47.2%, which is higher than that recorded for the Shargun coal sample. However, the elevated oxygen content (37.5%) also indicates a high degree of oxidation in this sample [16].

Spectral analysis revealed that the aluminum and silicon contents in the Angren brown coal are 5.0% and 3.3%, respectively, both higher than the corresponding values for the Shargun coal. The predominance of aluminosilicate minerals such as kaolinite and quartz were confirmed in this sample. These elevated concentrations lead to substantial ash formation and slag buildup on equipment surfaces during combustion [17]. Furthermore, the sulfur content of the Angren brown coal sample is 1.9%, which is considerably higher than that of the Shargun coal sample.

Overall, the XRF spectral data obtained from Figures 2 and 3 confirm that the coal samples from both the Shargun and Angren deposits belong to the brown coal type, are characterized by the predominance of aluminosilicate mineral phases, and require thorough technological evaluation prior to their use in industrial, energy, and broader economic applications.

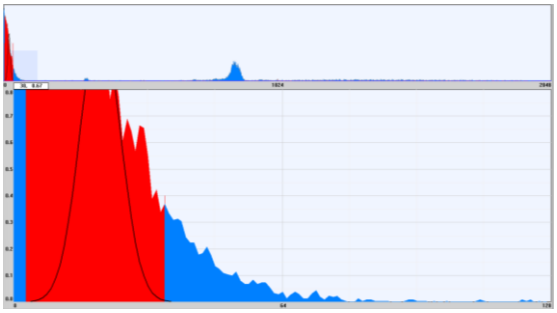

Figure 2 - Spectral intensity of the elements present in coal samples from the Shargun deposit

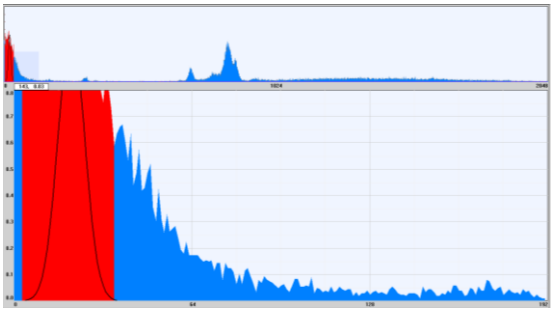

Figure 3 - Spectral intensity of elements present in coal samples from the Angren brown coal deposit

Morphological and particle size analysis of the Shargun coal sample was carried out using optical microscopy at magnifications ranging from 50× to 2,000×. At 50× magnification, particles displayed irregular, angular, and polyhedral geometries (Fig. 4), consistent with the fragmentation patterns produced by mechanical grinding.

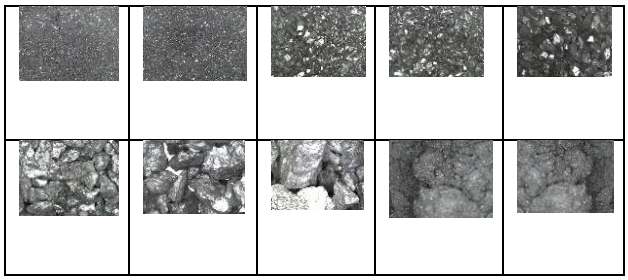

Figure 4 - Microscopic images of a sample from the Shargun coal deposit

The magnified images clearly reveal that the coal particles possess polyhedral, multi-angular, and irregular geometric shapes. This morphology confirms the high mechanical resistance of the coal to grinding and its rigid fractional composition. The angular structure of the particles indicates a dense mineralogical arrangement and the presence of inorganic mineral phases, including quartz and aluminosilicates [18].

Visual morphometric analysis indicated that the average equivalent particle diameter ranged from approximately 0.2 to 2.5 mm. Particle shape was assessed using the circularity factor (Equation 1):

$$C = \frac{4\pi S}{P^2} \quad (1)$$

where S is the projected particle area, and P is the particle perimeter. The measured values of C<0.7 confirms that the particles possess angular and irregular morphologies, reflecting the mechanical strength of the coal and its response to grinding.

At magnifications of 200-400×, light-colored mineral inclusions with high reflectivity were identified within the organic matrix. The area fraction of these mineral phases, determined by image segmentation, ranged from Fm/Ft≈0.20 to 0.27, where Fm is the mineral phase area, and Ft is the total image area. These values confirm a significant mineral content and are consistent with the Si and Al intensities recorded by XRF. The morphology of these inclusions - predominantly platy and granular - is characteristic of silicate phases, particularly kaolinite ($Al_2Si_2O_5(OH)_4$) and quartz (SiO_2) [[19], [20], [21], [22]].

At magnifications of 800-1,000×, a well-developed porous structure was clearly visible. Porosity was quantified by image analysis according to Equation 2:

$$\gamma = \frac{V_p}{V_t} \quad (2)$$

where Vp is the pore volume, and Vt is the total volume. The calculated porosity ranged from γ=0.10 to 0.20, consistent with the high porosity characteristic of brown coal. This pore structure is a key parameter governing the reactivity, adsorption capacity, and desorption behavior of the material [23]. At 1,600× magnification, mineral inclusions were observed to be distributed within the organic matrix as discrete, fine-grained clusters. The average mineral particle diameter ranged from approximately 5 to 60 μm, and the particle size distribution followed a log-normal function (Equation 3):

$$f(d) = \frac{1}{d\sigma\sqrt{2\pi}} \exp\left(-\frac{(lnd-\mu)^2}{2\sigma^2}\right) \quad (3)$$

This distribution is consistent with the natural sedimentary origin of the mineral phases [24, 25].

Comparative analysis of fractions at equivalent magnification revealed that finer fractions exhibit more uniform and finely dispersed mineral phases, whereas coarser fractions contain larger, heterogeneously distributed mineral inclusions. The particle size distribution of the granulometric composition was characterized using the Rosin–Rammler equation (Equation 4):

$$R(d) = \exp\left[-\left(\frac{d}{d_o}\right)^n\right] \quad (4)$$

where d_o is the characteristic diameter and n is the distribution modulus.

Microphotographs also revealed lamellar (platy) textures, indicating a low degree of coalification (metamorphism) and the presence of vitrinite and inertinite macerals in the organic fraction.

The integrated microstructural and spectrometric analysis demonstrates that the Shargun coal sample is a brown coal characterized by a heterogeneous, highly mineralized, and porous structure with a substantial mineral fraction. This is reflected in the ash formation relationship (Equation 5):

$$S_{osh} < SiO_2+Fe_2O_3+Al_2O_3 \quad (5)$$

which shows that increasing concentrations of SiO_2, Fe_2O_3, and Al_2O_3 directly raise the ash yield upon combustion. Accordingly, microscopic analysis of the mineral phases and their spatial distribution within the coal matrix provides scientific justification for the necessity of comprehensive beneficiation (enrichment) of Shargun coal prior to its use as fuel.

Conclusions

Combined XRF spectrometric and optical microscopic analyses - carried out at magnifications of up to 1,600× - enabled a comprehensive mineralogical, chemical, and microstructural characterization of coal from the Shargun deposit. The high spectral intensities of silicon and aluminum confirm an elevated content of aluminosilicate minerals, primarily kaolinite and quartz. The detection of iron, calcium, and sulfur signals the presence of pyrite and related sulfide phases, as well as carbonate minerals.

Microscopic imaging revealed a heterogeneous particle morphology characterized by angular and polyhedral forms, with mineral inclusions dispersed in clusters throughout the organic matrix. The mineral phase area fraction ranged from 0.20 to 0.27, and the polydisperse particle size distribution confirms that the sample belongs to the brown coal type, distinguished by a highly mineralized and highly porous structure with microporosity values of γ=0.10-0.20.

Integrated interpretation of the analytical results indicates that the elevated concentrations of aluminosilicates and iron oxides increase the coal's susceptibility to ash formation and slagging during combustion. At the same time, the developed porous microstructure and the presence of microcracks enhance reactivity during thermal treatment and gasification. Taken together, these findings demonstrate that comprehensive beneficiation of Shargun coal is a necessary prerequisite for its efficient and environmentally responsible use as a fuel source.

Conflict of interest. On behalf of all authors, the corresponding author declares that there is no conflict of interest.

***CRediT author statement*: M. Rabatuly:** Conceptualization, Methodology, Software; **Kh. Sharopov:** Data Curation, Writing - Original Draft Preparation; **D. Makhmarezhabov, B. Satbek:** Visualization, Investigation; **T. Daminov, D. Beisembay:** Software, Validation.

Cite this article as: Sharopov Kh, Makhmarezhabov D, Rabatuly M, Daminov T, Beisembay DS, Satbek BA. Assessment of the mineral composition, microstructure, and energy properties of the sample from the Shargun coal field based on instrumental analysis methods. Kompleksnoe Ispolzovanie Mineralnogo Syra = Complex Use of Mineral Resources. 2028; 344(1):90-98. https://doi.org/10.31643/2028/6445.09

Шарғұн көмір кен орнынан алынған үлгінің минералдық құрамын, микроқұрылымын және энергетикалық қасиеттерін аспаптық талдау әдістері негізінде бағалау

[1] Шаропов Х., [2] Махмарежабов Д., [3] Рабатулы М., [1] Даминов Т., [3] Бейсембай Д.С., [3] Сатбек Б.А.

[1]Ислам Каримов атындағы ташкент Мемлекеттік Техникалық Университеті, Ташкент, Өзбекстан
[2]Өзбекстан Республикасы Президенті Әкімшілігі жанындағы Білім сапасын қамтамасыз ету ұлттық агенттігі, Ташкент, Өзбекстан
[3]Ә. Сағынов атындағы Қарағанды техникалық университеті, Қарағанды, Қазақстан

Мақала келді: *5 наурыз 2026*
Сараптамадан өтті: *18 наурыз 2026*
Қабылданды: *8 мамыр 2026*

ТҮЙІНДЕМЕ

Бұл ғылыми мақалада Шарғұн көмір кен орнынан алынған үлгінің заттық құрамы мен микроструктурасы кешенді аспаптық әдістер негізінде зерттелді. Жүргізілген зерттеулер нәтижесінде элементтік құрам AL-NP-5010A рентген-флуоресценттік спектрометр көмегімен анықталды, микроскопиялық талдаулар 1600 есеге дейін үлкейтумен жүргізілді. Спектрометриялық талдау нәтижесінде кремний мен алюминий элементтерінің жоғары интенсивтілігі каолин мен кварцтың алюмосиликаттар түріндегі жоғары үлесіне байланысты екені көрсетілді. Сондай-ақ темір, кальций және күкірт элементтерінің анықталуы темір құрамдас және карбонатты фазаларда қосымша сульфидтердің бар екенін көрсетеді. Микроскопиялық талдау нәтижелеріне сүйене отырып, көмір үлгісінің әртекті және кеуекті құрылымы бар екені, ал органикалық матрица ішіндегі минералдық қосындылар дисперсті және кластерлі күйде орналасқаны, микрокеуектілікпен сипатталатыны анықталды. Сонымен қатар, морфометриялық бағалау бойынша минералды фаза ауданының үлесі 18–

	27 % құрайды, ал микрокеуектілік коэффициенті 0,12–0,20 аралығында болды. Бөлшектердің бұрыштық пішіні мен полидисперсті гранулометриялық құрамы Розин таралуына сәйкес келетіні атап өтілген. Алынған нәтижелердің интегралдық талдауы негізінде алюмосиликаттар мен темір оксидтерінің жоғары құрамы күл түзілу және шлак түзілу процестеріне бейімділікті арттыратыны анықталды. Сонымен қатар, кеуекті микроқұрылымдар мен микрожарықтардың болуы термиялық өңдеу және газдандыру процестерінде реактивтіліктің жоғарылауына мүмкіндік береді.
	Түйін сөздер: спектрометриялық талдау, микроскопиялық талдау, гранулометриялық құрам, флуоресцентті спектрометр, Шарғұн көмірі.
Шаропов Хусанжон Неъмат угли	***Авторлар туралы ақпарат:*** *Ислам Карим атындағы Ташкент мемлекеттік техникалық университетінің PhD докторанты, 100095, Алмазар ауданы, Университетская көшесі 2, Ташкент, Өзбекстан. E-mail: sharopovhusanjon@gmail.com; ORCID ID: https://orcid.org/0009-0001-2042-3057*
Махмарежабов Дилмурод Бахтиярович	*DSc, доцент, Өзбекстан Республикасы Президенті Әкімшілігі жанындағы Білім сапасын қамтамасыз ету ұлттық агенттігінің бас инспекторы, 100100, Бобур Көшесі, 30, Ташкент, Өзбекстан. E-mail: dmahmarejabov@mail.ru; ORCID ID: https://orcid.org/0000-0002-7708-6485*
Рабатұлы Мұхаммедрахым	*PhD докторы, Әбілқас Сағынов атындағы Қарағанды техникалық университетінің Пайдалы қазбалар кенорындарын өндіру кафедрасының қауымдастырылған профессоры, 100027, Нұрсұлтан Назарбаев даңғ. 56, Қарағанды, Қазақстан. E-mail: mukhammedrakhym@mail.ru; ORCID ID: https://orcid.org/0000-0002-7558-128X*
Даминов Темурбек Зокир угли	*Ислам Карим атындағы Ташкент Мемлекеттік Техникалық Университетінің PhD докторанты, 100095, Алмазар ауданы, Университетская көшесі, 2, Ташкент, Өзбекстан. E-mail: daminov.temurbek@tdtu.uz; ORCID ID: https://orcid.org/0009-0007-2798-2752*
Бейсембай Дарын Сағынтайұлы	*Магистрант, Әбілқас Сағынов атындағы Қарағанды техникалық университетінің Пайдалы қазбалар кенорындарын өндіру кафедрасының қауымдастырылған профессоры, 100027, Нұрсұлтан Назарбаев даңғ. 56, Қарағанды, Қазақстан. E-mail: sagynta1evv09@gmail.com; ORCID ID: https://orcid.org/0009-0002-4225-487X*
Сатбек Балғынбек Айбарұлы	*Магистрант, Әбілқас Сағынов атындағы Қарағанды техникалық университетінің Пайдалы қазбалар кенорындарын өндіру кафедрасының қауымдастырылған профессоры, 100027, Нұрсұлтан Назарбаев даңғ. 56, Қарағанды, Қазақстан. E-mail: balgynbekoff@gmail.com; ORCID ID: https://orcid.org/0009-0006-6408-8445*

Оценка минерального состава, микроструктуры и энергетических свойств образца из Шаргунского угольного поля на основе методов инструментального анализа

[1] Шаропов Х., [2] Махмарежабов Д., [3] Рабатулы М., [1] Даминов Т., [3] Бейсембай Д.С., [3] Сатбек Б.А.

[1] Ташкентский государственный технический университет имени Ислама Каримова, Ташкент, Узбекистан

[2] Национальное агентство по обеспечению качества образования при Администрации Президента Республики Узбекистан, Ташкент, Узбекистан

[3] Карагандинский технический университет имени А. Сагинова, Караганда, Казахстан

Поступила: *5 марта 2026*
Рецензирование: *18 марта 2026*
Принята в печать: *8 мая 2026*

АННОТАЦИЯ

В данной научной статье изучены вещественный состав и микроструктура образца, полученного из Шаргунского угольного месторождения, на основе комплексных инструментальных методов. По результатам проведённых исследований определён элементный состав с использованием рентгенофлуоресцентного спектрометра AL-NP-5010A, а микроскопические анализы выполнены при увеличении до 1600 раз. Проведённый спектрометрический анализ показал, что высокая интенсивность элементов кремния и алюминия обусловлена значительной долей каолина и кварца в виде алюмосиликатов. Также обнаружение элементов железа, кальция и серы свидетельствует о присутствии дополнительных сульфидов в железосодержащих и карбонатных фазах. На основании результатов микроскопических анализов установлено, что образец угля обладает неоднородной и пористой структурой, а минеральные включения в органической матрице расположены в дисперсном и кластерном состоянии, характеризуемом микропористостью. При этом доля площади минеральной фазы, по морфометрической оценке, составляет 18–27 %, а коэффициент микропористости находится в диапазоне 0,12–0,20. Отмечено, что угловатая форма частиц и полидисперсный гранулометрический состав соответствуют распределению Розина. В результате интегрального анализа полученных данных установлено, что высокое содержание алюмосиликатов и оксидов железа повышает склонность к процессам золообразования и шлакования. Кроме того, наличие пористых микроструктур и микротрещин позволяет повысить реакционную способность процессов термообработки и газификации.

	Ключевые слова: спектрометрический анализ, Микроскопический анализ, гранулометрический состав, флуоресцентный спектрометр, Шаргунский уголь.
Шаропов Хусанжон Неъмат угли	***Информация об авторах:*** *PhD докторант Ташкентского государственного технического университета имени Ислама Карима, 100095, Алмазарский район, ул. Университетская, 2, Ташкент, Узбекистан. E-mail: sharopovhusanjon@gmail.com; ORCID ID: https://orcid.org/0009-0001-2042-3057*
Махмарежабов Дилмурод Бахтиярович	*Доктор педагогических наук, доцент, главный инспектор Национального агентства по обеспечению качества образования при Администрации Президента Республики Узбекистан, 100100, ул. Бобура, 30, Ташкент, Узбекистан. E-mail: dmahmarejabov@mail.ru; ORCID ID: https://orcid.org/0000-0002-7708-6485*
Рабатулы Мухаммедрахым	*PhD, ассоциированный профессор кафедры Разработки месторождений полезных ископаемых Карагандинского технического университета имени Абылкаса Сагинова, 100027, пр. Нурсултана Назарбаева, 56, Караганда, Казахстан. E-mail: mukhammedrakhym@mail.ru; ORCID ID: https://orcid.org/0000-0002-7558-128X*
Даминов Темурбек Зокир угли	*PhD докторант Ташкентского государственного технического университета имени Ислама Карима, 100095, Алмазарский район, ул. Университетская, 2, Ташкент, Узбекистан. E-mail: daminov.temurbek@tdtu.uz; ORCID ID: https://orcid.org/0009-0007-2798-2752*
Бейсембай Дарын Сагынтайулы	*Магистрант кафедры Разработки месторождений полезных ископаемых Карагандинского технического университета имени Абылкаса Сагинова, 100027, пр. Нурсултана Назарбаева, 56, Караганда, Казахстан. E-mail: sagynta1evv09@gmail.com; ORCID ID: https://orcid.org/0009-0002-4225-487X*
Сатбек Балгынбек Айбарулы	*Магистрант кафедры Разработки месторождений полезных ископаемых Карагандинского технического университета имени Абылкаса Сагинова, 100027, пр. Нурсултана Назарбаева, 56, Караганда, Казахстан. E-mail: balgynbekoff@gmail.com; ORCID ID: https://orcid.org/0009-0006-6408-8445*

References

[1] Resolution of the President of the Republic of Uzbekistan dated October 4, 2019 No. PP-4477 On Approving the Strategy for the Transition of the Republic of Uzbekistan to a Green' Economy for the Period 2019-2030. Тошкент. 2019.

[2] Law of the Republic of Uzbekistan dated 23.11.2020 No. ЗРУ-648 'On Subsoil. Tashkent. 2020.

[3] Law of the Republic of Uzbekistan On Rational Use of Energy. April 25, 1997, No. 412-I. Tashkent. 1997.

[4] Law of the Republic of Uzbekistan No. 754-XII of 09.12.1992 On Environmental Protection. Tashkent. 1992.

[5] Decree of the President of the Republic of Uzbekistan dated October 4, 2019 No. PP-4477 On Approving the Strategy for the Transition of the Republic of Uzbekistan to a Green Economy for the Period 2019-2030.

[6] Ma F, Tao Y, Xian Y. Study on maceral liberation characteristics of ball grinding and rod grinding for low-rank coal. International Journal of Coal Preparation and Utilization. 2022; 42:2923-2939.

[7] Akkoyunlu M T, Pekel E, Akkoyunlu M C, Pusat S, Ozkan C, and Kara S S. Determination of effective parameters for coal moisture content determination using a 'design of experiment' method. International Journal of Coal Preparation and Utilization. 2018; 38:443-450.

[8] Dai S, Hou X, Ren D, & Tang Y. Surface analysis of pyrite in the No. 9 coal seam, Wuda Coalfield, Inner Mongolia, China, using high-resolution time-of-flight secondary ion mass-spectrometry. International Journal of Coal Geology. 2003; 55(2-4):139-150.

[9] Bekpulatov J M, Makhmarezhabov D B, Umirzokov A A. On the possibility of waste-free use of mineral resources of the Angrensky Brain coal deposit. E3S Web of Conferences. EDP Sciences. 2024; 491:08.

[10] Vassilev S V, Vassileva C G. Mineralogy of combustion wastes from coal-fired power stations. Fuel Processing Technology. 1996

[11] Vassilev S V, et al. An overview of the organic and inorganic phase composition of biomass. Fuel. 2012; 94:1-33.

[12] Raask E. Mineral impurities in coal combustion: behavior, problems, and remedial measures. CRC Press. 1985.

[13] Rabatuly M, Demin VF, Kenetaeva AA, Steflyuk YuYu, Toshov JB. Evaluation of modern methods and techniques for calculating parameters during coal bed degassing. Kompleksnoe Ispolzovanie Mineralnogo Syra = Complex Use of Mineral Resources. 2025; 334 (3):110-120. https://doi.org/10.31643/2025/6445.33

[14] Ward C R. Coal geology and coal technology. 1984.

[15] Alikulov Sh, Toshov J, Mussin R, Rabatuly M, Tolovkhan B, Bogzhanova Zh, Gabitova A. Study of rational solution parameters during in-situ uranium leaching. Mining of Mineral Deposits. 2025; 19(1):37-46. https://doi.org/10.33271/mining19.01.037

[16] Van Krevelen D W. Coal: Typology-physics-chemistry-constitution. 1993.

[17] Reid W T. External corrosion and deposits: boilers and gas turbines. 1970.

[18] Stach E, Mackowyky M-Th, Teichmüller M, Taylor GH, Chandra D, Teichmüller R. (Eds.), Stach's Textbook of Coal Petrology, Gebruder Borntraeger, Berlin. 1982.

[19] O'Keefe JM, Bechtel A, Christanis K, Dai S, DiMichele WA, Eble CF, Hower JC. On the fundamental difference between coal rank and coal type. International Journal of Coal Geology. 2013; 118:58-87.

[20] Kelisbekov AK, Daniyarov NA. Prospects of application in the coal industry of multi-motor plate conveyor with frequency-controlled electric drive. Scientific, technical and production-economic journal Coal, M. 2020; 5:45-48. https://doi.org/10.18796/0041-5790-2020-5-45-48

[21] Safarov JE, Sultanova ShA, Najafli MR, Ponasenko AS, Samandarov DI, Usenov AB, Mirkomilov AM, Dadayev GT, Huseynli M, Makhmudova LA. Modeling of equilibrium heat and mass transfer in three-dimensional connected media. Processes of Petrochemistry and oil Refining. PPOR. 2026; 27(2):521-534.

[22] Vassilev SV. Mineral matter in coal and its transformations. Fuel. 2005

[23] Vassilev S V, Vassileva C G. Mineralogy of combustion wastes from coal-fired power stations. Fuel Processing Technology. 1996; 47(3):261-280.

[24] Kenetayeva AA, Usupayev SE, Kryazheva TV, Rabatuly M. Demethanization of coal seams in the Karaganda basin. IOP Conference Series: Earth and Environmental Science. 2021; 677(4), https://doi.org/10.1088/1755-1315/677/4/042118

[25] Rabatuly M, Myrzathan SA, Toshov JB, Nasimov J, Khamzaev A. Views on drilling effectiveness and sampling estimation for solid ore minerals. Kompleksnoe Ispolzovanie Mineralnogo Syra = Complex Use of Mineral Resources. 2026; 336(1):5-14. https://doi.org/10.31643/2026/6445.01

Crossref
DOI: 10.31643/2028/6445.10
Earth and Planetary Sciences: Earth-Surface Processes

Analytical Review of the Methods of Studying Open Pit Slope Stability Under the Conditions of Mining Operations Digitalization

[*]Vishnevskaya N.A., Ozhigina S.B., Ozhigin S.G., Kubaidullina U.A., Baigali R.K., Babazhanov R.T.

Abylkas Saginov Karaganada Technical University, Karaganda, Kazakhstan

** Corresponding author email: n.vishnevskaya@ktu.edu.kz*

Received: *January 26, 2026*
Peer-reviewed: *April 22, 2026*
Accepted: *May 8, 2026*

ABSTRACT

Open-pit slope stability is one of the key factors determining the safety and efficiency of open-pit mining operations. With increasing pit depth, growing complexity of rock mass structure, and intensification of mining activities, the need for advanced methods for studying slope stability based on digital technologies is steadily increasing. The aim of this study is to systematize and comparatively analyze modern methods for investigating open-pit slope stability, taking into account their capabilities and limitations under mining conditions. The paper presents an analytical review of computational geomechanical approaches, geodetic instrumental methods, terrestrial laser scanning, UAV-based photogrammetry, and satellite radar interferometry (InSAR). A comparative analysis of these methods is performed based on key parameters, including data type, spatial coverage, and capabilities for deformation analysis. The results show that each method has specific advantages and limitations related to data characteristics, observation conditions, and analytical potential. It is established that none of the methods, when used individually, provides a complete and reliable description of slope stability. The highest level of informativeness is achieved through the integration of different methods within comprehensive analytical approaches. The results of this study provide a systematic understanding of the role of modern digital methods in slope stability research and confirm the перспективность of developing integrated digital systems for monitoring and assessing open-pit slope stability.

Keywords: Slope stability, Computational Method, Instrumental Method, Terrestrial Laser Scanning, Earth Remote Sensing, Integrated Digital System.

Information about authors:

Vishnevskaya Natalya — *Phd Student, Teacher of the Department of Mine Surveying and Geodesy, Abylkas Saginov Karaganda Technical University, ave. Nursultan Nazarbayev, 56, 100027, Karaganda, Kazakhstan. Email: n.vishnevskaya@ktu.edu.kz; ORCID ID: https://orcid.org/0009-0001-2434-2019*

Ozhigina Svetlana — *Candidate of Technical Sciences, Associate professor of the Department of Mine Surveying and Geodesy, Abylkas Saginov Karaganda Technical University, Ave. Nursultan Nazarbayev, 56, 100027, Karaganda, Kazakhstan. Email: s.ozhigina@ktu.edu.kz; ORCID ID: https://orcid.org/0000-0001-7986-2858*

Ozhigin Sergey — *Doctor of Technical Sciences, Professor of the Department of Mine Surveying and Geodesy, Abylkas Saginov Karaganda Technical University, Ave. Nursultan Nazarbayev, 56, 100027, Karaganda, Kazakhstan. Email: s.ozhigin@ktu.edu.kz; ORCID ID: https://orcid.org/0000-0003-2432-3851*

Kubaidullina Ulpan — *Phd Student, Teacher of the Department of Mine Surveying and Geodesy, Abylkas Saginov Karaganda Technical University, ave. Nursultan Nazarbayev, 56, 100027, Karaganda, Kazakhstan. Email: u.kubaidullina@ktu.edu.kz; ORCID ID: https://orcid.org/0000-0002-2445-5590*

Baigali Ruslan — *Phd Student, Teacher of the Department of Mine Surveying and Geodesy, Abylkas Saginov Karaganda Technical University, ave. Nursultan Nazarbayev, 56, 100027, Karaganda, Kazakhstan. Email: r.baigali@ktu.edu.kz; ORCID ID: https://orcid.org/0000-0003-4431-2172*

Babazhanov Ruslan — *Phd Student, Teacher of the Department of Mine Surveying and Geodesy, Abylkas Saginov Karaganda Technical University, ave. Nursultan Nazarbayev, 56, 100027, Karaganda, Kazakhstan. Email: r.babazhanov@ktu.edu.kz; ORCID ID: https://orcid.org/0000-0003-0498-8899*

Introduction

Open pit slope stability is one the key factors defining safety and productivity of open pit mining operations. Increase of open mine depths, growing complexity of rock massif structure and intensification of mining operations lead to slope failures, disturbance of production processes and significant economic losses. In this regard, the study of the stability state of open pit slopes remains an actual scientific and practical task in the mining industry.

Currently, a wide range of methods are used to research the open pit slope stability, including computational geomechanical approaches, instrumental geodetic observations, and remote sensing methods. Digital technologies gained their momentum,

these are terrestrial laser scanning, photogrammetry based on unmanned aerial photography, SAR interferometry and numerical modeling have been significantly developed to obtain spatial data on the geometry of slopes and the development of deformation processes.

Modern studies of the open pit slope stability are increasingly based on the use of digital methods that expand possibilities of assessing the condition of open pit slopes and analyzing the development of deformation processes. At the same time, the applied methods are focused on solving various problems of stability research, including assessment of the current condition of slopes, identification of potentially dangerous zones, analysis of deformation mechanisms and justification of deformation development forecast, which conditions need for their comparative and integrated consideration.

The aim of this study is to systematize and comparatively analyze modern methods for investigating the stability of open-pit slopes, taking into account the capabilities of digital technologies and assessing their applicability in open-pit mining conditions. The study examines the capabilities and limitations of computational, geodetic, and remote sensing methods, compares them according to key parameters, and determines the role of their integration in the analysis and prediction of deformation processes.

In this context, the following research questions are addressed: which methods provide the most informative description of open-pit slope stability, what are the limitations of their application under real mining conditions, and to what extent the integration of different approaches improves the reliability of stability assessment and deformation prediction.

Analytical Review of Modern Methods of Studying the Open Pit Slope Stability

Computational Methods

Computational methods of assessing open pit slope stability traditionally occupy a central place in the practice of open pit mining operations design and operation. Their basis is analysis of the limit equilibrium of the rock massif with determination of the stability coefficient for the assumed failure surface. Classical methods, such as the methods of Fellenius, Bishop, Yanbu, Spencer and their modifications, have become widespread due to their relative ease of implementation and normative confidence [[1], [2], [3]].

Application of computational methods allows for taking into account geometrical parameters of slopes, physical and mechanical properties of rocks, and influence of underground waters and external loads. At the same time, these approaches, as a rule, assume a priori setting of the failure surface shape and use of averaged massif characteristics, which significantly limits their applicability under the conditions of complex geological structure and pronounced structural heterogeneity of rocks [[2, [[4]].

Introduction of numerical modeling methods, including finite element, finite difference and discrete element methods, has ensured further development of classical design schemes. Numerical models allow for analyzing the stress-strain state of the massif in two- and three-dimensional presentation, for taking into account the layer-by-layer structure, tectonic disturbances and stages of mining operations [[5], [6]]. The application of such approaches expands possibilities of studying the mechanisms of slope failure and assessing influence of various factors on their stability.

In one of the studies [7], computational methods are complemented by multiple-factor analysis oriented at identifying key geological and geomechanical factors that determine slope stability. At the same time, classification and empirical approaches based on the use of integral indices of the massif state are used, which allow for performing rapid assessment of stability, but they are of general nature and expedient mainly for preliminary analysis [[8], [9]].

A number of studies address risks and typical methodological errors that occur in calculations of open pit slope stability. It is noted that the reliability of the obtained results is largely determined by the quality of the input data, correctness of the choice of the calculation scheme and validity of the accepted assumptions [4]. These aspects become particularly important when assessing stability in specific environments including layered massifs, man-made formations and non-metallic mineral open pit mines [[10], [11], [12]].

Computational methods provide a basic engineering assessment of open pit slope stability and remain an important tool for geomechanical analysis. At the same time, their application is not oriented at operative detection of deformations and direct analysis of hazardous processes development. In this regard, it is advisable to consider computational methods as a part of complex approaches that provide for the integration of computational models

with the results of instrumental geodetic observations and remote sensing data, which is discussed in the following sections of this review.

Geodetic Instrumental Methods

Geodetic instrumental methods are widely used in the study of the open pit slope stability as an instrumental basis for obtaining data on the deformations of rock massifs. In contrast to computational approaches, geodetic observations make it possible to record actual slope displacements in time, which provides a transition from computational stability assessment to the analysis of its current state [[13], [14]].

The tacheometric method is traditionally used to study deformation processes in the zones of potential instability of open pit slopes. Repeated high-precision measurements of survey marker coordinates allow for identifying directions and velocities of displacements, and for assessing nature of deformations, which is an important part of the rock massif stability analysis. At the same time, the point nature of tacheometric observations and the need to ensure direct visibility between the instrument and the object of observation limit the possibilities of spatial analysis of the slope condition, especially in case of their considerable length and complex configuration [[15], [16]].

Satellite geodetic methods based on the use of GNSS technologies are applied in the studies of open pit slope stability to form time series of displacements and arrange quasi-continuous observations. The use of stationary GNSS points allows for analyzing dynamics of deformation processes and identifying trends in their development, which is taken into account when assessing massif stability under the conditions of active mining operations [[17], [18]]. However, it should be emphasized that the accuracy and reliability of GNSS measurements in deep quarries can be reduced due to the screening of satellite signals, reflection from the surfaces of mining equipment and structures, and influence of dynamic loads, which requires a reasonable choice of observation schemes [18].

The joint use of tacheometric and satellite geodetic measurements is applied in the studies of open pit slope stability. This approach improves the reliability of open pit slope stability assessment due to mutual validation of data and compensating for the limitations of individual methods. Geodetic data in this case are used not only to record deformations, but also to analyze compliance of the actual behavior of the slope with the design geomechanical models [[13], [14]].

The scientific literature discusses the issues of methodological support of the geodetic observations in the open pit slope stability studies, including selection of the system of survey markers and working survey markings, justification of the frequency of measurements and methods for the results processing. Correct interpretation of geodetic data is a key condition for their use in stability assessment and in the process of making engineering decisions [[16], [19]].

Geodetic methods play an important role in studying the open pit slope stability, while providing highly accurate reliable information on the actual deformations of the rock massifs. At the same time, the limited spatial coverage and point nature of the observations necessitate their integration with other numerical methods of stability studies to ensure a holistic understanding of the slope stability condition.

Terrestrial Laser Scanning

Terrestrial Laser Scanning (TLS) has become widespread in recent years in the study of open pit slope stability due to the possibility of obtaining a detailed three-dimensional representation of their geometry. Unlike point geodetic measurements, TLS provides a continuous description of the slope surface with high spatial detailing, which significantly expands the possibilities of analyzing their condition [[20], [21], [22]].

One of the key areas of TLS application is the study of geometric parameters of slopes and their changes with time. Comparison of three-dimensional models formed based on multiple measurements by terrestrial laser scanning allows for detecting spatial displacements of the slope surface, analyzing the distribution of deformations and localizing zones of potential instability. Such data are used to assess the nature of deformation behavior of slopes and to clarify understanding of their failure mechanisms [[22], [23]].

The main advantage of TLS is the possibility of detailed analysis of structural features of rock massifs. Based on point clouds, the fracture systems, layering and other structural elements that determine the kinematic conditioning of slope stability are identified. The use of laser scanning data increase's reliability of stability assessment due to a more accurate specification of the geometry and orientation of structural disturbances in geomechanical models [[24], [25]].

TLS data have been successfully used in the verification of computational models of open pit slope stability. Comparison of the results of numerical modeling and actual deformations detected by laser

scanning data allows for refining the calculation schemes and improve the validity of engineering decisions [[20], [26]].

Application of terrestrial laser scanning has a number of limitations. These include dependence of the data quality on the observation environment, presence of shadow zones, and the need for complex processing and interpretation of point clouds. It is noted that the TLS results themselves do not allow for judging the stability reserve of slopes unambiguously without the use of computational and analytical methods, which emphasizes the auxiliary, although important, nature of this approach in the system of stability studies [[23], [26]].

Terrestrial laser scanning is used for detailed spatial analysis of the geometry and structural features of open pit slopes, while providing a detailed description of their geometry and structural features. The greatest information content of TLS is achieved when it is used as a part of complex approaches that provide for integration of laser scanning data with the results of geodetic observations, photogrammetry and computational geomechanical analysis [[20], [22]].

Photogrammetry Based on Unmanned Aerial Photography

In recent years photogrammetric methods based on unmanned aerial photography have become widespread in the studies of open pit slope stability due to that they combine efficiency, high information content and ability to cover large areas. Use of unmanned aerial vehicles (UAVs) allows for obtaining detailed images of open pit slopes and adjacent areas, based on which digital surface models are formed; the latter are used to analyze the geometric condition of slopes and identify signs of deformation processes [[27], [28]].

Photogrammetric processing of aerial photography data is usually implemented using Structure from Motion (SfM) methods, which ensures construction of three-dimensional slope models and their subsequent comparison in time. Multitemporal analysis of digital surface models makes it possible to detect changes in slope geometry, analyze changes in the shape and volume of surface elements and record development of deformation processes, which is important in the studies of open pit slope stability [[29], [30]].

Numerical models allow for analyzing dynamics of deformation processes and identifying preliminary potential instability zones. At the same time, it is of fundamental importance to ensure sufficient accuracy of the three-dimensional models and correctness of geodetic referencing, since these factors determine the validity of the use of photogrammetric data in slope stability studies [31].

A significant advantage of photogrammetry based on unmanned aerial photography is the possibility to perform surveys under the conditions that are complicated or unsafe for ground-based observations. This makes it possible to obtain information on the condition of slopes along their entire length and in hard-to-reach areas, which expands the possibilities of spatial analysis of the open pit slope stability compared to point instrumental methods [[27], [32]].

Studies show that photogrammetric methods have a number of limitations for the performance of open pit slope stability studies. These include dependence of the results quality on meteorological conditions, illumination, and survey equipment characteristics, and the possible decrease in accuracy in areas with poor surface texture. Moreover, three-dimensional models derived from UAV data usually require verification by ground-based geodetic observations or laser scanning when they are used for engineering stability assessments [[28], [31]].

Photogrammetry based on unmanned aerial photography is widely used for spatial analysis of the condition of open pit slopes, especially at the stage of identification and localization of deformation processes. The greatest information content of this approach is achieved when it is integrated with terrestrial laser scanning, geodetic observations and computational geomechanical models, which ensures a comprehensive study of the open pit slope stability [[30], [32]].

Earth Remote Sensing Methods (InSAR)

Earth remote sensing methods based on satellite radar interferometry (InSAR) have become widespread in the studies of open pit slope stability due to the possibility of detecting deformations of the earth surface at large areas. Unlike ground-based instrumental methods, InSAR ensures spatial analysis of deformation processes without the need to place measuring instruments directly on the slopes, which is especially relevant for large and hard-to-reach mining objects [[33], [34]].

Modern interferometric approaches, including permanent scatterer methods (PS-InSAR) and small-basis methods (SBAS), allow for generating temporal series of displacements and for analyzing the dynamics of deformation processes in open pit mines over long periods of operation. The obtained data are used to identify zones of stable and unstable behavior of massifs, and to assess trends in defor-

mation development, which is of fundamental importance when studying the stability of open pit slopes [[35], [36]].

Use of InSAR methods is most appropriate for early detection of deformation processes preceding the development of dangerous stability failures. Analysis of spatial and temporal patterns of displacements allows for identifying areas with progressive deformations and for using the obtained information to justify engineering decisions aimed at ensuring stability of open pit slopes [[33], [37]].

At the same time, there are difficulties with the interpretation of InSAR data in the studies of open pit slope stability due to a number of methodological limitations. These include the single-component nature of the measured displacements along the satellite line of sight, influence of atmospheric effects, and decrease in accuracy under the conditions of intensive anthropogenic changes in relief. In this regard, InSAR data require comparison with the results of ground-based geodetic observations and other sources of information on the rock massif condition [[36], [38]].

Use of InSAR as a part of complex approaches allows for increasing the reliability of the studies of open pit slope stability due to the mutual complementation of spatial and point data, and refining of models of deformation behavior of massifs [[33], [38]].

Radar interferometry methods are widely used for spatial analysis of deformation processes related to the stability of open pit slopes. The greatest practical value of InSAR is manifested when it is used as a part of integrated digital stability research systems that provide for the joint use of satellite data, ground-based instrumental observations and computational geomechanical models, which creates prerequisites for the transition from deformation recording to analyzing and forecasting their development [[34], [35]].

A comparative analysis of the considered methods shows that they differ in terms of the nature of the data obtained, spatial coverage, and capabilities for analyzing deformation processes. Computational methods are focused on engineering assessment of slope stability and allow the analysis of loading scenarios; however, they do not reflect the actual behavior of the rock mass. Geodetic instrumental methods provide highly accurate measurements of displacements, but are limited by the point-based nature of observations. Terrestrial laser scanning and photogrammetry enable the acquisition of spatial data on slope geometry, although their application depends on acquisition conditions and data processing. Satellite interferometric methods (InSAR) allow the analysis of deformation over large areas and long time periods; however, they require careful interpretation and comparison with ground-based measurements. The results of the comparative analysis of the methods are presented in Table 1.

Table 1 - Comparative Analysis of Methods

Method	Data type	Spatial coverage	Informational capability	Main limitation
Computa-tional methods	Model-based	Full	Stability assessment	Assumptions
Geodetic methods	Point measure-ments	Local	Actual displace-ments	Limited coverage
TLS	3D spatial data	Local to near-full	Geometry and structure	Shadow zones
UAV photogram-metry	3D surface models	Areal	Surface deformation	Acquisition conditions
InSAR	Radar displace-ments	Wide-area	Deformation trends	Interpreta-tion

Thus, none of the methods considered individually provides a complete and reliable description of the stability state of open-pit slopes, which necessitates their combined application within integrated approaches.

Integrated Digital Systems and Prospects for the Methods Development

Modern trends in the development of methods for studying open pit slope stability are characterized by the transition from the use of separate instrumental and computational approaches to the formation of integrated digital systems. Such systems combine data from geodetic observations, laser scanning, photogrammetry, satellite interferometry and computational geomechanical analysis, which allows for considering slope stability as a dynamic state of rock massifs [[26], [39]].

The integration of heterogeneous data sources significantly expands possibilities for studying the open pit slope stability. The joint analysis of geospatial and point measurements allows a more complete description of massif deformation behavior, while revealing the relationship between geometric changes, structural properties and stress-strain state of massifs [[40], [41]]. This approach contributes to improving the reliability of interpretation of the observed deformations and reduction of uncertainty in the stability assessment.

A separate innovative direction in the development of integrated systems is associated with the use of methods of data mining and elements of artificial intelligence. Approaches based on the application of neural networks and machine learning algorithms are increasingly used for predicting the stability indicators for open pit slopes based on a set of geological, geomechanical and monitoring parameters [42]. Use of such methods allows for identifying patterns in large amounts of data and more validated assessments of stability status.

Efficiency of the integrated digital systems is largely determined by the quality of the input data and correctness of the methodical organization of their joint analysis. The difference of spatial and temporal scales of observations, heterogeneity of measurement accuracy and lack of unified data harmonization procedures remain significant methodological limitations in the studied of the open pit slope stability [[26], [39], [43]].

The integrated digital systems represent a promising direction in the development of methods for studying open pit slope stability. Their use creates prerequisites for transition from isolated recording of deformations to complex analysis and forecasting of deformation behavior of rock massifs, which is the key task in ensuring the safety of open pit mining operations [[42], [43]].

Conclusion

The paper presents the analytical review of modern methods of studying open pit slope stability from the point of view of introduction and development of digital technologies. Computational geomechanical approaches, geodetic instrumental methods, terrestrial laser scanning technologies, photogrammetry based on unmanned aerial photography, and satellite radar interferometry methods are considered. The analysis performed shows that each of the considered approaches has specific capabilities and limitations that determine specifics of their use in the studies of the open pit slope stability.

It is shown that computational methods retain a key role in engineering assessment of slope stability, but under the conditions of complex geological structure and dynamic development of deformation processes, their use requires mandatory comparison with instrumental observation data. Geodetic methods provide reliable information on actual slope displacements, but due to the point nature of observations, they have limited opportunities for spatial analysis of stability conditions. Digital methods based on laser scanning, photogrammetry and Earth remote sensing significantly expand the possibilities of stability studies due to the formation of spatial representation of slope geometry and the properties of deformation processes development.

Analysis of literature sources indicates that the greatest information content in the study of open pit slope stability is achieved by integrating data obtained by different methods. Formation of integrated digital systems allows for considering slope stability as a dynamic state of rock massifs, for taking into account spatial and temporal peculiarities of deformation development and for increasing validity of conclusions on the stability state.

At the same time, it was revealed that further development of methods for studying open pit slope stability is largely constrained by the lack of unified approaches to the coordinated interpretation of the data of different scales and complexity of their joint use within a single methodological scheme. In this regard, improvement of the analysis and interpretation the actual scientific and practical task remains for digital monitoring data remain a relevant scientific and practical problem, with the focus on the transition from the fixation of deformations to a reasonable analysis and forecasting of their development.

Therefore, the results of the review confirm feasibility of the integrated use of computational and numerical methods in the study of open pit slope stability and emphasize prospects for further research focused on the development of integrated digital approaches and improving the efficiency of safety of open pit mining operations.

Conflicts of interest. The authors have no financial or personal conflicts of interest related to this work.

CRediT author statement: **N. Vishnevskaya:** Conceptualization, Writing draft preparation; **S. Ozhigina:** Data curation, Methodology; **S. Ozhigin:** Supervision.; **U. Kubaidullina:** Software, Validation; **R. Baigali:** Investigation; **R. Babazhanov:** Reviewing and Editing.

Cite this article as: Vishnevskaya NA, Ozhigina SB, Ozhigin SG, Babazhanov RT, Kubaidullina UA, Baigali RK. Analytical Review of the Methods of Studying Open Pit Slope Stability Under the Conditions of Mining Operations Digitalization. Kompleksnoe Ispolzovanie Mineralnogo Syra = Complex Use of Mineral Resources. 2028; 344(1):99-108. https://doi.org/10.31643/2028/6445.10

Тау-кен жұмыстарын цифрландыру жағдайында карьерлік беткейлердің тұрақтылығын зерттеу әдістеріне аналитикалық шолу

***Вишневская Н.А., Ожигина С.Б., Ожигин С.Г., Кубайдуллина У.А., Байгали Р.К., Бабажанов Р.Т.**

Әбілқас Сағынов атындағы Қарағанды техникалық университеті, Қарағанды, Қазақстан

Мақала келді: *26 қаңтар 2026*
Сараптамадан өтті: *22 сәуір 2026*
Қабылданды: *8 мамыр 2026*

ТҮЙІНДЕМЕ

Карьерлік еңістердің тұрақтылығы ашық тау-кен жұмыстарының қауіпсіздігі мен тиімділігін айқындайтын негізгі факторлардың бірі болып табылады. Карьерлердің тереңдеуіне, жыныс массивінің геологиялық құрылымының күрделенуіне және тау-кен жұмыстарының қарқындылығының артуына байланысты цифрлық технологияларға негізделген карьерлік еңістердің тұрақтылығын зерттеу әдістерін қолдану қажеттілігі арта түсуде. Осы зерттеудің мақсаты — ашық тау-кен жұмыстары жағдайында қолданылу мүмкіндіктері мен шектеулерін ескере отырып, карьерлік еңістердің тұрақтылығын зерттеудің заманауи әдістерін жүйелеу және салыстырмалы талдау жүргізу. Жұмыста есептік геомеханикалық тәсілдерге, геодезиялық аспаптық әдістерге, жерүсті лазерлік сканерлеу технологияларына, ұшқышсыз ұшу аппараттарына негізделген фотограмметрияға, сондай-ақ спутниктік радиолокациялық интерферометрия әдістеріне аналитикалық шолу ұсынылған. Әдістерге деректер түрі, кеңістіктік қамту және деформациялық процестерді талдау мүмкіндіктері сияқты негізгі параметрлер бойынша салыстырмалы талдау жүргізілді. Әрбір әдістің қолданылу саласын айқындайтын өзіндік артықшылықтары мен шектеулері бар екені көрсетілген. Жеке қарастырылған әдістердің ешқайсысы карьерлік еңістердің тұрақтылық жағдайын толық әрі сенімді сипаттай алмайтыны анықталды. Ең жоғары ақпараттылық әртүрлі әдістерді кешенді тәсілдер аясында біріктіру кезінде қол жеткізіледі. Алынған нәтижелер карьерлік еңістердің тұрақтылығын зерттеудегі заманауи цифрлық әдістердің орны мен рөлі туралы тұтас түсінік қалыптастырып, олардың мониторинг пен бағалауға арналған интеграцияланған цифрлық жүйелерін дамытудың перспективалы екенін дәлелдейді.

Түйін сөздер: беткейнің тұрақтылығы, есептеу әдісі, аспаптық әдіс, жердегі лазерлік сканерлеу, Жерді қашықтықтан зондтау, интеграцияланған цифрлық жүйе.

Авторлар туралы ақпарат:

Вишневская Наталья Александровна — *Phd докторант, Маркшейдерлік іс және геодезия кафедрасының оқытушысы, Әбілқас Сағынов атындағы Қарағанды техникалық университеті, Н. Назарбаев 56, 100027, Қарағанды, Қазақстан. Email: n.vishnevskaya@ktu.edu.kz; ORCID ID: https://orcid.org/0009-0001-2434-2019*

Ожигина Светлана Борисовна — *Т.ғ.к., Маркшейдерлік іс және геодезия кафедрасының қауымдастырылған профессоры, Әбілқас Сағынов атындағы Қарағанды техникалық университеті, Н. Назарбаев 56, 100027, Қарағанды, Қазақстан. Email: s.ozhigina@ktu.edu.kz; ORCID ID: https://orcid.org/0000-0001-7986-2858*

Ожигин Сергей Георгиевич — *Т.ғ.д., Маркшейдерлік іс және геодезия кафедрасының профессоры, Әбілқас Сағынов атындағы Қарағанды техникалық университеті, Н. Назарбаев 56, 100027, Қарағанды, Қазақстан. Email: s.ozhigin@ktu.edu.kz; ORCID ID: https://orcid.org/0000-0003-2432-3851*

Кубайдуллина Улпан Айткужиевна — *Phd докторант, Маркшейдерлік іс және геодезия кафедрасының оқытушысы, Әбілқас Сағынов атындағы Қарағанды техникалық университеті, Н. Назарбаев 56, 100027, Қарағанды, Қазақстан. Email: u.kubaidullina@ktu.edu.kz; ORCID ID: https://orcid.org/0000-0002-2445-5590*

Байғали Руслан Қанатұлы — *Phd докторант, Маркшейдерлік іс және геодезия кафедрасының оқытушысы, Әбілқас Сағынов атындағы Қарағанды техникалық университеті, Н. Назарбаев 56, 100027, Қарағанды, Қазақстан. Email: r.baigali@ktu.edu.kz; ORCID ID: https://orcid.org/0000-0003-4431-2172*

Бабажанов Руслан Тахирович — *Phd докторант, Маркшейдерлік іс және геодезия кафедрасының оқытушысы, Әбілқас Сағынов атындағы Қарағанды техникалық университеті, Н. Назарбаев 56, 100027, Қарағанды, Қазақстан. Email: r.babazhanov@ktu.edu.kz; ORCID ID: https://orcid.org/0000-0003-0498-8899*

Аналитический обзор методов исследования устойчивости карьерных откосов в условиях цифровизации горных работ

***Вишневская Н.А., Ожигина С.Б., Ожигин С.Г., Кубайдуллина У.А., Байгали Р.К., Бабажанов Р.Т.**

Карагандинский технический университет имени Абылкаса Сагинова, Караганда, Казахстан

Поступила: *26 января 2026*
Рецензирование: *22 апреля 2026*
Принята в печать: *8 мая 2026*

АННОТАЦИЯ

Устойчивость карьерных откосов является одним из ключевых факторов, определяющих безопасность и эффективность открытых горных работ. С увеличением глубины карьеров, усложнением геологического строения массивов и интенсификацией горных работ возрастает необходимость применения методов исследования устойчивости карьерных откосов, основанных на использовании цифровых технологий. Целью настоящего исследования является систематизация и сравнительный анализ современных методов исследования устойчивости карьерных откосов с учётом их возможностей и ограничений в условиях открытых горных работ. В работе представлен аналитический обзор расчётных геомеханических подходов, геодезических инструментальных методов, технологий наземного лазерного сканирования, фотограмметрии на основе беспилотной аэрофотосъёмки, а также методов спутниковой радиолокационной интерферометрии. Выполнен сравнительный анализ методов по ключевым параметрам, включая тип данных, пространственный охват и возможности анализа деформационных процессов. Показано, что каждый из методов обладает специфическими преимуществами и ограничениями, определяющими область его применения. Установлено, что ни один из методов, рассматриваемый отдельно, не обеспечивает полного и достоверного описания состояния устойчивости карьерных откосов. Наибольшая информативность достигается при интеграции различных методов в рамках комплексных подходов. Полученные результаты формируют целостное представление о роли современных цифровых методов в исследовании устойчивости карьерных откосов и подтверждают перспективность развития. интегрированных цифровых систем мониторинга и оценки их устойчивости.

Ключевые слова: устойчивость откоса, расчетный метод, инструментальный метод, Наземное лазерное сканирование, дистанционное зондирование Земли, интегрированная цифровая система.

Информация об авторах:

Вишневская Наталья Александровна — *Phd докторант, преподаватель кафедры Маркшейдерского дела и геодезии, Карагандинский технический университет имени Абылкаса Сагинова, пр. Н.Назарбаева 56, 100027, Караганда, Казахстан. Email: n.vishnevskaya@ktu.edu.kz; ORCID ID: https://orcid.org/0009-0001-2434-2019*

Ожигина Светлана Борисовна — *К.т.н., ассоциированный профессор кафедры Маркшейдерского дела и геодезии, Карагандинский технический университет имени Абылкаса Сагинова, пр. Н.Назарбаева 56, 100027, Караганда, Казахстан. Email: s.ozhigina@ktu.edu.kz; ORCID ID: https://orcid.org/0000-0001-7986-2858*

Ожигин Сергей Георгиевич — *Д.т.н., профессор кафедры Маркшейдерского дела и геодезии, Карагандинский технический университет имени Абылкаса Сагинова, пр. Н.Назарбаева 56, 100027, Караганда, Казахстан. Email: s.ozhigin@ktu.edu.kz; ORCID ID: https://orcid.org/0000-0003-2432-3851*

Кубайдуллина Улпан Айткужиевна — *Phd докторант, преподаватель кафедры Маркшейдерского дела и геодезии, Карагандинский технический университет имени Абылкаса Сагинова, пр. Н.Назарбаева 56, 100027, Караганда, Казахстан. Email: u.kubaidullina@ktu.edu.kz; ORCID ID: https://orcid.org/0000-0002-2445-5590*

Байғали Руслан Қанатұлы — *Phd докторант, преподаватель кафедры Маркшейдерского дела и геодезии, Карагандинский технический университет имени Абылкаса Сагинова, пр. Н.Назарбаева 56, 100027, Караганда, Казахстан. Email: r.baigali@ktu.edu.kz; ORCID ID: https://orcid.org/0000-0003-4431-2172*

Бабажанов Руслан Тахирович — *Phd докторант, преподаватель кафедры Маркшейдерского дела и геодезии, Карагандинский технический университет имени Абылкаса Сагинова, пр. Н.Назарбаева 56, 100027, Караганда, Казахстан. Email: r.babazhanov@ktu.edu.kz; ORCID ID: https://orcid.org/0000-0003-0498-8899*

References

[1] Fakir M, Ferentinou M. A holistic open pit mine slope stability index using artificial neural networks. ISRM International Symposium, Cape Town. South Africa. 2–7 October. 2017, 331-348

[2] Tsevegmid T, Kim Y, Lee S, Kim B. A Comparative Analysis of Slope Stability Methods for an Open-Pit Mine in Mongolia. Applied Sciences. 2025; 15:9984. https://doi.org/10.3390/app15189984

[3] Jiang J, Sun J, Wang D, Wang L, Cao L, Cai M. An evaluation method of open pit slope stability based on Poset theory. Geomechanics and Geophysics for Geo-Energy and Geo-Resources. 2024; 10:11. https://doi.org/10.1007/s40948-023-00708-y

[4] Vujić L, Čebašek V, Gajić G, Gojkovićn, Miljanović I, Petrovski A. Potential traps and risks in slope stability calculations at open pit mines. 4th Balkanmine Congress, Slovenia, Ljubljana. 2011, 527-531.

[5] Sun Z, Balasubramanian GR, Fager A, Crouse B, Barlow G, Abouaali M. Numerical Analysis of Slope Stability in Open Pit Mining based on an Integrated Geology and Geomechanics Approach. 58th U.S. Rock Mechanics. Geomechanics Symposium, USA, Colorado, Golden. 2024, 8. https://doi.org/10.56952/ARMA-2024-0499

[6] Steiakakis E, Xiroudakis G, Lazos I, Vavadakis D, Bazdanis G. Stability Analysis of a Multi-Layered Slope in an Open Pit Mine. Geosciences. 2023; 13(12):359. https://doi.org/10.3390/geosciences13120359

[7] Cao H, Ma G, Liu P, Qin X, Wu C, Lu J. Multi-Factor Analysis on the Stability of High Slopes in Open-Pit Mines. Applied Sciences. 2023; 13(10):5940. https://doi.org/10.3390/app13105940

[8] Yang X, Hao Z, Ma G, Li G. Research on Slope Stability Evaluation Based on Improved Set Pair Analysis Method: A Case of Tonglvshan Open-Pit Mine. Shock and Vibration. 2021; 6713581:16. https://doi.org/10.1155/2021/6713581

[9] Koriawan GP, Mawaleda M, Pachri H. Slope Stability analysis based on rock mass rating (RMR) method at an open pit mine, east Java, Indonesia. IOP Conference Series: Earth and Environmental Science, Mataram, Indonesia. 2024; 1422:012006. https://doi.org/1755-1315/1422/1/012006

[10] Liu Q, Ren YQ, Wu XY, Chen JY, Chen XM. Slope Stability Analysis of the Mining Pit in an Open Pit Nonmetallic Mine. Engineering Technology Trends. 2025; 3(1):6-11.

[11] Lin B. Stability Analysis of Dump Slope: Taking Zijinshan Open-Pit Mine as an Example. Mobile Information Systems. 2022; 9009528:20. https://doi.org/10.1155/2022/9009528

[12] Pykhteeva NF, Andreeva ON, Koltsov PV. Stability analysis of pit slopes in ZapadnoOzerny quarry to ensure mine safety. ICITE 2023. E3S Web of Conferences. 2024; 474. https://doi.org/10.1051/e3sconf/202447401072

[13] Nguyen HV, Pham KC, Nguyen DB, Nguyen LQ. Application of the GNSS Method in the Monitoring of Mine Surface Displacement: A Systemic Review. Inzynieria Mineralna. 2024; 2(1):247-255. http://doi.org/10.29227/IM-2024-01-115

[14] Shi S, Guo Z, Ding P, Tao Y, Mao H, Jiao Z. Failure Mechanism and Stability Control Technology of Slope during Open-Pit Combing Underground Extraction: A Case Study from Shanxi Province of China. Sustainability. 2022; 14(14);8939. https://doi.org/10.3390/su14148939

[15] Afeni TB, Cawood FT. Slope Monitoring using Total Station: What are the Challenges and How Should These be Mitigated. South African Journal of Geomatics. 2013; 2(1):41-53.

[16] Nizametdinov FK, Murat G, Mustafin, Sergey G Ozhigin, Asem Serikkyzy Tuyakbai. Geomonitoring sostoyaniya ustoychivosti karyernykh otkosov [Geomonitoring of stability state of career slopes]. Interekspo Geo-Sibir = Interexpo GEO-Siberia. 2020, 176-185. (in Russ.). https://doi.org/10.33764/2618-981X-2020-1-1-176-185

[17] Brown N, Kaloustian S, Roeckle M. Monitoring of Open Pit Mines Using Combined GNSS Satellite Receivers and Robotic Total Stations. Slope Stability. 2007, 417-429.

[18] Kazakov AN, Fazilova DH, Khamitov NA. Monitoring slope displacements at the kalmakyr open-pit mine using gnss and gamit/globk processing. Technical science and innovation. 2025; 3(5):31-36. https://doi.org/10.59048/2181-1180.1708

[19] Ponomarenko MR. Razrabotka metoda deformatsionnogo monitoringa otkrytykh gornykh rabot v usloviyakh kraynego severa s ispolzovaniyem kosmicheskogo radiolokatsionnogo zondirovaniya [Development of a method for deformation monitoring of open-pit mining operations in the Far North using space radar sensing]. Sankt-Peterburg. 2018, 155. (in Russ.).

[20] Yin C, Li H, Hu Z, Li Y. Application of the Terrestrial Laser Scanning in Slope Deformation Monitoring: Taking a Highway Slope as an Example. Applied Sciences. 2020; 10:2808. https://doi.org/10.3390/app10082808

[21] Guo Y, Li X, Ju S, Lyu Q, Liu T. Utilization of 3D Laser Scanning for Stability Evaluation and Deformation Monitoring of Landslides. Journal of Environmental and Public Health. 2022; 8225322:14. https://doi.org/10.1155/2022/8225322

[22] Lefu N, Nokwe V. Use of laser scanner technology as part of the slope stability risk management strategy at Letšeng diamond mine. Slope Stability. Proceedings of the 2020 International Symposium on Slope Stability in Open Pit Mining and Civil Engineering, Australian Centre for Geomechanics, Perth. 2020, 241-254. https://doi.org/10.36487/ACG_repo/2025_11

[23] Bazarnik M. Slope stability monitoring in open pit mines using 3D terrestrial laser scanning. AG 2018 – 4th International Conference on Applied Geophysics. E3S Web of Conferences. 2018; 66. https://doi.org/10.1051/e3sconf/20186601020

[24] Yartseva VF, Ozhigin DS, Dolgonosov VN, Ozhigina SB, Ozhigin SG. Study of rock mass structural features based on laser scanning results. Kompleksnoe Ispolzovanie Mineralnogo Syra = Complex Use of Mineral Resources. 2026; 338(3):72-80. https://doi.org/10.31643/2026/6445.30

[25] Zarovnyayev BN, Shubin GV, Vasilyev IV, Varlamova LD. Monitoring sostoyaniya bortov glubokikh karyerov s primeneniyem tekhnologii nazemnogo lazernogo skanirovaniya [Monitoring of the condition of the sides of deep quarries using ground-based laser scanning technology]. Mining Journal. 2016; 9;37–40. (in Russ.). https://doi.org/10.17580/gzh.2016.09.07

[26] Kazantseva VV, Ozhigin DS, Kosarev NS, Satbergenova AK, Ozhigina SB. Development of complex system of geotechnical monitoring of technogenic objects based on geospatial data. Journal of Mining Institute. 2025; 16590:1-15.

[27] Tangadzani JP, Paradzayi C, Muromo TG. Application of UAV-based Photogrammetry in Monitoring Slope Deformations in Open Pit Mining Environments: A Systematic Review. Proceedings of the FIG Working Week. 2024.

[28] Tsachouridis S, Pavloudakis F, Sachpazis C, Tsioukas V. Monitoring Slope Stability: A Comprehensive Review of UAV Applications in Open-Pit Mining, Land. 2025; 14:1193. https://doi.org/10.3390/land14061193

[29] Ciccarese G, Tondo M, Mulas M, Bertolini G, Corsini A. Rapid Assessment of Landslide Dynamics by UAV-RTK Repeated Surveys Using Ground Targets: The Ca' Lita Landslide (Northern Apennines, Italy). Remote Sensimg. 2024; 16(6):1032. https://doi.org/10.3390/rs16061032

[30] Yigit AY, Senol HI. Surface Change and Stability Analysis in Open-Pit Mines Using UAV Photogrammetric Data and Geospatial Analysis. Drones. 2025; 9:472. https://doi.org/10.3390/drones9070472

[31] Avrunev EI, Yambayev KhK, Opritova OA, Chernov AV, Gogolev DV. Otsenka tochnosti 3D-modeley, postroyennykh s ispolzovaniyem bespilotnykh aviatsionnykh system [Evaluation of the accuracy of 3D models built using unmanned aircraft systems]. Vestnik Sgugit = Vestnik Ssugt. 2018; 23(3):211-228. (in Russ.).

[32] Junaid M, Al-Atroush ME, Mahmood S, Shah KS, Ullah A. Recent developments in unmanned aerial vehicle (UAV) surveys for rock slope stability analysis-a review. Geocarto International. 2025; 40;1:2519915. https://doi.org/10.1080/10106049.2025.2519915

[33] Maulana F R, Wattimena R K, Sulistianto B. Integrated D-InSAR and Ground-based Radar for Open Pit Slope Stability Monitoring and Implications for Rock Mass Young's Modulus Reduction. Journal of Engineering and Technological Sciences. 2023; 55(3):247-260. https://doi.org/10.5614/j.eng.technol.sci.2023.55.3.3

[34] Mozer DV, Karaneyeva AD, Isainova GO, Satbergenova AK, Estayeva AR. Kosmicheskiy monitoring za deformatsiyami zemnoy poverkhnosti na territorii Ekibastuzskogo mestorozhdeniya [Space monitoring of deformations of the Earth's surface in the territory of the Ekibastuz field]. Interekspo Geo-Sibir = Interexpo GEO-Siberia. 2016; 4(1):55-58. (in Russ.).

[35] Haupt S, Sibolla B, Mdakane LW. Time series insar analysis for slope stability monitoring using sentinel-1 in open pit mining. The International Archives of the Photogrammetry, Remote Sensing and Spatial Information Sciences, Volume XLVIII-1/W2-2023 ISPRS Geospatial Week 2023. Cairo, Egypt. 2023, 945-951. https://doi.org/10.5194/isprs-archives-XLVIII-1-W2-2023-945-2023

[36] Gorbunov VA, Kantemirov YuI. Rezultaty kosmicheskogo radarnogo monitoringa deformatsiy bortov i ustupov karyerov OAO Gayskiy GOK i smeshcheniy zemnoy poverkhnosti i sooruzheniy na promyshlennoy ploshchadke predpriyatiya [The results of space radar monitoring of deformations of the sides and ledges of JSC Gaisky GOK quarries and displacements of the Earth's surface and structures at the industrial site of the enterprise]. Geomatika = Geomatics. 2013; 2:70-76. (in Russ.).

[37] Nunu S. Issledovaniye problemy neustoychivosti bortov karyerov Britanskoy Kolumbii [Investigation of the problem of instability of the sides of British Columbia quarries]. Fiziko-tekhnicheskiye problemy razrabotki poleznykh iskopayemykh = Journal of Mining Science. 2018; 5:115-123. (in Russ.). https://doi.org/10.15372/FTPRPI20180511

[38] Nguyen H V, Pham K C, Vo D N, Dinh T T, Pham C V. Monitoring subsidence of open pit mine slope based on GNSS/CORS technology - case study at the Coc Sau open-pit coal mine. Journal of Mining and Earth Sciences. 2024; 65(3):109–122. https://doi.org/10.46326/JMES.2024.65(3).10

[39] Le Roux R, Sepehri M, Khaksar S, Murray I. Slope Stability Monitoring Methods and Technologies for Open-Pit Mining: A Systematic Review. Mining. 2025; 5:32. https://doi.org/10.3390/mining5020032

[40] Cheng Y, Hou K. Open-Pit Slope Stability Analysis Integrating Empirical Models and Multi-Source Monitoring Data. Applied Sciences. 2025; 15:9278. https://doi.org/10.3390/app15179278

[41] Nguyen PMV, Marciniak M. Stochastic Rock Slope Stability Analysis: Open Pit Case Study with Adjacent Block Caving. Geotechnical and Geological Engineering. 2024; 42:5827–5845. https://doi.org/10.1007/s10706-024-02862-w

[42] Wang S, Zhang Z, Wang C. Prediction of stability coefficient of open-pit mine slope based on artificial intelligence deep learning algorithm. Scientific Reports. 2023; 13:12017. https://doi.org/10.1038/s41598-023-38896-y

[43] Fomenko IK, Novgorodova MA, Sirotkina ON. Sovremennyye sredstva otsenki ustoychivosti bortov karyerov i otkosov otvalov [Modern tools for assessing the stability of quarry sides and landfill slopes]. Nauchno-prakticheskaya konferentsiya, posvyashchennaya 60-letiyu Yakutskogo nauchno-issledovatelskogo i proyektnogo instituta almazodobyvayushchey promyshlennosti Yakutniproalmaz. Gornodobyvayushchaya Promyshlennost V 21 Veke: Vyzovy I Realnost [Scientific and practical conference dedicated to the 60th anniversary of the Yakut Scientific Research and Design Institute of the Diamond Industry Yakutniproalmaz. Mining Industry In The 21st Century: Challenges And Reality. Russia, Mirniy. 2021, 29-32. (in Russ.).

Crossref
DOI: 10.31643/2028/6445.11
Earth and Planetary Sciences: Earth-Surface Processes

Research and Improvement of Methods for Predicting Hidden Fracturing in a Rock Mass at a Polymetallic Mine

Bakhtybayev N.B., *Abil O.A., Bakhtybayeva A.S.

Mining Research Group LLP, Karaganda, Kazakhstan

** Corresponding author email: orazabil@minrg.com*

Received: *April 15, 2026*
Peer-reviewed: *April 25, 2026*
Accepted: *May 28, 2026*

ABSTRACT

This paper presents the results of a study aimed at improving the reliability of predicting hidden fracturing in the near-contour rock mass adjacent to underground mine workings at a polymetallic mine. The relevance of the study is associated with the fact that hidden discontinuities are not always identified during conventional visual inspection of the rock mass, which increases the risk of local collapses and complicates the selection of support parameters. The work aimed to improve methods for predicting hidden fracturing through the integrated application of ground-penetrating radar profiling, three-dimensional surveying, spatial fracture mapping, and geomechanical modeling. The study included analysis of the mining and geological conditions of the deposit, laser scanning of mine working sections, spatial fracture analysis in ShapeMetriX, numerical modeling in RocTunnel3, and GPR profiling using the GROT 12N system. It was established that the highest reliability of hidden fracturing prediction is achieved through the sequential integration of 3D survey data, spatial fracture analysis, and GPR investigation. The practical effect of the proposed approach lies in improving the validity of selecting existing support schemes rather than introducing new support types.

Keywords: hidden fracturing, rock mass, underground mine workings, ground-penetrating radar profiling, laser scanning, fracture mapping, geomechanical modeling, mine support.

Information about authors:

Bakhtybayev N.B. — *Candidate of Technical Sciences, Director of the Mining Research Group LLP, Karaganda, Kazakhstan. E-mail: bakhtybayev@minrg.com; ORCID ID: https://orcid.org/0000-0002-9816-9765*

Abil O.A. — *Executive Director of the Mining Research Group LLP, Karaganda, Kazakhstan. E-mail: orazabil@minrg.com; ORCID ID: https://orcid.org/0000-0001-9939-9039*

Bakhtybayeva A.S. — *PhD, Senior researcher of the Mining Research Group LLP, Karaganda, Kazakhstan. E-mail: bakhtybayeva_a@minrg.com, ORCID ID: https://orcid.org/0000-0001-7163-6274*

Introduction

The stability of underground mine workings is largely determined by the structural condition of the surrounding rock mass, primarily by the presence of fractures that form weakened zones and potential failure surfaces. Under conditions of underground mining, hidden fracturing represents a particular hazard because such discontinuities are not exposed on the contour of workings and cannot always be reliably identified by visual inspection alone [[1], [2], [3]]. This reduces the reliability of assessing the state of the sidewall rock mass and may lead to local collapses, roof slabbing, block formation, and disturbances to normal mining operations.

For a polymetallic mine, predicting hidden fracturing is of practical importance because geotechnical disturbances have been recorded in workings where hazardous discontinuity planes could not be reliably identified by visual observations. Analysis of mining-geological and geotechnical documentation showed that manifestations of instability are most often observed near junctions, while some hazardous disturbances remain hidden.

Modern studies indicate that the most reliable results in detecting hidden fracturing are achieved by combining direct and indirect methods, including structural mapping, seismic and electrical tomography, ground-penetrating radar, and numerical modeling [[1], [2], [3], [4], [5], [6]]. At the same time, the quantitative prediction of fracture parameters and the spatial localization of hidden weakened zones remain the most challenging aspects [[4], [5], [6]].

Recent studies show that the prediction of hidden fracturing in underground excavations is developing along four main directions: high-resolution GPR imaging, integration of geophysical

methods, digital fracture mapping from 3D data, and geomechanical interpretation for support design [[3], [7], [8], [9], [10], [11], [12], [13], [14]]. In the first direction, ground-penetrating radar has proven to be a promising tool for detecting concealed fractures, disturbed zones, moisture-related heterogeneities, and shallow structural discontinuities in rock masses [[3], [9], [10], [11], [16]]. At the same time, its efficiency strongly depends on signal attenuation, lithological contrast, moisture, metallic interference, and the correctness of radargram interpretation [[9], [10], [15], [16]]. Recent work has therefore focused not only on fracture detection itself, but also on improving image quality, interpretation robustness, and data constraints [[10], [15], [16]].

A second active direction is the integration of GPR with other geophysical methods. In fractured and heterogeneous rock masses, single-method interpretation often remains ambiguous because similar anomalies may be caused by fracturing, water saturation, lithological contacts, or altered zones [[2], [7], [8]]. For this reason, recent studies increasingly combine GPR with electrical resistivity tomography, borehole logging, seismic methods, or joint inversion strategies [[7], [8]]. Hasan et al. showed that non-invasive geophysical data can be linked to rock mass quality indicators [[2], [7]], while Huayllazo et al. demonstrated that ERT-supported interpretation can improve the identification of fractured zones and geomechanical inferences [8]. Yuan et al. proposed a GPR workflow constrained by logging data for fractured rock mass detection [10]. These developments are especially relevant for underground mining, where local geological complexity and limited access often make single-method diagnosis insufficient [[3], [8], [10]].

The third major trend concerns the transition from conventional visual mapping to digital characterization of discontinuities using LiDAR, photogrammetry, and point-cloud-based analysis [6]. This is highly relevant for mine workings where access is restricted, exposure conditions are incomplete, and shotcrete masks part of the structural pattern [[6], [12]]. Recent work has shown that semi-automatic extraction of discontinuity parameters from 3D data can significantly improve the consistency of fracture orientation analysis and the geometric basis for stability assessment [[6], [12]]. The value of such digital methods lies not only in documenting visible fracture traces, but also in building a coordinate-consistent structural model that can then be transferred into geomechanical calculations [[6], [11], [17]]. This is directly aligned with the present study, where LiDAR and ShapeMetriX are used as the first step before geomechanical analysis and targeted GPR profiling [[18], [19], [20]].

The fourth direction is the integration of structural observations into geomechanical and probabilistic stability analysis. Recent studies indicate that the engineering effect of fracture characterization is maximized when mapped discontinuities are not treated as descriptive information only, but are further used to assess parameter inversion, stress sensitivity, and support adequacy [[12], [13], [13], [14]]. This is particularly important in underground excavations affected by intersecting fracture sets and local weakening [11]. Recent publications address stress-field selection, inversion of surrounding rock parameters, and support-related geomechanical interpretation in fractured ground [21]. These studies support the logic of the present work, in which fracture geometry obtained from 3D mapping is used to guide RocTunnel3 modeling and to prioritize GPR survey locations [[18], [22]].

This study aimed to investigate and improve methods for predicting hidden fracturing in a rock mass under conditions of a polymetallic mine through the integrated use of ground-penetrating radar profiling, three-dimensional surveying, and spatial fracture mapping, as well as to develop recommendations for refining the selection of support types and parameters for underground mine workings.

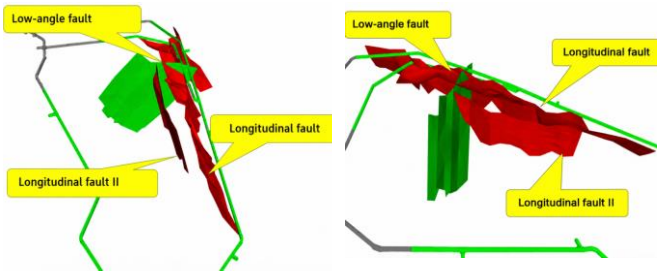

Figure 1 – Layout of faults at the polymetallic deposit

Experimental part

The study included experimental investigations using laser scanning, ground-penetrating radar profiling, and specialized software packages RocTunnel3 and ShapeMetriX. At the first stage, mine workings were visually inspected in order to identify sections suitable for instrumental investigation within the fault-controlled zone (Figure 1). It was found that a significant part of the workings had been covered with shotcrete. Therefore, six

unshotcreted sections located at the +335, +315, +295, +275, +255, and +235 m levels were selected for detailed study. An example of an investigated section is shown in Figure 2.

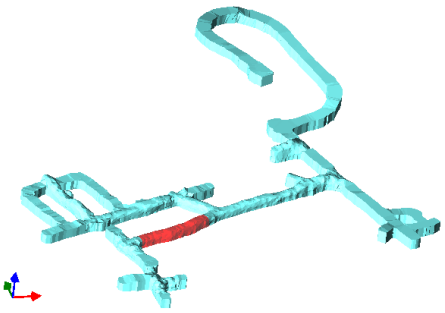

Figure 2 – Section No. 6 at the +235 m level

To obtain spatially oriented models of the workings, a Greenvalley ARTGEO LIGRIP O2 LITE (Figure 3) handheld laser scanner was used. Scanning was carried out along the contours of all selected sections, as well as at observation stations with naturally exposed fractures. Based on dense point clouds, three-dimensional models of the investigated sections (Figure 4-5) were constructed [18].

Figure 3 – Handheld LiDAR Greenvalley ARTGEO LIGRIP O2 LITE

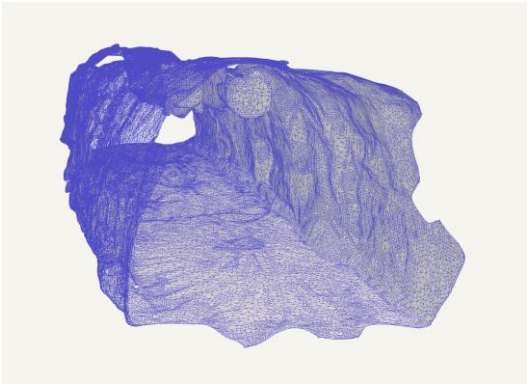

Figure 4 – Example of a 3D model of the processed section

Figure 5 – 3D model of the observation station

Spatial fracture analysis was performed in the ShapeMetriX software package (Figure 6), where fracture surfaces, strike azimuths, dip angles, and fracture sets were identified from digital models. The obtained data were then used as input for geomechanical analysis in RocTunnel3, where the formation of potentially unstable wedges and blocks was assessed. This approach made it possible to move from a generalized assessment of the rock mass to the analysis of its actual spatial fracture structure [[18], [22]].

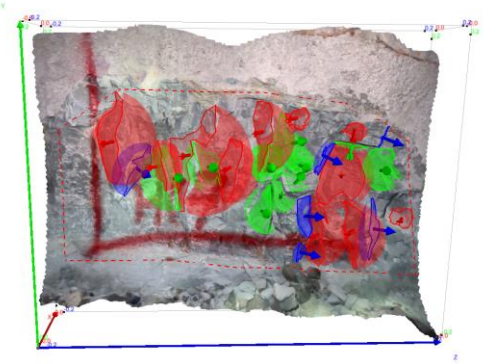

Figure 6 – Identification of fracture systems in ShapeMetriX software

Ground-penetrating radar profiling of the near-contour rock mass was carried out using the GROT 12N radar equipped with a 2 m antenna (Figure 7). Under polymetallic mine conditions, a hodograph-based measurement approach was applied, which made it possible to determine the depth of reflecting boundaries, the geometry of structural disturbances, and the electrophysical properties of the medium [[3], [4]]. According to the field program, GPR investigations were performed at four sections located at the +315, +295, +275, and +255 m levels. The interpretation quality was significantly affected by metallic support elements, wet clay-rich deposits on the surface, and the high electrical conductivity of the medium.

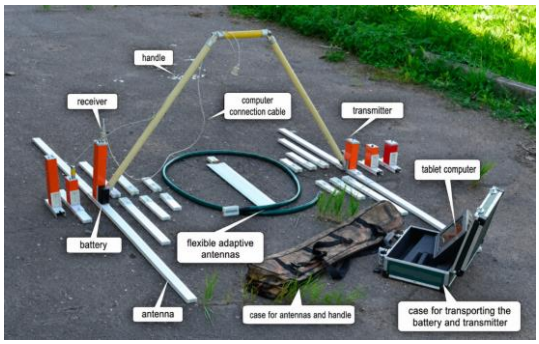

Figure 7 – General layout of the GROT 12N ground-penetrating radar

In the investigated workings, the use of alternative geophysical methods was limited by water saturation and the presence of metallic support elements, including mesh and rock bolts. Under such conditions, ERT and other resistivity-based or electromagnetic methods may be significantly distorted by conductive water and metal inclusions. Seismic methods are less suitable for rapid local near-contour investigation because they require more complex acquisition geometry under underground operating conditions. Therefore, GPR was considered the most suitable method for the selected task, while LiDAR-based fracture mapping and geomechanical modeling were used to improve the reliability of interpretation (Figure 8).

Figure 8 – Process of ground-penetrating radar survey along the floor

Results and Discussion

The performed investigations showed that visual inspection of the rock mass under polymetallic mine conditions does not provide sufficient information about the actual condition of the near-contour rock mass. Fine wet deposits, shotcrete coverage, and secondary infill of fractures reduce the reliability of determining the number, orientation, and aperture of fractures by conventional visual mapping.

Laser scanning and subsequent processing in ShapeMetriX made it possible to identify fracture systems and obtain a spatially oriented model of the rock mass structure. This provided reliable initial data for stability assessment and for planning targeted GPR investigations.

According to the results of geomechanical modeling in RocTunnel3, the most hazardous zones are associated with intersections of fracture systems and with locally weakened sectors of the rock mass where wedge and block failure structures may form. Using Section No. 3 at the +275 m level as an example, the factors of safety for the sidewall rock mass were determined, thereby allowing the localization of zones requiring additional verification by GPR (Figure 9).

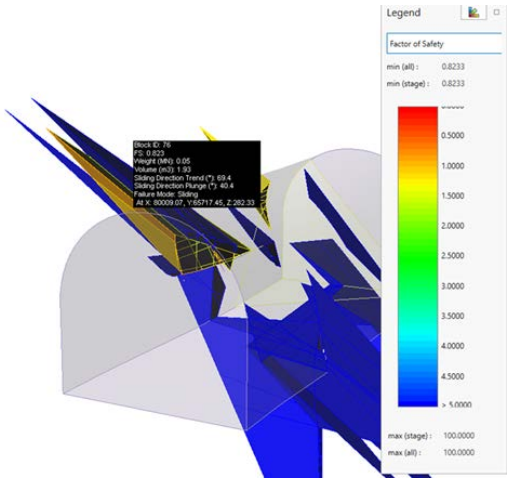

Figure 9 – Factor of safety of the side rock mass of Section No. 3 at the +275 m level in RocTunnel3 software

Ground-penetrating radar profiling confirmed the presence of hidden weakened zones that could not be detected on exposed surfaces of the workings. In addition to potentially disturbed areas, radargrams revealed zones of increased mineralization characteristic of ore bodies (Figures 10-12). Considering the combined effect of interference factors under deposit conditions, the GROT 12N radar provided an effective investigation depth of up to 18 m [[18], [22]].

As a result of the work, an integrated methodology for predicting hidden fracturing was developed, including section selection, 3D surveying, spatial fracture mapping, geomechanical modeling, and targeted GPR profiling.

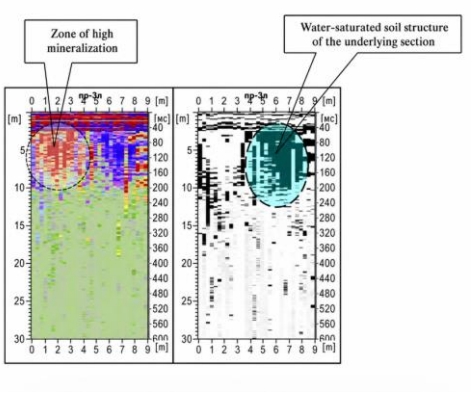

Figure 10 – Radargram of Profile 3L

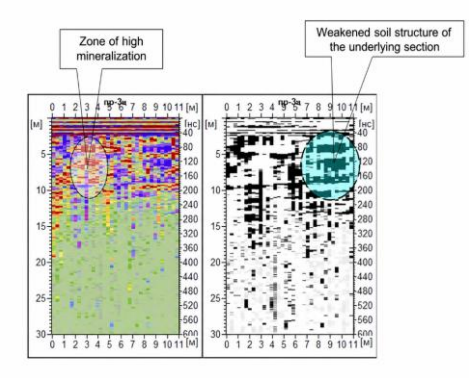

Figure 11 – Radargram of Profile 3C

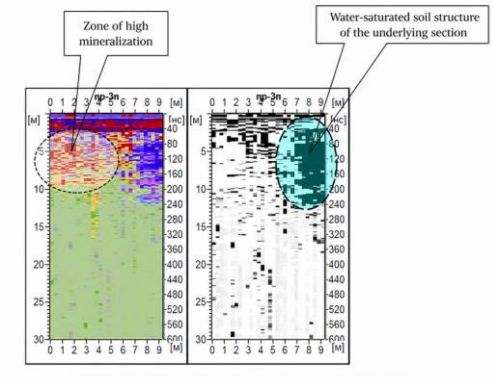

Figure 12 – Radargram of Profile 3P

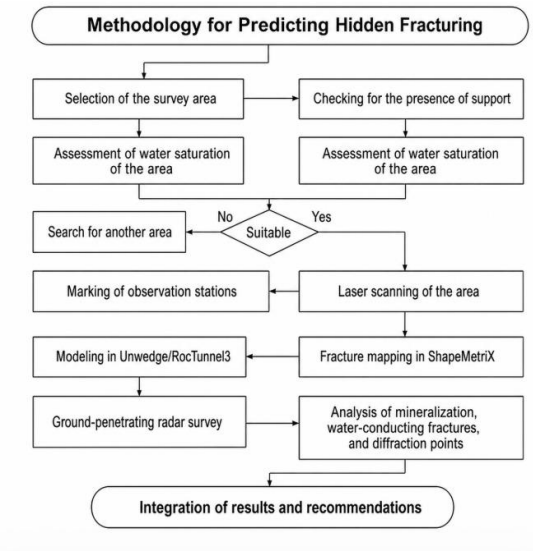

Figure 13 – Flowchart of the methodology for predicting hidden fracturing

The obtained results show that under polymetallic mine conditions, the highest reliability of predicting hidden fracturing is achieved through the integration of laser scanning, spatial fracture mapping, geomechanical modeling, and ground-penetrating radar investigation [[3], [4], [5], [6], [7], [8]]. This approach makes it possible to first record the actual geometry of the working and visible fracturing, then develop a calculated scheme of possible block-type failures, and only after that perform targeted GPR profiling to identify hidden discontinuities.

The practical significance of the results lies in the possibility of a more accurate selection of support parameters. The performed analysis showed that the current mine support regulations already include a sufficient set of support methods and support types, including anchor, friction, steel-polymer, cable, and reinforced schemes. Therefore, the main direction of improvement should not be the introduction of new support types but rather the enhancement of the validity of selecting existing solutions while taking into account the actual spatial fracture structure of the rock mass [18].

The proposed methodology (Figure 13) is especially advisable when opening new levels, driving capital mine workings, working in areas with complicated geological structure, water inflows, and signs of instability in the surrounding rock mass.

The present study had an experimental and methodological character and was primarily aimed at testing the applicability of an integrated workflow for hidden fracturing prediction under actual mine conditions. For this reason, a full quantitative validation of the method, including statistical performance assessment and large-sample comparison with documented instability cases, was beyond the scope of the current work. These aspects represent an important direction for further research.

Conclusion

1. Hidden fracturing was found to be one of the key factors controlling local instability of the near-contour rock mass in underground workings of a polymetallic mine.

2. Conventional visual inspection does not provide sufficient completeness in identifying hazardous zones under conditions of shotcrete coverage, secondary fracture infill, and complex tectonic structure of the rock mass.

3. An integrated methodology for predicting

hidden fracturing was developed based on the sequential use of LiDAR surveying, spatial fracture mapping, RocTunnel3 modeling, and GPR profiling with the GROT 12N system.

4. The application of the integrated approach improves the reliability of identifying hidden weakened zones and enhances the engineering justification for selecting support parameters.

5. The main practical conclusion is that improvement of the technological regulation should be aimed at refining the conditions for applying existing support schemes rather than expanding the range of support types.

Credit author statement: **N. Bakhtybayev, O. Abil:** Conceptualization, Methodology, Software, Data curation, Writing – original draft, Writing – review & editing; **A. Bakhtybayeva:** Investigation, Visualization, Validation, Supervision.

Funding. This study was carried out within the framework of R&D work “Research on improving methods for predicting hidden fracturing of the rock mass” (state registration No. 0126RKN0029) under Contract No. 27-01/2026-0001 dated 12 January 2026.

Cite this article as: Bakhtybayev NB, Abil OA, Bakhtybayeva AS. Research and Improvement of Methods for Predicting Hidden Fracturing in a Rock Mass at a Polymetallic Mine. Kompleksnoe Ispolzovanie Mineralnogo Syra = Complex Use of Mineral Resources. 2028; 344(1):109-116. https://doi.org/10.31643/2028/6445.11

Полиметалл кенішінде тау жыныстары массивінің жасырын жарықшақтылығын болжау әдістерін зерттеу және жетілдіру

Бахтыбаев Н.Б., Әбіл О.А., Бахтыбаева А.С.

Mining Research Group ЖШС, Қарағанды, Қазақстан

Мақала келді: *15 сәуір 2026*
Сараптамадан өтті: *25 сәуір 2026*
Қабылданды: *28 мамыр 2026*

ТҮЙІНДЕМЕ

Мақалада полиметалл кенішінің жерасты тау-кен қазбаларының жапсарлас массивіндегі жасырын жарықшақтылықты болжау дәлдігін арттыруға бағытталған зерттеу нәтижелері қарастырылған. Жұмыстың өзектілігі жасырын үзілімдік бұзылыстардың бақылауға қолжетімді беттерде әрдайым байқала бермейтіндігімен және осыған байланысты тау жыныстары массивін дәстүрлі визуалды тексеру кезінде анықталмай қалуымен түсіндіріледі, бұл жергілікті опырылулар қаупін арттырып, бекіту параметрлерін таңдауды қиындатады. Зерттеудің мақсаты георадарлық профильдеу, үшөлшемді түсірілім, жарықшақтарды кеңістіктік карталау және геомеханикалық модельдеуді кешенді қолдану негізінде жасырын жарықшақтылықты болжау әдістерін жетілдіру болды. Жұмыс барысында кен орнының тау-кен-геологиялық жағдайларына талдау жасалды, қазба учаскелеріне лазерлік сканерлеу жүргізілді, ShapeMetriX бағдарламасында жарықшақтылықтың құрылымдық талдауы, RocTunnel3 бағдарламасында сандық модельдеу және «ГРОТ 12Н» георадары арқылы георадарлық профильдеу орындалды. Жасырын жарықшақтылықты болжаудың ең жоғары сенімділігіне 3D-түсірілім, құрылымдық талдау және георадарлық зерттеу деректерін дәйекті түрде біріктіру арқылы қол жеткізілетіні анықталды. Тәжірибелік нәтиже жаңа бекіту түрлерін енгізуде емес, қолданыстағы бекіту сұлбаларын таңдаудың негізділігін арттыруда екені көрсетілді.

Түйін сөздер: жасырын жарықшақтылық, тау жыныстары массиві, жерасты тау-кен қазбалары, георадарлық профильдеу, лазерлік сканерлеу, жарықшақтарды кеңістіктік карталау, геомеханикалық модельдеу, қазбаларды бекіту.

Авторлар туралы ақпарат:

Бахтыбаев Н.Б. *Т.ғ.к., Mining Research Group ЖШС директоры, Қарағанды, Қазақстан. E-mail: bakhtybayev@minrg.com; ORCID ID: https://orcid.org/0000-0002-9816-9765*

Әбіл О.А. *Mining Research Group ЖШС атқарушы директоры, Қарағанды, Қазақстан. E-mail: orazabil@minrg.com; ORCID ID: https://orcid.org/0000-0001-9939-9039*

Бахтыбаева А.С *PhD, Жетекші ғылыми қызметкер, Mining Research Group ЖШС, Қарағанды, Қазақстан. E-mail: bakhtybayeva_a@minrg.com, ORCID ID: https://orcid.org/0000-0001-7163-6274*

Исследование и совершенствование методов прогноза скрытой трещиноватости горного массива на полиметаллическом руднике

Бахтыбаев Н.Б., Абиль О.А., Бахтыбаева А.С.

ТОО Mining Research Group, Караганда, Казахстан

Поступила: *15 апреля 2026*
Рецензирование: *25 апреля 2026*
Принята в печать: *28 мая 2026*

АННОТАЦИЯ
В статье рассмотрены результаты исследований, направленных на повышение достоверности прогноза скрытой трещиноватости прибортового массива вблизи подземных горных выработок полиметаллического рудника. Актуальность работы обусловлена тем, что скрытые разрывные нарушения не всегда выявляются при традиционном визуальном обследовании массива, что повышает риск локальных вывалов и осложняет выбор параметров крепления. Целью исследования являлось совершенствование методов прогноза скрытой трещиноватости на основе комплексного применения георадарного профилирования, трехмерной съемки, пространственного картирования трещин и геомеханического моделирования. В работе выполнены анализ горно-геологических условий месторождения, лазерное сканирование участков выработок, пространственный анализ трещиноватости в ShapeMetriX, численное моделирование в RocTunnel3 и георадарное профилирование георадаром «ГРОТ 12Н». Установлено, что наибольшая достоверность прогноза достигается при последовательной интеграции данных 3D-съемки, пространственного анализа трещиноватости и георадарного обследования. Показано, что практический эффект заключается в повышении обоснованности выбора уже действующих схем крепления, а не во введении новых типов крепи.

Ключевые слова: скрытая трещиноватость, горный массив, подземные горные выработки, георадарное профилирование, лазерное сканирование, картирование трещин, геомеханическое моделирование, крепление выработок.

Информация об авторах:

Бахтыбаев Н.Б. *Кандидат технических наук, директор ТОО Mining Research Group, Караганда, Казахстан. E-mail: bakhtybayev@minrg.com; ORCID ID: https://orcid.org/0000-0002-9816-9765*

Абиль О.А. *Исполнительный директор ТОО Mining Research Group, Караганда, Казахстан. E-mail: orazabil@minrg.com; ORCID ID: https://orcid.org/0000-0001-9939-9039*

Бахтыбаева А.С *PhD, Ведущий научный сотрудник ТОО Mining Research Group, Караганда, Казахстан. E-mail: bakhtybayeva_a@minrg.com, ORCID ID: https://orcid.org/0000-0001-7163-6274*

References

[1] Butchibabu B, Sandeep N, Sivaram YV, Jha PC, Khan PK. Bridge pier foundation evaluation using cross-hole seismic tomographic imaging. Journal of Applied Geophysics. 2017; 144:104–114. https://doi.org/10.1016/j.jappgeo.2017.07.008

[2] Hasan M, Shang Y, Meng Q. Application of electrical resistivity tomography (ERT) for rock mass quality evaluation. Scientific Reports. 2021; 11:24529. https://doi.org/10.1038/s41598-021-03217-8

[3] Song Z, Zheng J, Zhang R, Zhu A, He T, Wang J. The potential of ground penetrating radar in rock fracture detection: insights from physical model tests and numerical simulations. Journal of Rock Mechanics and Geotechnical Engineering. 2025. https://doi.org/10.1016/j.jrmge.2025.04.036

[4] Hunziker J, Greenwood A, Minato S, Barbosa ND, Caspari E, Holliger K. Bayesian full-waveform inversion of tube waves to estimate fracture aperture and compliance. Solid Earth. 2020; 11:657–668. https://doi.org/10.5194/se-11-657-2020

[5] Ringel LM, Jalali M, Bayer P. Characterization of the highly fractured zone at the Grimsel Test Site based on hydraulic tomography. Hydrology and Earth System Sciences. 2022; 26:6443–6455. https://doi.org/10.5194/hess-26-6443-2022

[6] Pavičić I, Galić I, Kucelj M, Dragičević I. Fracture system and rock-mass characterization by borehole camera surveying: application in dimension stone investigations in geologically complex structures. Applied Sciences. 2021; 11(2):764. https://doi.org/10.3390/app11020764

[7] Hasan M, Shang Y, Meng Q. Evaluation of rock mass units using a non-invasive geophysical approach. Scientific Reports. 2023; 13:14493. https://doi.org/10.1038/s41598-023-41570-y

[8] Huayllazo Y, Infa M, Frodella W, et al. Using electrical resistivity tomography method to determine the inner 3D geometry and the main runoff directions of the large active landslide of Pie de Cuesta in the Vitor Valley, Peru. Geosciences. 2023; 13(11):342. https://doi.org/10.3390/geosciences13110342

[9] Rhee J-Y, Park K-T, Cho J-W, Lee S-Y. A study of the application and the limitations of GPR investigation on underground survey of the Korean expressways. Remote Sensing. 2021; 13(9):1805. https://doi.org/10.3390/rs13091805

[10] Yuan W, Liu S, Zhao Q, Deng L, Lu Q, Pan L, Li Z. Application of ground-penetrating radar with the logging data constraint in the detection of fractured rock mass in Dazu Rock Carvings, Chongqing, China. Remote Sensing. 2023. 15(18):4452. https://doi.org/10.3390/rs15184452

[11] Chen N, Hao Y, Wang C, Zheng J. Semi-automatic identification of discontinuity parameters in rock masses based on unmanned aerial vehicle photography. Geological Journal. 2024; 59(9):2401–2415. https://doi.org/10.1002/gj.4905

[12] Liu Y, Hua W, Chen Q, Liu X. Characterization of complex rock mass discontinuities from LiDAR point clouds. Remote Sensing. 2024; 16:3291. https://doi.org/10.3390/rs16173291

[13] Tomilov A, et al. Expert system for stability assessment of underground mine workings and automatic selection of rock bolt support schemes. Applied Sciences. 2025; 15(16):8951. https://doi.org/10.3390/app15168951

[14] Isfahani NS, et al. Optimizing rock bolt support for large underground excavations in fractured rock masses using three-dimensional DEM-DFN modeling. Geosciences. 2025; 15(8):293. https://doi.org/10.3390/geosciences15080293

[15] Zhang X, Pei J, Sha X, Feng X, Hu X, Chen C, Song Z. Experimental co-polarimetric GPR survey on artificial vertical concrete cracks by the improved time-varying centroid frequency scheme. Remote Sensing. 2024; 16(12):2095. https://doi.org/10.3390/rs16122095

[16] Elshaboury N, Mohammed Abdelkader E, Al-Sakkaf A, Zayed T. A critical review and bibliometric analysis on applications of ground penetrating radar in science based on Web of Science database. Eng. 2023; 4(1):984–1008. https://doi.org/10.3390/eng4010059

[17] Wang C, Liu Z, Dong Z, Zhang F, Ma C, Xu X, Guo Q. Comprehensive application of borehole fine detection methods: a case study in Shantou Bay subsea tunnel. Geofluids. 2024; 2024:5546191. https://doi.org/10.1155/2024/5546191

[18] Research report Study on improving methods for predicting hidden fracturing of a rock mass. Karaganda: Mining Research Group LLP. 2026.

[19] Salvini R, Rindinella A, Brogi A, et al. Stress–strain investigation of the rock mass based on overcoring with CSIRO HI cell test and numerical modeling: a case study from an Italian underground marble quarry. Geosciences. 2022; 12(12):441. https://doi.org/10.3390/geosciences12120441

[20] Shi C, Yan X, Yang J, Liu Y. An inversion method for surrounding rock parameters of tunnels based on a probabilistic baseline model under a constructional environment. Geosciences. 2024; 14(4):107. https://doi.org/10.3390/geosciences14040107

[21] Liu Y, Chen J, Zhan J. Revisiting each fracture size and spatial pattern: inference from rock mass surface to interior. Journal of Rock Mechanics and Geotechnical Engineering. 2025; 17(3):1399–1417. https://doi.org/10.1016/j.jrmge.2024.08.026

[22] Technological regulations for selecting the types and parameters of support at the Dolinnoye mine. Version 3. 2025.

МАЗМҰНЫ
СОДЕРЖАНИЕ
CONTENTS

MINING & MINERAL PROCESSING

METALLURGY AND METALLURGICAL ENGINEERING

EARTH AND PLANETARY SCIENCES: EARTH-SURFACE PROCESSES

Техникалық редакторлар:
Г.К. Қасымова, Н.М.Айтжанова, Т.И. Қожахметов

Компьютердегі макет:
Г.К. Қасымова

Дизайнер:
Г.К. Қасымова, Н.М.Айтжанова

“Металлургия және кен байыту институты” АҚ
050010, Қазақстан Республикасы, Алматы қаласы, Шевченко к-сі, 29/133

Жариялауға 28.05.2026 жылы қол қойылды

Технические редакторы:
Г.К. Касымова, Н.М. Айтжанова, Т.И. Кожахметов

Верстка на компьютере:
Г.К. Касымова

Дизайнер:
Г.К. Касымова, Н.М.Айтжанова

АО “Институт металлургии и обогащения”
050010, г. Алматы, Республика Казахстан. ул. Шевченко, 29/133

Подписано в печать 28.05.2026 г.

Technical editors:
G.K. Kassymova, N.M. Aitzhanova, T.I. Kozhakhmetov

The layout on a computer:
G.K. Kassymova

Designer:
G.K. Kassymova, N.M. Aitzhanova

“Institute of Metallurgy and Ore Beneficiation” JSC
050010, Almaty city, the Republic of Kazakhstan. Shevchenko str., 29/133

Signed for publication on 28.05.2026